

If you have discovered material in AURA which is unlawful e.g. breaches copyright, (either yours or that of a third party) or any other law, including but not limited to those relating to patent, trademark, confidentiality, data protection, obscenity, defamation, libel, then please read our [Takedown Policy](#) and [contact the service](#) immediately

**A STUDY OF THE DRYING OF SINGLE  
DROPLETS IN FREE-FLIGHT**

by

**Saleem Akbar**

**Doctor of Philosophy**

**The University of Aston in Birmingham**

**October 1988**

This copy of the thesis has been supplied on condition that anyone who consults it is understood to recognise that its copyright rests with its author and that no information derived from it may be published without the author's prior, written consent.

'A Study of the Drying of Single Droplets  
in Free-Flight '

Saleem Akbar

Doctor of Philosophy

1988

SUMMARY

The literature relating to evaporation from single droplets of pure liquids and the drying of solution and slurry droplets, and of droplet sprays has been reviewed.

The heat and mass transfer rates for individual droplets suspended in free-flight, were investigated using a specially-designed vertical wind tunnel, to simulate conditions in a spray drier. The technique represented a unique alternative method for investigating evaporation from unrestrained single droplets with variable residence times.

The experiments covered droplets of pure liquid (water, isopropanol) and of significantly different solutions (sucrose, potassium sulphate) over a range of temperatures of 37°C to 97°C, initial concentrations of 5 to 40wt/wt%, and initial drop sizes of 2.8 to 4.6mm. Drop behaviour was recorded photographically and dried particles were examined by Scanning Electron Microscopy.

Correlations were developed for mass transfer coefficients for pure water droplets in free-flight ;

(i) experiencing oscillations, rotation and deformation,

$$Sh = -105 + 3.9 \left[ \frac{T_a - T_d}{T_{amb}} \right]^{0.18} Re^{0.5} Sc^{0.33}$$

for Re approx. > 1380

(ii) when these movements had ceased or diminished,

$$Sh = 2.0 + 0.71 \left[ \frac{T_a - T_d}{T_{amb}} \right]^{0.18} Re^{0.5} Sc^{0.33}$$

for Re approx. < 1060

Data for isopropanol drops were correlated reasonably well by these equations. The heat transfer data showed a similar transition range.

The drying rate curves for drops of sucrose and potassium sulphate solution exhibited three distinct stages; an initial increase in the drying rate as drop temperature reduced to the wet-bulb temperature, a short constant-rate period and a falling-rate period characterised by formation of a crust which controlled the mass transfer rate. Due to drop perturbation the rates in the high Re number region were up to 5 times greater than predicted from theory for spherical droplets. In the case of sucrose solution a 'skin' formed over the drop surface prior to crust formation. This provided an additional resistance to mass transfer and resulted in extended drying times and a smooth crust of low porosity. The relevance of the results to practical spray drying operations is discussed.

**Key Words :** Droplet Drying, Free-Flight Drop.

## **Dedicated**

To The Almighty One,  
My Parents, Brothers and Sisters

## Acknowledgements

I wish to express my sincere gratitude to Doctor C.J. Mumford and Professor G.V. Jeffreys for their supervision, encouragement and unfailing interest throughout the course of this work and compilation of the report, for which I am greatly indebted.

I also wish to thank Mr. N. Roberts and the entire staff of the Chemical Engineering Department's workshop, stores and also Mr. J. Holloway for his assistance with photographic work.

I would also like to thank the University of Aston in Birmingham for the award of a University Studentship.

Finally, I am most grateful to my very kind parents for their moral support through my studies and wish to thank my family for their encouragement.

# CONTENTS

	<b>Page</b>
<b>SUMMARY</b>	<b>2</b>
<b>DEDICATION</b>	<b>3</b>
<b>ACKNOWLEDGEMENTS</b>	<b>4</b>
<b>CONTENTS</b>	<b>5</b>
<b>LIST OF FIGURES</b>	<b>8</b>
<b>LIST OF TABLES</b>	<b>11</b>
<b>LIST OF APPENDICES</b>	<b>12</b>
<b>1 <u>INTRODUCTION</u></b>	<b>13</b>
<b>2 <u>MASS TRANSFER FUNDAMENTALS</u></b>	<b>21</b>
<b>2.1 Mass Transfer Across a Phase Boundary</b>	<b>21</b>
<b>2.2 Two - Film Theory</b>	<b>23</b>
<b>2.3 Penetration Theory</b>	<b>24</b>
<b>2.4 Surface - Renewal Theory</b>	<b>24</b>
<b>2.5 Film Penetration Theory</b>	<b>25</b>
<b>2.6 Boundary - Layer Theory</b>	<b>25</b>
<b>3 <u>DROPLET HEAT AND MASS TRANSFER</u></b>	<b>26</b>
<b><u>-EVAPORATION FROM PURE LIQUID DROPLETS</u></b>	
<b>3.1 Evaporation From Single Droplets and Spheres         under Natural Convection</b>	<b>29</b>
<b>3.2 Evaporation From Fixed Droplets and Spheres         under Forced Convection</b>	<b>33</b>
3.2.1 Mass Transfer	<b>33</b>
3.2.2 Heat Transfer	<b>42</b>
<b>3.3 Evaporation From Single Droplets in Free - Fall</b>	<b>44</b>
<b>3.4 Evaporation From Single Droplets in High Temperature         Surroundings</b>	<b>48</b>

	Page	
<b>4</b>	<b><u>DRYING OF DROPLETS CONTAINING DISSOLVED OR SUSPENDED SOLIDS</u></b>	
4.1	Constant - Rate Period	56
4.2	Falling - Rate Period	58
4.3	Mechanisms of Internal Moisture Transfer	59
4.3.1	Capillary Flow Theory	60
4.3.2	Diffusion Theory	61
4.3.3	Evaporation-Condensation Theory	62
4.4	Evaporation and Drying of Single Droplets Containing Dissolved and Suspended Solids	62
4.5	Evaporation From Sprays of Droplets	70
4.5.1	Sprays of Pure Liquids	71
4.5.2	Sprays Containing Dissolved and Suspended Solids	74
4.6	Temperature of Evaporating Droplets	75
<b>5</b>	<b><u>MATHEMATICAL MODELS FOR EVAPORATION FROM AND DRYING OF SINGLE DROPLETS</u></b>	<b>79</b>
5.1	Pure Liquid Drops	79
5.1.1	Mass Transfer Rate	81
5.1.2	Mass Transfer Coefficient	82
5.1.3	Nusselt Number	84
5.1.4	Heat Transferred to a Drop by Radiation	86
5.1.5	Heat Transferred to a Drop Through the Suspension Device	86
5.2	Drops Containing Dissolved Solids	
	-The Receding Evaporation Interface Model	87
5.2.1	Crust Thickness	90
5.2.2	Mass Transfer Coefficient	91
5.2.3	Crust Porosity	92
<b>6</b>	<b><u>EXPERIMENTAL INVESTIGATION</u></b>	<b>93</b>
6.1	Description Of Apparatus	
6.1.1	Overall Arrangement	93
6.1.2	The Drop Forming System	99
6.1.3	The Drop-Catching Mechanism	101

	<b>Page</b>
6.1.4 Shaped Wire Gauze to Produce the Inverted Velocity Profile	<b>103</b>
6.1.5 Strobe Light	
<b>7</b>	
<b><u>EXPERIMENTAL PROCEDURE</u></b>	
7.1 Operation Of Apparatus	<b>106</b>
7.2 Flow Rate Calibration For Axial Velocity	<b>107</b>
7.3 Measurement of Air Temperature and Velocity Profile in the Working Section	<b>107</b>
7.4 Measurements of Drop Dimensions	<b>110</b>
7.5 Measurement of Dry and Wet-Bulb Temperatures	<b>114</b>
7.6 Evaporation of Pure Liquid Drops	<b>114</b>
7.6.1 Drops of Water and Isopropanol	
7.7 Drying of Solution Drops	
7.7.1 Drops of Sucrose Solution	<b>114</b>
7.7.2 Drops of Potassium Sulphate Solution	<b>115</b>
<b>8</b>	
<b><u>PRESENTATION AND DISCUSSION OF RESULTS</u></b> <b><u>-EVAPORATION FROM PURE LIQUID DROPLETS</u></b>	<b>116</b>
<b>9</b>	
<b><u>PRESENTATION AND DISCUSSION OF RESULTS</u></b> <b><u>-DROPLETS CONTAINING SOLIDS</u></b>	
9.1 Drops of Sucrose Solution	<b>142</b>
9.1.1 Rates of Evaporation	<b>142</b>
9.1.2 Effect of Air Temperature on the Rate of Mass Transfer	<b>154</b>
9.1.3 Effect of Concentration on the Rate of Mass Transfer	<b>154</b>
9.1.4 Effect of Operating Temperature, Drop Diameter and Concentration on the Critical Moisture Content	<b>154</b>
9.1.5 Film Resistance Prior to Crust Formation	<b>159</b>
9.2 Drops of Potassium Sulphate Solution	<b>161</b>
9.2.1 Drying Rates	<b>161</b>
9.2.2 Appearance Changes and Drop Behaviour During Drying	<b>168</b>
9.2.3 Comparison Between Predicted and Measured Drying Rates	<b>169</b>
9.3 Applicability of Single Drop Studies to Spray Drying	<b>177</b>

	Page
<b>10 <u>CONCLUSIONS AND RECOMMENDATIONS</u></b>	
<b>10.1 Pure Liquid Droplets</b>	<b>181</b>
<b>10.2 Droplets Containing Dissolved Solids</b>	
10.2.1 Skin-Forming Materials	182
10.2.2 Rigid Crust Forming Materials	183
<b>10.3 Experimental Technique</b>	<b>184</b>
<b>10.4 Recommendations For Further Work</b>	<b>184</b>
<b>NOMENCLATURE</b>	<b>186</b>
<b>REFERENCES</b>	<b>195</b>
<b>APPENDICES</b>	<b>204</b>

### LIST OF FIGURES

1.0 Drying Rate Curve	18
4.1 Drying Characteristics of Droplets at Air Temperatures Below the Boiling Point	65
4.2 Drying Characteristics of Droplets at Air Temperatures Above the Boiling Point	65
5.1 Suspended Drop of Pure Liquid	80
5.2 Suspended Drop Containing Solids	80
6.1 General Arrangement of the Vertical Wind Tunnel	94
6.2 Schematic Diagram of the Vertical Wind Tunnel for Free-Flight Drop Studies	95
6.3 Working Section of the Experimental Apparatus	97
6.4 Working Section of Free-Flight Drop Experimental Apparatus	98
6.5 Drop-Forming System	100
6.6 Drop-Catching Mechanism	100
6.7 Drop-Forming Unit Connected to a Syringe Pump	102
6.8 Drop-Catching Unit	102
6.9 Schematic Diagram of a Strobe Synchronised with a Video Camera	105
7.1 Velocity Calibration Curves	108
7.2 Temperature Distribution of Air in the Working Section	109

	<b>Page</b>
for Different Operating Temperatures	
7.3 Velocity Distribution and Profile of Air in the Working Section of the Vertical Wind Tunnel	<b>111</b>
7.4 Schematic Diagram of Spheroid Droplet Geometry	<b>113</b>
8.1 Drop Mass-vs-Time For Pure Water Drops (N.S = 2mm)	<b>117</b>
8.2 Drop Mass-vs-Time For Pure Water Drops (N.S = 4mm)	<b>117</b>
8.3 Drop Mass-vs-Time For Drops of Isopropanol	<b>118</b>
8.4 Equivalent Drop Diameter-vs-Time For Water Drops (N.S = 2mm)	<b>118</b>
8.5 Equivalent Drop Diameter-vs-Time For Water Drops (N.S = 4mm)	<b>119</b>
8.6 Equivalent Drop Diameter-vs-Time For Drops of IPA	<b>119</b>
8.7 $Sh$ -vs- $Re^{1/2}Sc^{1/3}$ For Drops of Water (N.S = 2mm)	<b>130</b>
8.8 $Nu$ -vs- $Re^{1/2}Pr^{1/3}$ For Drops of Water (N.S = 2mm)	<b>130</b>
8.9 $Sh$ -vs- $Re^{1/2}Sc^{1/3}$ For Drops of Water (N.S = 4mm)	<b>131</b>
8.10 $Nu$ -vs- $Re^{1/2}Pr^{1/3}$ For Drops of Water (N.S = 4mm)	<b>131</b>
8.11 $Sh$ -vs- $Re^{1/2}Sc^{1/3}$ For Drops of Isopropanol	<b>132</b>
8.12 $Nu$ -vs- $Re^{1/2}Pr^{1/3}$ For Drops of Isopropanol	<b>132</b>
8.13 Correlation Of Mass Transfer Data (N.S = 2mm)	<b>134</b>
8.14 Correlation Of Mass Transfer Data (N.S = 4mm)	<b>135</b>
8.15 Oscillation of a Pure Water Drop at 30°C	<b>136</b>
8.16 Water drop showing increased tendency to sphericity with increasing $\theta$ at 97°C	<b>138</b>
8.17 Correlation of Mass Transfer Film Coefficients of Water Drops	<b>140</b>
9.1 Drying Rate Curves For Drops of Sucrose Solution at 20 w/w% Solids and a 2mm Diameter Nozzle	<b>143</b>
9.2 Drying Rate Curves For Drops of Sucrose Solution at 20 w/w% Solids and a 4mm Diameter Nozzle	<b>144</b>
9.3 Drying Rate Curves For Drops of Sucrose Solution at 40 w/w% Solids and a 2mm Diameter Nozzle	<b>145</b>
9.4 Drying Rate Curves For Drops of Sucrose Solution at 40 w/w% Solids and a 4mm Diameter Nozzle	<b>146</b>
9.5 Drop Mass-vs-Time For Sucrose Solution (20w/w%) using a 2mm Diameter Nozzle	<b>149</b>
9.6 Drop Mass-vs-Time For Sucrose Solution (20w/w%) using a 4mm	<b>149</b>

	<b>Page</b>
Diameter Nozzle	
9.7 Drop Mass-vs-Time For Sucrose Solution (40w/w%) using a 2mm Diameter Nozzle	<b>150</b>
9.8 Drop Mass-vs-Time For Sucrose Solution (40w/w%) using a 4mm Diameter Nozzle	<b>150</b>
9.9 Electron micrographs of dried crusts of sucrose solution (40w/w%) at 68°C	<b>151</b>
9.10 Photographs of a sucrose solution (40w/w%) drop exhibiting a ' ballooning ' effect	<b>153</b>
9.11 Effect of Concentration on the Evaporation Rate ( $T_a = 68^\circ\text{C}$ )	<b>156</b>
9.12 Effect of Concentration on the Evaporation Rate ( $T_a = 95^\circ\text{C}$ )	<b>157</b>
9.13 Drying Rate Curves and Water Content of 5w/w% Solution Drops of Potassium Sulphate using a 2mm Diameter Nozzle	<b>162</b>
9.14 Drying Rate Curves and Water Content of 10w/w% Solution Drops of Potassium Sulphate using a 2mm Diameter Nozzle	<b>163</b>
9.15 Drying Rate Curves and Water Content of 5w/w% Solution Drops of Potassium Sulphate using a 3mm Diameter Nozzle	<b>164</b>
9.16 Drying Rate Curves and Water Content of 10w/w% Solution Drops of Potassium Sulphate using a 3mm Diameter Nozzle	<b>165</b>
9.17 Drying Rate Curves and Water Content of 5w/w% Solution Drops of Potassium Sulphate using a 4mm Diameter Nozzle	<b>166</b>
9.18 Drying Rate Curves and Water Content of 10w/w% Solution Drops of Potassium Sulphate using a 4mm Diameter Nozzle	<b>167</b>
9.19 Changes of Appearance of Potassium Sulphate Drops	<b>170</b>
9.20 A drop of potassium sulphate solution forming a truncated spheroid ( conc = 5w/w%, N.S. = 4mm, T = 65°C )	<b>171</b>
9.21 Photographs showing various configurations of dried crusts of potassium sulphate solution	<b>171</b>
9.22 Comparison Between Measured and Predicted Drying Rates of Potassium Sulphate Solution Drops at 36°C using 10 w/w% Solids and a 2mm Diameter Nozzle	<b>172</b>
9.23 Comparison Between Measured and Predicted Drying Rates of Potassium Sulphate Solution Drops at 65°C using 10 w/w% Solids and a 2mm Diameter Nozzle	<b>172</b>

	<b>Page</b>
9.24 Comparison Between Measured and Predicted Drying Rates of Potassium Sulphate Solution Drops at 95°C using 10 w/w% Solids and a 2mm Diameter Nozzle	<b>173</b>
9.25 Comparison Between Measured and Predicted Drying Rates of Potassium Sulphate Solution Drops at 36°C using 10 w/w% Solids and a 3mm Diameter Nozzle	<b>173</b>
9.26 Comparison Between Measured and Predicted Drying Rates of Potassium Sulphate Solution Drops at 65°C using 10 w/w% Solids and a 3mm Diameter Nozzle	<b>174</b>
9.27 Comparison Between Measured and Predicted Drying Rates of Potassium Sulphate Solution Drops at 95°C using 10 w/w% Solids and a 3mm Diameter Nozzle	<b>174</b>
9.28 Comparison Between Measured and Predicted Drying Rates of Potassium Sulphate Solution Drops at 36°C using 10 w/w% Solids and a 4mm Diameter Nozzle	<b>175</b>
9.29 Comparison Between Measured and Predicted Drying Rates of Potassium Sulphate Solution Drops at 65°C using 10 w/w% Solids and a 4mm Diameter Nozzle	<b>175</b>
9.30 Comparison Between Measured and Predicted Drying Rates of Potassium Sulphate Solution Drops at 95°C using 10 w/w% Solids and a 4mm Diameter Nozzle	<b>176</b>
A8.1 Spherical slurry droplet after crust formation	<b>231</b>

### **LIST OF TABLES**

4.5.1 Droplet Size Distribution Functions	<b>72</b>
7.5.1 Vapour-Pressure Lowering Effects of Dissolved Solute	<b>115</b>
8.1 Evaporation of Water Drops at 37°C using a 2mm Diameter Nozzle	<b>121</b>
8.2 Evaporation of Water Drops at 67°C using a 2mm Diameter Nozzle	<b>122</b>
8.3 Evaporation of Water Drops at 97°C using a 2mm Diameter Nozzle	<b>123</b>
8.4 Evaporation of Water Drops at 37°C using a 4mm Diameter Nozzle	<b>124</b>
8.5 Evaporation of Water Drops at 67°C using a 4mm Diameter Nozzle	<b>125</b>
8.6 Evaporation of Water Drops at 97°C using a 4mm Diameter Nozzle	<b>126</b>
8.7 Evaporation of Pure Isopropanol Drops at 37°C using a 4mm Nozzle	<b>127</b>

	<b>Page</b>
8.8 Evaporation of Pure Isopropanol Drops at 67°C using a 4mm Nozzle	<b>128</b>
8.9 Values of $\beta$ and $\phi$ for Drops of Water and Isopropanol	<b>137</b>
9.1 Effect of Operating Variables on the Moisture Content	<b>155</b>

### **LIST OF APPENDICES**

A1 Least Squares Method for Data Correlation	<b>186</b>
A1.1 Constant Air Temperature	<b>186</b>
A1.2 Variable Air Temperature	<b>187</b>
A2 Program Constant 1	<b>189</b>
Program Constant 2	<b>190</b>
Program VarTemp	<b>191</b>
A3.1 Tabulation of Results for Pure Liquid Drops	<b>193</b>
A3.1.1 Pure Water Drops	<b>193</b>
A3.1.2 Pure Isopropanol Drops	<b>196</b>
A4.1 Tabulation of Data for Evaluation of Drying Characteristics of Drops of Sucrose Solution	<b>197</b>
A4.2 Tabulation of Data for Evaluation of Drying Characteristics of Drops of Potassium Sulphate Solution	<b>201</b>
A5 Derivation of the Crust Coefficient , $k_c$	<b>210</b>
A6 List of videos deposited in the Departmental Library	<b>211</b>
A7 Determination of the pressure driving force for systems other than air-water vapour	<b>212</b>
A8 Mathematical Model for the Prediction of Drying Rates	<b>213</b>

## CHAPTER ONE

### INTRODUCTION

Drying is an operation in which a volatile liquid, normally water, is separated from a solid material by vaporization. It is of widespread importance in the chemical industry and in the processing of natural products. A proper appreciation of the mechanisms of drying, and the equipment best able to solve a drying problem on an industrial scale, are correspondingly important. Most manufacturing operations entail stages where drying, in one form or another, is carried out. Many engineering manufacturing processes also require drying of the product before it is ready for the market.

There are many reasons, either technical or commercial, why drying is an essential step in the production of a final product. The product must be in suitable form either for subsequent processing or for marketing. For example clay granules which are fed to a press, in tile manufacture or the production of low tension insulators, must flow satisfactorily in the presses and the most suitable characteristics occur at a certain moisture content of the clay. A cup prepared in a Plaster-of-Paris mould must be of the correct moisture content for subsequent sponging or turning and for fitting the handle. Pharmaceutical granules require to be pre-dried for feeding to the tableting machine. Dyestuffs and pigments, food-stuffs, cereals and detergents require to be dried to the correct final moisture content ready for packaging and 'flowability'. Physical suitability of the final product for the market may be controlled by correct drying methods, as in the case of globular detergent powder of uniform size and appearance, or synthetic fertilizers of granular form to minimize dust losses during application. Pigments have to be marketed in a fine state of subdivision and adequate drying is imperative so that the pulverizing equipment can handle the product

satisfactorily.

A wide variety of dryer designs have been evolved over the years but, industrial dryers fall essentially into two main categories, namely convection dryers and conduction dryers, with additional special types involving almost entirely radiation or some other specialised form of heat generation or application. Vacuum freeze driers for coffee for example utilise radiant heat to sublime the moisture.

Dryers which depend on heat transfer and drying by convection are usually referred to as direct dryers, and those depending on conduction as indirect dryers. In direct dryers, such as rotary dryers, fluid bed dryers and spray dryers, the heating medium, comprising heated air or the products of combustion, is in direct contact with the wet material. In indirect dryers, such as vacuum tray dryers, pan dryers and film drum or roller dryers, the heat is transmitted indirectly by contact of the wet material with a heated surface (1). The present study relates specifically to spray drying, a form of direct, convective drying.

Spray drying is used in all major industries. In the chemical industry, for example, spray drying may be employed at some stage in the drying of plastics, resins, ceramic materials, detergents and surface active agents, pesticides, dyestuffs and pigments. Other industries include those utilising chemicals from timber and offal and fish industries in the drying of slaughterhouse products such as animal protein, blood, gelatin etc (2). In the food industry, milk, meat, egg, fruit and vegetable derivatives are dried for use as ingredients, such as thickeners and flavour and protein additives, or final consumables, such as dried milk, powdered eggs and instant coffee. Spray drying application to foods date back over 100 years, yet the process is still poorly understood. With increasing interest in improved product qualities, greater fundamental knowledge of the individual droplet drying behaviour,

and how this affects the final particulate form and moisture content, is therefore of considerable interest.

Food drying offers the unique problem of retaining volatile and sensitive flavour components while removing moisture. Many of the advantages of spray drying are partially offset by a perceived lowering of quality factors in the dried product. Volatile flavour and aroma components important to the smell and taste of foods are often lost during the drying process. Other food quality factors, such as bulk density and redispersibility, which are equally important to consumer appeal, can also suffer under poor drying conditions.

Quality factors are a direct result of the design and operating conditions used. The interactions between these are however, complex because of the presence of a distribution of drop sizes and complicated air-spray mixing patterns. In addition gross shape, or morphological changes of the droplets occur. These changes include skin formation and uneven shrinkage. Expansion and rupture can occur at high temperatures. The final morphology of the product can determine some quality attributes. Bulk density and redispersibility are directly associated with expansion and porosity. Other factors, such as moisture content and aroma retention, are affected by developing morphology.

Spray drying involves the transformation of feed from a fluid state into a dried particulate form by spraying it into a hot gaseous drying medium, normally air. It is a one step continuous particle-processing operation in which the feed may be a solution, suspension or paste. A high concentration feed is preferred to minimize the energy requirements to vaporize the free moisture. The feed is atomised into a spray to provide a large surface area, followed by contact with the drying medium resulting in moisture evaporation. A process of simultaneous heat and mass transfer occurs

between the droplets and the hot gas streams until the desired average moisture content in the dried particles is obtained, and the product is then recovered from the carrier gas in one or more separation stages .

Because atomization inevitably produces a distribution of drop sizes, generally in the range 10 to 1000 $\mu$ m, the dried particles result from a range of drying rates and residence times and hence vary in moisture content.

In short spray-drying consists of the following process stages:

- Atomization of feed into a spray (generally by use of a rotary or nozzle atomizer)
- Spray-air contact
- Drying of spray (moisture/volatiles evaporation)
- Separation of dried product from the air.

Each stage depends upon the dryer design and operation, and, together with the physical and chemical properties of the feed, these determine the characteristics of the dried product.

Of all the industrial dryer types available, few accept pumpable fluids as the feed material at the dryer inlet and discharge a dry particulate at the outlet. Spray drying is moreover unique in being able to produce powders within a narrow range of particle size and moisture content irrespective of dryer capacity and product heat sensitivity. These characteristics are of such importance to many industrial operations that spray drying is the only rational choice to dry fluid feedstock although since it is a convectional type dryer, its thermal efficiency is lower than competing conduction dryers that also receive fluid feed materials .

A desirable commercial spray-dried product is generally one which is dust-free, evenly dried (i.e. without any fraction degraded due to excessive temperature or residence time) and containing no agglomerates. The manner in which the spray contacts the air is an important factor in spray dryer design, since this affects dried product properties by influencing droplet

behaviour during drying. The gas flow may be countercurrent flow or mixed flow. Alternatively the spray can be contacted with air in which feed and air pass through the dryer in the same direction (co-current operation). This arrangement is widely used for products where rapid crust formation is desirable and the products are heat-sensitive, since the hottest gas contacts the wettest solid.

In spray-drying a droplet may enter the drying chamber at a feed temperature above, below, or equal to some dynamic-equilibrium temperature of the drying air. In the case of droplets of solution the dynamic equilibrium temperature will be higher than the wet-bulb temperature. For suspensions, the dynamic-equilibrium temperature may be equal to the wet-bulb temperature. If the initial drop temperature is not equal to the dynamic-equilibrium temperature of the drying air, it will endeavour to approach that temperature. During this initial unsteady-state period the amount of drying taking place is usually negligible although this may not always be true at very high temperatures. The drying-rate curve in Figure 1 illustrates the general drying characteristics. In phase AB, the drying rate is established immediately the droplet contacts the drying air. The droplet surface temperature increases slightly and the drying rate increases in the milliseconds required for heat transfer across the droplet - air interface to establish equilibrium.

If the droplet establishes a dynamic-equilibrium temperature with the drying air, it exhibits a constant-rate drying period, phase BC, during which the rate of drying per unit area is constant. During this period vaporization occurs as from a free liquid surface of constant composition and vapor pressure. Material structure has no influence and the constant rate period is controlled by the external conditions of air velocity, temperature and humidity. The entire resistance to mass transfer during this period lies in the

gas-film surrounding the droplet. The higher the drying temperature of the air and the higher the feed concentration the shorter will be the constant-rate period. It is entirely possible that the latter may be negligible at high temperatures and high solids contents. At the end of the constant-rate period, at point C, an average moisture content is reached designated the critical moisture content. This is a function of material properties, the constant-drying rate, and particle size and marks the beginning of the falling rate period wherein the internal mechanism of moisture flow controls. This period can exhibit more than one characteristic, if local areas of wetness remain on the droplet surface. Phase CD continues until no areas of wetness remain. In phase DE, resistance to mass transfer is wholly in the solid layer. Evaporation continues at a decreasing rate until the droplet acquires a moisture content in equilibrium with the surrounding gas. Approach to the equilibrium moisture content E is slow. However, in industrial spray-drying

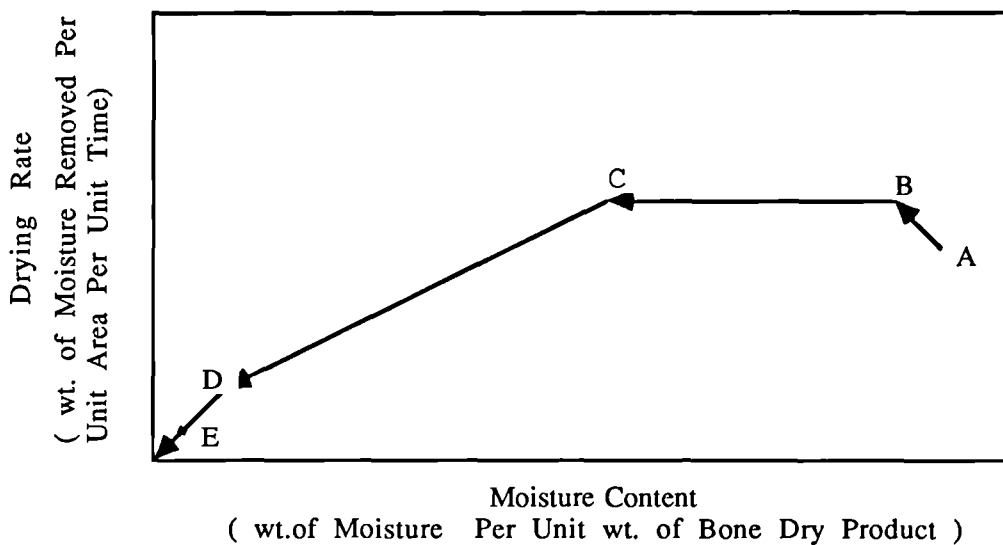


Figure 1 Drying Rate Curve

operations the product is removed before the equilibrium moisture content is reached. Droplet temperature rises throughout the two phases of the falling rate period. Figure 1 is diagrammatic and in reality drying curves may not show sharply defined points. Some of the drying zones as shown may not even occur, as in Figures 9.1-9.4, 9.13-9.18, later, where the constant rate period is very short indeed, compared to the falling-rate period.

The duration of the falling-rate period usually establishes the size of a dryer required to dry a given material at a specified rate to a specified final moisture content. During this period a skin or crust forms and there is a shift from external to internal mass-transfer control. Evaporation from the surface of the droplet is generally controlled by the thickness and porosity of the crust. As a particle dries, the crust increases in thickness resulting in an increase in the resistance to heat and mass transfer. This invariably increases the core temperature causing a reduction in the partial pressure and temperature driving force. The transfer process is therefore highly complex and difficult to model mathematically. Furthermore, following crust formation, fracture, shrinkage or inflation may occur; these further complicate the modelling of heat and mass transfer and, of course, affect final form .

Because of the complexities and the impracticability of investigating rate controlling mechanisms for the distribution of drop sizes travelling through a dryer, studies of spray drying have therefore tended to be divided into:

- (a) studies of atomization, with attempts to correlate drop size distribution with feed characteristics, atomiser design and flowrates ,
  - (b) studies of gas flow patterns and residence times ,
  - (c) single drop drying studies
- and (d) mathematical models which attempt to bring together the data from a-b to predict dryer performance.

The present study was concerned with a sophisticated study under (c)

Many experimental studies have been made on the drying of single droplets but in the majority of these the droplet was dried whilst suspended from the tip of a fine filament, thermocouple or a nozzle. The disadvantages of these techniques include:

- Heat conduction along the nozzle, which can represent a significant proportion of the total heat transferred to the droplet. This results from the large surface area (-33%) of the drop in contact with the nozzle.
- With a droplet suspended from a nozzle, evaporation occurs from a hemisphere.
- The presence of a filament significantly affects the drying behaviour near the end of drying.
- Whilst a nozzle may be rotated, the drop on a filament is subjected to a directional air flow.
- In other investigations single drops have been allowed to fall through still air in a vertical column but this generally allows insufficient residence time for drying.

These disadvantages were overcome in the present study by using a vertical wind tunnel in which a single droplet could be stabilised in free-flight, thus simulating more closely conditions existing in a spray dryer. The aim was to gain fundamental insight into the mechanisms involved in the evaporation of pure liquids and the drying of drops containing solids, with a view to eventually improving the design and operating performance of spray dryers. The experimental work covered a drop size range of 0.7 to 4.6 mm, the evaporation of pure liquid drops, and the drying of solutions of organic and inorganic drops.

**CHAPTER TWO**  
**MASS TRANSFER FUNDAMENTALS**

**2.1 Mass Transfer Across a Phase Boundary**

Drying of droplets, like most diffusional mass transfer operations, involves contact between two phases which allows transfer of the diffusing vapour from one phase to the other. The driving force for mass transfer is provided by the concentration gradient which exists across the interface.

The rate of transfer of diffusing substance may be described by means of Fick's Law of diffusion (3). According to this law, the rate of diffusion of substance A in a binary mixture of A and B, is proportional to the concentration gradient in the direction of diffusion;

$$N_A = - D_{AB} \frac{dC_A}{dZ} \quad \text{-----} \quad 2.1$$

where  $D_{AB}$  is the diffusivity of A in B.

The rate of mass transfer between the two phases is a function of the physical properties of the two phases, the interfacial area and the concentration driving force;

$$N_A = K_O A \Delta C \quad \text{-----} \quad 2.2$$

where  $K_O$  = Overall Mass Transfer Coefficient

A = Interfacial area

$\Delta C$  = Concentration driving force

Equation 2.2 defines the overall mass transfer coefficient, but in spray drying, or in the drying of single droplets containing solids, initially evaporation occurs from a saturated surface and the entire resistance to mass transfer lies in the boundary layer or gas-film around the droplet (see section 4.1). The gas-film mass transfer coefficient,  $k_g$ , is said to be rate controlling. However, once the critical moisture content is reached (see section 4.2) a crust begins to grow around the droplet and the controlling resistance to moisture movement shifts from the gas-film into the crust. The crust coefficient,  $k_c$ , then limits the overall mass transfer process. In the case of a droplet of solution/slurry which has a tendency to form a skin or membrane around the droplet prior to crust formation, such as sucrose solution (see section 9.1), an additional barrier to mass transfer has to be taken into account. Hence in this case the overall mass transfer coefficient should contain a term to include for the resistance to mass transfer due to this primary film. Therefore, prior to crust formation, the overall mass transfer coefficient,  $K_o$ , including a term for skin mass transfer coefficient,  $k_s$ , is given by,

$$\frac{1}{K_o} = \frac{1}{k_g} + \frac{1}{k_s} \quad \text{-----2.3}$$

The overall mass transfer coefficient for such a drop once the crust formed reverts to,

$$\frac{1}{K_o} = \frac{1}{H_1 k_g} + \frac{1}{k_c} \quad \text{-----2.4}$$

since the outer surface is, by definition, solid and not a film. The interfacial area,  $A$ , which may change if the droplet expands, shrinks or ruptures (see section 4.4) may also effect a change in the value of  $K_o$ .

A number of theories have been proposed to explain how transfer of mass takes place across an interface.

## 2.2 Two-Film Theory

In the two-film theory, proposed by Whitman (4) in 1923, equilibrium is assumed at the interface and the resistance to mass transfer in each phase is regarded as lying in a thin laminar layer on either side of the interface. The overall resistance is obtained by adding the individual film resistances, in an analogous manner to convective heat transfer. The theory postulates that the entire concentration difference in each phase is attributed to molecular diffusion within an 'effective' film of thickness  $Z_f$ . The latter depends upon the nature of the flow conditions. For the theory to have useful applications, the film would have to be very thin, so that the amount of solute within the film would be small relative to the quantity passing through it, or the concentration gradient would have to be set up quickly. The concentration gradient in the film is that characteristic of steady state.

The film theory predicts that the mass transfer coefficient,  $K_o$ , for a particular solute being transferred under particular fluid flow conditions is directly proportional to the diffusivity of the solute,  $D_v$ . However for turbulent flow a much smaller dependency is observed;

$$K_o \propto (D_v)^n \quad \text{-----} \quad 2.5$$

where  $n$  may be anything from nearly zero to 0.8 or 0.9, depending upon the circumstances. The simple film-theory, in conflict with what is observed under turbulent flow conditions, has therefore been largely discredited. Nevertheless, it does well in handling the effect of high mass transfer flux and the effect of mass transfer on heat transfer.

### 2.3 Penetration Theory

Higbie (5) emphasized that in many situations the time of exposure of a fluid to mass transfer is short, so that the concentration gradient of the film theory, characteristic of steady-state, would not have time to develop. The theory was actually conceived to describe the contact of two fluids in which an eddy or a particle of fluid rises from the depths of the bulk fluid to the interface. Here it remains exposed for a finite period of time to the action of the second fluid. In this theory, the time of exposure is taken as constant for all such eddies. During the exposure time the liquid particle is subject to unsteady-state diffusion or penetration of solute. This is followed by the elements being remixed with the bulk fluid. According to this concept the mass transfer coefficient was shown to be proportional to  $(D_v)^{0.5}$ .

### 2.4 Surface-Renewal Theory

Danckwerts (6) pointed out that the Higbie theory, with its constant time of exposure of the eddies of fluid at the surface, is a special case of what may be a more realistic picture, where the eddies are exposed for varying lengths of time. The interface is then a mosaic of surface elements of different exposure-time histories and since the rate of solute penetration depends upon exposure time, the average rates for a unit surface area must be determined by summing up the individual values. On the assumption that the chance of a surface element being replaced by another is quite independent of how long it has been in the surface, and if  $S$  is the fractional rate of replacement of elements, Danckwerts demonstrated that,

$$K_o \propto (D_v \cdot S)^{0.5} \quad \text{----- 2.6}$$

## 2.5 Film Penetration Theory

Toor and Marchello (7) developed a 'film-penetration' model, combining features of the earlier models. The theory suggests that for rapid penetration, or when the rate of surface renewal is small (i.e. long exposure times), or for thin surface elements, the mass-transfer coefficient takes on the character described by the film theory i.e.  $K_0 \propto D_v$  whereas for slow penetration or rapid renewal (short exposure times) the mass-transfer coefficient obeys the penetration model, i.e.  $K_0 \propto (D_v \cdot S)^{0.5}$ . Consequently  $K_0 \propto D_v^n$ , where n may have any value between the limits 0.5 and 1.0, could account for many observations.

## 2.6 Boundary - Layer Theory

For the theories discussed above, where the interfacial surface is formed between two fluids, the velocity at that surface will not normally be zero. But when one of the phases is a solid, the fluid velocity parallel to the surface at the interface must of necessity be zero, and consequently the two circumstances are inherently different.

For flow over spherical droplets, the equations of motion, continuity and energy can be solved approximately to obtain the velocity, concentration and temperature profiles in a thin boundary layer at the interface. Exact calculations done by Frössling (8) for drops of water, nitrobenzene and aniline, show that the mass-transfer coefficient according to this approach varies with  $(D_v)^{2/3}$ .

**CHAPTER THREE**  
**DROPLET HEAT AND MASS TRANSFER**  
**EVAPORATION FROM PURE LIQUID DROPLETS**

The subject of heat and mass transfer in dispersed phase systems has received close attention in recent years since it is of fundamental significance for design in a number of key operations. In many items of process equipment such as spray driers, the rate determining step is that of mass transfer from a liquid drop in forced convection conditions. The main consideration in the prediction of design and performance is then the rate of mass transfer. If the driving force, in the form of concentration or partial pressure difference, is known it is the mass transfer coefficient and the interfacial area that play the determining roles.

Evaporation from a liquid droplet is essentially a simultaneous heat and mass transfer process. Maxwell (9) in 1877 laid down the basis of the theory of evaporation from a droplet, stationary relative to an infinite gaseous medium. It was shown that for a spherical droplet, whose vapour concentration at the surface  $C_s$  is continuously saturated, the evaporation rate was given by,

$$\frac{dm}{d\theta} = 4 \pi r D_v (C_s - C_\alpha) \quad \text{-----3.1}$$

The evaporation rate can also be expressed as,

$$\frac{dm}{d\theta} = k_g 4 \pi r^2 (C_s - C_\alpha) \quad \text{-----3.2}$$

Thus, from equations (3.1) and (3.2) a gas phase mass transfer coefficient, under stagnant conditions, can be defined as,

$$k_g = D_v/r \quad \text{-----} \quad 3.3$$

The Sherwood number, under negligible relative velocity conditions, can therefore be expressed as,

$$\text{Sh}_0 = k_g \cdot 2r/D_v = 2.0 \quad \text{-----} \quad 3.4$$

For dynamic equilibrium the rate of heat transfer is equal to the product of mass transfer and latent heat of vaporization,  $\lambda$ . The evaporation rate in terms of heat transfer can therefore be expressed as,

$$\frac{dm}{d\theta} = \frac{dQ}{d\theta \cdot \lambda} = h_g A_h (T_a - T_d) / \lambda \quad \text{-----} \quad 3.5$$

From the heat and mass transfer analogy the Nusselt number, under stagnant conditions, is given by,

$$\text{Nu}_0 = h_g \cdot 2r/K_d = 2 \quad \text{-----} \quad 3.6$$

Although derived for the evaporation of an isolated drop into still air, equation 3.4 also describes the evaporation from a swarm of droplets co-currently entrained in turbulent air if the droplets are very fine ( $14 < d_p < 30 \mu\text{m}$ ) (23). Whenever the droplet size is much smaller than the scale of turbulence, the droplet appears to closely follow the continuous-phase motion with a negligible slip velocity (24). Moreover, the atomized droplets swiftly disperse, often to occupy less than 0.1% of the available space, the reported

threshold for significant droplet interaction (25,26). Measured integral scales of turbulence in one co-current spray-drier, 0.2 m in diameter, ranged between 90 and 520  $\mu\text{m}$  (27), and thus complete entrainment in that unit is likely with particles below 50  $\mu\text{m}$  in diameter.

Commercial atomizers usually produce droplets within the size range 10 to 1000  $\mu\text{m}$  (28). Drops bigger than 100  $\mu\text{m}$  will fall with significant slip velocities and particle Reynolds numbers up to 100 are possible.

Evaporation rates however, increase with increase in relative velocity between the droplet and air due to the additional evaporation caused by the convection in the boundary layer around the droplet. Frössling (29), using boundary-layer analysis, showed that to account for the contribution of forced convection to mass transfer equation 3.4 should be multiplied by a 'wind factor',  $f'$ , given by,

$$f' = 1 + \beta \text{Re}^{0.5} \text{Sc}^{0.33} \quad \text{-----} \quad 3.7$$

The value of  $\beta$  was evaluated from naphthalene - sublimation tests (10) as 0.276. Thus, the total evaporation is given by,

$$\text{Sh} = 2 (1 + 0.276 \text{Re}^{1/2} \text{Sc}^{1/3}) \quad \text{-----} \quad 3.8$$

Subsequently numerous other workers (11-22), notably Ranz and Marshall (22) who evaluated  $\beta$ , as 0.3, the more usually quoted value, have confirmed the form of equation (3.8). However, the data all relate to experiments carried out using drops or solid particles suspended at the end of a filament or a capillary. Indeed, investigations of mass transfer from unsupported drops, which is the practical situation, are extremely few in number.

### 3.1 Evaporation from Single Droplets and Spheres under Natural Convection

Rates of evaporation in still air were first determined by Sreznevskii (30). Experiments were carried out on the convex liquid meniscus at the upper end of a tube of 3mm diameter, and on drops of liquid placed on the flat top of vertical cylindrical columns of 1.8 - 3.6 mm diameter, such that the drop completely covered the top. Evaporation rates were determined by following the outline of the drop through a horizontal microscope. Rates were determined for hemispherical droplets (of height  $h$ ) of water, carbon disulphide, chloroform, ether and benzene with varying column (and hence droplet) radius  $r$ . The following relationship was established,

$$r \frac{dh}{d\theta} = \text{Constant} \quad \text{----- 3.9}$$

Morse (31) in 1910 studied the evaporation in air of spheres of iodine placed on the pan of a microbalance and found that the rate of evaporation was proportional to the radii of the spheres. Langmuir (32), from the results obtained by Morse, independently derived a modified form of the Maxwell equation (eq. 3.1) in terms of partial pressures.

Experiments were carried out by Whytlaw-Gray and Patterson (33) on drops of water, aniline, p-cresol, quinoline and methyl salicylate with radii of 1-2 mm, placed on the pan of a quartz microbalance. In every case the surface of the drop decreased linearly with time, although the volume decreased by a factor of almost a hundred. No further experiments were made with drops on a flat support; instead thin filaments were used to support the droplets, which gave a much better approximation to the conditions of evaporation of free droplets. This method gave more reliable and accurate results for the rates of evaporation of droplets both in still media

and in an air-stream.

Measurements by this method were first made in 1927 by Topley and Whytlaw-Gray (34) on spheres of iodine fused to a quartz fibre. The spheres of radius 1mm were placed in a cylindrical vessel of radius 2cm. The walls and bottom of the vessel were covered with a thin layer of KOH to absorb the iodine vapour. This work provided the first quantitative support for Maxwell's equation.

Houghton (35) determined the rate of evaporation of drops of water suspended from glass fibres using a horizontal microscope. Use of fibres of radii 1.25, 12.5, 42, and 125  $\mu\text{m}$ , facilitated the study of drops of radii 50-250, 150-600, 500-1000 and greater than 1000  $\mu\text{m}$  respectively. The fibres were covered with a thin layer of paraffin, firstly to reduce the distortion of the drop and secondly to prevent the drop creeping up the fibre. The temperature of the air in the chamber was 20°C and the drop temperature was assumed to equal the wet-bulb temperature.

Direct measurements of the temperature of an evaporating droplet suspended from the junction of a thermocouple were first made by Frössling (8). Experiments in still air were performed on drops of nitrobenzene and aniline. However, neither the gauge of the wires nor the size of the droplets used in the experiments were reported.

Kiriukhin (36) performed experiments on water drops with radii of 0.1 - 1 mm in a chamber whose humidity was maintained constant. However, neither the gauge nor the material of the thermocouple were reported. From measurements of the rate of evaporation by the optical method, Kiriukhin obtained a linear plot of  $r^2$  vs.  $\theta$ , as did other workers.

Langstroth et al. (37) in their work measured optically the rates of evaporation of drops of water and of a number of organic liquids with radii of approximately 0.7 mm. The experiments were carried out in a spherical

vessel of 10mm radius in which the drops were suspended from either a glass fibre of 50  $\mu\text{m}$  radius or from a copper-constantan thermocouple with wires of 40 gauge. The inside of the vessel was covered with a thin layer of active charcoal, or for water, a mixture of charcoal and  $\text{P}_2\text{O}_5$ , to absorb the vapour. The pressure inside the vessel was equalized with that in the atmosphere ( $\sim 690$  mm Hg) via a small opening. The temperature of the air was maintained at  $\sim 20^\circ\text{C}$ , although with water and n-butanol measurements were also made at  $10^\circ\text{C}$  and  $40^\circ\text{C}$ . Corrections were made for the finite size of the vessel and for radiation, but the flow of heat through the glass fibre was not accounted for.

A special dryer was used by Ranz and Marshall (22) for the study of evaporation rates of pure liquids such as water, aniline and benzene. The individual drops were evaporated with changing diameter whilst suspended on a thermoelement or with constant diameter whilst suspended from a capillary. Drop diameters ranged from 0.06 to 0.11 cm., and air temperatures ranged up to  $220^\circ\text{C}$ .

At zero relative velocity, if heat transfer is by simple conduction and mass transfer is by simple diffusion,  $\text{Nu} = \text{Sh} = 2.0$ . In the practical case, however, a density difference exists across the transfer path, and a fluid velocity caused by free convection contributes to the transfer path. To account for this, Ranz and Marshall correlated their data by the expressions:

$$\text{Nu}_0 = 2.0 + 0.6 \text{Pr}^{1/3} \text{Gr}^{0.25} \quad \text{-----} \quad 3.10$$

$$\text{Sh}_0 = 2.0 + 0.6 \text{Sc}^{1/3} \text{Gr}^{0.25} \quad \text{-----} \quad 3.11$$

Steinberger and Treybal (38) studied rates of solution of 12.7, 19.1, and 25.4 mm cast benzoic acid spheres under natural-convection conditions. A Dewar flask was filled with water and allowed to stand for 8 hours on a

6.35 mm thick rubber pad to damp fluid circulations. A benzoic acid sphere was gently lowered into the stagnant fluid, a lucite cover being used to support the sphere and a thermometer. The next day the sphere was gently removed from the flask, and the solution was mixed and titrated for its benzoic acid content. The data was separated according to whether (Gr.Sc) was < or > 10<sup>8</sup>, because of the onset of a turbulent boundary layer in the higher range. For (Gr.Sc) < 10<sup>8</sup> the data were correlated by ;

$$Sh_o = 2 + 0.569 (Gr.Sc)^{0.25} \quad \text{-----} \quad 3.12$$

with an average deviation of the data of 12.7%, and for (Gr.Sc) > 10<sup>8</sup> by;

$$Sh_o = 2 + 0.0254 (Gr.Sc)^{1/3} (Sc)^{0.244} \quad \text{-----} \quad 3.13$$

with an average deviation of 3.2%. Equation 3.13 was however established from only three data points. Therefore, the accuracy attributed to the constant and exponents is questionable.

Yuge (39) investigated the heat transfer under natural convection conditions from internally heated carbon-chrome steel and brass spheres. The sphere was suspended from two sides by thermocouple wires. The data were correlated by the expression,

$$Nu_o = 2 + 0.392 Gr^{0.25} \quad \text{-----} \quad 3.14$$

for  $1 < Gr < 10^5$

The evaporation of free drops has also been studied by supporting charged droplets in a Milikan condenser. Gudris and Kulikova (40) used this technique on drops of water, Nestle (41) on drops of mercury, and Woodland and Mack (42) on drops of dibutyl tartrate and dibutyl phthalate.

Whilst less accurate results are achieved using the Milikan condenser, it does allow droplets as small as a few microns to be studied.

### 3.2 Evaporation from Fixed Droplets and Spheres under Forced Convection

#### 3.2.1 Mass Transfer

The greatest practical interest centres on the evaporation of droplets moving relative to the gaseous medium under the influence of gravity and/or inertia, since this is the situation in spray drying. The majority of measurements of the rate of evaporation of droplets under forced convection have been performed as in the previous case of stationary droplets, using fixed drops, ventilated by a stream of gas. Very little work has been done with drops under free-fall due to the experimental difficulties.

Majama and Togino (43), working with water and a number of organic liquids first measured rates of evaporation from drops suspended in a gas stream. Drops of 0.1 mm initial radius were supported on a horizontal glass fibre of radius 2.5  $\mu\text{m}$  in an air current at velocities up to 18  $\text{ms}^{-1}$ . Their analysis revealed that the rate of change of diameter squared,  $d(D^2)/dt$ , was a constant.

Frössling's (8) extremely careful work produced the first accurate measurements relating to the rate of evaporation of drops suspended in a gas stream. Glass fibres of radius 10 to 100  $\mu\text{m}$  or a constantan-manganin thermocouple were used to suspend drops of water, aniline, nitrobenzene and spheres of naphthalene with initial radii in the range 0.1 - 0.9 mm, at an air temperature of 20°C. The drops were suspended 20 cm above the exit of a vertical wind tunnel. Vertical ventilation, according to Frössling, has the advantage over horizontal ventilation because with the latter the drop is displaced in the direction of the stream, its shape is distorted and the fibre

disturbs the flow around the drop.

The air velocity was varied over the range 0.2 - 7 m/s and the rate of evaporation was determined by periodically photographing the drop. Frössling correlated the experimental data by equation 3.8 over the complete range of Re, namely 2 to 1280, investigated. Interesting data were obtained by Frössling on the variation of the rate of evaporation over the surface of the naphthalene spheres. Evaporation rate from the forward face was found to be a maximum, reducing to a minimum just past the equator and increasing to a lower maximum rate on the trailing face, which experiences velocities in the reverse direction. The average rate of evaporation from the rear face of the sphere was roughly 1/10th the rate from the front stagnation point.

The work of Ranz and Marshall (22) using drops of aniline, benzene or water was performed at ambient temperature or at elevated temperatures up to 220°C. At ambient temperature, drops of water, of 0.6mm radius were suspended from the capillary end of a microburette of 30 to 50 µm radius. The drops were ventilated by dry air (Re = 0-200) from below and the drop size was kept constant by a continuous supply of water through the burette. The temperature of each drop was determined by inserting a constantan-manganin thermocouple into its side.

For experiments at elevated temperatures, up to 220°C, water drops were suspended from fibres and, since they evaporated very rapidly, were recorded by high-speed photomicrography.

Ranz and Marshall's results confirmed those of Frössling and differed only in the value of  $\beta$ . The results for heat and mass transfer were expressed by the equations;

$$\text{Nu} = 2.0 + 0.6 \text{ Re}^{1/2} \text{ Pr}^{1/3} \quad \text{-----} \quad 3.15$$

$$Sh = 2.0 + 0.6 Re^{1/2} Sc^{1/3} \quad \text{-----} \quad 3.16$$

Hsu, Sato and Sage (10) studied the evaporation of drops of n-heptane, placing particular emphasis on the influence of droplet size and shape. They developed a method of steady-state measurement which was similar, in some respects, to that used by Ranz and Marshall (22) and Ingebo (50); i.e. the droplet diameter was kept constant. Measurements of the rate of evaporation were made in an air jet at a free stream temperature of 38°C and at nominal velocities of 0.61, 1.3, 1.8 and 2.4 m/s. Experimental data on the evaporation of drops of n-heptane were obtained for 26 different drop configurations, the shapes varying from pendant contours with a large value of the height-diameter ratio to oblate spheroids with small values of this ratio. The data were correlated by,

$$Sh = [1 + 0.178 Re^{0.56} Sc^{0.37}] [1 + 2.292 (1 - \mu')] [1 - 0.257(1 - h'/d')] \quad \text{---} 3.17$$

where  $\mu' = 6V/S'd'$  (Sphericity)

V = Volume of drop

S' = Surface area of drop

d' = Maximum horizontal diameter of drop

h' = Height of drop

The evaporation rate increased rapidly with deviations from a sphere, the oblate spheroids yielding higher evaporation rates than the pendant drops.

Tverskaia (45-47) used a microscope to determine the rate of evaporation of drops of water of 0.4 to 1.6mm diameter, suspended from a thermocouple in an aerodynamic tube with varying air temperature and humidity. The results demonstrated an increase in the value of  $\beta$  with Re. At Re = 10, 20, 100, 200 and 300-500,  $\beta$  equalled 0.10, 0.15, 0.18, 0.24 and 0.26 respectively. The last value closely approached that obtained by

Frössling.

Sokol'skii and Timofeyeva (48) obtained similar results with drops of water with diameters of 1.0 - 2 mm. Their results, for Re in the range 0.7 - 200, were expressed by,

$$\text{Sh} = 2 (1 + 0.08 \text{Re}^{2/3}) \quad \text{-----} \quad 3.18$$

and for Re > 200 by,

$$\text{Sh} = 0.52 \text{Re}^{0.5} \quad \text{-----} \quad 3.19$$

corresponding to  $\beta = 0.29$ .

Van Krevelen and Hoftijzer (49) measured the rates of evaporation and heat transfer of particles of porous material soaked in water. Granules of wet marl in the diameter range 5.5 to 14.5 mm were suspended by a very thin wire from the beam of a torsion balance, and dried in a constant stream of dry air. Results for the first stage, or constant rate stage were found to correlate well by,

$$\text{Sh} = 0.50 \text{Re}^{1/2} \text{Sc}^{1/3} \quad \text{-----} \quad 3.20$$

The rate of evaporation of each of a number of organic liquids from the surface of cork spheres at 20 - 500°C was measured by Ingebo (50). For cork spheres of 6.88 mm diameter in the Re range 1000 - 1600 the data could be correlated by,

$$\text{Sh} = 2 + 0.30 (\text{ReSc})^{0.6} (\text{K}_d/\text{K}_v)^{0.5} \quad \text{-----} \quad 3.21$$

where  $\text{K}_d$  and  $\text{K}_v$  are the thermal conductivities of air and the vapours respectively.

Maisel and Sherwood (15) working with 2.55 and 3.48 cm diameter spheres of calcium silicate, wetted with water or benzene, found that in the Re range 2000 - 50,000 Sh was proportional to  $Re^{0.56}$ . Benzene was found to evaporate so quickly, especially at high values of Re, a factor of 5 to 10 faster than with water, that the surface of the spheres was not always completely wetted. Therefore, the water data are more reliable.

Garner and Grafton (14) studied the dissolution of 12.7mm diameter benzoic acid spheres into a stream of water at ambient temperature and correlated experimental mass transfer data by,

$$Sh = 44 + 0.48 Re^{0.5} Sc^{0.5} \quad \text{-----} \quad 3.22$$

in the Re range 20 to 1000. Equation 3.22 is of similar form to equations 3.8 and 3.16 by Frössling and Ranz and Marshall but differs in the value of the constant term due to natural convection. However, in Frössling's mass transfer to air, the diameters were 0.02 to 0.18 cm, and for Ranz and Marshall, 0.06 to 0.11 cm, which results in greatly reduced Gr numbers, which are proportional to  $d_p^3$ . Also for mass transfer to air, the Schmidt number (and the Prandtl number) is approximately unity. Therefore, the value of Sh for natural convection, which is a function of Gr and Sc, would have been much less in the work of Frössling and Ranz and Marshall and will approach the limiting value of 2.0. This consideration shows that the equations of Frössling and Ranz and Marshall do not differ greatly from that for the benzoic acid spheres if allowance is made for the effect of the system on the Grashof and Schmidt numbers. To measure the dissolution rates of 9.5 and 12.7mm diameter spheres of adipic acid and 9.5, 12.7, 15.8 and 19.0mm diameter spheres of benzoic acid, Garner and Suckling (11), in a later investigation, used a similar technique. Their results were correlated,

using an assumed limiting value of 2, by,

$$\text{Sh} = 2 + 0.95 \text{Re}^{0.5} \text{Sc}^{0.33} \quad \text{-----} \quad 3.23$$

for  $100 < \text{Re} < 700$

Garner and Kee (51) used a low-speed water - tunnel to investigate dissolution rates of pelleted 19.0 mm diameter benzoic acid spheres into water at 30°C at Reynolds numbers in the range 2.3 to 255. Extrapolation of results enabled the upper limit to be extended to 900. The results showed that free-convective effects were not entirely absent until  $\text{Re} = 750$ . Over the range  $900 > \text{Re} > 250$  the overall mass transfer results were in approximate agreement with the relationship,

$$\text{Sh} = 0.94 \text{Re}^{1/2} \text{Sc}^{1/3} \quad \text{-----} \quad 3.24$$

Subsequently, Garner and Hoffman (52), used a similar method and concluded that free-convective effects did not disappear entirely until  $\text{Re} = 250$  compared with  $\text{Re} = 750$  for the 19.0 mm spheres in the previous work. However, they used 9.5 mm spheres.

Pasternak and Gauvin (53) used a similar technique to the previous workers (18) with celite spheres impregnated with water suspended from a hypodermic needle. Each sphere was positioned inside a 38.1mm diameter horizontal glass column through which hot air was passed. For spheres of 5.59 to 11.63 mm diameter, the results were correlated by,

$$\text{Sh} = 0.692 \text{Re}^{0.514} \text{Sc}^{0.33} \quad \text{-----} \quad 3.25$$

In their later work (21) this expression was confirmed by using radioactive

celite spheres impregnated with acetone in free fall. Particle velocity was accurately determined using a radioactive tracer technique.

Fuchs (54) suggested that the rates of heat and mass transfer in a drop may be doubled by internal circulation. In a later theoretical analysis, by Bowman et al. (55), of the influence of internal circulation on the mass transfer rate from spherical fluid particles, it was postulated that the external flow pattern is affected by internal circulation thereby decreasing the resistance to transfer in the external fluid. Ward et al. (56) verified this hypothesis from their work on circulating spheres. They measured the rates of mass transfer from water drops in cyclohexanol and drops of cyclohexanol, isobutanol and o-toluidine into water. Sherwood numbers were found to be in good agreement with the theoretical predictions and the results showed a four to six-fold enhancement of mass transfer due to internal circulation for water drops falling in cyclohexanol. This effect was shown to depend on the ratio of continuous to disperse phase viscosity of the system. Thus, for a system such as water drops in cyclohexanol ( $\mu_c/\mu_d = 25$ ), the rates were as expected several times those of solid spheres. The reverse situation with cyclohexanol drops in water ( $\mu_c/\mu_d = 0.04$ ), resulted, as expected, in little enhancement due to circulation. Consequently, for liquid drops in air where the ratio  $\mu_c/\mu_d$  will be very small it is reasonable to assume that negligible enhancement in mass transfer will result from internal circulation.

Steinberger and Treybal (38) from their work with cast benzoic acid spheres, proposed that mass transfer by natural and forced convection to spheres are additive. From experiments in which spheres of 12.7, 19.1 and 25.4 mm diameter were suspended in an upward stream of water or propylene glycol they proposed the relationship,

$$Sh = Sh_0 + 0.347 (Re.Sc^{0.5})^{0.62} \text{ ----- 3.26}$$

where  $Sh_0$ , the natural convection contribution is given by equations 3.12 and 3.13. The correlation gave excellent agreement with data, on heat and mass transfer from gas and liquid streams published by eleven authors.

Kinard et.al. (57) reviewed theoretical approaches to the estimation of mass transfer from single spheres and suggested, that Boundary Layer Theory cannot accurately predict overall mass transfer since it neglects transfer from the rear surface of the sphere. They proposed a semi-theoretical equation based on the linear addition of forced convection in front of, and behind, the separation zone of the boundary layer. The proposed correlation,

$$Sh = 2.0 + Sh_0 + 0.45 Re^{0.5} Sc^{0.33} + 0.00484 Re.Sc.^{0.33} \text{ -----3.27}$$

was tested using selected data of Ranz and Marshall (22), Garner and Suckling (11) and Steinberger and Treybal (38), for mass transfer due to forced convection. The addition of a separate term describing mass transfer from the rear surface of the sphere resulted in a significant improvement over Frössling's correlation.

A novel method of drop suspension was used by Audu (58). Hemispherical drops of water were suspended from a rotating nozzle in a horizontal wind tunnel, such that all sides of the evaporating drop were exposed to the impinging air. For ambient conditions, the experimental data were correlated by the equation,

$$Sh = 2.0 + 0.473 Re^{0.5} Sc^{0.33} \text{ ----- 3.28}$$

A limitation may be however that the nozzle, which had a similar outside diameter to the hemispherical drop would affect the flow pattern of air around

the drop resulting in profiles differing from those for a spherical drop. Furthermore, heat conducted along the suspension nozzle and that due to radiation was not taken into account .

More recently, Sandoval-Robles et al. (59) investigated mass transfer around a sphere using the technique of electrolysis of an electroactive species on the surface of a convenient metallic spherical electrode. The electrodes were brass spheres 5,7,9 or 10mm in diameter, coated with an electrodeposited gold film of 5 $\mu$ m thickness. The sphere was rotated at constant velocity, in the range  $2 \times 10^{-3}$  to  $2.5 \text{ ms}^{-1}$ , around a circular channel containing the motionless electrolytic solution, namely ferricyanide and ferrocyanide ion concentration of  $2 \times 10^{-6} \text{ mole m}^{-3}$  in a 0.5 N sodium hydroxide aqueous solution. This provided conditions of no turbulence and a flat velocity profile. The data showed a significant dependency on the Reynold's number and was correlated by,

$$\begin{aligned} \text{Sh} &= 1.032 \text{ Re}^{0.385} \text{ Sc}^{0.33}, \text{ for} & 2 < \text{Re} < 20 & \text{-----}3.29 \\ \text{Sh} &= 0.803 \text{ Re}^{0.475} \text{ Sc}^{0.33} & 20 < \text{Re} < 2000 & \text{-----}3.30 \\ \text{and } \text{Sh} &= 0.300 \text{ Re}^{0.593} \text{ Sc}^{0.33} & 2000 < \text{Re} < 23000 & \text{-----}3.31 \end{aligned}$$

However, the main drawback of the system was that after a revolution the probe no longer rotated in a stagnant liquid but in its own wake; which suggests that the accuracy of the measurement technique may not justify the implied precision of the exponents in the above equations.

Sandoval-Robles et.al. (60) also studied electrochemically, mass transfer around single spheres in a highly turbulent liquid. A 94 mm diameter, vertical column was used in which a brass sphere was suspended. Turbulence in the liquid flowing past the sphere was generated by a polyethylene porous plate fixed at the bottom of the column. Mass transfer

rates were determined using an equimolecular mixture,  $2 \times 10^{-3}$  N, of potassium ferricyanide and potassium ferrocyanide in 0.5 N sodium hydroxide and turbulence intensities - up to 30% - by hot wire anemometry. An electrochemical method was used to measure the rate of mass transfer. Their results were correlated by the expression,

$$Sh = 6.82 Re^{0.559} f^{0.069}, \quad \text{for } 330 < Re < 1720 \quad \text{-----} 3.32$$

where  $f$  = the turbulence intensity. At low  $f$  values the data obtained were in good agreement with that previously published for laminar conditions (53).

### 3.2.2 Heat Transfer

Heat transfer to a suspended droplet takes place by a combination of convection, radiation and conduction. However, for the case of a droplet falling freely as in spray drying only the first two mechanisms are operational.

Kramers (62) developed an empirical equation for the film coefficient of a fluid flowing past a steel sphere heated by high frequency induction and maintained at a constant, uniform temperature. Individual spheres, of 7.0 to 12.7 mm diameter, were suspended vertically by a pair of fine thermocouple leads in a vertical stream of air, water or oil. The experimental results were correlated by,

$$Nu = 2.0 + 1.3 Pr^{0.15} + 0.66 Pr^{0.31} Re^{0.50} \quad \text{-----} 3.33$$

for  $Re$  up to  $10^5$  and  $0.7 < Pr < 400$

The second term on the right side of equation 3.33 was necessary to bring together data for air, water and oil. However the physical properties of the

liquids appear likely to have been affected by temperature gradients at the surface of the spheres. Film coefficients calculated from equation 3.33 are probably applicable to heat transfer between continuous fluid and a stagnant drop. However, in the case of a circulating drop, such as a drop in free-fall, such a coefficient would serve only as an approximation.

Tsubouchi and Sato (63) investigated steady state heat transfer between single particles and a fluid by means of an original technique. Thermistor spheres of 0.3 to 2.0 mm diameter were suspended in two types of wind tunnel: the first a revolving-arm type with a speed range of 0.01 to 0.5 ms<sup>-1</sup> and the second the Eiffel type, with a speed range of 1 to 20 ms<sup>-1</sup>. A current was supplied to the sphere and from the voltage, current and resistance measurements the temperature and the amount of heat dissipated were obtained. The data were correlated by,

$$\text{Nu} = 2.0 + 0.5 \text{Re}^{0.5} \quad \text{-----} \quad 3.34$$

for  $0.3 < \text{Re} < 3000$

Yuge (39) in a detailed study on heat transfer from carbon-chrome steel and brass spheres in different wind tunnels, compared the effects of cross, counter and parallel flows. Metal spheres less than 6 mm in diameter were preheated in an electric furnace outside the wind tunnel prior to being inserted into the flowstream. The larger spheres (6-60mm) were heated internally. The experimental results were expressed by,

$$\text{Nu} = 2 + 0.493 \text{Re}^{0.5} \quad \text{-----} \quad 3.35$$

for  $10 < \text{Re} < 1.8 \times 10^3$

and

$$\text{Nu} = 2 + 0.300 \text{Re}^{0.5664} \quad \text{-----} \quad 3.36$$

for  $1.8 \times 10^3 < \text{Re} < 1.5 \times 10^5$

Rowe et al (64), reviewed past work on heat and mass transfer and presented new results on heat transfer on the cooling of internally heated copper spheres in air and in water. The sublimation of naphthalene in air and the dissolution of benzoic acid spheres in water were also studied. For heat and mass transfer in air, the results were correlated as,

$$\text{Nu (Sh)} = 2 + 0.69 \text{Re}^{0.5} \text{Pr}^{0.33} (\text{Sc}^{0.33}) \quad \text{-----} \quad 3.37$$

and for water by,

$$\text{Nu (Sh)} = 2 + 0.79 \text{Re}^{0.5} \text{Pr}^{0.33} (\text{Sc}^{0.33}) \quad \text{-----} \quad 3.38$$

A dilatometric method, combined with cinematography, was used by Adams and Pinder (65) to obtain an average heat transfer coefficient for the evaporation of cyclopentane and isopentane in a continuous phase of glycerine-water solution. Different size air bubbles were injected into a drop, and as evaporation occurred, the increase in volume of the air bubble was determined by a dilatometric tube. The data were correlated by the equation,

$$\text{Nu} = 7550 \text{Pr}^{-0.75} [ \mu_c / (\mu_c - \mu_d) ]^{4.3} \text{Bo}^{0.33} \quad \text{-----} \quad 3.39$$

### **3.3 Evaporation From Single Droplets In Free-Fall**

The earliest work on the evaporation of free drops was initiated by Gudris and Kulikova (40) who supported charged droplets in a Milikan's condenser. The droplet, previously charged, was introduced into the apparatus and the potential across the condenser continuously varied so that the electrostatic and gravitational fields were exactly balanced i.e. the droplet remained stationary. The rates of evaporation of water droplets of diameter

1.2 to 2.5  $\mu\text{m}$  were measured in an atmosphere saturated with water vapour at room temperature. The rate was found to be negligible in carbon dioxide and slow in air. However, when a mixture of 70% hydrogen and 30% air was used, the rate was several times faster than in air itself. Other workers (38,66,67) using a similar technique studied systems such as benzophenone, benzil, dibutyl tartrate, mercury and diamyl sebacate.

Experiments with Milikan's condenser strictly relate to drops moving freely with respect to the medium but with such small radii ( $\sim 1 - 2\mu$ ) and correspondingly small  $\text{Re}$  ( $\sim 10^{-5} - 10^{-4}$ ) that the effect of movement on the rate of evaporation is vanishingly small. The first measurements on the rate of evaporation for larger drops were those of Vyubov (68) who studied the rate of water drops of 2 mm diameter falling freely in a vertical tube 1 m long. Air heated to 40 - 100°C at  $1 \text{ ms}^{-1}$  passed down the tube and the droplets were collected on a weighing pan. The experimental data were correlated by,

$$\text{Sh} = 0.52 \text{ Re}^{1/2} \quad \text{-----} \quad 3.40$$

for  $100 < \text{Re} < 500$

Kinzer and Gunn (69) studied the rate of evaporation from water drops at 0 to 40°C using the method of instantaneous photography with illumination from the side. Small droplets of diameter 10 to 140  $\mu\text{m}$  were charged and allowed to fall freely through detector rings. Droplets greater than 1 mm were supported in free-flight by a hydrodynamic force, and as evaporation proceeded they moved up the tube. The same relationship as Frösslings i.e.  $\text{Sh} = 2 (1 + \beta \text{Re}^{1/2} \text{Sc}^{1/3})$  was obtained for droplets in the size range 0.6 to 3.0 mm diameter, with a  $\beta$  value of 0.23 for  $100 < \text{Re} < 1600$ . They found that at very small  $\text{Re}$  ( $< 0.9$ ) the 'wind factor' was unity, i.e.  $\beta=0$ . On increasing  $\text{Re}$ ,  $\beta$  rose to a value of 0.46 at  $\text{Re} = 4$ , then

gradually fell to 0.23 at  $Re = 100$ .

Jones and Smith (70) studied the evaporation of freely-suspended spheres of benzoic acid, camphor and naphthalene in an air stream moving at high velocity through rotameter tubes. Despite the fact that the particle spun erratically, the mass transfer coefficient showed no significant difference when compared to that from stationary particles. A possible reason for this is that when one side of a spinning sphere is stationary relative to the gas the other side meets the flow at twice its linear velocity. Relationships were proposed which take into account the Reynolds number of the gas,  $Re_g$ .

For the laminar region,

$$Sh = 2 + 25 (Re.Sc.Re_g^{0.5})^{0.33} \quad \text{-----} \quad 3.41$$

and for the turbulent region,

$$Sh = 2 + 0.055 (Re.Sc.Re_g^{0.5})^{0.5} \quad \text{-----} \quad 3.42$$

A number of workers (71-73) have studied the shapes, oscillations and internal circulations of drops suspended at their terminal velocity in gases, and the absorption of gases into these drops. Of particular significance is the work of Finlay (72) who suspended drops of water, iso-butane, n-heptane and iso-octane in an air stream within a wind-tunnel. After a known time, drops were collected and weighed and values of Sh number were calculated for drop diameters in the range 1 to 5 mm. Comparing his results with those of Ranz and Marshall, Finlay found a marked discrepancy in rates of mass transfer from drops of a diameter greater than 3 mm. This was attributed to enhanced droplet oscillation. This was later confirmed by Ahmadzadeh and Harker (74) who studied the evaporation of drops of 50%

acetone-water mixture, in free-fall. They also found that the equation did not fully correlate the data and that the nozzle diameter became an additional parameter. For the acetone-water system the mass transfer data were correlated by the empirical equation,

$$Sh = 3.0 (0.345 d_e - 0.744) Re \quad \text{-----} \quad 3.43$$

Garner and Lane (75) investigated the absorption of carbon dioxide in water and hydrocarbons and the absorption of water into glycols and an amine. Their study revealed that drops oscillate in three different ways:

- 1) Prolate - oblate oscillations about an equilibrium spheroidal shape.
- 2) Oscillations about axes 90° apart in the horizontal plane.
- 3) Eccentric rotation about the vertical axis whilst horizontal axes remains constant.

Yao and Schrock (77) studied heat and mass transfer of water drops 3 to 6 mm in diameter falling through an atmosphere of lower temperature. The experiment was designed to provide accurate data on the relationship between the mean temperature of the drop and its position in free-fall for different drop size, initial drop temperature, and the temperature and humidity of the air through which it falls. The apparatus consisted of a drop generator, a vertical plastic column 3 m in height containing the conditioned air, air conditioning equipment, and a calorimeter that could be positioned at any elevation to catch and measure mean drop temperature. Drop sizes and oscillations were observed photographically.

The results showed that the models predicted much less cooling than observed experimentally. This suggested that deformation and vibration of drops had an important effect of decreasing the resistance of the external

field. To bring the model prediction into agreement with the data a correction factor was obtained for the Ranz-Marshall correlation. This in effect was a transient correction factor that corrected the Ranz - Marshall equation for the effects of vibration and distortion of drop shape as it falls. The modified Ranz - Marshall equations were then:

$$\text{Nu} = 2.0 + 15.0 \text{Re}^{1/2} \text{Pr}^{1/3} (x/d)^{-0.7} \quad \text{-----} \quad 3.44$$

$$\text{Sh} = 2.0 + 15.0 \text{Re}^{1/2} \text{Sc}^{1/3} (x/d)^{-0.7} \quad \text{-----} \quad 3.45$$

for  $3\text{mm} \leq d \leq 6\text{mm}$ ;  $10 \leq x/d \leq 600$

where  $x$  = falling distance measured from rest

$d$  = diameter of drop

Miura et al (76) employed an experimental apparatus similar to that of Garner and Kendrick (78) to study the rates of heat and mass transfer from floating droplets in an ascending air current. Distilled water droplets were used with an initial diameter range of 2.9 - 3.3 mm at air temperatures of 53 and 75°C. Their experimental data were well represented by the Ranz - Marshall equations (3.15, 3.16) over the Reynolds range 2 to 1600.

More recently Flick et al (135) using an experimental device similar to that of King (136), studied the drying of free-falling droplets of concentrated milk. The device generated a single stream of droplets of uniform size with a mean diameter ranging from 200 to 400  $\mu\text{m}$ , and allowed them to fall into a hot air column. The column was 2m high with a 16cm internal diameter. A limitation of the technique was that even at an air temperature of 180°C only partially dried crusts could be collected, because of the short residence time.

### 3.4 Evaporation from Single Droplets in High-Temperature Surroundings

In a high-temperature environment where the free stream temperature is considerably greater than the wet-bulb temperature, heat is transferred to a

liquid drop by convective transfer directly from the drying medium and by radiative transfer from the surrounding enclosure. For a droplet in a wind tunnel, the radiative heat transfer to the droplet comes mainly from the hot walls, and the contribution from the gas is negligible. The convective heat-transfer  $Q_C$  is therefore:

$$Q_C = Q - Q_R \quad \text{-----} \quad 3.46$$

The contribution of natural convection for a Reynolds number of  $\sim 200$  has been estimated (79) to be negligible, i.e:

$$\frac{Q \text{ free convection}}{Q \text{ forced convection}} \cong 0 \text{ (0.01)}$$

Thus, in equation 3.46,  $Q_C$  represents only heat transfer by forced convection.

Yuen et al (79) and Eisenklam et al (80) have demonstrated that at higher temperatures, the effect of mass transfer on heat transfer of liquid droplets cannot be neglected. At higher temperatures, evaporation reduces heat-transfer rates directly as a result of a considerable amount of the heat conducted inwards being used to heat up the vapour diffusing outwards. It has been shown by Ranz (82) that the actual heat available for vaporisation for an evaporating droplet may be as little as 25% of the total heat transferred. Indirectly evaporation affects heat-transfer rates through the changes in both the composition and the temperature of the surrounding gaseous medium, unless this can be considered infinite in extent.

Marshall studied droplet evaporation at high air temperatures and developed a differential equation to describe the differential heat balance over a spherical shell (81). Solution of this gave an expression for the temperature

T, as a function of distance x , through the gas film surrounding the drop:

$$\frac{T - T_s}{T_g - T_s} = \frac{\exp(-E/x) - \exp(-E/r_1)}{\exp(-E/r_2) - \exp(-E/r_1)} \quad \text{-----3.47}$$

where  $E = m C_{pV} / 4\pi K_V$

$r_1$  = radius of the evaporating droplet

$r_2$  = outer radius of the gas film

One obvious simplification was that any variations in the heat capacity and the thermal conductivity of the gas film, caused by temperature and concentration gradients, were neglected. When equation 3.47 is differentiated at the drop surface, an expression for Nusselt number is obtained as,

$$Nu = \frac{2 E/r_1}{\exp\left(E\left(1/r_1 - 1/r_2\right)\right) - 1} \quad \text{-----3.48}$$

Ranz (82), including an additional term for radiation effects, derived a similar expression.

Hoffman and Gauvin (83) measured evaporation rates of individual drops of water, methanol, cumene, pentane and benzene suspended on a thin glass fibre inside an electrically-heated, 22.9 cm diameter stainless steel sphere. Temperatures ranged from 100°C to 550°C and drop diameters from 0.4 to 1.4 mm. The rates of evaporation were recorded photographically. For stationary droplets at high temperatures the evaporation rate was not governed by the rate of heat transfer by natural convection, but depended on the Transfer Number B, where  $B = C_p \Delta T/\lambda$ . They expressed their results by the correlation:

$$B' Nu (Pr)^{-0.33} = 3.2 B^{0.97} \quad \text{-----} \quad 3.49$$

where  $B'$  is the Spalding transfer number,  $C_p \Delta T / (\lambda - q/m)$ . However, equation 3.49 is only valid when the gas and the containing walls are at the same temperature.

In a later investigation, Pei and Gauvin (84), using essentially the same apparatus as that of Hoffman and Gauvin studied the evaporation of water, benzene and methanol. Stationary porous, hollow spheres 6.35 to 12.7 mm diameter, at 204°C to 537°C, were used to measure the rates of evaporation. Their results were correlated well by the correlation,

$$(Nu/Re^{0.5}) (B'/Pr^{0.33}) = 3.32 (Gr/Re^2)^{0.007} \quad \text{-----} \quad 3.50$$

However, an exponent as small as 0.007 effectively reduces the right side to 3.32.

In an investigation by Pei et.al. (85) the stainless steel sphere used by Pei and Gauvin (84) was modified to provide a stream of superheated steam at 150°C to 750°C with a Reynolds range of 5.5 to 510. The effects of natural and forced convection were demonstrated as non-additive and the transition was found to be gradual. It was concluded that when  $Gr/Re^2$  is less than 0.2 the effects of natural convection was negligible, and for values greater than 10 forced convection had little influence. However, they were unable to propose a correlation to account for this dependency.

Downing (86) performed extensive measurements on individual suspended droplets of water, acetone, benzene or n-hexane, each of the order of 1mm diameter. These were in laminar air jets and covered a temperature range of 27°C to 340°C;  $Re$  ranged from 24 to 325 and the Transfer Number ranged from 0 to 2. The correlation of data was expressed as,

$$Nu = MN \frac{\ln(1+B)}{B} (2.0 + 0.6 Re^{0.5} Pr^{0.33}) \quad \text{-----3.51}$$

and

$$Sh = M (2.0 + 0.6 Re^{0.5} Sc^{0.33}) \quad \text{-----3.52}$$

where,

$$M = 1 - 0.4 (1 - T_s/T_g)$$

$$N = 1 - 0.4 \left( 1 - \frac{\ln(1+B)}{B} \right)$$

The average physical and transport properties were calculated at an average film temperature,  $T_f$ , defined as,

$$(T_f - T_s) / (T_g - T_s) = 0.6$$

Eisenklam et al (80) have investigated the evaporation of single water and other hydrocarbon droplets in high temperature (up to 1000°C) air streams. The Reynolds numbers varied from 0.01 to 15 and the Mass Transfer Number from 0 to 3. The data were correlated as,

$$Nu_f (1 + B_f) = 2 + 1.6 Re_f^{1/2} \quad \text{----- 3.53}$$

where the properties are evaluated using the film conditions.

Narashimhan and Gauvin (87) investigated the evaporation of water from porous Celite spheres in superheated steam at temperatures from 500 K to 1000 K. They expressed their results by the equation,

$$Nu_f (1 + B_f)^{2/3} = 0.68 Re_s^{1/2} \quad \text{----- 3.54}$$

Lee and Ryley (88) suspended drops of water on a 50µm glass fibre

in a horizontal test section. Evaporation rates were followed optically and superheated steam and air were used as the gaseous media at Reynolds numbers between 64 and 250. The correlation obtained was found to be similar to that of Ranz and Marshall (3.15) with a coefficient of 0.74. Radiation effects however, were ignored in their analysis.

In a study by Frazier and Hellier (89), rates of evaporation of droplets of 440  $\mu\text{m}$  diameter Freon 113 were determined by injecting a stream of droplets passing through a 669°C air jet. A photographic technique was used to monitor changes in drop size. It was concluded that the mass transfer coefficient was underestimated by a factor of 4 by the Ranz and Marshall correlation. Using corrections for the net flow through the interface based on the film theory, Crosby and Stewart (90) recalculated the results of Frazier and Hellier and found a much smaller deviation of 33% between experimental and predicted values.

Trommelen and Crosby (91) determined the evaporation of 1.56 mm diameter drops of water in air and superheated steam at velocities of 1.5 to 2.1 m/s. Temperature of the drying medium ranged between 150°C and 250°C. The experimental procedure was similar to that followed by Sano and Nishikawa (92) which, in turn, was based on the method developed by Charlesworth and Marshall (93). The drop was suspended at the junction of a chromel-constantan thermocouple which itself was affixed to the end of a fine horizontal glass fibre. This allowed the simultaneous measurement of drop temperature and drop weight. Their results revealed that at equal temperatures and velocities the evaporation rate was greater for air than for superheated steam. However, as the drying temperature increased, this difference between the rates of evaporation in the two media decreased. This phenomena may be explained by the fact that at higher temperatures the thermal driving forces in the two media approach one another. From the

results it was concluded that the accepted correlation of heat transfer coefficients which is applicable for evaporation of small drops of pure liquid in air is also valid for evaporation in a superheated vapour. Their analysis took account of heat transferred by direct radiation and conducted through the thermocouple wires. In the estimate of the latter however, they used the cross-sectional area of the wires which underestimated the area of the bead at the junction by at least a factor of 4.

Audu (58) used a horizontal wind tunnel in which water drops were suspended at the end of a rotating nozzle, to determine rates of evaporation. A temperature correction factor was proposed to account for the results at temperatures > 46°C,

$$Sh = 2.0 + 0.44 \left( \frac{T_g - T_s}{T_{amb}} \right)^{-0.008} Re^{0.5} Sc^{0.33} \quad \text{-----3.55}$$

However, an exponent of 0.008 is too small to have any significant effect.

Kadota and Hiroyasu (94) derived a mathematical model for a single evaporating drop at high pressures and high temperatures. The quasi-steady state model included the effects of natural convection, non-ideal behaviour and effects of high mass transfer rates on temperature and concentration profiles and boundary layer thickness. Results from an earlier study (95) on the evaporation of ethanol, n-heptane, benzene and water droplets were found to be in good agreement with the model.

Yuen and Chen (79) simulated a droplet by using a porous sphere soaked in the liquid and regulated the supply of liquid so that the surface was always wetted. The heat transfer rates to simulated water and methanol droplets were measured in an atmospheric vertical, hot air, tunnel. The experiments were limited to a Reynolds number range of 200 - 2000, a free stream air temperature range of 150 - 960°C and a velocity range of 2.1 to 11.4 m/s. They correlated the experimental data by,

$$\text{Nu}_f (1 + B) = 2 + 0.6 \text{Re}_m^{1/2} \text{Pr}_f^{1/3} \quad \text{-----3.56}$$

where  $\text{Re}_m$  is defined as  $\rho_g v_g d / \mu_f$

The experimental data therefore showed that at higher temperatures, evaporation reduces heat transfer rates directly by a factor of  $(1 + B)$ . However, the study was limited to droplets with maximum  $B = 0.5$  and Reynolds numbers from 200 - 2000.

Renksizbulut and Yuen (96) recently used the same experimental technique as Yuen and Chen (79) to measure heat transfer to single water, methanol and heptane droplets. However, a broader Reynolds number range of 25 to 2000, and a Transfer Number range of 0.07 to 2.79 were used. Their data were correlated by the expression,

$$\text{Nu}_f (1 + B_f)^{0.7} = 2 + 0.57 \text{Re}_m^{1/2} \text{Pr}_f^{1/3} \quad \text{-----} \quad 3.57$$

The validity of simulation of pure liquids by using spheres saturated with the liquid may however, be open to question because of local vapour pressure depression at micro-undulations and surface tension effects.

In summary, different techniques of drop suspension, ranging from a stationary drop suspended on a glass filament or thermocouple to a drop retained in free-flight, have been used to cover an extensive range of temperatures, drop sizes and gas velocities. However, evaporation from single droplets suspended freely in an air stream has been incompletely studied. This was therefore included in the present study using a vertical wind tunnel designed to support a droplet in free-flight.

Although the results of the majority of previous workers support the Ranz and Marshall correlations, the effects of turbulence, circulation within a drop and drop oscillation had not been thoroughly investigated. These aspects were therefore considered.

**CHAPTER FOUR**  
**DRYING OF DROPLETS CONTAINING DISSOLVED OR**  
**SUSPENDED SOLIDS**

As summarised in Chapter 3, the mechanisms of evaporation from pure liquid droplets have been described by many workers. However, the much more complicated problem of evaporation from drops containing dissolved or suspended solids, the situation in spray drying has received less attention. Thus, information on the evaporation from droplets containing solids and on the formation of a solid phase is sparse.

In the presence of nonvolatile dissolved solids in a droplet having a velocity relative to the surrounding air, the complexity of the process of evaporation is greatly increased. Whereas, in the consideration of heat and mass transfer from a droplet of pure liquid, conditions within the droplet may justifiably be assumed uniform, they cannot be if there is a non-volatile material present.

In general, the concentration of solute in the droplet is initially uniform, but as soon as some evaporation has taken place from the surface of the droplet, concentration gradients are set up and there is diffusion of solvent toward the surface and solute toward the centre. Furthermore, since except in a few cases, the drop is necessarily decreasing in size, the solute in the surface layer is swept inward by the retreating interface, which is impermeable to the solute. The concentration profiles are consequently not simple. Furthermore, the droplet may experience internal circulation from density gradients caused by temperature and concentration and from the viscous drag of the passing air. Droplet rotation as a whole may also be present.

Therefore, the drying of droplets containing solids is not susceptible to a simple analysis and the drying characteristics are related to the formation of a solid structure on the surface of the droplet. The latter provides an additional resistance to moisture transfer into the surrounding media.

When a droplet contains dissolved, or in certain circumstances to a lesser degree suspended, materials, the normal vapour pressure of the liquid is lowered, with the result that the evaporation rate becomes lower than that for pure drops of the same size. The surface temperature of the evaporating droplet will consequently increase above the thermodynamic wet bulb temperature. As in most drying operations, the process of drying a single droplet can be sub-divided into two periods; the 'constant-rate' period and the 'falling-rate' period.

#### **4.1 Constant-Rate Period**

This period is characterised by evaporation from a free liquid surface of constant composition and vapour pressure and the rate of drying per unit surface area depends entirely on parameters external to the solid being dried, such as the velocity, flow pattern, temperature and humidity of the drying air. If the external conditions are constant, then the drying rate in this period is constant.

In this period drying proceeds by diffusion of vapour from the saturated surface through a stagnant gas-film around the drop into the environment. The surface is kept saturated as long as moisture movement from within the material is sufficiently rapid to maintain a completely wet surface. The vaporization rate is controlled by the heat transfer rate to the evaporating surface; the mass transfer rate adjusts to the heat transfer rate, and the liquid reaches a steady-state temperature. The drying rate is therefore, constant as long as the heat transfer rate is held constant by external

conditions. If heat is transferred solely by convection from a gas, the steady-state surface temperature is the gas wet-bulb temperature. When conduction or radiation contribute to heat transfer, e.g. the drop is suspended from a filament or a nozzle or receives radiation from a warm enclosure, a surface temperature somewhere between the wet-bulb temperature and the liquids boiling point is obtained.

#### **4.2 Falling-Rate Period**

The falling-rate period commences at the 'critical moisture content' when the constant-rate period ends. The critical moisture content is the average material moisture content at the end of the constant rate drying period. During the falling rate period a crust begins to form, starting from a preferential site, usually the point of maximum mass transfer, and spreads around the droplet. The drying characteristics are then determined by the nature of the solid structure. When the range of moisture content is above the critical moisture content, the whole drying process will occur under constant-rate conditions. If, on the other hand, the initial moisture content is below the critical moisture content, the entire drying process will occur in the falling-rate period. This period is usually divided into two zones; the zone of unsaturated surface drying and the zone where internal moisture movement controls. In the first zone, the entire evaporating surface can no longer be maintained and saturated by moisture movement within the solid. The drying rate decreases from the unsaturated portion and hence the rate for the total surface decreases.

As drying proceeds, the point is reached where all the exterior surface is unsaturated. The plane of evaporation recedes into the solid, and the drying process enters the second falling-rate period. The drying rate is now governed by the rate of internal moisture movement; the influence of external variables diminishes. This period usually predominates in determining the

overall drying time.

### **4.3 Mechanisms of Internal Moisture Transfer**

Internal moisture movement may occur by several different mechanisms within the material, depending on the nature of the material, the type of moisture bonding, the moisture content, temperature and pressure in the pores, etc. The following mechanisms are mentioned in the literature (97):

- (a) Liquid moisture movement due to capillary forces in granular and porous solids;
- (b) Vapour and liquid diffusion due to differences in moisture concentration in continuous, homogeneous solids;
- (c) Flow caused by shrinkage and pressure gradients. The situation is however complex when drying droplets since drop rupture, partial disintegration and vapour explosions are additional possibilities.
- (d) Flow caused by gravity (mainly in coarse-pored materials);
- (e) Flow caused by a vaporization-condensation sequence;
- (f) Flow caused by a temperature gradient (thermo-diffusion effect)

Of the several theories so far suggested the diffusion theory, capillary flow theory and evaporation-condensation theory appear to have gained general recognition. Although more than one of these mechanisms of flow may be effective at one time, generally only one predominates at a given time in a solid during drying. However, a different mechanism may predominate at a different time in the drying operation. The mechanism of moisture flow can be determined experimentally by a determination of moisture gradients.

Hougen, McCauley, and Marshall (98) have discussed the conditions under which capillary flow and diffusional flow may be expected to occur in a solid. They showed that capillary flow gives a moisture gradient having a double curvature and point of inflection while diffusional flow results in a gradient with a smooth curve, concave downwards. They also showed that for diffusional flow the liquid diffusivity, usually assumed constant, is not constant but decreases as the moisture content decreases. Hougen et al also classified solids with respect to capillary and diffusional internal liquid flow.

#### **4.3.1. Capillary Flow Theory**

Buckingham (99) introducing the concept of capillary potential and, by postulating the mechanisms of unsaturated capillary flow, laid down the fundamentals of capillary flow theory.

The outer surface of a porous solid has pore entrances of various sizes. As surface liquid is evaporated during the constant rate period, a liquid meniscus is formed across each entrance and capillary forces are set up by interfacial tension between the liquid and solid. These forces draw liquid from the interior to the outer surface. At the critical moisture content, some of the menisci begin to retreat into the pores. Wetted outer surface gradually decreases and, although the drying rate per unit area of wetted outer surface remains constant, drying rate based on total outer surface decreases. This stage of unsaturated surface drying of porous materials is the first falling rate drying period. During this stage, gas begins to enter the pores, but the internal liquid phase is continuous; the liquid is said to be in the funicular state. If the pores are small and not of uniform size, the retreat of the liquid phase is not uniform. Small pores produce stronger capillary forces than large pores; thus small pores draw liquid out of large pores. As more liquid is removed, the outer surface dries completely and a point is reached where there is not enough internal liquid left to maintain a continuous phase linking

all interior pores. Residual liquid retreats to isolated pockets in the smallest pores, and gas enters far enough into the material so that gas forms the continuous phase. The liquid then obtains the so called pendular state. This point is the second critical moisture content in porous materials because there is a second break in the drying rate profile. All heat for vaporization must now pass by conduction through the material to the liquid pockets; the temperature rises, and the residual liquid vaporizes and diffuses in the gas phase to the surface.

#### **4.3.2. Diffusion Theory**

Diffusion is proposed as the major mechanism of moisture movement by a number of research workers (100,101). Assuming this to be valid, Sherwood (102) regarded the drying process as taking place in two characteristically different ways:

- (a) diffusion of liquid from the interior to the solid surface, followed by the evaporation of the liquid at the surface and diffusion of vapour into the surrounding air; or
- (b) evaporation of the liquid at a point beneath the surface of the solid, followed by diffusion of water vapour through the pores to the surface and into the ambient air.

It is necessary to note however that, when drying droplets, severe drying conditions after crust formation, resulting in internal steam generation at a rate exceeding the permissible vapour diffusion rate, can lead to local ruptures or explosions. Clearly in such cases the idealised vapour diffusion model is inapplicable.

Although it has been suggested (Section 4.3.1) that capillarity is the principle mechanism of moisture flow in porous materials, diffusion theory may also be used to study moisture movement in porous materials.

However, all estimates based on relationships that assume constant diffusivity are approximations. Liquid diffusivity in solids usually decreases with moisture concentration; liquid and vapour diffusivity also change as material shrinks during drying.

### **4.3.3 Evaporation-Condensation Theory**

This theory assumes that movement of moisture takes place entirely in the gaseous phase through the pores. It was shown by some workers (103,104) that when the system was subjected to a temperature gradient, even at relatively high pore saturation, the assumption was essentially correct. A model based on this theory was developed by Harmathy (105) to successfully predict the drying rates of clay bricks.

### **4.4 Evaporation and Drying of Single Droplets Containing Dissolved and Suspended Solids**

Apart from their work on pure liquids, Ranz and Marshall (22) presented experimental data on the evaporation from droplets of sodium chloride and ammonium nitrate solutions, droplets of a non-soluble, suspended green dye and from droplets containing reconstituted dried whole milk. Their results from ammonium nitrate solution suggested that droplets of solutions prior to membrane or crust formation evaporated at all times as if they were saturated, even though the average solute concentration in the droplet was well below the saturation value. Using calcium chloride solutions of four different initial concentrations, this hypothesis was later tested and challenged by Charlesworth and Marshall (93).

In a study by Duffie and Marshall (106) a vertical, cylindrical co-current spray dryer, 20.32 cm in diameter and 6.1 m high, was developed to carry out a qualitative study on a wide range of products. Their results were

reported from two points of view. One analysis was based on a study of the bulk densities of the materials and the way in which they varied with drying-air temperature, liquid-feed temperature, feed concentration and material properties. The second analysis was based on a classification of materials according to the nature of their spray-dried products.

Their observations revealed that four factors contributed to the formation of hollow particles;

- (a) Hollow particles may arise due to the formation of films causing puffing or ballooning of the particle;
- (b) A hollow particle may be formed if the rate of evaporation exceeds the rate of diffusion of solids back into the drop, creating internal voids;
- (c) A hollow particle may be formed by the capillary action of the rigid porous shell on the drop surface drawing liquid and solids to the surface and creating sub-atmospheric pressures within the particle;
- (d) The presence of entrained gases in the feed may also result in hollow particles.

They characterised the materials studied into three categories; 'film forming' such as sodium silicate, 'crystalline' materials such as most inorganic salts and intermediate materials such as coffee extract. However, they found that the mechanism of hollow particle formation differed within each category.

Charesworth and Marshall (93) made a study of evaporation from single drops of aqueous solutions of various materials, e.g. sodium sulphate, copper sulphate, coffee extract and whole fresh milk. The suspension device adopted was a vertical glass filament the tip of which was drawn to small diameter and then touched to a flame to give a small knob on the end. Typical diameters were 340 $\mu\text{m}$  for the main filament, 70 $\mu\text{m}$  for the necked-in

to another horizontal glass filament, the deflection of which determined the weight of the drop. They proposed a correlation for the experimental data concerning the time for formation of a solid phase around a droplet,

$$\theta_c = \frac{x_o^2}{4D} \ln \left( \frac{C_s/C_o}{\phi_y^2 + 2\gamma \ln(C_s/C_o)} \right) \quad \text{---- 4.4.1}$$

They further presented a generalized description of the appearance and behaviour of a drying droplet as shown in Figures 4.1 and 4.2. The sequence of events up to the point of crust formation were similar for all droplets no matter what the solute concentration or drying conditions. The results of further drying after the completion of the crust differed depending on the nature of the crust and the temperature of the surrounding air.

Trommelen and Crosby (91) investigated the changes in weight and temperature as a function of time of approximately 2 $\mu$  litre drops of four food products and various inorganic salts, and used steam and air as the drying media. They observed that for the four food products studied air generally gave equivalent or more rapid drying than steam at temperatures near 150°C, whereas superheated steam gave equivalent or slightly faster drying than air at around 250°C. However, it was noted that the relative rates of drying and the differences in properties of the dried particles for these drying media were product specific. Examination of the dried particle properties showed no real differences from drying in steam as compared with air. However, drops dried in steam sometimes yielded denser particles.

Miura et al (107) in the study of the drying of single droplets characterised the solids contained in the droplets from the standpoint of changing properties during the process of drying as follows:

- (1) Those which educe crystals and produce crusts on the surface such as ammonium chloride, sodium sulphate and sodium chloride;

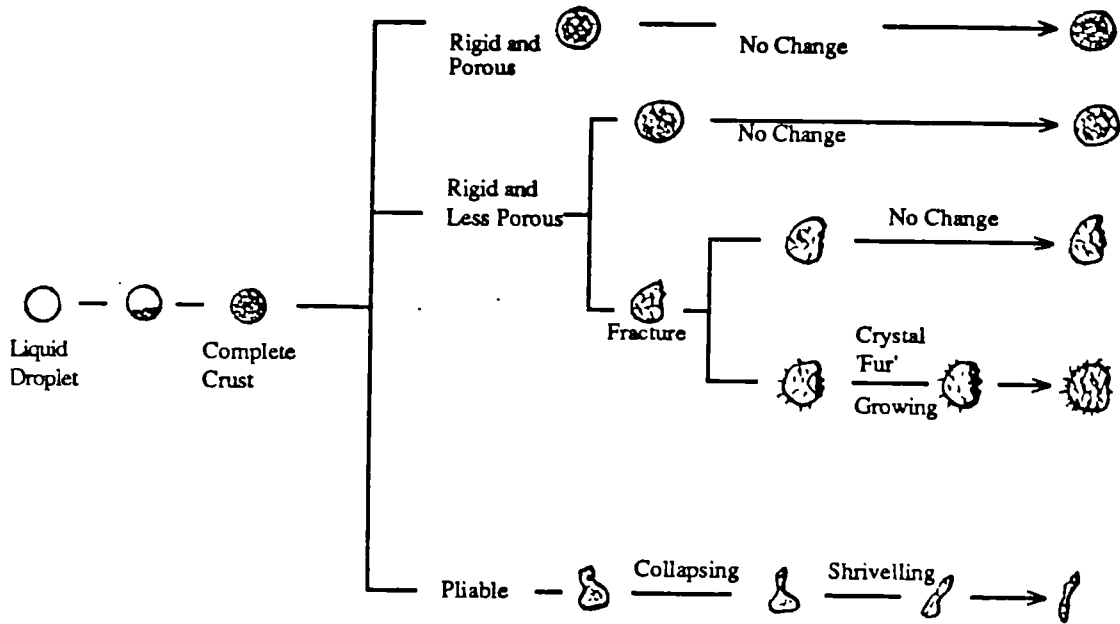


Figure 4.1 Drying Characteristics of Droplets at Air Temperatures Below the Boiling Point

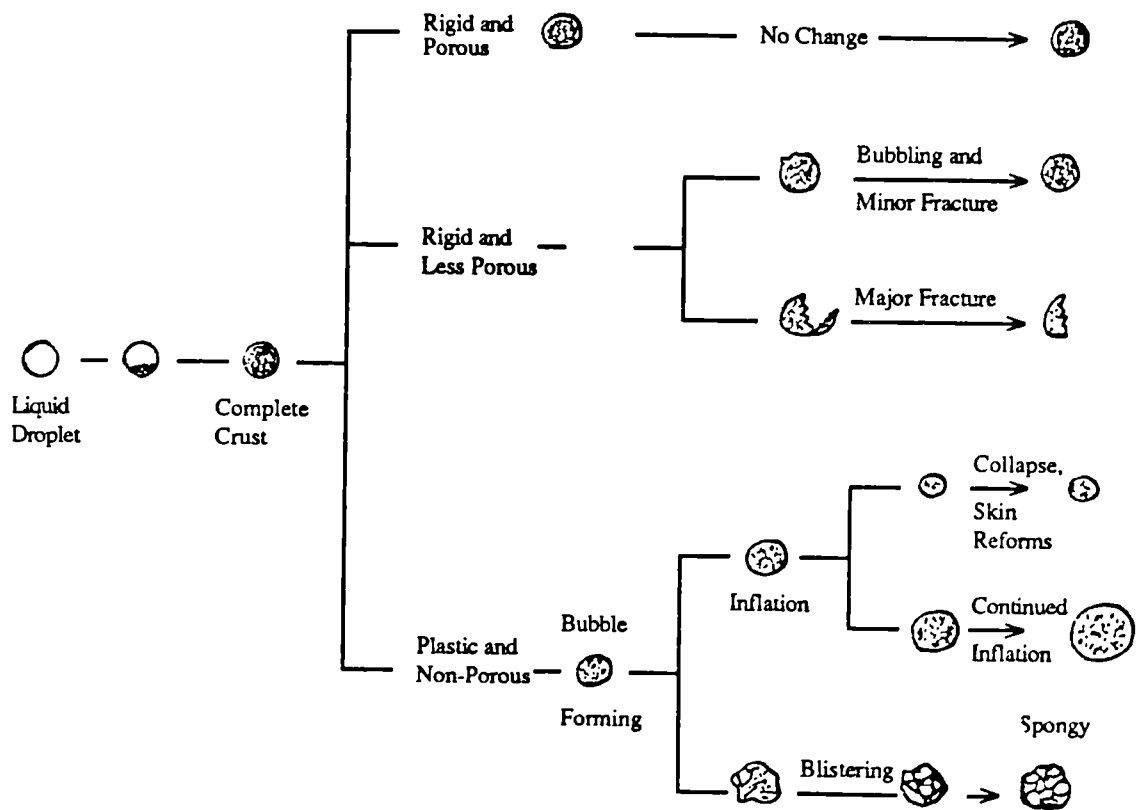


Figure 4.2 Drying Characteristics of Droplets at Air Temperatures Above the Boiling Point

- (2) Those which form a skin on the surface of the drop such as skim milk and gelatin;
- (3) Those which produce neither crusts nor skins such as bentonite.

A theory was proposed for the cases of (1) and (2) to determine the skin/crust thickness of a droplet and the time of eduction of crystals. From a mass balance of solids in a droplet the following equation was proposed to predict the skin/crust thickness;

$$(Y - 1) = \frac{1 - W^3}{3G'W^2 - 3G'^2W + G'^3} \quad \text{---- 4.4.2}$$

where  $W = r/r_0$

$Y = c/c_0$

$G' = \psi/r_0$

They used the equation proposed by Charlesworth and Marshall (93) to predict the time of appearance of a crust, and found that although it was in reasonable agreement with experimental data, the latter were generally greater than the calculated values. For the case of bentonite, where no skin or crust was observed, the curve of evaporation rate and temperature rise was nearly the same as that for a pure liquid droplet.

The drying of single droplets of sodium sulphate and detergent slurries, suspended in a wind tunnel, were studied by Audu and Jeffreys (108). A crust mass transfer coefficient  $k_c$ , was proposed and expressed as,

$$k_c = \frac{D_v \epsilon^{1.5}}{\psi} \quad \text{----4.4.3}$$

With the systems studied the crust resistance to mass transfer could account for as much as 64.2% of the total resistance. However heat conducted along the suspension nozzle and that due to radiation was not taken into consideration. Based on a mass balance of moisture in the surrounding air, a crust thickness model was also proposed as,

$$\psi = R - \left[ R^3 - \frac{3G}{2\pi C_0} (H_d - H_j) \Delta\theta \right]^{0.33} \quad \text{---4.4.4}$$

However, the calculated values were as much as 20% higher than experimental results.

Basing their work on the experimental results of Van der Lijn (109), who introduced a concentration and temperature dependent diffusion coefficient, Wijlhuizen et al (110) proposed a 'solid sphere' and 'hollow sphere' model for an evaporating droplet of skimmed milk. The 'hollow sphere' model assumed an initial gas bubble of known size in a droplet and a uniform concentration profile. Using the necessary boundary conditions the diffusion equations were solved to predict moisture concentrations and droplet temperatures during drying. The model however, has limited applications since it does not allow for the formation of a crust.

Haertling (111) developed a model to predict the drying rates for porous hygroscopic materials such as clay brick and burned clay. The model assumed that mass transfer within the droplet occurred by a simultaneous process of vapour diffusion and liquid moisture movement by capillary suction. The model however, overestimates the drying rates by about 21% particularly at high air temperatures.

A mathematical model for estimating crust mass transfer coefficient,  $k_C$ , was developed by Esubiyi (112) based on an assumed vapour velocity



through the pores of a solid crust described by the Kozeny equation (113).  
The crust coefficient was expressed as,

$$k_c = \frac{\varepsilon^3 \rho}{5(1-\varepsilon)^2 \mu_s b^2 \psi} \quad \text{----4.4.5}$$

He confirmed the validity of this model by using five different sources of Portland cement.

A more realistic model to describe the drying of single droplets containing colloidal material into solid hollow spheres was presented by Sano and Keey (114). To describe the mechanisms for the formation of hollow spheres they assumed that once the equilibrium vapour pressure of the moisture inside the droplet exceeds the pressure of the ambient air, the particle inflates instantaneously and ruptures. After inflation, two limiting ways of deformation were proposed;

- (a) The maximum radius remains constant, but the void radius increases due to the moisture loss; or
- (b) The void radius does not change, but the outer radius shrinks.

For the drying of droplets of skimmed milk suspended on a fine glass filament in the temperature range between 100°C and 150°C, the second proposal gave the best approximation to the experimental results. Theoretical computations, however, required an experimentally determined inflation ratio, which was the ratio of the maximum radius after inflation to the initial radius. Their results were computed with an inflation ratio of 0.88, but to fit the data of Trommelen and Crosby (91), for the same material and

temperatures, they found that a ratio of 1.1 was required.

Cheong (115) recently developed a receding interface model to describe the drying characteristics of single drops of slurries of sodium sulphate decahydrate. A unique thermocouple was developed for the simultaneous measurement of drop weight and drop temperature during drying. Single drops of slurries, 1.0 to 1.5 mm in diameter, were suspended on the tip of a flexible glass cantilever inserted in a vertical wind tunnel. The thermocouple consisted of a 50  $\mu\text{m}$  diameter nickel wire passing through the centre of a glass filament and the outer surface coated with a thin film of copper. A junction was formed at the tip where about 0.5 mm of nickel wire was exposed. The thermocouple measured the temperature of the core of the drop and the deflection of the beam gave the loss in weight during drying. Three equations were derived which on simultaneous solution give the crust thickness, core temperature and weight of the drop as a function of time. For the crust thickness predictions the model gave good results. However, the drying of sodium sulphate decahydrate was found to be complicated by the enantionmorphic changes taking place at 33°C. When the heats of solution of the different hydrates and the heats of transition of the crystal forms were included in the model the agreement between the predicted and the experimental drying behaviour, over the temperature range 20 to 78°C was good. The model however, takes no account of the constant rate period, and the effects of fractures, 'blow' holes etc. Consequently, since the model does not take into account the loss of small fragments when the crust fractures, it overestimates the drop weight after complete crust formation.

Ali et al (137) investigated the drying of single droplets suspended from a rotating nozzle in a horizontal wind-tunnel. Their study covered pure liquid (water), solutions (eg sodium sulphate decahydrate, organic and inorganic products), and slurries of various organic products over a range of air temperatures (20-200°C) and air velocities (0.1-2.1  $\text{ms}^{-1}$ ). Revised

correlations were obtained for mass and heat transfer coefficients from pure liquid drops. In the drying of drops of solutions and slurries good agreement was obtained between experimental and predicted overall mass transfer coefficients.

In summary, the drying characteristics of drops containing dissolved/suspended solids, as in the case for the evaporation of pure liquid drops, have been primarily investigated by suspension of a drop at the end of a filament, thermocouple or a nozzle. The attempt, therefore, in the present work has been to study the drying behaviour of drops in free-flight. The experimental technique therefore, simulates more closely conditions in a spray dryer and avoids extraneous effects such as heat conduction along the suspension device, and the droplet climbing up the filament in later stages of the drying process.

#### **4.5 Evaporation from Sprays of Droplets**

The evaporation characteristics of droplets within a spray differ from those of single droplets. Although the basic theory is similar in both cases, it is difficult to apply to the case of a large swarm of droplets evaporating close to the atomiser. Any analysis of spray evaporation depends upon defining the spray in terms of a representative size distribution, the relative velocity between any droplet and its surrounding air, droplet trajectory and the number of droplets present at any given time per give volume of drying air. Furthermore, there are grave difficulties in determining parameters in the vicinity of the atomiser and spray evaporation data are subsequently limited. For non-homogeneous sprays the droplet mean diameter generally shows an initial increase prior to a decrease until completion of evaporation, since the finest droplets disappear reducing the total number of droplets in the spray. Therefore, the use of a mean droplet size is unlikely to adequately characterize

the evaporation process for a non-uniform spray. The best representation of droplets during evaporation is the droplet size distribution function. Table 4.5.1 gives the more common distribution functions discussed extensively by Masters (2).

The shape of the product particle depends upon droplet formation during atomization and upon droplet/particle behaviour during drying. An agglomerate can be formed through interdrop impingement in the proximity of the atomiser or through partially dried droplets adhering to each other in the lower regions of the chamber, due to their sticky surfaces. Impingement of two liquid sprays for example by using a two nozzle arrangement may also cause significant increase in the droplet particle size.

#### **4.5.1 Sprays of Pure Liquids**

Using the Rosin-Rammler equation (116), Probert (138) attempted to represent the drop size distribution of a fuel spray. It was assumed that the spray droplets had no relative velocity and that there were negligible temperature driving force changes during evaporation. The prediction was, with the same mean diameter, a spray with a narrow size distribution will evaporate completely in less time than one with a wider distribution. Fledderman and Hanson (117) extended this study to cover conditions of relative velocity assuming a Nukiyama-Tanasawa type distribution (118).

A comprehensive stepwise method for the evaluation of spray evaporation was proposed by Marshall (81). Division of the size distribution into small size groups enabled the change in the average droplet diameter in each selected group to be calculated over short time intervals. Although the method was only presented for pure liquid droplets at zero relative velocity, the results are useful in illustrating the nature of changes likely to take place in a dryer. For example it predicted that in the majority of spray drying

**TABLE 4.5.1 DROPLET SIZE DISTRIBUTION FUNCTIONS**

EQUATION

DISTRIBUTION

Normal

$$\frac{d(N)}{d(d_p)} = \frac{1}{S_N(2\pi)^{0.5}} \cdot \exp - \left[ \frac{(\bar{d}_p - d_p)^2}{2S_N^2} \right]$$

Log-Normal

$$\frac{d(N)}{d(d_p)} = \frac{1}{d_p S_G(2\pi)^{0.5}} \cdot \exp - \left[ \frac{(\log d_p - \log d_{gm})^2}{2S_G^2} \right]$$

Square Root Normal

$$\frac{d(N)}{d(d_p)} = \frac{1}{2(2\pi d_p S_G)^{0.5}} \cdot \exp - \left[ \frac{(d_p^{0.5} - d_{gm}^{0.5})^2}{2S_G^2} \right]$$

Upper Limit

$$\frac{d(N)}{d(d_p)} = \frac{1}{d_p S_G(2\pi)^{0.5}} \cdot \exp - \left[ \frac{\log((d_{max} - d_p)/d_{gm})^2}{2S_G^2} \right]$$

Nukiyama-Tanasawa

$$\frac{d(N)}{d(d_p)} = a_n d_p^2 \cdot \exp (-b_n d_p^f)$$

Rosin-Rammler

$$V_p = 100 \cdot \left( \frac{d_p}{d_r} \right)^2$$

operations 90% of the evaporation will be completed during the first 1.5 seconds, and that during this period the air temperature will fall to within 17°C of the outlet temperature.

Useful measuring techniques were developed by Manning and Gauvin (12) in their study of heat and mass transfer of water sprays in co-current and countercurrent air flows. A colourimetric method using a red dye was used to measure the progressive evaporation from a spray and the droplet size distribution was determined on samples obtained by traversing the spray with an immersion cell containing varsol. However, there was considerable scatter amongst the experimental data. This may have arisen, in part, due to the uncertainty in predicting relative velocities and droplet sizes in the vicinity of the atomising nozzle.

Bose and Pei (119) investigated the evaporation of water sprays in a 152.4mm I.D. cocurrent drier. Contrary to the findings of Dlouhy and Gauvin (23), the relative velocity between spray and air stream was observed to cause a substantial increase in the heat and mass transfer rates. Indeed, this is to be expected from the dependency of both Sherwood and Nusselt Number on the Reynolds number. They showed that the Ranz and Marshall correlations, which take account of relative velocities, represented their data well.

Dickinson and Marshall (120) presented a computational study of the evaporation of sprays of pure liquid. They considered spray droplets under conditions of both negligible and significant relative velocities, and took account of non-uniform size distributions. However, their analysis has limited use because of the assumptions of idealized conditions of constant droplet temperature and ideal flow.

The effects of drop to drop interaction on the rate of drop to fluid heat and mass transfer were investigated by Miura et al (76). Single water droplets

were surrounded by glass beads and the resulting experimental equations proposed were;

$$\text{for } b/d_g \leq 2, \text{ Nu/Nu}_R \text{ or Sh/Sh}_R = 0.71 (b/d_g)^{0.25} (d_p/d_g) + 0.07 \quad \text{-----4.5.1}$$

and

$$\text{for } b/d_g > 2, \text{ Nu/Nu}_R \text{ or Sh/Sh}_R = 0.42 (b/d_g)^{0.125} + 0.41 \quad \text{-----4.5.2}$$

where  $b$  = distance between water droplet surface and glass bead surface.

Using results from water sprays generated from a pneumatic nozzle the validity of the above equations was confirmed by a model proposed by Miura and Ohtani (121). However, the evaluation of  $b$  and  $d_g$  values was tedious and relied on probability theory.

#### **4.5.2 Sprays containing Dissolved and Suspended Solids**

The surface tension of a solvent, and hence its vapour pressure, is lowered considerably by the addition of a solute. This is given by the 'Kelvin equation' as,

$$-\Delta P = \frac{2\sigma'}{r} \quad \text{-----4.5.3}$$

It is clear from equation 4.5.3 that for small droplets the reduction in pressure due to surface tension is greater. Furthermore as evaporation proceeds, the concentration of solids in the smaller droplets will increase much faster than in the larger droplets resulting in a wide variation in the concentration driving force. The solid phase not appearing simultaneously throughout the size distribution is a consequence of this phenomenon. For droplets containing insoluble solids there are no surface tension effects and the lowering of vapour pressure is considered negligible. Therefore, the analysis of spray evaporation is complex and investigations in this field are limited.

Using experimental techniques similar to Manning and Gauvin (12), Dlouhy and Gauvin (23) investigated the evaporation of sprays of calcium

lignosulphonate solution in a 203.2mm diameter cocurrent dryer. Accurate prediction of the drying rate curves was achieved employing the stepwise method of calculation proposed by Marshall (81). However, their method requires a knowledge of the drop size distribution which must be determined experimentally.

Baltas and Gauvin (122) used the same dryer as Dlouhy and Gauvin (23) and studied evaporation from a spray of sodium nitrate solution. They developed a step-by-step prediction procedure and found that the predicted evaporation rates were 3.5 times greater than the observed rates. Results from computer calculations of local humidity and mass flow profiles showed good agreement with observed profiles. Their model is however only applicable to the free fall zone.

Equations based on assumed size distributions and ideal flow patterns in the drying chamber, were proposed by Katta and Gauvin (123). These predicted the three dimensional motion of droplets in a spray drier. Their model which predicts droplet trajectories and evaporation rates was experimentally verified by work with solutions of calcium lignosulphonate in a 122 cm diameter, 183 cm high, circular cocurrent chamber with a conical base. It was concluded that there is an optimum nozzle depth and an optimum air temperature for maximum efficiency and capacity.

Miura et al (124) investigated the drying of solutions of skimmed milk and sodium chloride using a two fluid pneumatic nozzle and a hollow cone nozzle for atomization. A Nukiyama-Tanasawa distribution was assumed in their analysis and the results were correlated more accurately by equations 4.5.1 and 4.5.2 for evaporation in a spray cloud, than by Ranz and Marshall equations for single droplets.

#### 4.6 Temperature of Evaporating Droplets

To evaluate the temperature driving force so that evaporation times and rates can be estimated, it is necessary to be able to specify, or estimate, the droplet surface temperature. For pure liquid droplets if a dynamic equilibrium between the rate of heat and mass transfer is established, and assuming that all heat transferred is consumed for evaporation, then the surface temperature of the droplet may be estimated from the equality ,

$$\frac{T_g - T_s}{p_s - p_g} = \frac{k_g A_m \lambda}{h_g A_h} \quad \text{----4.6.1}$$

and if  $A_m = A_h$

$$\frac{T_g - T_s}{p_s - p_g} = \frac{k_g \lambda}{h_g} \quad \text{----4.6.2}$$

which is the familiar expression for the surface temperature or the wet-bulb temperature.

When a droplet contains solids in solution the temperature of the droplet will be higher than that predicted from the wet-bulb temperature for water at its normal vapour pressure. This elevation above the wet-bulb depends upon the extent to which the vapour pressure is depressed due to the dissolved solids. When a droplet contains insoluble suspended solids however, there are negligible vapour pressure lowering effects and the surface temperature will initially approximate that for a pure liquid droplet. In both cases the formation of a crust about the droplet will provide additional resistance to moisture diffusion resulting in the core temperature rising above the saturated wet-bulb temperature.

William and Schmidt (125) have shown from their study that when drying salt solutions the heat of crystallization should be taken into account.

The heat of crystallization for ammonium nitrate solutions is, for example, 20% of the latent heat of vaporization. Consequently equation 4.6.2 becomes,

$$\frac{T_g - T_s}{P_s - P_g} = \frac{k_g(\lambda - C_d)}{h_g} \quad \text{----4.6.3}$$

Ranz and Marshall (22) and Charlesworth and Marshall (93) followed drop temperature histories, during evaporation, by embedding a thermoelement junction inside a suspended droplet. Unlike later workers (91,115) they were unable to measure the evaporation rates and droplet temperatures simultaneously. With drops containing  $3.0 \times 10^{-4}$  gm of ammonium nitrate, Ranz and Marshall observed that there was a gradual increase in the drop temperature initially, due to the heat of solution, followed by a sharp rise as crystallization occurred. Their analysis took no account of the heat conducted along the thermocouple wires.

Using thermocouple leads of increasing diameter Downing (86) measured drop temperatures and extrapolated the results to zero diameter to estimate the heat conducted along the wire. Organic liquid drops were observed to climb up the wires and the wet-bulb temperature was found to depend on the position of the thermocouple junction in the drop.

Trommelen and Crosby (91) were the first investigators to carry out a simultaneous measurement of drop weight and drop temperature. They suspended a drop from a chromel-constantan thermocouple fixed to the end of a glass filament which acted as a torsion balance. From a heat balance along the thermocouple wires an expression was derived, and solved, giving an estimate of the rate at which heat was transferred to the drop along each of the two thermocouple leads. In contrast to clay slurries and inorganic salts their results revealed that food products generally did not exhibit a period of

constant temperature. However, the rise in temperature was interrupted by one or more cycles of inflation, rupture or collapse which varied from one drop to another.

In a recent study by Sano and Keey (114) on droplets containing colloidal material, a hollow sphere model (section 4.4) was proposed and equations derived to predict the temperature of an evaporating drop. The temperature history was followed by suspending a drop at the junction of a manganin-copper thermocouple, with wire diameters of  $30\mu\text{m}$ . At high temperatures ( $150^{\circ}\text{C}$ ) the model slightly underestimated the drop temperature, probably because no correction term was included to take account of heat conducted along the thermocouple wires.

As described in section 4.4, Cheong (115) developed a unique method of the simultaneous measurement of drop weight and core temperature. Working with drops of sodium sulphate decahydrate solution he found that at an air temperature of  $20^{\circ}\text{C}$  the core temperature curve showed an initial transient period before equilibrium was established and the core temperature reduced to the wet-bulb temperature. There was then a steady rise in the core temperature as the resistance to heat and mass transfer increased with crust thickness. This was followed by a sharp rise as the core temperature approached the air temperature. This sudden rise in temperature was due to the evaporation interface receding away from the thermojunction resulting in the dry crust temperature being measured. The trend of the core temperature curves at higher temperatures of  $40.7$ ,  $59.3$ , and  $78.3^{\circ}\text{C}$  was found to be rather unusual. After the initial transient period, the core temperature rose gradually until it reached  $33^{\circ}\text{C}$  when there was a sudden fall, before again increasing steeply to the particular air temperature. This was explained by the knowledge that at  $33^{\circ}\text{C}$  sodium sulphate decahydrate crystals melt absorbing heat in the process.

**CHAPTER FIVE**  
**MATHEMATICAL MODELS FOR EVAPORATION FROM**  
**AND DRYING OF SINGLE DROPLETS**

The models which have been developed by previous investigators, to characterise drying of single drops will be described in the following sections. One is for pure liquid drops and the other, a Receding Evaporation Interface model, was proposed to predict the core temperature, evaporation rate and crust thickness of a drop of slurry during drying.

**5.1 Pure Liquid Drops**

This model will be discussed with reference to water drops. A hemispherical drop suspended on a nozzle, with a constant air flow, having an initial temperature  $T_1$  and humidity  $H_1$ , is shown diagrammatically in Figure 5.1 .

Following moisture transfer the downstream or outlet temperature is  $T_0$  and humidity  $H_0$  . In deriving the model Audu (58) made the following assumptions :

- (i) The drop radius  $R$ , was kept constant ( achieved in his experimentation by a controlled liquid feed ) ,
- (ii) The physical properties of air are constant over the temperature range studied ,  
and
- (iii) The air flow rate and inlet temperature are constant.

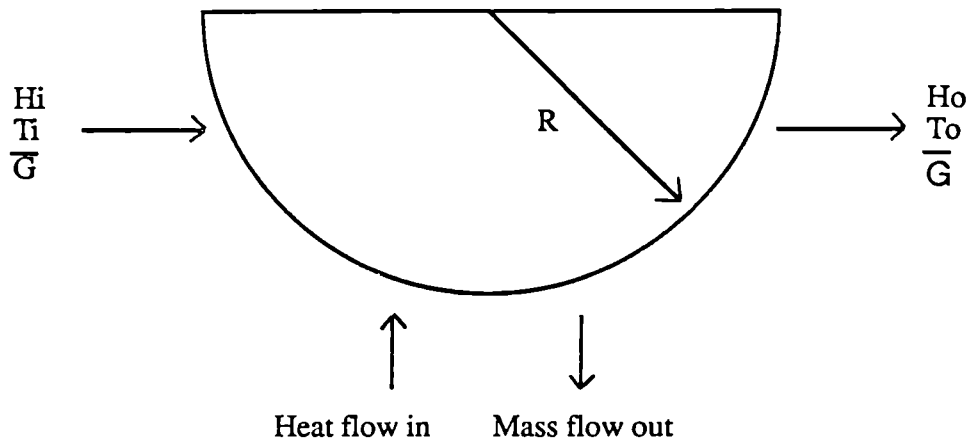


Figure 5.1 Suspended Drop of Pure Liquid

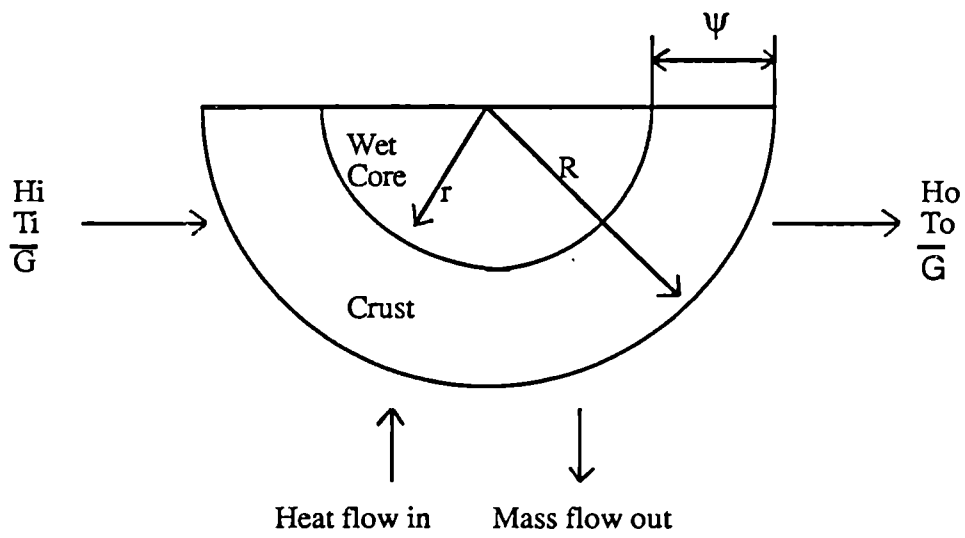


Figure 5.2 Suspended Drop Containing Solids

### 5.1.1 Mass Transfer Rate

#### Suspended Drops

The amount of water evaporated per unit weight of air is, from a mass balance over the suspended drop,

$$\Delta H = H_0 - H_1 \quad \text{---5.1}$$

Therefore, the rate of evaporation,  $N_A$ , is given by,

$$N_A = \frac{G \cdot \Delta H}{A_m} \quad \text{---5.2}$$

where  $A_m$  = area for mass transfer

$$G = \bar{G} / (1 + H_1) \quad \text{---5.3}$$

#### Extension to Free-Flight Drops

By analogy the rate of mass transfer for drops in free-flight can be expressed as,

$$N_A = \frac{dm}{d\theta} \frac{1}{A_e} \quad \text{---5.4}$$

where the equivalent surface area of the drop  $A_e$ , and the equivalent diameter,  $d_e$  are ;

$$A_e = \pi d_e^2 \cdot \text{and } d_e = (2d_h + d_v)/3$$

As explained and illustrated in Sections 7.4, drops in free-flight were not spherical and therefore an equivalent diameter must be defined. The values of  $dm/d\theta$  were obtained from plots of mass against time (see Chapter 8).

### 5.1.2 Mass Transfer Coefficient

The rate of mass transfer is directly proportional to the driving force, and the proportionality constant was denoted K. The driving force used is the humidity driving force defined as,

$$\Delta H = H_s - H_i \quad \text{---5.5}$$

where  $H_s$  = the saturation humidity at the drop temperature  $T_s$ .

The rate of mass transfer can therefore, be expressed as,

$$N_A = k_H (H_s - H_i) \quad \text{---5.6}$$

where  $k_H$  is the mass transfer coefficient in terms of a humidity driving force.

Equation (5.5), can be transformed to yield the pressure driving force  $\Delta P$ , by converting the humidities to pressure analogues (126). Therefore, assuming ideal gas behaviour,

$$H = (M_w \cdot p) / (M_a (P - p)) \quad \text{---5.7}$$

whence,

$$p = \frac{H.P}{\left(\frac{M_w}{M_a}\right) + H} \quad \text{---5.8}$$

Where  $p$  = partial pressure of water vapour

$P$  = total pressure

$H$  = absolute humidity

$M_w$  = molecular weight of water

$M_a$  = molecular weight of air

According to Hinchley and Himus (127), the rate of evaporation is directly

proportional to the pressure driving force;

$$N_A = k_p (p_s - p) \quad \text{---5.9}$$

where  $N_A$  = mass transfer rate per unit area

$k_p$  = the mass transfer coefficient

$p_s$  = vapour pressure of water at wet-bulb temperature

$p$  = partial pressure of water vapour in the environment

The mass transfer coefficient is obtained from equation (5.9) after substituting for  $N_A$  from equations (5.2) and (5.4) ;

$$k_p = \frac{G \cdot \Delta H}{A_m (p_s - p)} \quad \text{---5.10}$$

Equation (5.10) can, however, be modified to give the mass transfer coefficient as,

$$k_g = \frac{G \cdot \Delta H}{A_m (p_s - p)} \cdot \frac{R_c T_i}{M_w} \quad \text{---5.11}$$

where  $k_g$  has units of cm/s.

Audu was the first to apply equation (5.11) to suspended drops.

Similarly for the new case of a free-flight drop, the mass transfer coefficient can be expressed as,

$$k_g = \frac{dm \cdot l}{d\theta A_e} \frac{R_c T_i}{M_w (p_s - p)} \quad \text{---5.12}$$

The Sherwood number is defined as,

$$Sh = \frac{k_g d_e}{D_v} \quad \text{---5.13}$$

Substituting equation ( 5.12 ) into ( 5.13 ) gives,

$$Sh = \frac{dm \cdot l}{d\theta A_e} \frac{R_c T_i}{M_w (p_s - p)} \frac{d_e}{D_v} \quad \text{---5.14}$$

### **5.1.3 Nusselt Number**

Cheong (115) made the following assumptions in determining the experimental value of the Nusselt number :

- (i) The drop is spherical with a constant density ;
- (ii) The temperature driving force remains constant ;
- (iii) The temperature at the surface of the drop is equal to the wet-bulb temperature ;
- (iv) The latent heat of vaporisation and thermal conductivity are evaluated at the mean temperature between the air and the drop.

The rate of mass transfer from a spherical drop can be expressed as ,

$$\frac{dw}{d\theta} = \frac{dQ/d\theta}{\lambda} \quad \text{---5.15}$$

The heat transfer to the drop can be determined from,

$$dQ/d\theta = h_g A_h \Delta T \quad \text{---5.16}$$

Substituting equation (5.16) into (5.15) gives,

$$\frac{dw}{d\theta} = \frac{h_g A_h \Delta T}{\lambda} \quad \text{---5.17}$$

Since the weight of a spherical drop is,  $w = \pi d_p^3 \rho_d / 6$  , and for the present case

of a spheroidal free-flight drop,  $w = \pi d_e^3 \rho_d / 6$ , equation (5.17) becomes,

$$h_g = - \frac{\lambda \rho_d \cdot 1}{6 \Delta T d_e^2} \cdot \frac{d(d_e^3)}{d\theta} \quad \text{---5.18}$$

where the area of a spheroidal drop  $= \pi d_e^2$ .

The Nusselt number Nu, is defined as,

$$Nu = \frac{h_g d_e}{K_d} \quad \text{---5.19}$$

Substituting equation (5.18) into the above expression gives,

$$Nu = - \frac{\lambda \rho_d \cdot 1}{6 K_d \Delta T d_e} \cdot \frac{d(d_e^3)}{d\theta} \quad \text{---5.20}$$

Since ,

$$\frac{d(d_e^3)}{d\theta} = 3d_e^2 \cdot \frac{d(d_e)}{d\theta}$$

therefore,

$$Nu = - \frac{\lambda \rho_d \cdot d_e}{2 K_d \Delta T} \cdot \frac{d(d_e)}{d\theta} \quad \text{---5.21}$$

The instantaneous value of  $d(d_e)/d\theta$  at each drop size can be determined from a

plot of  $d_e$  against  $\theta$  ( see Figures 8.4-8.6 ).

#### **5.1.4 Heat Transferred to a Drop by Radiation**

A droplet within a spray tower, or in a wind tunnel, receives some heat by radiation in addition to the main contribution from forced convective heat transfer. Therefore, radiation effects may have to be taken into account.

The radiative heat transfer rate  $q_e$ , can be expressed as,

$$q_e = \sigma A F_a e (T_g'^4 - T_s'^4) \quad \text{---5.22}$$

The geometry factor  $F_a$ , may be assumed to be unity since the drop is surrounded by the drying chamber.

#### **5.1.4 Heat Transferred to a Drop Through the Suspension Device**

Since the drop suspension device will itself be exposed to the drying air, some heat will be transferred to the drop along the nozzle/filament by conduction. In deriving the expression for this heat input Cheong (115) made the following assumptions, for conduction along a glass filament :

- (i) Heat is transferred to the filament from the surroundings by radiation and convection ;
- (ii) The physical properties of the filament are constant ;
- (iii) The temperature around the filament is constant and equal to the temperature of the air ;
- (iv) There is no radial temperature gradient ;
- (v) The length of the filament is much longer than the diameter, i.e infinite length ;
- (vi) The heat transfer coefficient on the surface of the filament is constant.

Considering the filament as a cylinder the final expression for the heat transferred through the filament was,

$$q_f = \frac{\pi}{2} \left[ \frac{K_t d_f^3}{5} \left( 2\sigma e_g (T_s'^5 - T_g'^5) - 10\sigma e_g T_g'^4 (T_s' - T_g') + 5h_f (T_s' - T_g')^2 \right) \right]^{0.5} \quad \text{---5.23}$$

## 5.2 Drops Containing Dissolved Solids -The Receding Evaporation Interface Model

Consider a hemispherical drop suspended from a nozzle as shown in Figure 5.2 and let the following assumptions be valid (58,115),

- (i) There is a receding evaporation interface between the solution and the crust. As drying proceeds, the crust grows inwards and the external radius of the drop remains constant. The internal radius,  $r$ , is therefore a function of time,  $\theta$  ;
- (ii) The crust, once formed, is porous and thus pore diffusion is the mechanism of moisture movement from the interior of the drop to the exterior ;
- (iii) The water-vapour storage within the crust is negligible ;
- (iv) The core temperature,  $T_c$ , is uniform throughout the core ;
- (v) Air flow rate, air temperature and other physical properties of the air are constant ;
- (vi) Heat is transferred from the drying air to the crust by convection and it is transferred through the crust by conduction ;
- (vii) The core density remains constant during the evaporation process, i.e as water evaporates at the interface, it precipitates an equivalent mass of solid as crust.

Cheong (115) in his work on the drying of drops of aqueous solutions of sodium sulphate used this model to derive three equations which on simultaneous solution give the crust thickness, core temperature and weight of the drop as a function of time, viz.

$$\frac{dx}{d\theta} = \frac{b_1}{b_2x^2 + b_3x} \cdot \frac{p_g - p_c}{T_c} \quad \text{---5.24}$$

$$\frac{dT_c}{d\theta} = \frac{a_1/a_2}{a_2x^2 + a_3x} \cdot \frac{T_g - T_c}{x} + \frac{b_1/a_4}{b_2x^2 + b_3x} \cdot \frac{p_g - p_c}{T_c x} \quad \text{---5.25}$$

and,

$$\frac{dw}{d\theta} = 4 \pi x^2 \rho_c \frac{b_1}{b_2x^2 + b_3x} \cdot \frac{p_g - p_c}{T_c} \quad \text{---5.26}$$

where,

$$a_1 = R^2 h_g k_c / \rho_c x_w (\lambda - C_c)$$

$$a_2 = k_c - R h_g$$

$$a_3 = R^2 h_g$$

$$a_4 = Cp / 3x_w (1 - C_c)$$

$$b_1 = R^2 D_v M_w k_g / \rho_c x_w R_c$$

$$b_2 = D_v - R k_g$$

and,  $b_3 = R^2 k_g$

The major drawbacks of this model as related to the present investigation are the following :

- (i) The model assumes that the drop is a rigid sphere. However, in free-flight, prior to rigid crust formation, the drop undergoes oscillations, rotations and random deformations. With such drop behaviour the model will tend to substantially underestimate the mass transfer rates (see section 9.2.3 ).
- (ii) The model does not take into account drop inflation, fracture or shrinkage.

and,

- (iii) The model is restricted to conditions whilst there is still a wet core, yet hollow spheres may result from extended drying times.

Of these (ii) is most fundamental since many droplets undergo dimensional changes in practical spray-drying which would strongly influence drying. If fracture or a blow-hole occurs, the interfacial area and the path and mechanism of moisture transfer may change .

### **5.2.1 Crust Thickness**

From a mass balance over the drop, the amount of water-vapour evaporated during any time interval  $\Delta\theta$  is,

$$\Delta w = G ( H_d - H_u ) \Delta\theta \quad \text{---5.27}$$

However,  $\Delta w$  is also equal to the quantity of water displaced in forming a crust of

thickness ( R - r ). This is represented mathematically for a hemi-spherical drop as;

$$\Delta w = 2/3 \pi C_o ( R^3 - r^3 ) \quad \text{---5.28}$$

By rearrangement of equations (5.27) and (5.28) the crust thickness  $\psi$  , becomes ;

$$\psi = R - \left[ R^3 - \frac{3}{2} \frac{G}{\pi C_o} [H_d - H_w] \Delta \theta \right]^{1/3} \quad \text{---5.29}$$

The crust thickness can thus be predicted from equation (5.29) , which was first developed by Audu (58).

### 5.2.2 Mass Transfer Coefficient

The overall resistance to transfer of water-vapour from the wet core to the air is obtained by treating the resistances to mass transfer through the crust and the boundary-layer or gas-film in series. Thus,

$$\frac{1}{K_o} = \frac{1}{k_g H_1} + \frac{1}{k_c} \quad \text{---5.30}$$

where,

$K_o$  = overall mass transfer coefficient ;

$k_g$  = gas-film mass transfer coefficient for pure water drops, deduced from equation (5.11) ;

$H_1$  = Henry's law constant.

The mass transfer coefficient of the crust  $k_c$ , is a function of the diffusivity of the

water-vapour, porosity and the crust thickness and may be expressed as ,

$$k_c = \frac{D_v \varepsilon^{1.5}}{\psi} \quad \text{---5.31}$$

The basis of the above equation is given in Appendix A5. Therefore , the value of the mass transfer coefficient of the crust can be obtained from equation (5.31) and then used in equation (5.30), to evaluate the overall transfer coefficient.

### **5.2.3 Crust Porosity**

An increase in porosity,  $\varepsilon$  , would tend to increase the drying rate of drops containing dissolved or suspended solids. Audu (58) used a modified form of the Kozeny (128) equation , given below, to calculate the porosity of detergent slurry drops:

$$\varepsilon = \left[ \frac{5G \cdot S_b^2 \cdot v \cdot \psi}{2\pi d_c \cdot \Delta P} \right]^{1/3} \quad \text{---5.32}$$

The above equation was subsequently, used by Ali (137) in his work using drops of sodium sulphate decahydrate, and organic and inorganic products. For this purpose the crust thickness  $\psi$  was obtained using a high resolution Scanning Electron Microscope and the pressure drop across a crust,  $\Delta p$ , by using an apparatus consisting of two tubes, a rotameter, a U-tube manometer and a crust support ; this enabled dry air to be blown through the crust.

The fundamental assumption in such single drop studies is that the particle morphology is independent of size, i.e., that a 1mm - 5mm drop forms

crusts of similar structure to drops in the size range 10 - 1000 $\mu$ m in a spray drier, providing only that the initial slurry or solution concentration and the air temperature are identical. This is being examined in a separate investigation (140).

## **CHAPTER SIX**

### **EXPERIMENTAL INVESTIGATION**

#### **6.1 Description Of Apparatus**

##### **6.1.1 Overall Arrangement**

The vertical wind tunnel for free-flight drop studies, which followed the original design of Lihou (149), is shown in Figure 6.1 and illustrated diagrammatically in Figure 6.2. It consisted of a closed circuit of rectangular and circular ducting constructed of 10 gauge mild steel sheet. Air from the 0.75 kw 3-phase centrifugal fan, A, expanded through the horizontal duct, B, to a large cubical settling chamber, C, where two rows of five and three 1kw heater elements, D, were mounted to heat the circulating air. To reduce the size of the turbulent eddies, and to assist the 90° change in direction of the air flow, a fine stainless steel gauze of 30/30 mesh was placed diagonally across the flow and another at the exit to the settling chamber. The suction flare, E, reduced the cross-section without re-introducing turbulence.

In the smoothing section, F, four damping screens, G, served to provide the gas stream with a reasonably uniform velocity across its cross-section. In the smooth contraction, H, the parallel filaments of air were brought together and accelerated while further reducing the intensity of turbulence. Between the smooth contraction and the working section, J, an aluminium 20/20 screen mesh, I, was inserted. This was shaped specifically to modify the uniform velocity profile of the air stream, producing an inverted velocity profile on the axis of the working section, as described in section 6.1.4 and illustrated in Figure 7.3. The mesh was placed in a

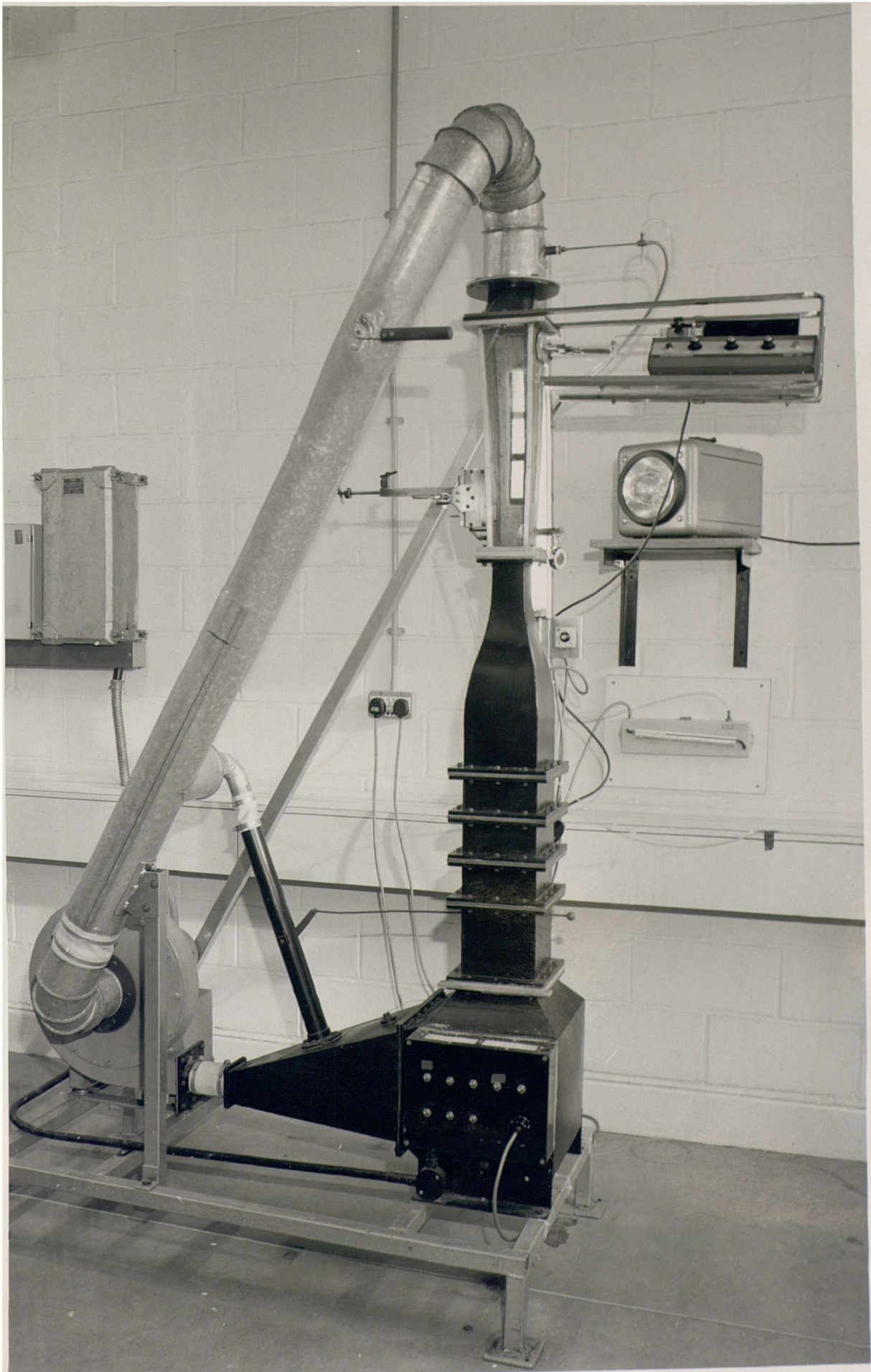
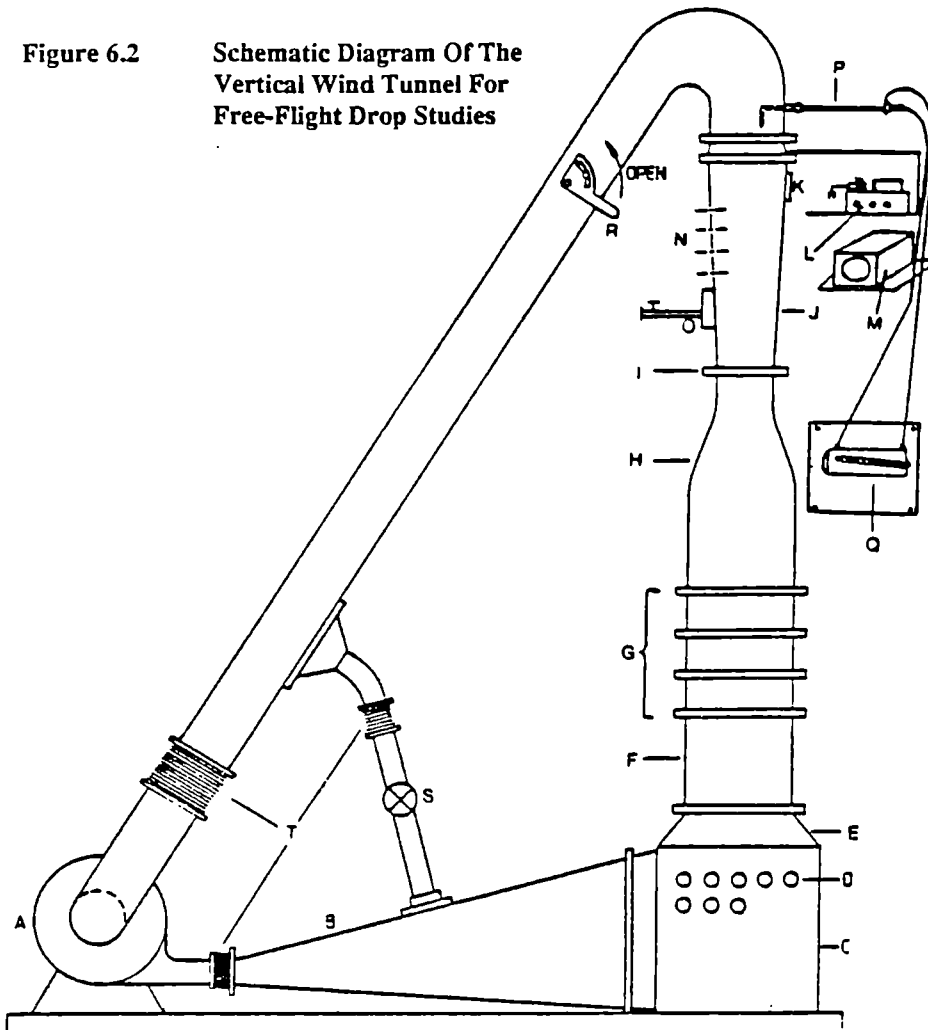


**Figure 6.1 General Arrangement of the Vertical Wind Tunnel**

**Figure 6.2**      **Schematic Diagram Of The  
Vertical Wind Tunnel For  
Free-Flight Drop Studies**



A Fan	H Smoothing Contraction	N Tapped Hole For Thermocouple And Pitot Tube
B Expansion Duct	I Screen Mesh	O Drop-Catching Mechanism
C Settling Chamber	J Working Chamber	P Fixed Pitot Tube
D Heater Elements	K Tapped Hole For Drop Producing Unit	Q Inclined Manometer
E Suction Flare	L Drop Forming System	R Velocity Control Valve
F Smoothing Section	M Stroboscope	S Butterfly Valve
G Damping Screens	T Rubber Connections	

removable frame to enable rapid access for cleaning. Another screen mesh was installed above the working section to protect the fan from any item dropped into the working section accidentally, and to prevent blocking of the damping screens in the smoothing section by any dried particles carried away in the air flow during drying experiments.

The working section shown in Figure 6.3 and illustrated diagrammatically in Figure 6.4 diverged with a  $3^\circ$  total angle. This divergence provided a vertical velocity gradient such that the velocity decreased downstream i.e in the upward direction to a droplet. This enabled the droplet to find its own level of stability. The front wall was of glass cemented into the other three walls of aluminium. Similar glass windows were let-in to one side and the back for illumination purposes, using a stroboscope, M. A 5.2 cm diameter hole, K, was cut at the top right hand wall through which the drop-forming unit, L, described in section 6.1.2, was inserted. After the drop had been produced and the drop forming unit removed the hole was sealed by sliding a flat aluminium plate, measuring 5.5cm x 6.5cm x 0.5cm across the hole. Four 6mm diameter holes, N, drilled in the left hand wall and spaced 5.2cm apart vertically allowed insertion of a pitot tube and a thermocouple. When not in use these holes were plugged with removable bolts to allow easy access. The drop-catching mechanism, O, attached to the same side of the working chamber is fully described in section 6.1.3.

A pitot tube P, was fixed at the top of the working section to allow measurements of the flowrate by direct calibration of an inclined manometer Q, against another pitot tube (see section 7.2).

A control valve R, was used to regulate the air flowrate at the test section, to adapt to the change in the terminal velocity of the droplet due to mass transfer. A butterfly valve S, was used for delicate alterations.

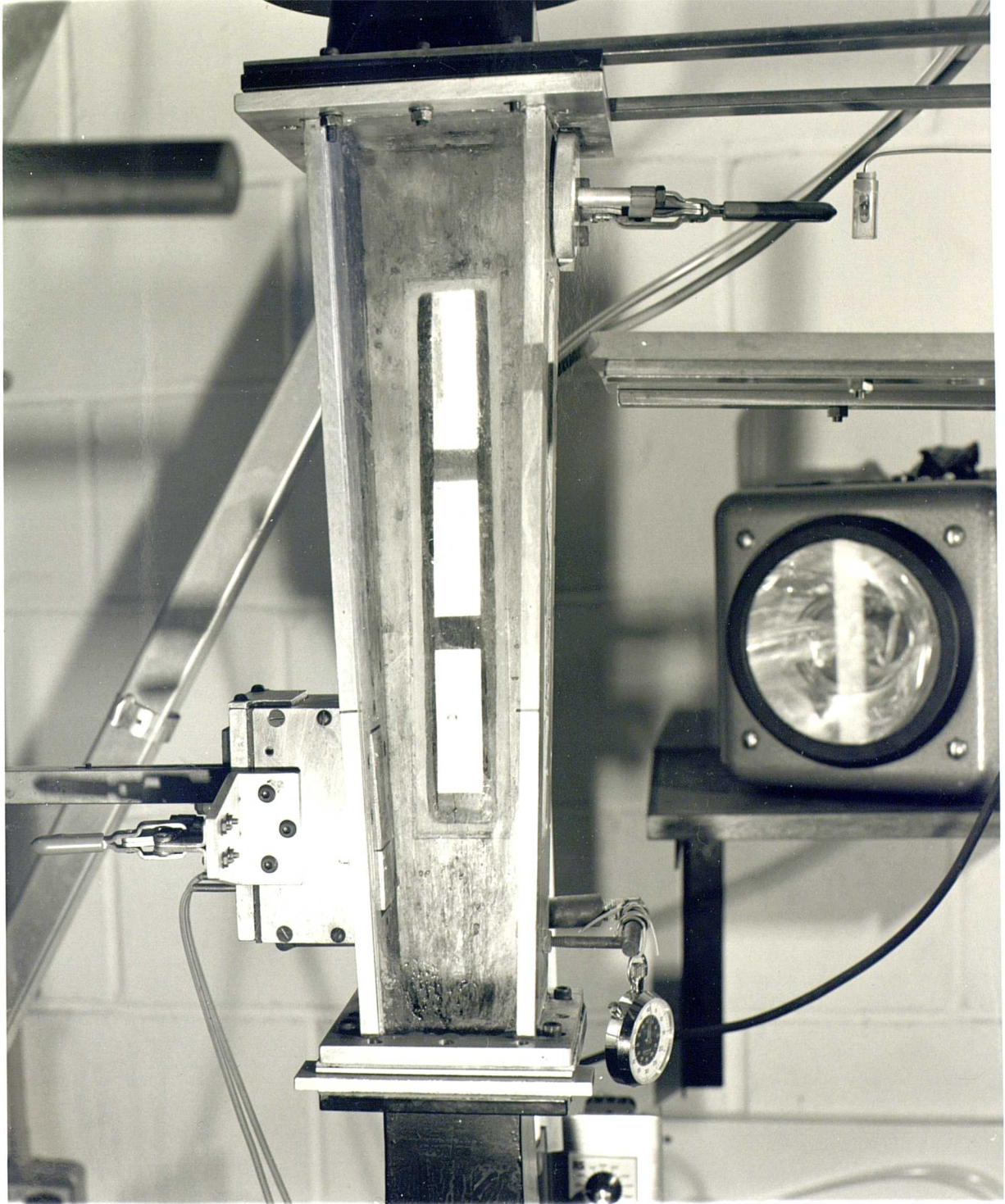
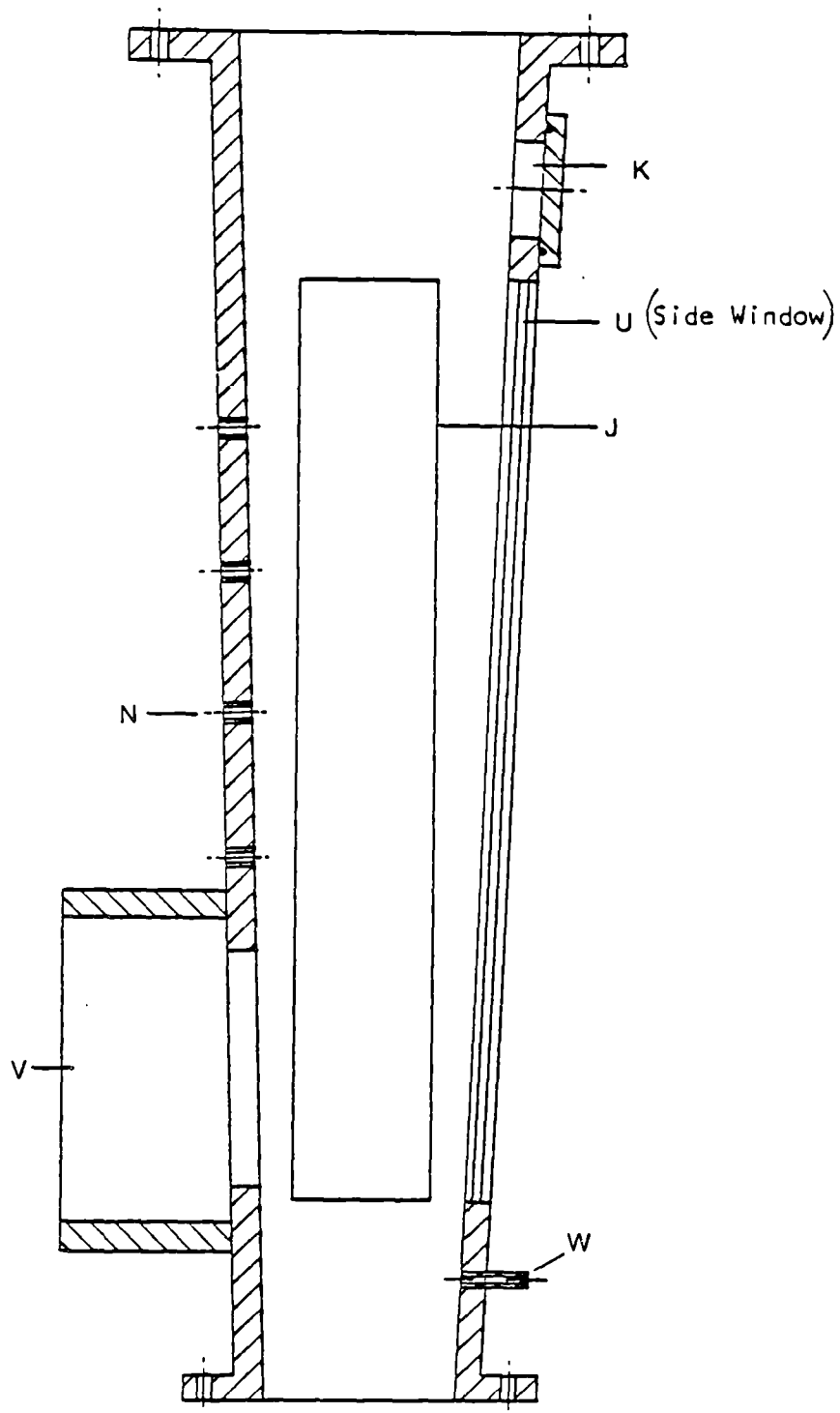


**Figure 6.3 Working Section of the Experimental Apparatus**



Item	Description
W	Standard Pressure Tapping
V	Housing for Drop-Catching Unit
J	Rear Window
K	Hole for Drop-Forming Unit
N	Pitot Tappings

Figure 6.4 Working Section of Free-Flight Drop Experimental Apparatus.

### **6.1.2 The Drop-Forming System**

Details of the apparatus are shown schematically in Figure 6.5. It comprised a 10ml. plastic syringe A, containing the liquid to be studied. The liquid was then passed via a hypodermic needle B, to a plastic nozzle C, mounted in a rubber bung D. Nozzles with different outer diameters, in the range 2-4mm, were used to obtain different drop sizes. Before the drop was released from the nozzle i.e during its formation, it was shielded from the air flow by a short length of perspex tubing E.

The plastic syringe was connected to a syringe pump (model 351 by Sage Instruments) as shown in Figure 6.7 and the whole system mounted upon two parallel grooves. With this arrangement it was possible to slide the drop forming system into the air stream, inject the drop and remove the system again, all with one hand-the other hand being used to start the stop watch.

In previous work (141) drops were introduced into the wind tunnel by inserting the drop forming device into the working chamber by hand and generating a drop by depressing the syringe plunger manually. However, in practice the nozzle could not always be replaced exactly in a vertical position and it also tended to shake, due to the unsteadiness of the operator's hand when depressing the plunger. Hence, this method of drop insertion resulted in an error of about 12% in drop size repeatability.

Introduction of a syringe pump minimised operator intervention. The syringe plunger was controlled automatically to give a fixed flowrate and the nozzle inserted into the wind tunnel exactly in the same position each time. This technique reduced the error in drop size repeatability to < 2%.

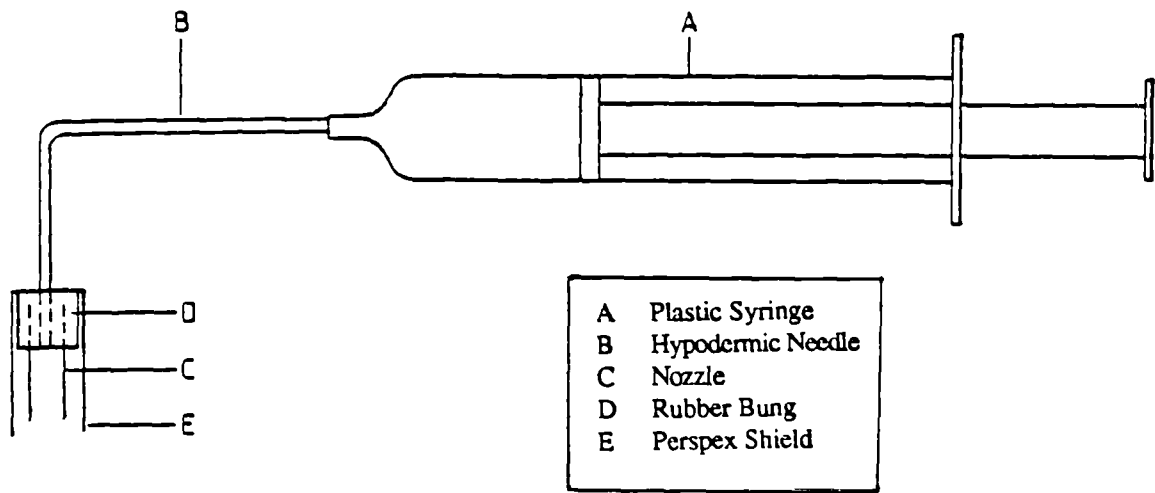


Figure 6.5 Drop-Forming System

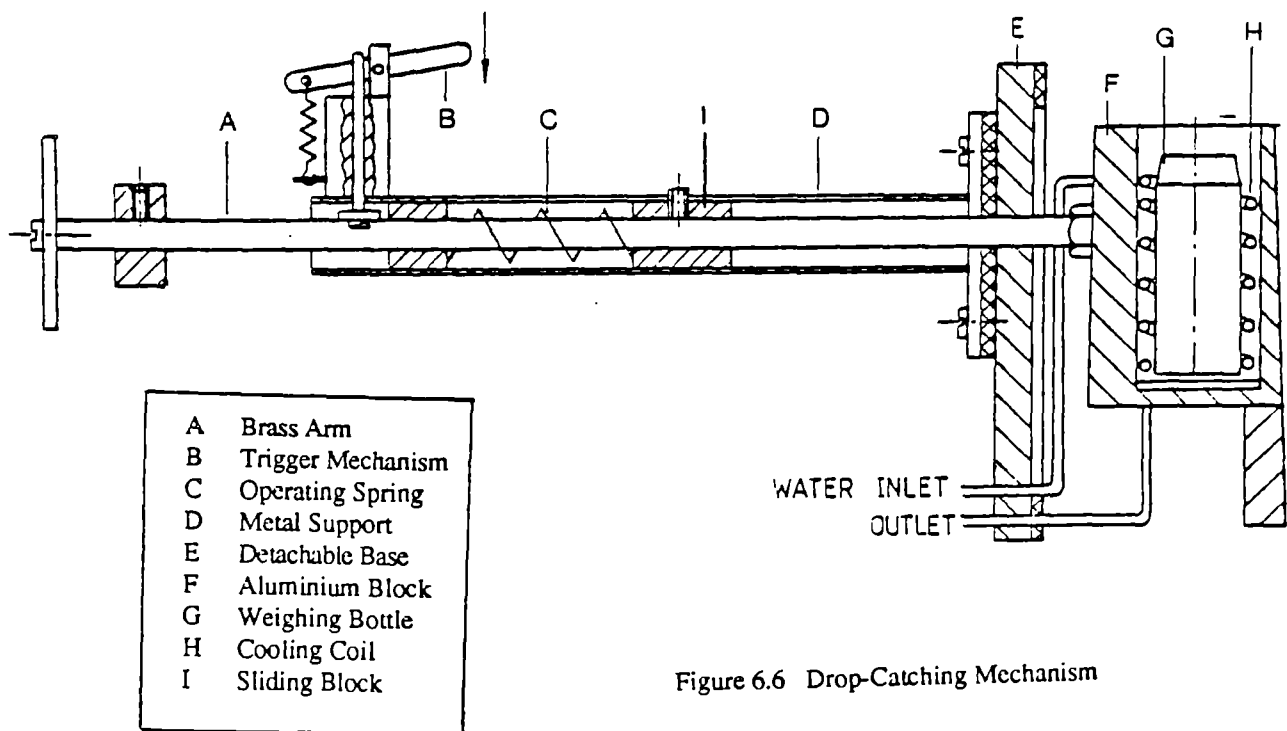


Figure 6.6 Drop-Catching Mechanism

### 6.1.3 The Drop-Catching Mechanism

Drops were produced and stabilised in the working section one at a time, each being caught and removed before the next was produced. A special cup was designed to retrieve drops from the working section for weighing. It held a small bottle for catching the drops so that they were removed rapidly from the air stream without further mass transfer during, or after, collection. Except during collection the cup remained retracted through the wall of the working section.

The design for the introduction and removal of the cup is shown in Figure 6.6 and Figure 6.8. The aluminium block F, which carried the weighing bottle G, was supported from a brass rod, A. The latter carried a square section block I, which slid in a square section tube, D. This tube was rigidly fixed to the detachable back E, of a box fixed to the side of the working section. The movement of the slide was controlled by adjustable stops at either end of its travel. The slide was pushed forward by means of a spring, and drawn back by hand. A trigger mechanism B, was used for retaining the slide in the retracted position and for releasing it when required.

When the wind tunnel was operating at temperatures above ambient the temperature of the cup could be maintained at 25°C by the use of a cooling coil, H. The coil of 2mm outside diameter and 1.5mm inside diameter stainless steel tube lined the recess in F. Cooling water was fed to the coil via rubber tubing which did not hinder the rate at which the block could be shot into the working chamber.

Drops were caught in the cup by introducing it quickly through the side wall of the working section. The presence of the cup cut off the air stream in the region where the drop was stabilised and so the drop, losing its support, fell into the bottle which was then immediately withdrawn. After catching the drop it was important to seal the bottle as quickly as possible to reduce subsequent mass

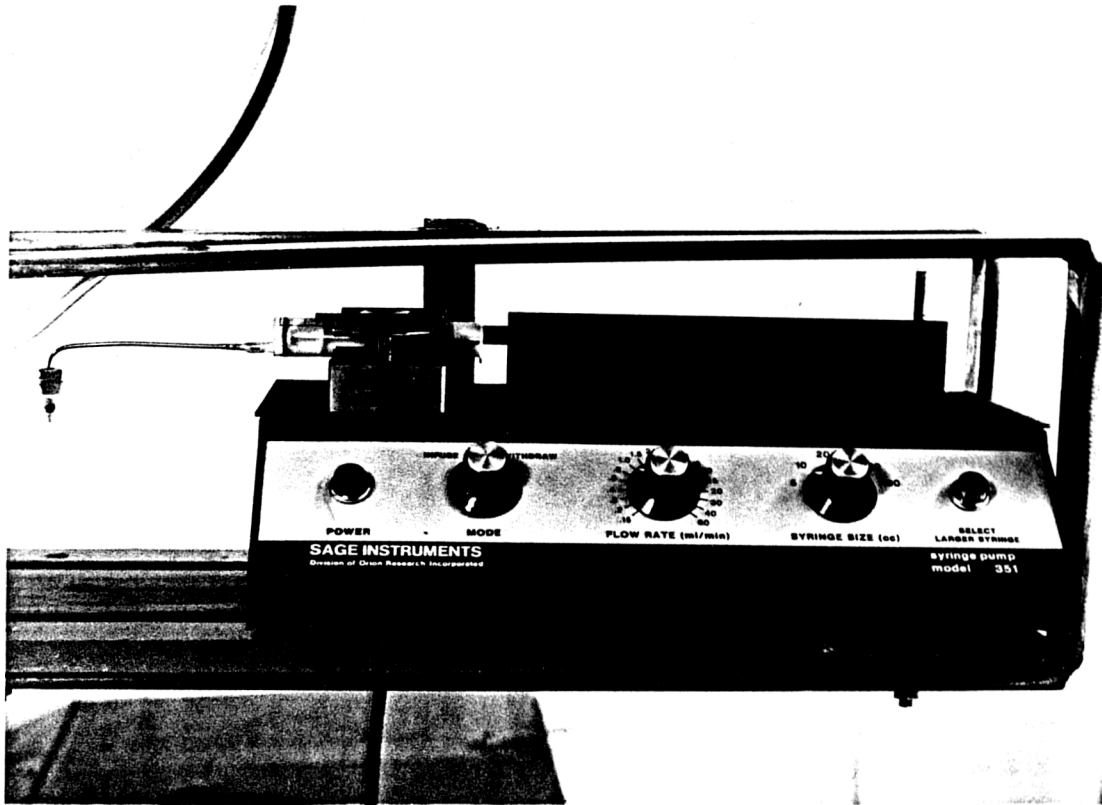


Figure 6.7 Drop Forming Unit Connected to a Syringe Pump

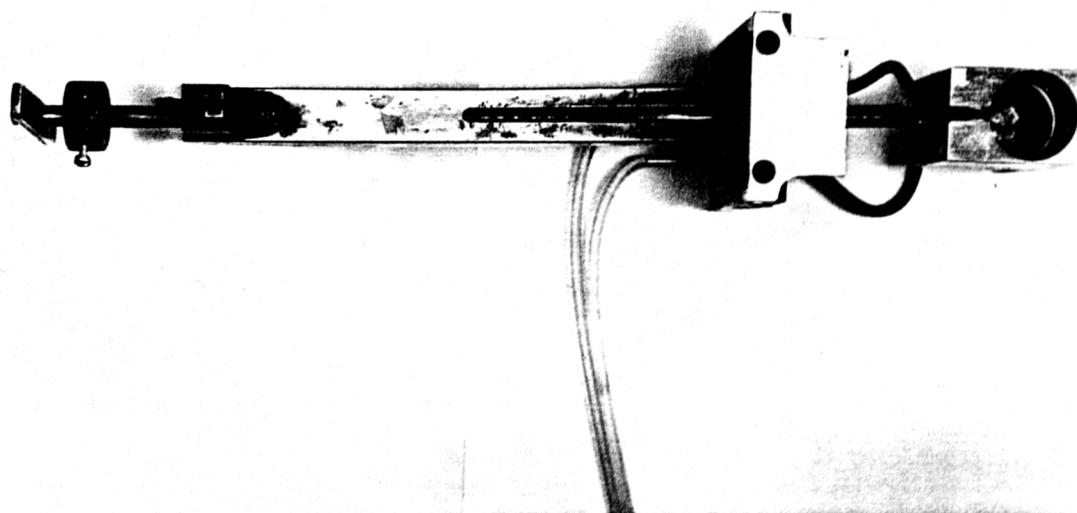


Figure 6.8 Drop-Catching Unit

transfer.

#### **6.1.4 Shaped Wire Gauze To Produce The Inverted Velocity Profile**

When a droplet is placed in an ascending air current with a velocity equivalent to the terminal velocity of the droplet, the droplet may remain suspended in the air stream. In practice however, a floating droplet cannot be maintained for long before it is carried away by the air stream. This occurs because the droplet shape varies continuously and a gradual decrease in droplet diameter results in a reduction in its terminal velocity.

A droplet can however, be made to float in the working section for a much longer time period ranging to several hours, the exact time depending on the initial drop size and the nature of the material being investigated, by modifying the uniform velocity profile(1). The modified profile assumed an 'inverted' parabolic shape. This was achieved in the present study by inserting a screen mesh in the entrance to the working section. The screen mesh modified the shape of the velocity profile to produce a reduced velocity region in the central part of the air stream, surrounded by an annular region of higher velocity flow. When the air velocity was adjusted to the terminal velocity of a droplet injected in the low velocity region, the drop floated for a longer time than in the uniform stream without the screen mesh. Even if the droplet moved in a radial direction due to turbulence, it was returned to the central, low velocity, region by the higher velocity air currents in the annular region. If the droplet was injected into the higher velocity region it was carried away in the air stream. However, if the droplet was inserted at the boundary of these two flow regimes, it rotated and moved back to the low velocity region.

Droplet oscillations, rotation and deformation which were seen to take place, were predominant in the initial stages of its life but diminished as it became smaller and more spherical. However, each individual drop adjusted its position of balance automatically to accommodate these changes. This caused occasional rapid,

though stable, up-and-down movements of a drop over a range up to 8-12 cm. Lateral movement of drops was negligible. A number of screen meshes of different shapes and mesh sizes were tested in order to establish the best possible velocity profile giving the most stable droplet. After looking at a number of possibilities, it was found that an aluminium screen with a 20/20 mesh size, assuming the shape shown in Figure 7.3, gave the best results. Thus an aluminium gauze, producing the required minimum at the axis, as shown in Figure 7.3, was used for subsequent experiments.

### **6.1.5 Strobe Light**

As mentioned in section 6.1.4 a droplet experienced occasional rapid vertical movements especially in the earlier stages of its drying history. When using an ordinary fluorescent tube to illuminate the drop for video recording it was found that the drop appeared as a blurr during its vertical movements. However, by using a strobe which was synchronised with the video camera it was found that the extremely short pulse width of the light very effectively froze the movements of the drop in its vertical motion. The brief exposure clearly showed details of the droplet in its axial movements previously recorded only as a blurr. To produce a stroboscopic effect capable of being recorded by a video camera it was necessary to synchronize the triggering of the strobe light to precisely match that of the start of the individual frame signal from the video camera. A Sony black and white video monitor was used for this purpose. It was connected in parallel with the camera and recorder, as shown in Figure 6.9, and at this point was capable of producing its own internal line and frame pulses synchronised with that of the camera. A suitable frame signal was identified within the monitor's circuitry and brought out to the 'strobe light

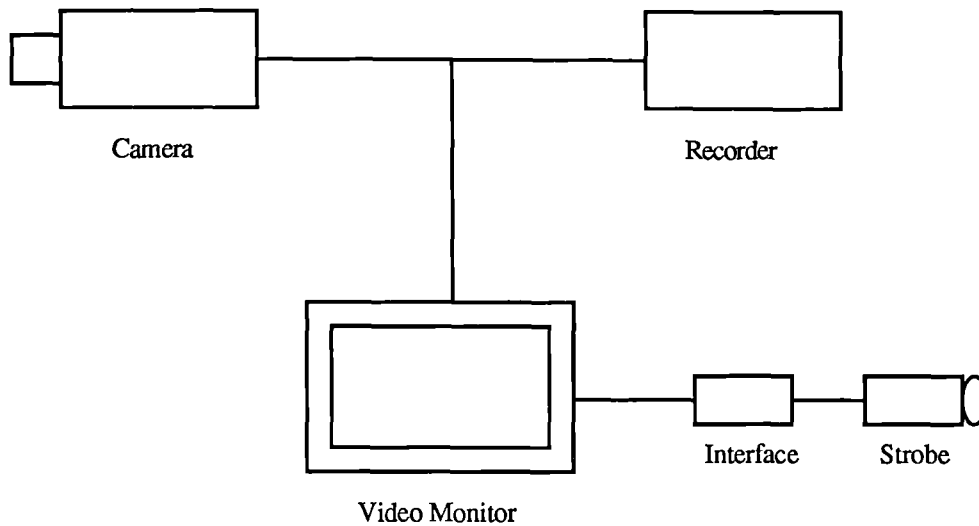


**Figure 6.9 Schematic Diagram of a Strobe Synchronised with a Video Camera**

interface'. This consisted briefly of simple buffer/amplifiers and output driver stage to produce the correct voltage level signal to trigger the input stage of the strobe light. The maximum repetitive flash rate of the strobe light was well in excess of that of the frame rate.

The videos obtained are listed in Appendix A6 and the tapes have been deposited in the Department Library.

## Chapter Seven

### Experimental Procedure

#### 7.1 Operation Of Apparatus

At the start of a series of experiments the fan was started and the appropriate heaters were turned on to provide any air temperature within the range 35 to 145 °C. The apparatus reached a steady temperature after about 2 hours. During this time 12 weighing bottles were washed out with acetone, polished free of any remaining grease or dirt, and left to stand for at least 20 minutes in the balance room before being carefully weighed.

When the apparatus had reached the desired operating temperature a weighing bottle was introduced in the hole in the collection block and the nozzle was prepared. The cooler around the collection cup was now turned on to prevent further evaporation taking place once the drop had been caught. Before doing a run a few drops were purged from the nozzle to make sure no air bubbles or small particles of rubber from the bung were included in the drop. The 5.2cm hole was then uncovered, the nozzle slid into the working section and a drop was released. A range of drop sizes for pure liquids and for solutions was covered (see section 7.6). The nozzle was then removed and the hole covered again. The evaporative and drying behaviour of a drop was recorded using a photographic technique (see section 7.4).

After a predetermined time interval the drop was caught in the weighing bottle, which was shot under the drop by the spring loaded carrier as described in section 6.1.3. The air flow was cut off and the drop fell into the bottle, which was then removed with the carrier. In order to catch a drop cleanly it had to be stabilised at the correct height in the working section, which was found to be

about 2-3cm above the collection cup. With experience it was found that most drops, especially the smaller ones, could be caught cleanly. After a drop was caught the cover was placed on the weighing bottle, another placed in the collection block and the drop unit clamped into position again. The period between pressing the trigger on the unit and placing the cover on the weighing bottle was about 5 seconds. The unit was replaced as quickly as possible to prevent too much cold atmospheric air being drawn into the apparatus.

## **7.2 Flow Rate Calibration For Axial Velocity**

As mentioned in section 6.1.1 a manometer (Type 504) was calibrated against a pitot tube which was inserted at a height of about 2cm above the collection cup and the mid-point of the velocity profile. The differential pressure readings from this pitot tube were converted to the axial velocities. These were then plotted against manometer readings as shown in Figure 7.1, for air temperatures of 37,67 and 97°C. These calibration charts were subsequently used to determine the droplet terminal velocity at any instant during a run.

## **7.3 Measurement Of Air Temperature And Velocity Profile In The Working Section**

After about 2 hours, when no further change in temperature was observed, a Ni-Cr/Ni-Al thermocouple was inserted through a side hole into the centre of the working chamber. The air stream temperature distribution was obtained by taking temperature readings at different distances from the centre of the test section. Typical temperature profiles for different working temperatures

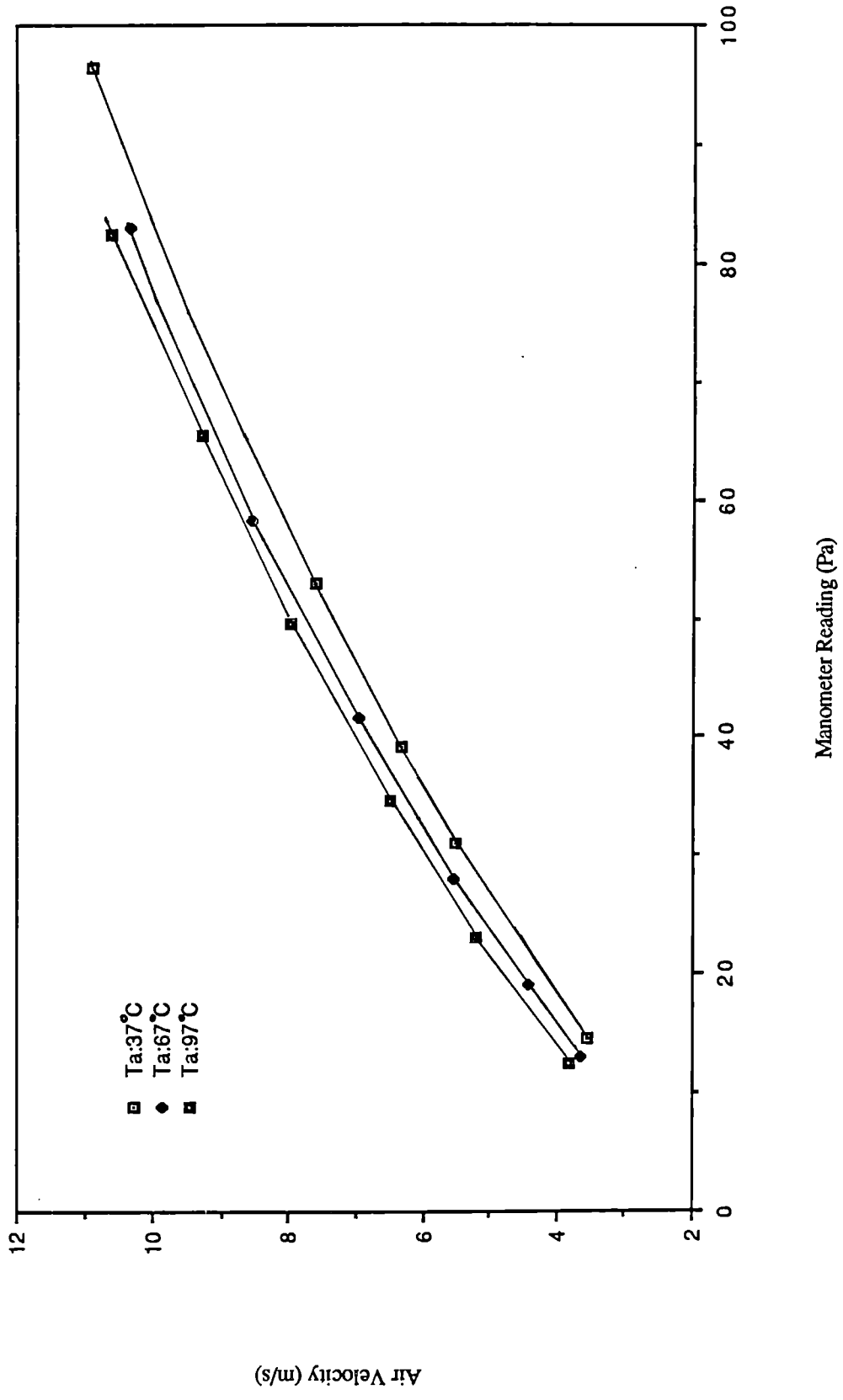


Figure 7.1 Velocity Calibration Curves

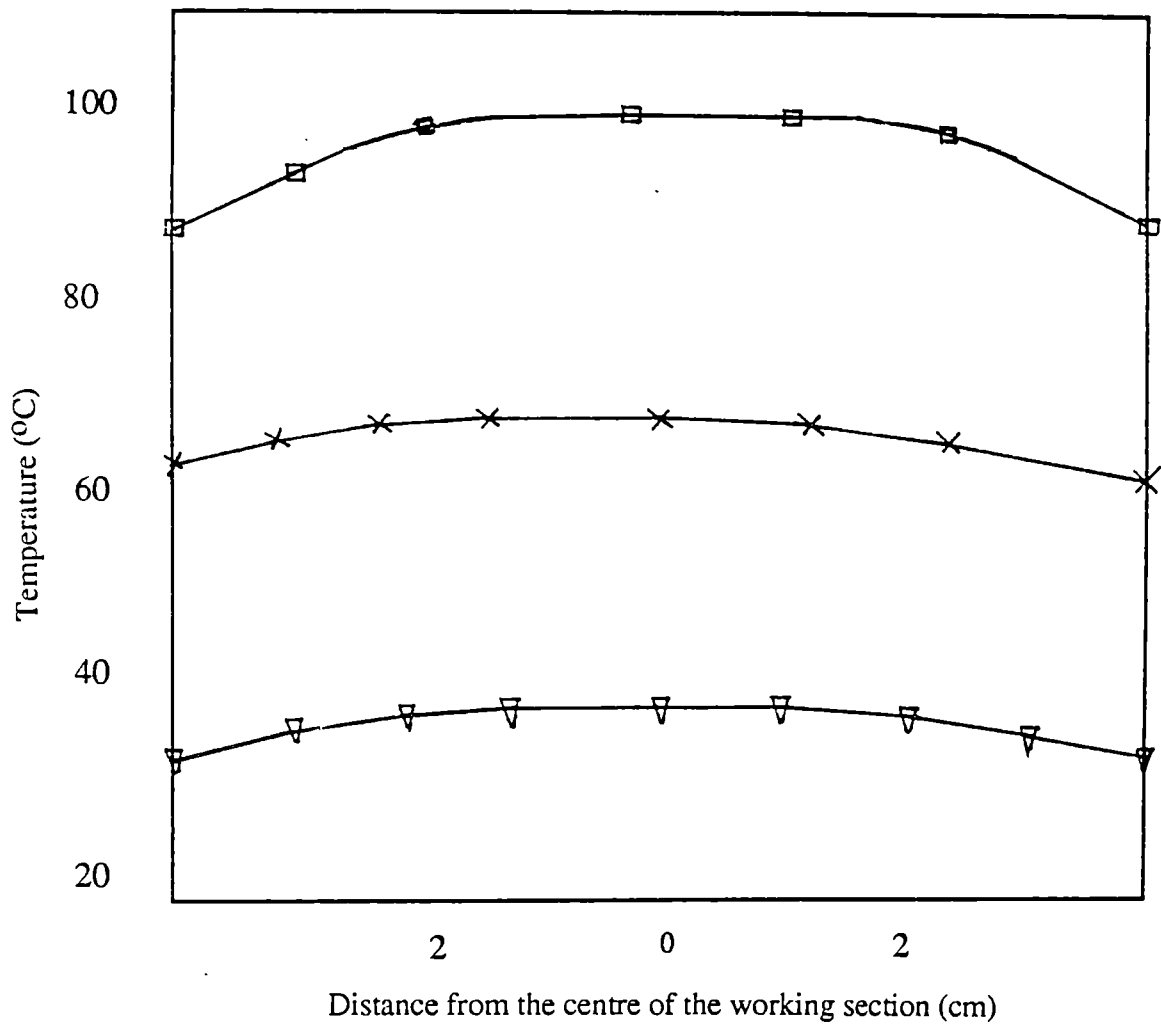


Figure 7.2 Temperature Distribution of Air in the Working Section for Different Operating Temperatures

are shown in Figure 7.2.

The velocity profile in the test section was determined by traversing a pitot tube across the test section and Figure 7.3 shows the profiles at varying heights from the screen mesh. As explained in section 6.1.4 the profiles were uniform with the required minimum on the axis of the wind tunnel.

#### **7.4 Measurement of Drop Dimensions**

A photographic technique was used to record drop dimensions. A JVC video camera ( model GX-N70E ) was placed at a fixed distance in front of the test section and at the beginning of each run an accurate perspex rule was brought next to the working section to give the magnification. The exact time of each diameter measurement was accurately determined since the camera contained an inbuilt timer.

A stroboscope was used for illumination purposes ( see section 6.1.5 ) which was fixed to shine through the glass window at the back of the working section. Translucent white paper was positioned over the glass to diffuse the light and black stripes were sealed on the window to give a sharp definition of the droplet.

The video film was viewed on a T.V screen and for each measurement the drop was stabilised on the screen and the drop dimensions measured using an accurate perspex rule.

In the present study photographic evidence has shown that as a good approximation to the equilibrium shape, deformed drops in air can be represented by a spheroid, having major horizontal axes and a minor vertical axis. Figure 7.4 shows such a spheroid having a leading front (ADC) facing the oncoming air, and a rear side (ABC). The rear section resembles a hemisphere whilst the front section is slightly flat-bottomed due to impingement of the air stream.

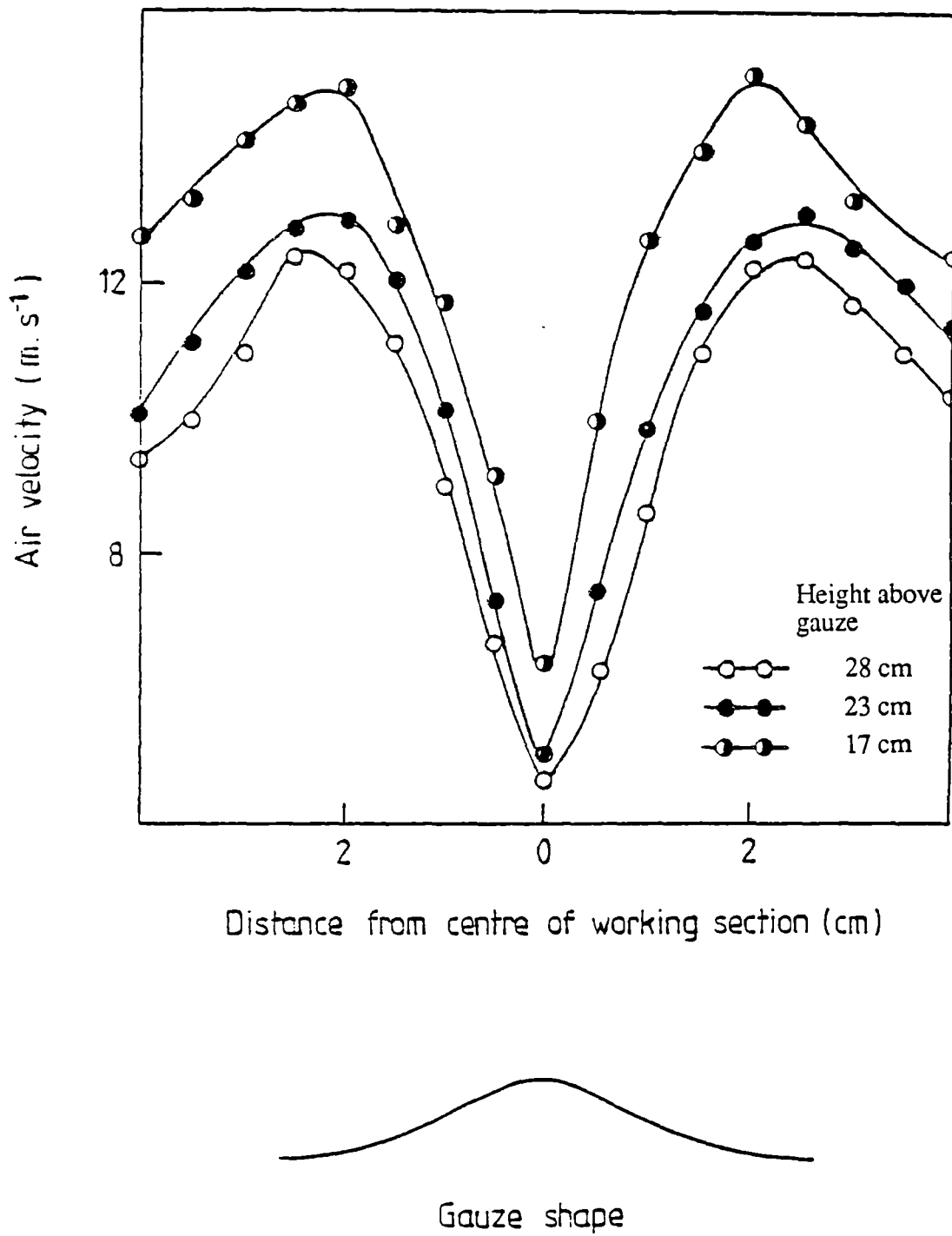


Figure 7.3 Velocity Distribution and Profile of Air in the Working Section of the Vertical Wind Tunnel

The spheroid has a vertical diameter in the y-direction comprising a major length  $b_1$  and a minor length  $b_2$ , and two identical diameters in the horizontal direction (x and z axes). As evaporation occurs  $b_2$  increases due to the tendency of small drops to approach a more spherical shape as the lower half tends further towards sphericity. This is illustrated in Figure 8.16, showing the changing configuration of a pure water droplet with increasing residence time.

From the geometry of the spheroid, for a stable drop, the horizontal diameter in the x and z directions ( $d_x$  and  $d_z$ ) had to be equal whilst the vertical diameter ( $d_y$ ) is always smaller due to the flattening of the drop. Thus, the equivalent diameter of the drop was calculated as,

$$d_e = \frac{d_x + d_y + d_z}{3}$$

and since  $d_x = d_z$

$$d_e = \frac{2d_x + d_y}{3} \quad \text{-----7.1}$$

Equation 7.1 was therefore used to calculate the drop equivalent diameter and hence drop area ( $A_e$ ).

### **7.5 Measurement of Dry and Wet-Bulb Temperatures**

The dry bulb temperature was determined by inserting a thermocouple inside the test section at the axial position at which a drop was normally suspended. Since in the present study a direct measurement of the drop temperature was not possible, for water drops the latter was assumed equal to the wet-bulb temperature. The equilibrium or wet-bulb determinations for water drops were carried out using a thermocouple whose thermojunction was covered with a piece of tissue soaked with the liquid. The lowest temperature was then assumed to be the equilibrium temperature. For isopropanol drops however, the

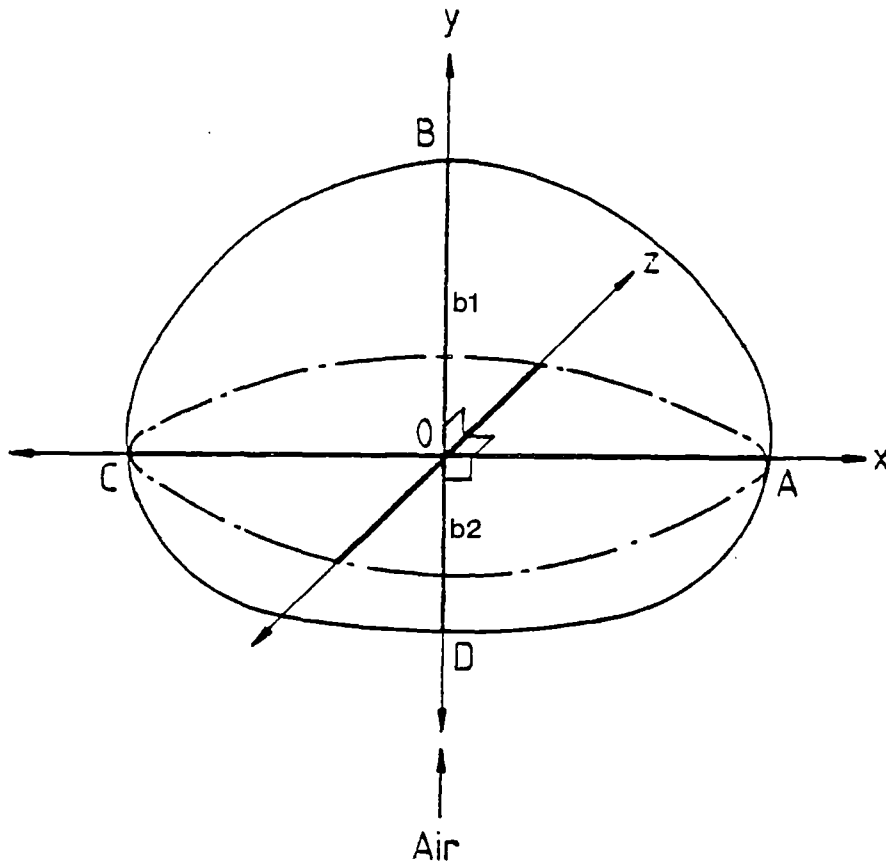


Figure 7.4 Schematic diagram of spheroid droplet geometry  
 AC = Drop diameter in horizontal direction ( x and z axes )  
 DB = Drop diameter in the vertical direction ( y axis )

wet-bulb and adiabatic-saturation temperatures are substantially different, and for this system the partial pressure driving force was determined by using a correlation proposed by Bedingfield and Drew (139) (Appendix A7).

For drops of potassium sulphate and sucrose solutions where there is a lowering of water vapour pressure, as shown in Table 7.5.1, the drop surface temperature would tend to be slightly higher than the wet-bulb temperature. However, it may be assumed equal to the wet-bulb temperature, at least during surface evaporation, without significant error. Once the crust begins to form however, the drop temperature will steadily rise to the air temperature when the drop has completely dried.

## **7.6 Evaporation Of Pure Liquid Drops**

### **7.6.1 Drops of Water and Isopropanol**

The procedure for evaporation rate and drop size measurements was as described in sections 5.1.1 and 7.4, respectively. Drop evaporation rates were then studied at a range of air temperatures from 37 to 97°C using 2 and 4mm diameter nozzles to cover an initial drop diameter size range of 2.8 to 4.6mm. Water and isopropanol were selected to test existing mass transfer correlations of pure liquid systems. Isopropanol was chosen since it has not been investigated by previous workers and because its diffusivity in air is very different from that of water ( $D_v(\text{H}_2\text{O}) = 2.4 D_v(\text{isopropanol})$ ).

## **7.7 Drying Of Solution Drops**

### **7.7.1 Drops of Sucrose solution**

Sucrose solution was selected for study as an example of a film or 'skin' forming material. Drying characteristics were determined at two initial concentrations, 20 and 40%w/w, two nozzle sizes, 2 and 4mm, and two operating temperatures, 68 and 95°C.

System	Concentration (wt/wt%)	Temperature (°C)	Vapour Pressure of Pure Solvent (mmHg)	Reduced Vapour Pressure of Solvent (mmHg)
Potassium Sulphate	0	30	31.824	31.824
"	1.74	"	"	31.711
"	13.92	"	"	30.951
Sucrose	0	100	760	760
	10.26	"	"	755.85
	27.36	"	"	748.57
	41.04	"	"	742.58

Table 7.5.1 Vapour-Pressure Lowering Effects of Dissolved Solute

### 7.7.2 Drops of Potassium Sulphate solution

The drying of potassium sulphate solution has not been studied comprehensively by previous workers and was selected as an example of a material forming a rigid porous crust. Drying rates were determined to cover a concentration range of 5-10%w/w, three nozzle sizes, 2,3 and 4mm and an operating temperature in the range 35 to 95°C. Once a crust had formed however, the particle started to bounce quite vigorously which made drop collection very difficult. In fact , it was not possible to collect a completely dried crust. Hence, analysis of crust structure under the electron microscope was not possible.

**CHAPTER EIGHT**  
**PRESENTATION AND DISCUSSION OF RESULTS**  
**EVAPORATION OF PURE LIQUID DROPLETS**

The experimental results for pure liquid droplets of water and isopropanol are presented as Sherwood and Nusselt numbers calculated from equations 5.14 and 5.21, respectively. The data are tabulated in Appendix A3.

The mass transfer rates were calculated using equation 5.4, and the mass transfer coefficients from equation 5.12. The value of  $dm/d\theta$  was obtained in each case from a plot of drop mass against time as shown in Figures 8.1 - 8.3. In order to obtain the experimental Nusselt number during a run using equation 5.21, the instantaneous value of  $d_e/d\theta$  at each drop size was obtained from a plot of equivalent drop diameter,  $d_e$ , against time, as shown in Figures 8.4 to 8.6.

Each data point in Figures 8.1 - 8.6 for water and isopropanol drops represents an average of three readings. Due to the vertical movements that accompanied the drops, it was not always possible to remove drops at precisely the desired moment, but the maximum delay was < 2 seconds on residence times of 16 to 600s.

There was found to be very little variation in the drop size produced from the same nozzle. Indeed, with the modified drop producing unit (see section 6.1.2) the error was < 2%. The time of evaporation could be recorded within 0.5 seconds, representing an error of < 1% for one minute suspension times. The apparatus was allowed to run for 2 to 2<sup>1</sup>/<sub>2</sub> hours before doing a run so that the air stream conditions within the tunnel could reach an equilibrium, providing a constant dry and wet-bulb temperature. Some errors were inevitably introduced in weighing the bottles due to

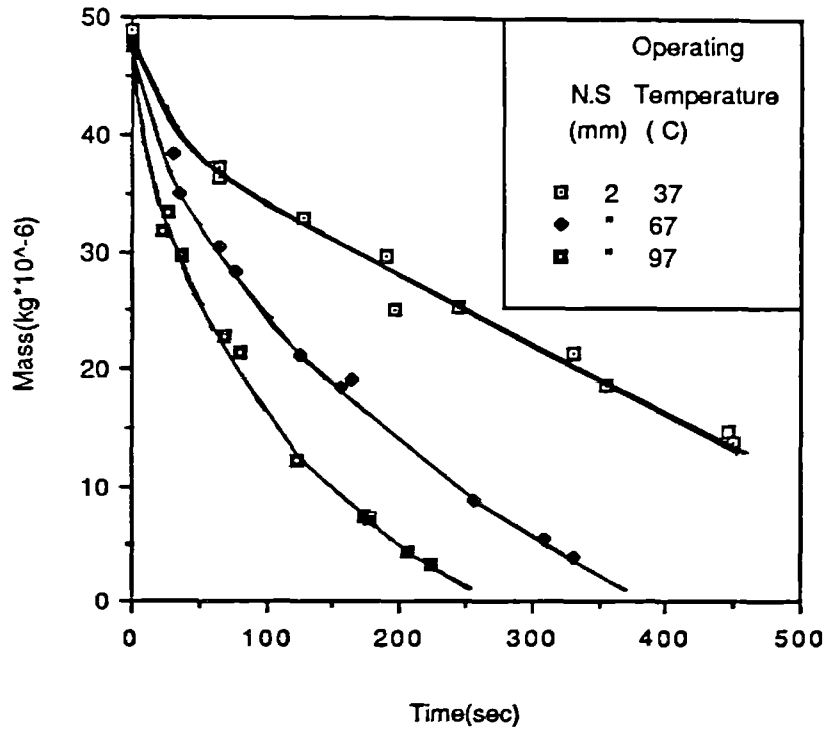


Figure 8.1 Drop Mass-vs-Time For Pure Water Drops

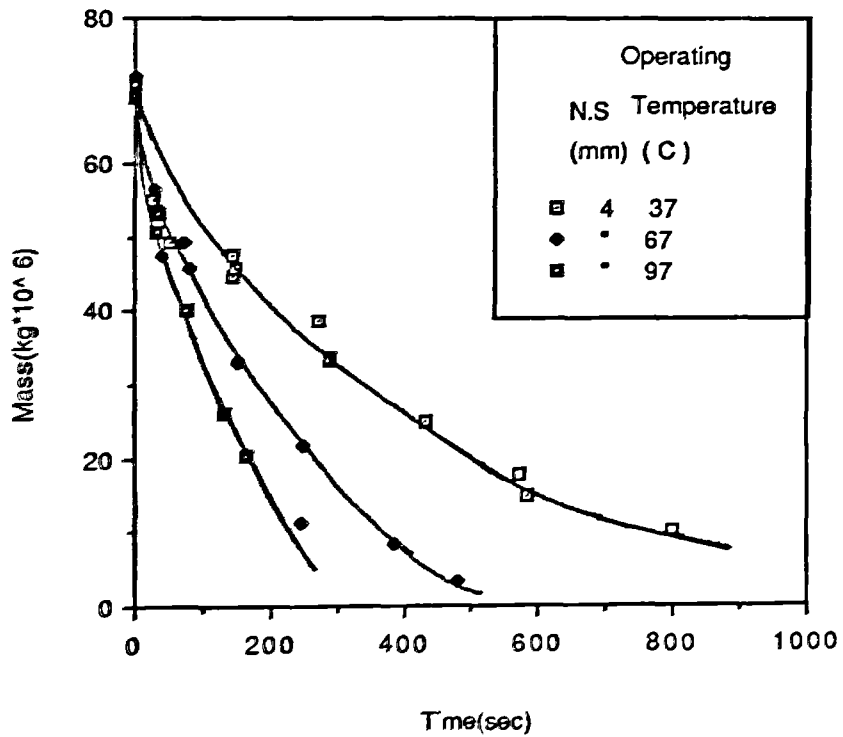


Figure 8.2 Drop Mass-vs-Time For Pure Water Drops

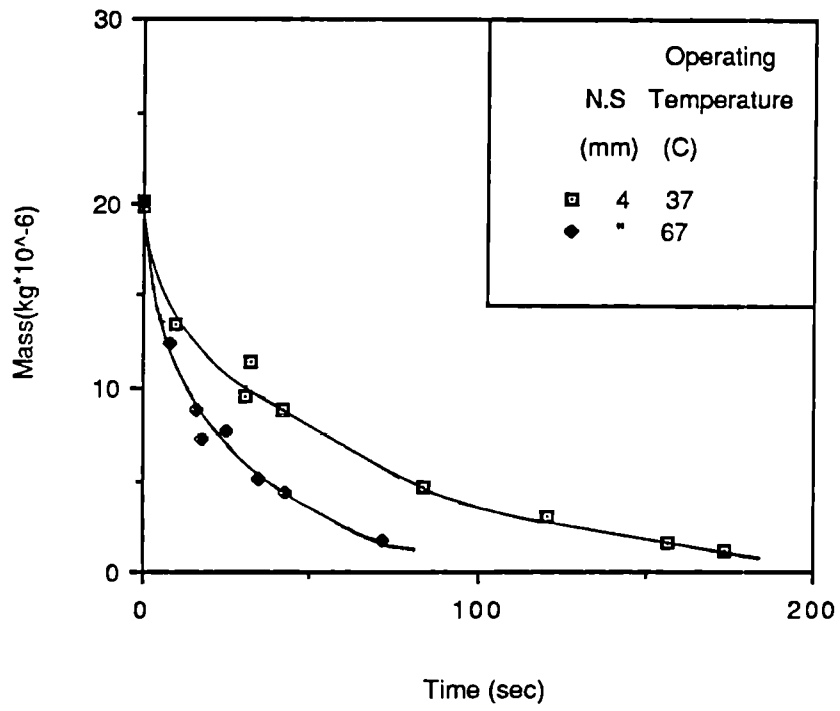


Figure 8.3 Drop Mass-vs-Time For Drops Of Iso-propanol

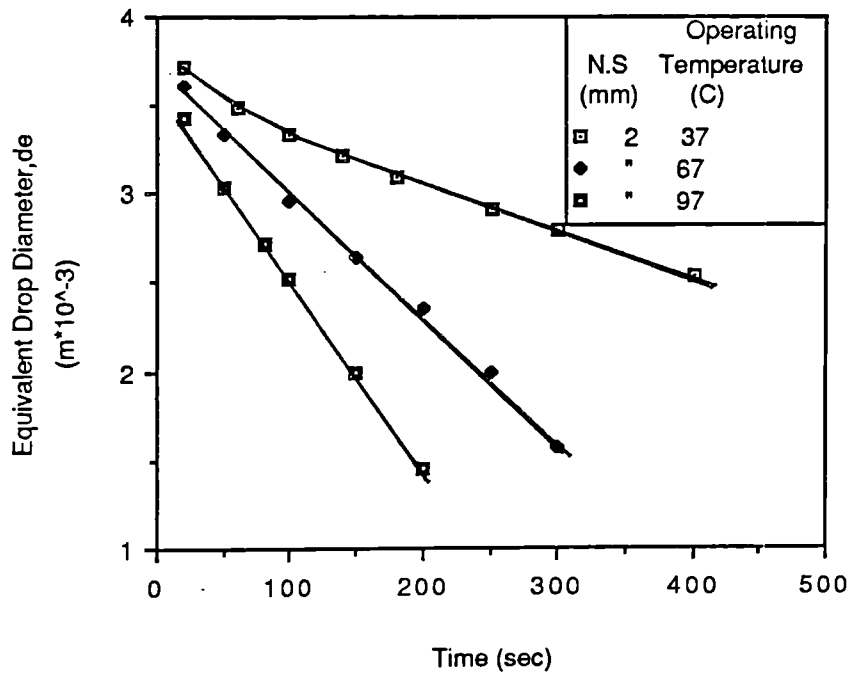


Figure 8.4 Equivalent Drop Diameter-vs-Time For Water Drops

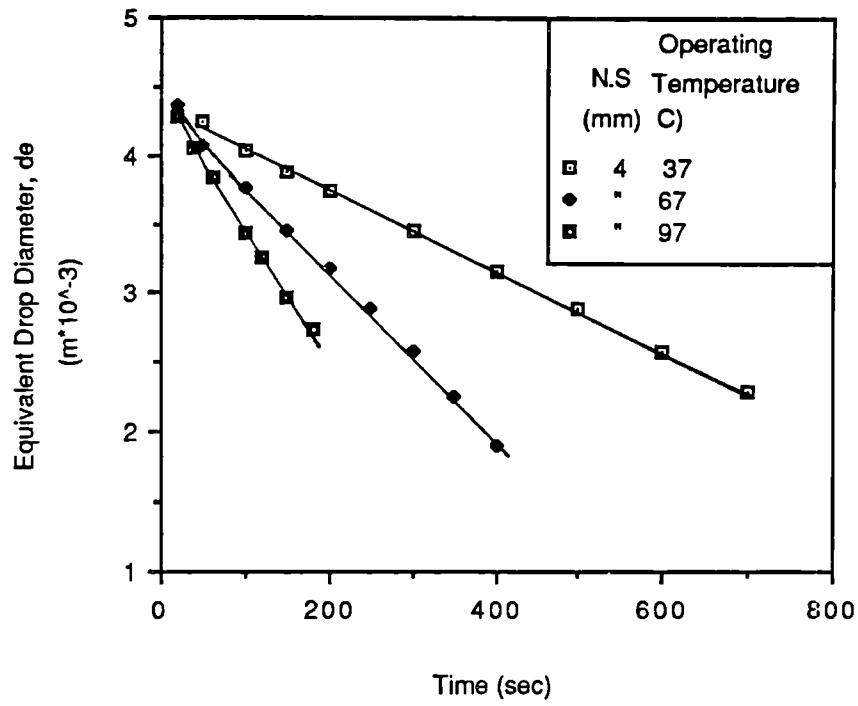


Figure 8.5 Equivalent Drop diameter-vs-Time For Water Drops

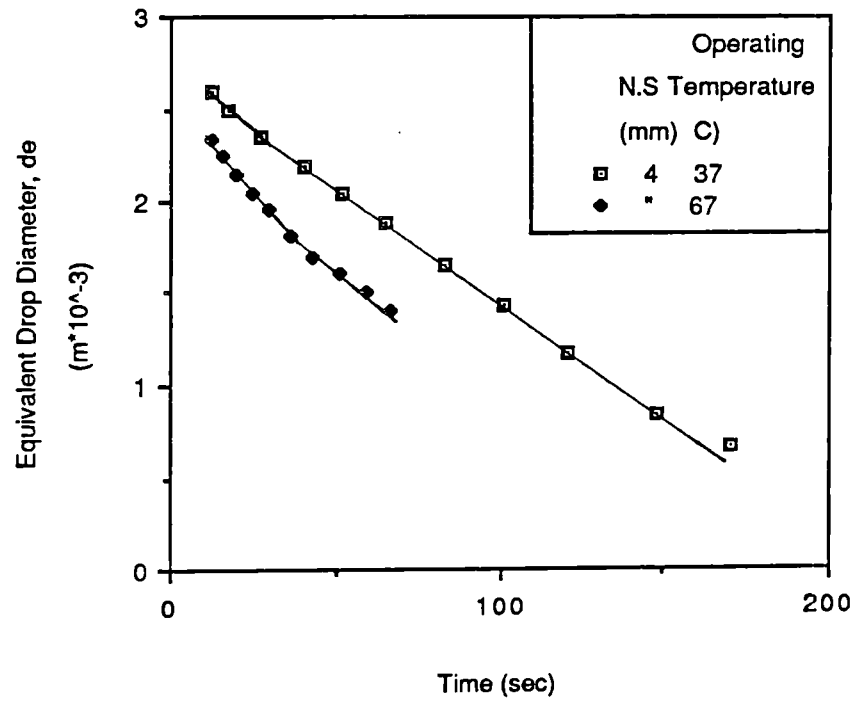


Figure 8.6 Equivalent Drop Diameter-vs-Time For Drops Of IPA

variations in adsorbed moisture caused by the differing conditions inside and outside the working sections and, from handling of the weighing bottles. Evaporation of drops after catching was not a serious source of error, and the maximum error from this cause was not  $> 0.2$  mg. However, it was concluded that the greatest errors were introduced in measuring drop diameters from the T.V. screen, which were estimated to be  $< 10\%$ .

The results of the experiments on pure liquid droplets are summarised in Tables 8.1 - 8.8. and Appendix A3. They are also presented graphically in Figures 8.7 - 8.12 in the form of Sherwood number versus  $Re^{1/2} Sc^{1/3}$  and Nusselt number versus  $Re^{1/2} Pr^{1/3}$ . The results demonstrate that the expressions of Ranz and Marshall, equations 3.15 and 3.16, in the case of water drops do not fully correlate the data and the operating temperature becomes an additional parameter.

Since the investigation by Ranz and Marshall many workers (10-21) have obtained similar correlations, but the experiments have in every case been carried out using drops suspended from either a filament or a capillary. Investigations of the more practical situation of mass transfer from unsupported drops are extremely few in number, although the work of Finlay (72) and of Ahmadzadeh and Harker (74) is of special significance.

Finlay (72) suspended individual water, iso-butane, iso-octane and n-heptane drops in an air stream within a wind tunnel. After a known time interval the drop was collected and weighed and values of  $Sh$  were calculated for drop diameters in the range 1 to 5mm. Ahmadzadeh and Harker (74) allowed single drops of a 50% acetone-water mixture, to fall down a square-section column into a collecting device which prevented further evaporation of acetone. The gas phase, either air or nitrogen, was passed up the column after being metered at a carefully controlled temperature. To compare their results with those of Ranz and Marshall, both Finlay and Ahmadzadeh and

**TABLE 8.1 Evaporation of Water Drops at 37°C using a 2mm Nozzle**

Residence Time (sec)	Mass Transfer Rate $\text{kgm}^{-2}\text{s}^{-1} \times 10^{-3}$	Mass Transfer Coefficient (m/s)	Sherwood Number Sh	Nusselt Number Nu	$\text{Re}^{0.5} \text{Sc}^{0.33}$	$\text{Re}^{0.5} \text{Pr}^{0.33}$
60	3.4	0.33	41.4	39.7	34.9	37.0
80	2.8	0.27	33.6	39.4	34.4	36.4
100	2.4	0.24	28.6	24.6	33.9	35.9
120	2.3	0.23	26.8	22.8	33.6	35.5
140	2.3	0.23	26.3	20.2	33.1	35.1
160	2.0	0.20	22.6	19.0	32.8	34.7
200	2.0	0.19	21.3	18.8	32.0	33.9
250	1.9	0.18	19.2	16.9	31.1	32.9
300	1.9	0.18	18.4	15.8	30.1	31.9

**TABLE 8.2 Evaporation of Water Drops at 67°C using a 2mm Nozzle**

Residence Time (sec)	Mass Transfer Rate $\text{kgm}^{-2}\text{s}^{-1} \times 10^{-3}$	Mass Transfer Coefficient (m/s)	Sherwood Number Sh	Nusselt Number Nu	$\text{Re}^{0.5} \text{Sc}^{0.33} \text{Pr}^{0.33}$
40	5.8	0.34	35.7	34.2	31.8
80	5.4	0.31	30.1	27.8	31.7
100	5.0	0.29	26.6	24.2	31.0
120	4.8	0.28	24.4	22.0	30.1
140	4.9	0.28	23.7	20.4	29.3
160	4.8	0.28	22.2	19.1	28.6
180	5.1	0.29	22.2	18.9	27.7
200	5.3	0.31	22.3	17.0	24.1
					35.2
					33.3
					32.4
					31.6
					30.7
					29.9
					29.0
					28.3

**TABLE 8.3 Evaporation of Water Drops at 97°C using a 2mm Nozzle**

Residence Time (sec)	Mass Transfer Rate $\text{kgm}^{-2}\text{s}^{-1} \times 10^{-3}$	Mass Transfer Coefficient (m/s)	Sherwood Number Sh	Nusselt Number Nu	$\text{Re}0.5 \text{ Sc}0.33$	$\text{Re}0.5 \text{ Pr}0.33$
40	8.9	0.36	30.4	27.8	29.7	30.7
60	7.5	0.31	23.8	21.2	28.6	29.5
80	7.5	0.31	22.3	19.8	27.5	28.4
100	8.4	0.34	19.5	18.2	26.3	27.1
120	8.6	0.35	17.1	16.6	24.9	25.7
140	9.0	0.37	14.0	15.2	23.6	24.3
160	9.9	0.41	13.8	13.7	22.2	22.8

**TABLE 8.4 Evaporation of Water Drops at 37°C using a 4mm Nozzle**

Residence Time (sec)	Mass Transfer Rate $\text{kgm}^{-2}\text{s}^{-1} \times 10^{-3}$	Mass Transfer Coefficient (m/s)	Sherwood Number Sh	Nusselt Number Nu	$\text{Re}^{0.5} \text{Sc}^{0.33}$	$\text{Re}^{0.5} \text{Pr}^{0.33}$
50	3.3	0.32	49.3	46.5	39.5	41.8
100	2.2	0.22	36.3	34.2	38.4	40.7
150	1.8	0.18	29.1	28.0	37.5	39.7
200	1.8	0.18	26.3	25.1	36.6	38.8
300	1.8	0.18	23.5	22.1	34.8	36.8
400	1.9	0.18	21.6	20.9	32.9	34.9
500	2.1	0.19	20.9	19.7	31.1	32.9
600	2.3	0.22	20.8	17.6	28.9	30.6

**TABLE 8.5 Evaporation of Water Drops at 67°C using a 4mm Nozzle**

Residence Time (sec)	Mass Transfer Rate $\text{kgm}^{-2}\text{s}^{-1} \times 10^{-3}$	Mass Transfer Coefficient (m/s)	Sherwood Number Sh	Nusselt Number Nu	Re0.5 Sc0.33	Re0.5 Pr0.33
50	4.3	0.25	31.7	31.3	35.4	37.2
100	3.7	0.22	25.2	24.1	33.7	35.5
150	4.0	0.23	23.1	22.2	31.9	33.6
200	3.9	0.23	22.4	20.5	30.3	31.9
250	4.2	0.25	19.5	18.1	28.5	30.0
300	4.8	0.28	17.9	18.0	26.6	27.9
400	5.7	0.33	15.8	14.5	21.4	22.5

**TABLE 8.6 Evaporation of Water Drops at 27°C using a 4mm Nozzle**

Residence Time (sec)	Mass Transfer Rate $\text{kgm}^{-2}\text{s}^{-1} \times 10^{-3}$	Mass Transfer Coefficient (m/s)	Sherwood Number Sh	Nusselt Number Nu	Re0.5 Sc0.33	Re0.5 Pr0.33
40	7.8	0.32	35.4	33.5	34.4	35.5
50	6.5	0.26	27.8	26.8	33.3	34.4
80	6.4	0.26	25.3	24.1	31.7	32.7
100	6.5	0.26	24.3	22.7	30.6	31.5
120	6.1	0.25	21.6	20.1	29.6	30.5
140	5.8	0.24	19.6	21.8	28.5	29.4
160	5.8	0.24	18.5	19.1	27.5	28.3
180	5.0	0.20	14.8	17.5	26.4	27.3

**TABLE 8.7 Evaporation of Pure Drops of Iso-Propanol at 37°C using a 4mm Nozzle**

Residence Time (sec)	Mass Transfer Rate $\text{kgm}^{-2}\text{s}^{-1} \times 10^{-3}$	Mass Transfer Coefficient (m/s)	Sherwood Number Sh	Nusselt Number Nu	$\text{Re}^{0.5} \text{Sc}^{0.33}$	$\text{Re}^{0.5} \text{Pr}^{0.33}$
27	8.2	0.20	25.3	24.5	35.7	37.6
40	7.8	0.19	23.2	22.7	34.3	36.1
52	7.8	0.19	19.9	21.0	32.9	33.5
65	8.0	0.19	21.5	20.8	31.4	33.2
83	8.0	0.19	20.7	19.2	30.0	31.9
101	7.2	0.17	15.1	18.9	26.6	27.5

**TABLE 8.8 Evaporation of Pure Drops of Iso-Propanol at 67°C using a 4mm Nozzle**

Residence Time (sec)	Mass Transfer Rate $\text{kgm}^{-2}\text{s}^{-1} \times 10^{-3}$	Mass Transfer Coefficient (m/s)	Sherwood Number Sh	Nusselt Number Nu	$\text{Re}0.5 \text{ Sc}0.33$	$\text{Re}0.5 \text{ Pr}0.33$
20	19.2	0.21	24.5	23.0	32.0	33.8
25	15.8	0.18	22.3	21.1	31.1	32.9
30	14.2	0.16	20.1	19.3	30.2	31.8
43	13.1	0.15	18.1	18.9	27.6	29.2
51	12.3	0.14	17.9	19.0	26.3	28.1
59	11.5	0.13	16.1	17.5	24.6	25.0
67	10.2	0.11	14.9	16.9	22.9	24.0

Harker plotted  $Sh$  against  $Re^{1/2} Sc^{1/3}$  as shown in Figures 8.13 - 8.14 but found a marked discrepancy in rates of mass transfer from drops  $> 3\text{mm}$  diameter. They attributed this to enhanced droplet oscillation.

Results from the present investigation were also compared with those of previous workers in Figures 8.13 and 8.14, and were found to bear out Finlay's and Ahmadzadeh and Harkers' findings in so far as drop rotation, deformation and oscillation contribute to enhanced rates of mass transfer. Thus, some discrepancies from the Ranz and Marshall equations will result from the limitations inherent in these equations viz,

- (i) Droplet structure was assumed stable i.e. the droplet approximated to a rigid sphere. However, any oscillation or surface distortion of the droplet as shown in Figure 8.15 will increase heat and mass transfer rates due to a thinning of the boundary layer and an increase in the interfacial surface area of the droplet.
- (ii) Droplets were assumed stable in the air flow. In the present investigation however the droplet experienced occasional rapid vertical movements and rotation. Such droplet behaviour would tend to reduce the boundary layer, thus increasing evaporation rates.
- (iii) Ranz and Marshall carried out their experimentation over a Reynolds number range of 0 to 200 compared to 395 to 2211 in the present investigation . Furthermore, their experiments were limited to the largest initial drop size of 1.1mm compared with 4.6mm in this study.

Figures 8.7 - 8.10 show that the evaporation of a pure water droplet appeared to occur in two distinct stages separated by a transition region, shown on the Figures as dotted lines. In stage one or Regime 1 (R1) heat and mass transfer occurred to and from a droplet which was observed to experience deformation, oscillation and rotation and consequently the

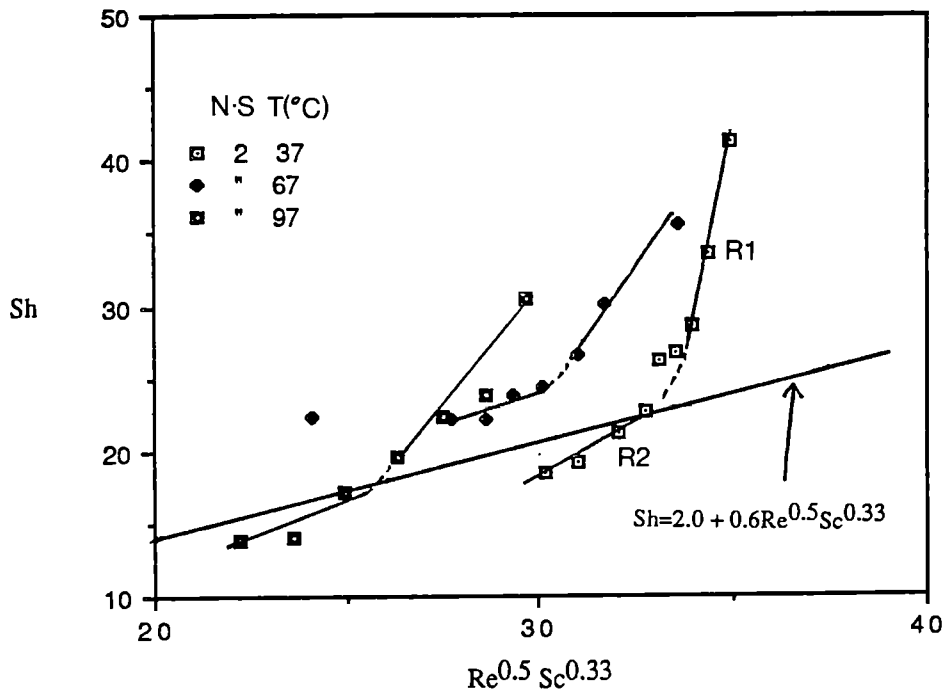


Figure 8.7 Sh-vs- $Re^{0.5}Sc^{0.33}$  For Drops of Water

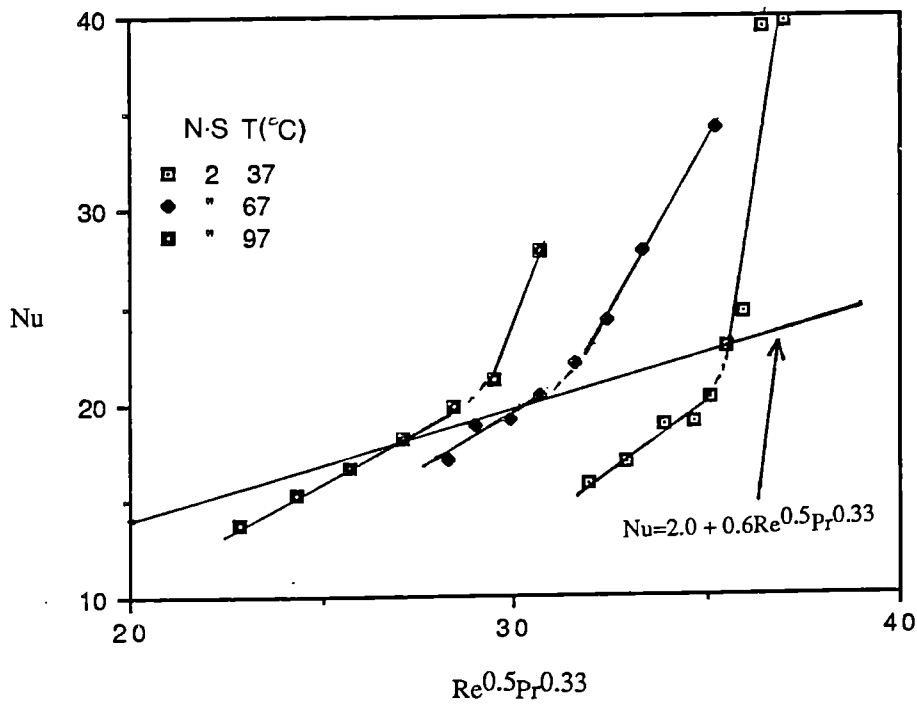


Figure 8.8 Nu-vs- $Re^{0.5}Pr^{0.33}$  For Drops of Water

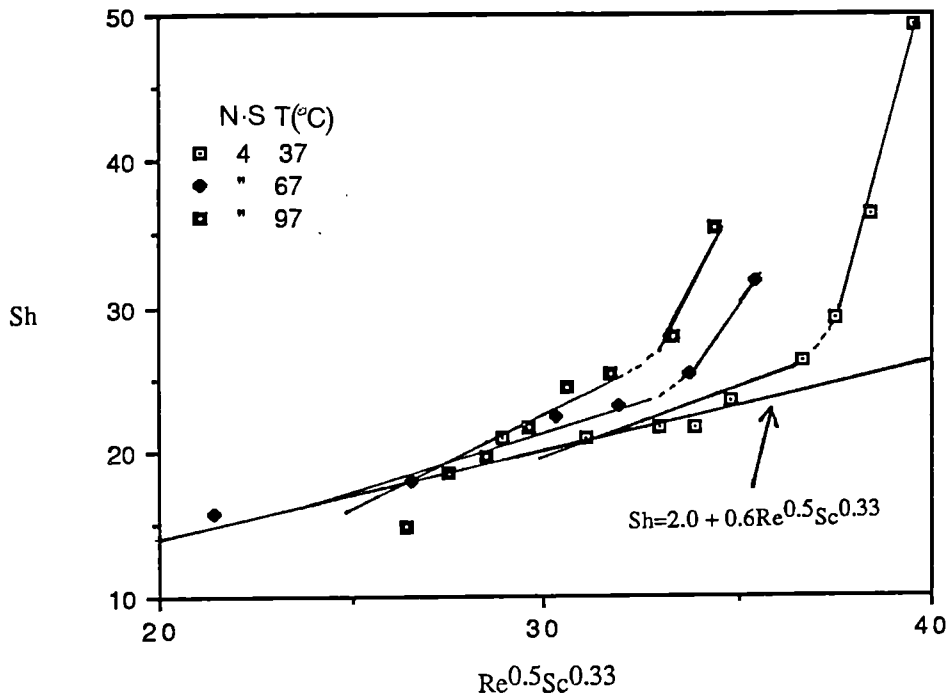


Figure 8.9 Sh-vs- $Re^{0.5}Sc^{0.33}$  For Drops of Water

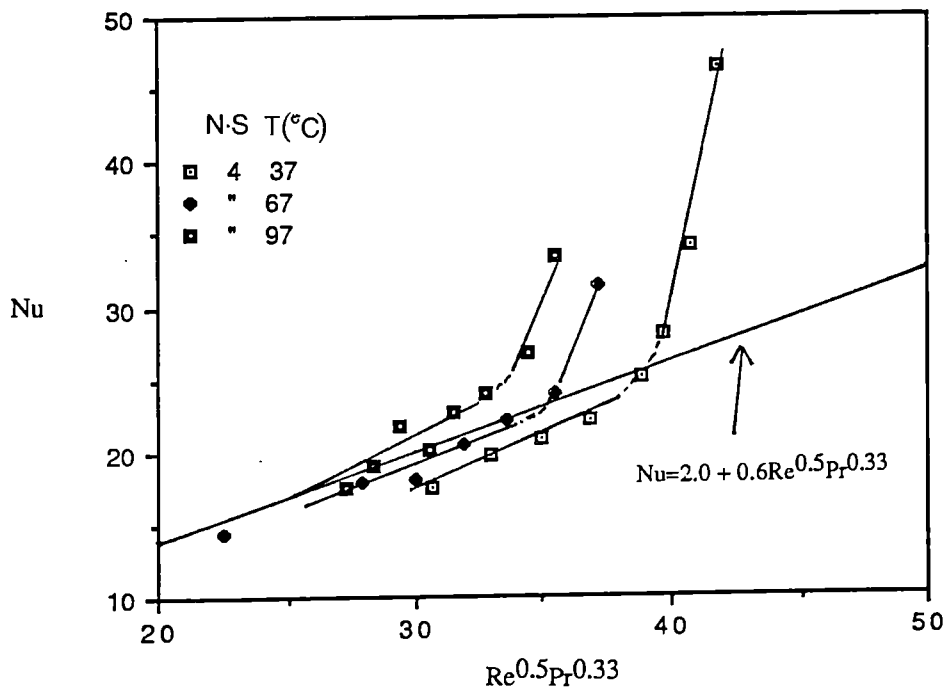


Figure 8.10 Nu-vs- $Re^{0.5}Pr^{0.33}$  For Drops of Water

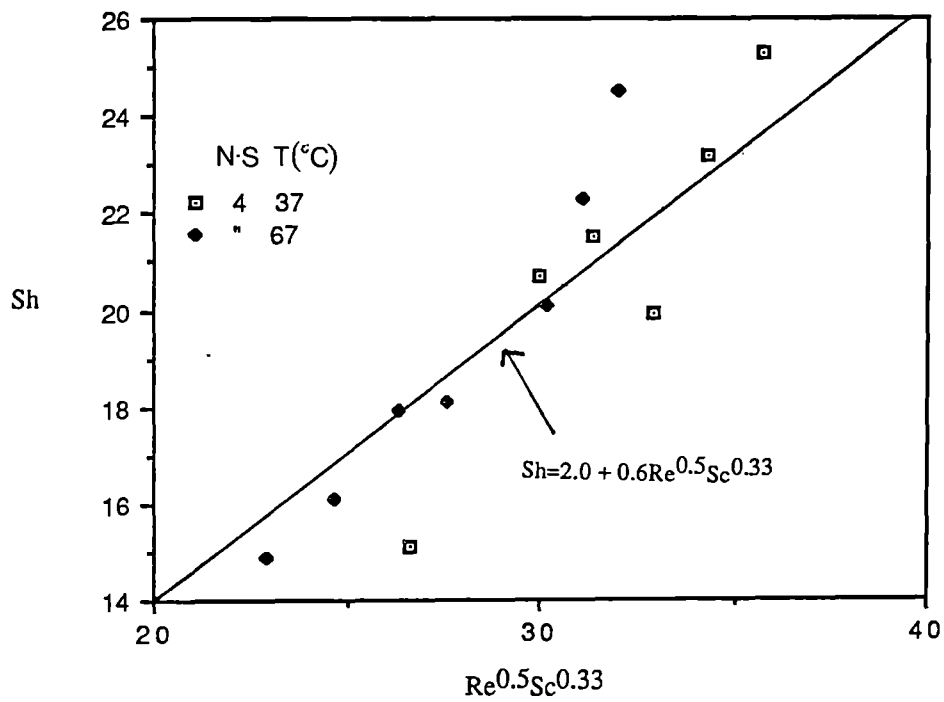


Figure 8.11 Sh-vs- $Re^{0.5} Sc^{0.33}$  For Drops of Isopropanol

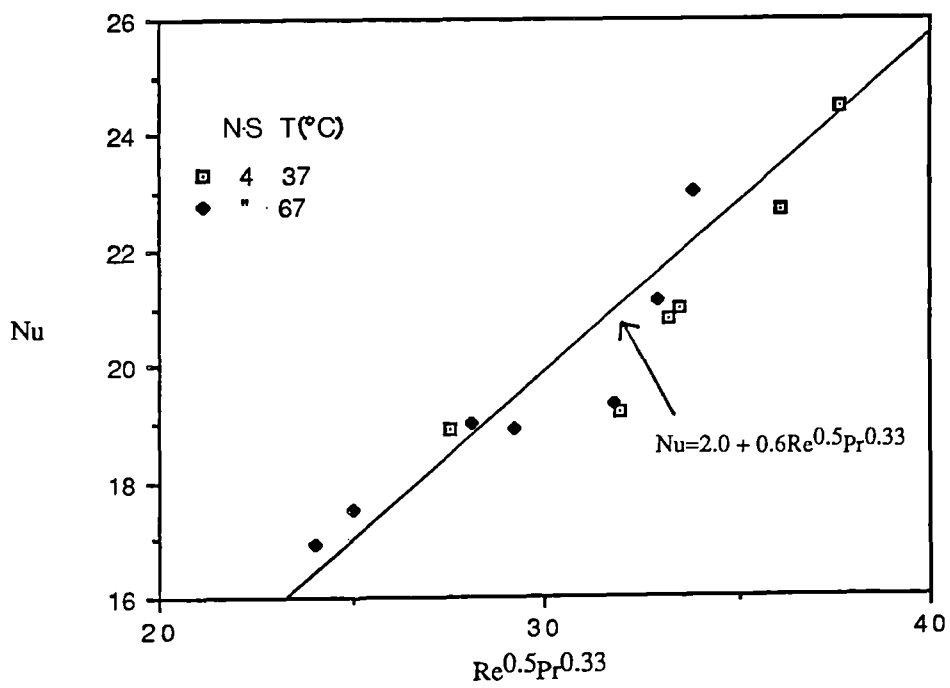


Figure 8.12 Nu-vs- $Re^{0.5} Pr^{0.33}$  For Drops of Isopropanol

enhanced rates of heat and mass transfer lie well above the theoretical Ranz and Marshall line. As the droplet size reduced, it became more spherical as shown in Figure 8.16, and more stable with regard to droplet oscillation and deformation. In Regime 2 (R2) mass transfer took place from a more spherical droplet and consequently the data lie much closer to the theoretical Ranz and Marshall line.

Therefore, the two regimes have been analysed separately and correlated according to the equations.

$$\text{Sh} = 2.0 + \beta \text{Re}^{1/2} \text{Sc}^{1/3} \quad \text{-----} \quad 8.1$$

$$\text{Nu} = 2.0 + \phi \text{Re}^{1/2} \text{Pr}^{1/3} \quad \text{-----} \quad 8.2$$

A least square correlation technique described in Appendix A1.1 was used to correlate the data. The values of  $\beta$  and  $\phi$  for water and isopropanol are shown in Table 8.9. It is apparent from Table 8.9 that temperature is an additional parameter which should be taken into account. The experimental results were therefore correlated using the equation for Sherwood number proposed by Audu(15),

$$\text{Sh} = A + \beta \left[ \frac{T_a - T_s}{T_{\text{amb}}} \right]^n \text{Re}^{1/2} \text{Sc}^{1/3} \quad \text{-----} \quad 8.3$$

where the empirical correction factor involving the group  $(T_a - T_s)/T_{\text{amb}}$  accounts for the fact that the film properties were considered to be constant in the theoretical development while they are functions of temperature in the actual system. A least squares technique, described in Appendix A1.2 was used to correlate the data according to the above equation. The resulting correlations were:

Regime 1

$$\text{Sh} = -105 + 3.9 \left[ \frac{T_a - T_s}{T_{\text{amb}}} \right]^{0.18} \text{Re}^{1/2} \text{Sc}^{1/3} \quad \text{-----} \quad 8.4$$

For Re approx. > 1380

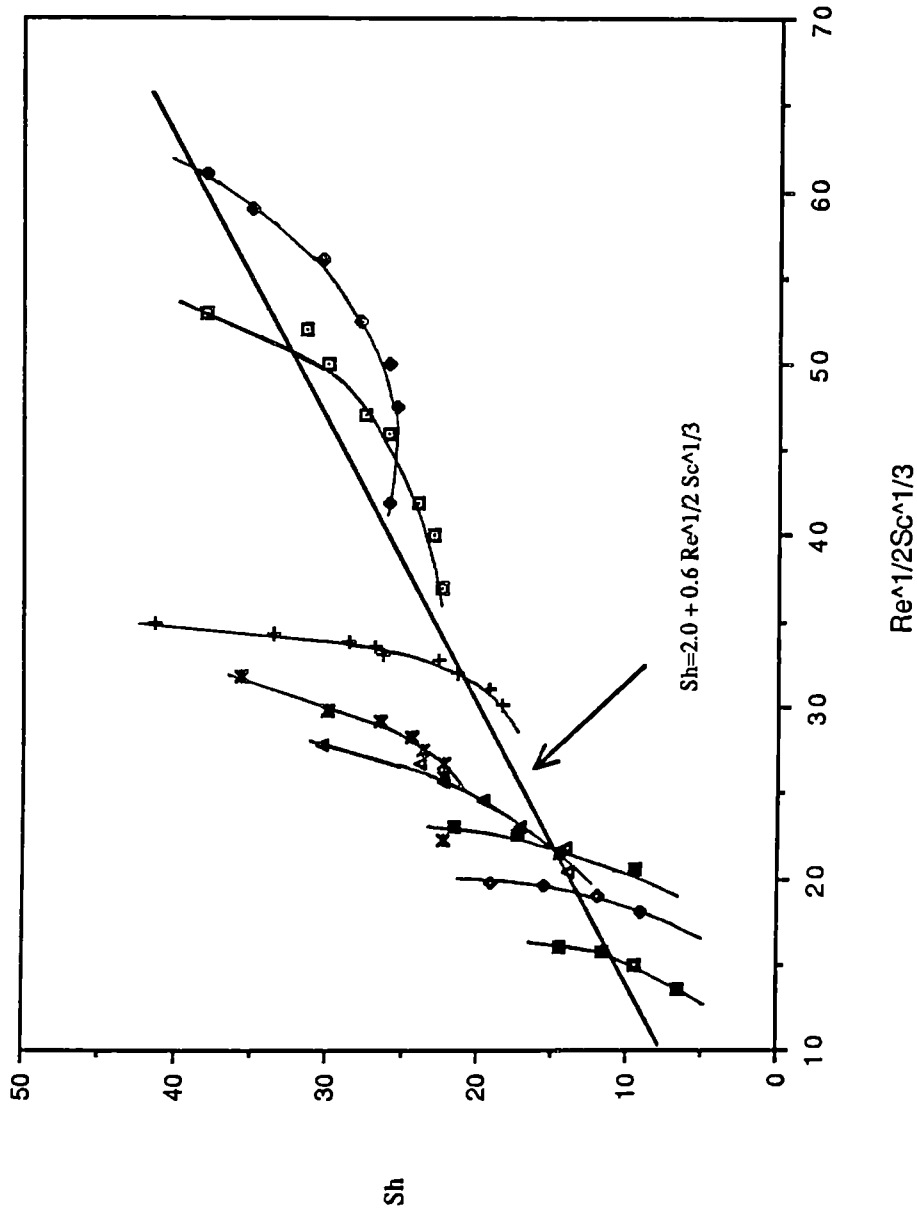


Figure 8.13 Correlation Of Mass Transfer Data

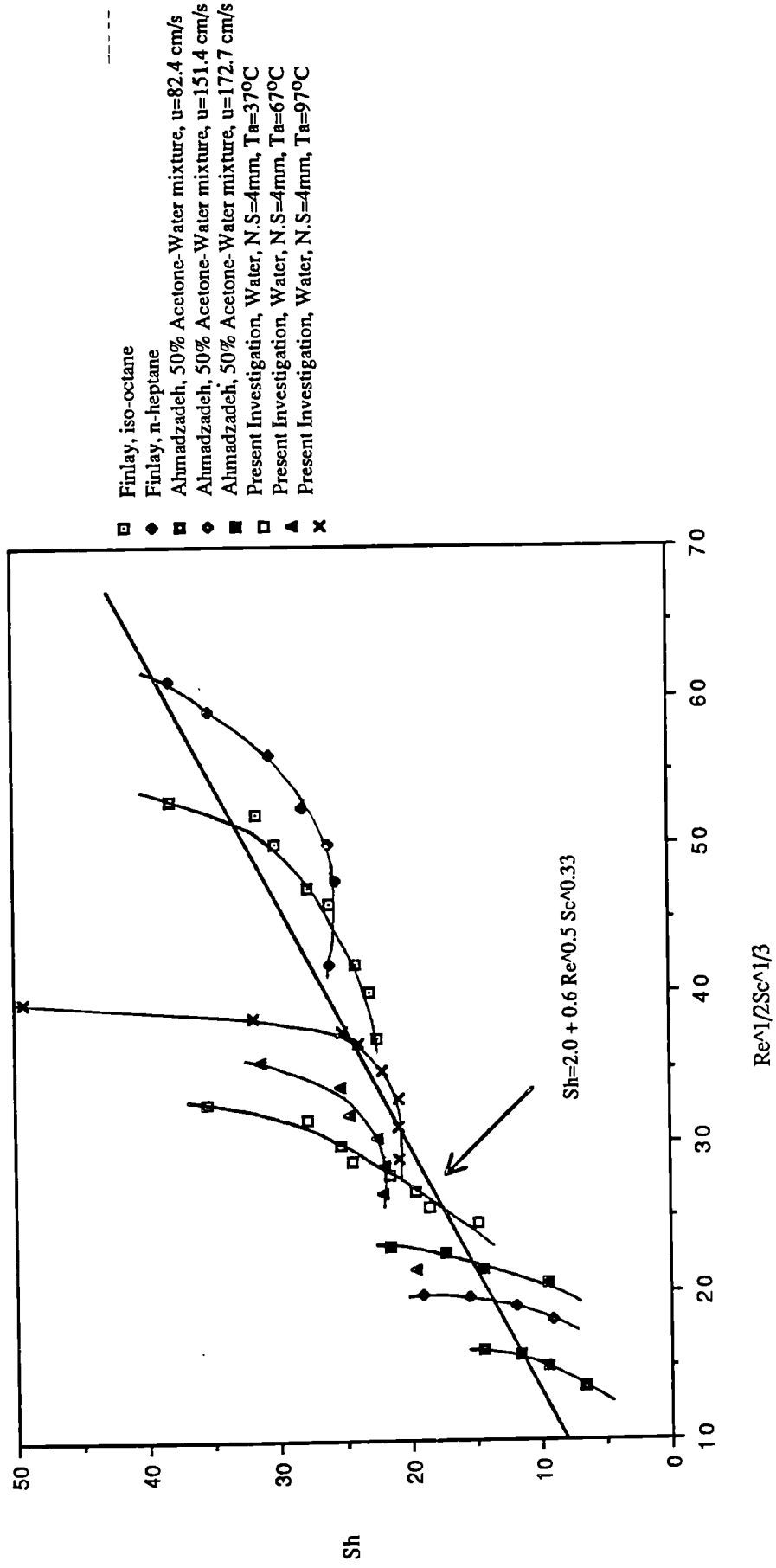


Figure 8.14 Correlation Of Mass Transfer Data

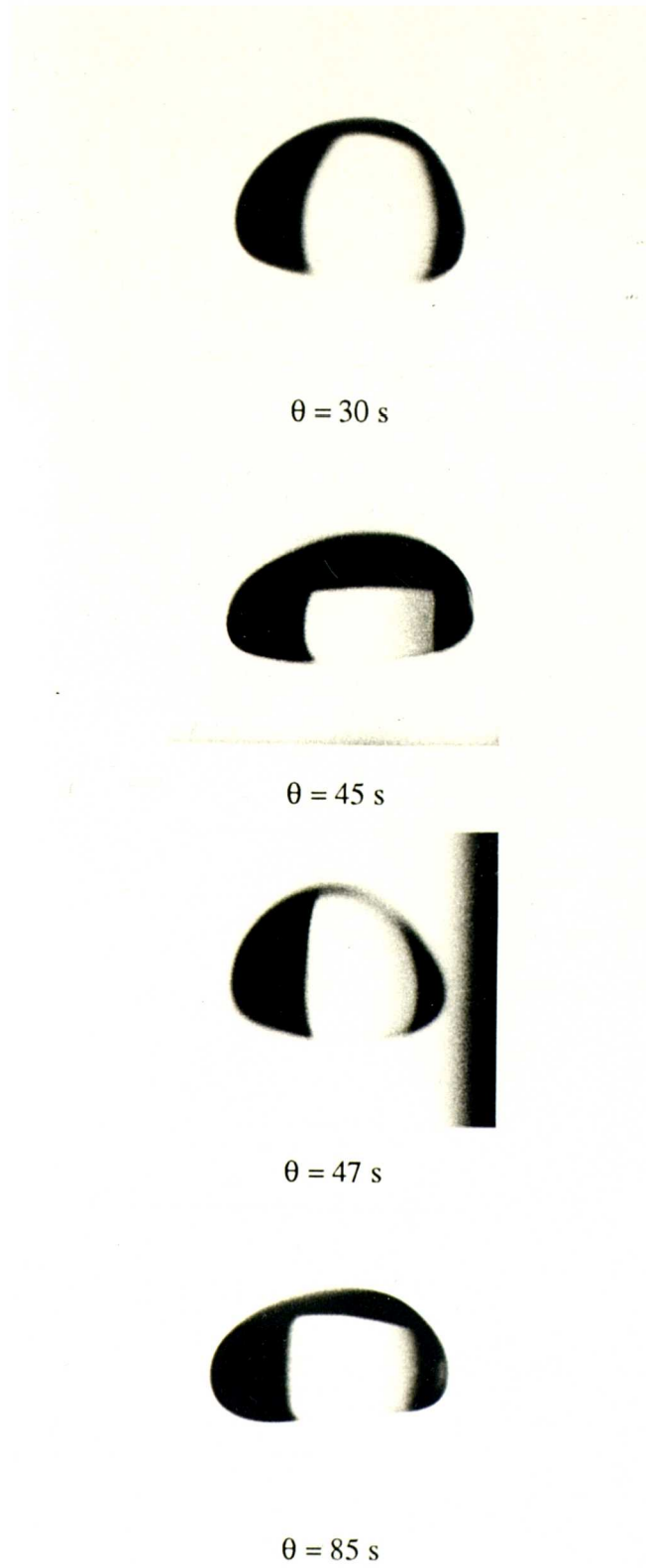


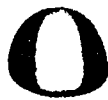
Figure 8.15 Oscillation of a Pure Water Drop at 30°C

**TABLE 8.9 Values of  $\beta$  and  $\phi$  for Drops of Water and Iso-propanol**

System	Nozzle Size (mm)	Operating Temperature (°C)	Regime I $\beta_1$	Regime 2 $\beta_2$	Regime 1 $\phi_1$	Regime 2 $\phi_2$
Water	2	37	4.50	0.86	4.10	0.85
"	2	67	3.72	0.82	3.94	0.74
"	2	97	2.91	0.79	3.61	0.74
"	4	37	4.21	0.73	4.10	0.71
"	4	67	3.58	0.71	3.81	0.62
"	4	97	2.80	0.63	3.78	0.72
IPA	4	37		0.63		0.64
"	4	67		0.61		0.62



$\theta = 15$  s



$\theta = 29$  s



$\theta = 33$  s



$\theta = 65$  s

Figure 8.16 Water drop showing increased tendency to sphericity with increasing  $\theta$  at 97°C

Regime 2

$$\text{Sh} = 2.0 + 0.71 \left[ \frac{T_a - T_s}{T_{\text{amb}}} \right]^{0.18} \text{Re}^{1/2} \text{Sc}^{1/3} \quad \text{-----8.5}$$

for Re approx. < 1060

The Re number at the start of the transition region of 1060 is in good agreement with Finlays work (72) who found that his data for the evaporation of water drops were slightly higher than the correlation proposed by Ranz & Marshall for spheres for Re > 1100. Equation 8.4 for oscillating drops shows some similarity with the empirical expression for circulating liquid-liquid drops proposed by Foord (148),

$$\text{Sh} = -126 + 1.8\text{Re}^{1/2}\text{Sc}^{0.42} \quad \text{-----8.6}$$

The absolute average deviations of equations 8.4 and 8.5 from the experimental values are 5.76 and 6.23%, respectively, indicating a reasonable fit.

Figure 8.17 shows a plot of Sh against  $\left[ \frac{T_a - T_s}{T_{\text{amb}}} \right]^{0.18} \text{Re}^{1/2} \text{Sc}^{1/3}$

Figures 8.11 and 8.12 demonstrate that the data for the isopropanol system, within the limits of experimental error, are represented reasonably well by the traditional Ranz & Marshall equations with an absolute average deviation of 8.31%. However the new proposed correlation for mass transfer, equation 8.5, correlates the data slightly better with an absolute average deviation of 6.62%. It is interesting to note that Regime 1 does not exist in the case of an isopropanol droplet because the largest drop size formed from a 4mm nozzle was 2.5mm, corresponding to a Reynolds number of 1012. Consequently the entire life span of a drop lay in Regime 2, and the drop experienced no significant shape dilations except for the initial instability caused by detachment from the nozzle.

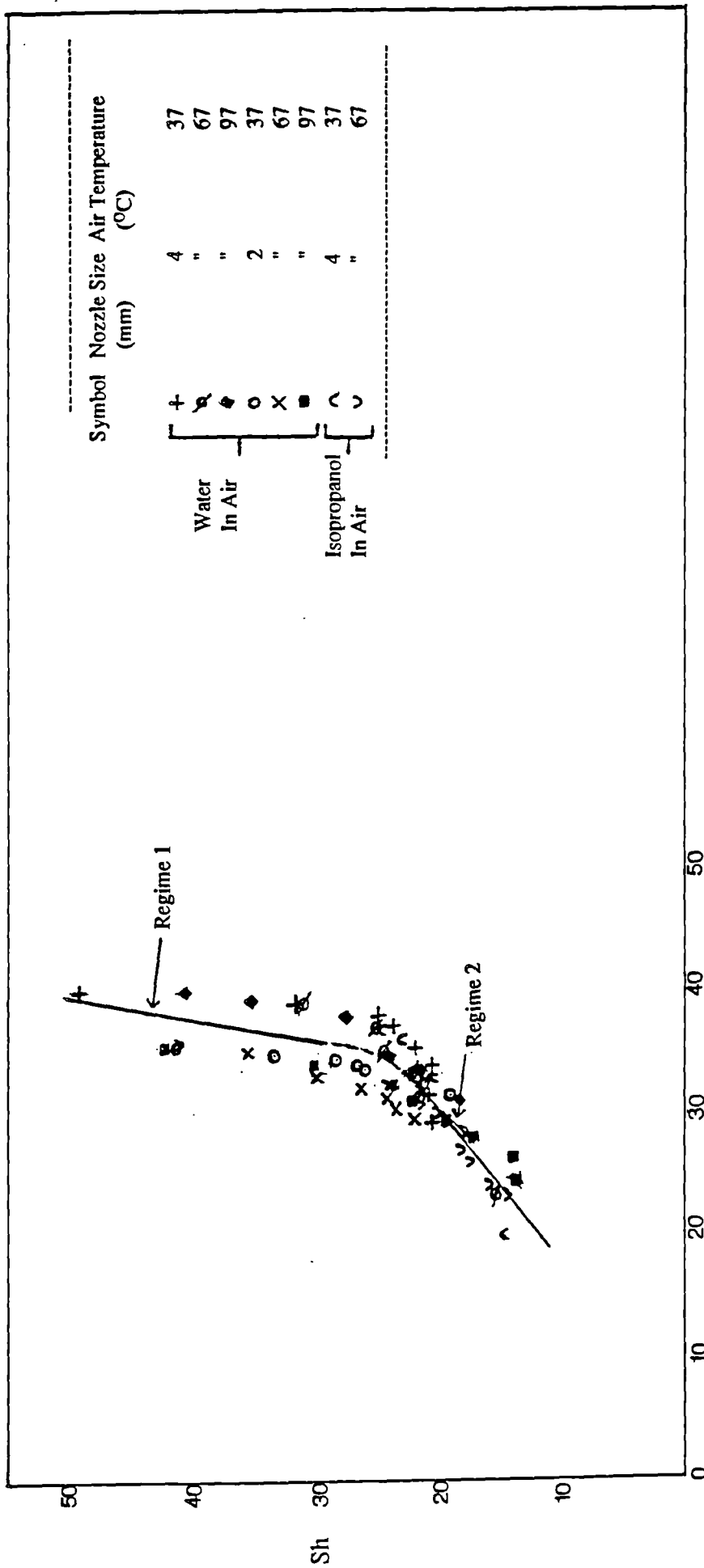


Figure 8.17 Correlation of Mass Transfer Film Coefficients of Water and Isopropanol Drops

The heat transfer data appear to follow a similar pattern to the mass transfer data and if allowance is made for experimental error, the transition occurs at roughly similar values of  $Re^{0.5}Pr^{0.33}$ . Hence, the two processes are almost identical, showing a common trend and may be termed 'analogous'. Since the Schmidt number must equal the Prandtl number, the diffusion coefficients governing the two processes,  $D_v$  and  $K_d$  must be equal. Therefore since  $D_v$  is due to molecular migration, whereas  $K_d$  is due to molecular collision, the strict analogy between heat and mass transfer will not be applicable. However, attempts to correlate the experimental heat transfer data by incorporating the transfer number  $B$ , where  $B = Cp\Delta T/\lambda$ , proved unsuccessful.

The nozzle size also had some effect upon the rate of mass transfer as shown in Figures 8.7 and 8.9. However, this displacement of the experimental data is due to the different histories, ie. equi-sized drops will have spent different lengths of time in the working chamber if they were produced using different nozzles. Consequently, a drop of e.g. 3.8 mm diameter will have spent 4 seconds using a 2mm nozzle and a drop of identical size from a 4 mm nozzle will have spent 275 seconds. Therefore, the drop from the 2 mm nozzle will still be experiencing some initial instability whereas the drop from the 4 mm nozzle will be far more stable. Thus, the instantaneous rate of mass transfer from a 3.8mm drop from the 2mm nozzle would be expected to be higher. This was indeed found to be the case. For the drop from the 2 mm nozzle the rate was found to be  $4.3 \times 10^{-3} \text{ kg m}^{-2} \text{ s}^{-1}$  compared with  $1.8 \times 10^{-3} \text{ kg m}^{-2} \text{ s}^{-1}$  for the drop from the 4 mm nozzle.

The initial instability mentioned above, which is essentially oscillation and deformation of the drop following detachment from the nozzle and free fall, does not however affect the validity of the overall results since it only lasted for a few seconds.

**CHAPTER NINE**  
**PRESENTATION AND DISCUSSION OF RESULTS**  
**-DROPLETS CONTAINING SOLIDS**

In general, as discussed in Chapter 4, the presence of a solid increases the time to remove a given mass of moisture compared to that if all the moisture were present as a drop of pure liquid. Thus, a solid in solution will cause a vapour pressure lowering during the initial period of surface evaporation, while during the falling rate period it creates a solid phase through which liquid and/or vapour must pass in order to escape from the particle. The nature of this solid-phase resistance is extremely variable, and it has considerable influence on the properties of the dried particle.

**9.1 Drops of Sucrose Solution**

In this series of experiments investigations were carried out at two concentrations; 20 and 40w/w% solids , at varying air temperatures , initial drop diameters and air velocities.

**9.1.1 Rates of Evaporation**

The evaporation rates presented in Figures 9.1-9.4, were calculated using equation 5.4, the values of  $dm/d\theta$  and  $1/A_e$  being determined, respectively, from plots of drop mass versus time and drop diameter versus time. The data are tabulated in Appendix A4.1.

Figures 9.1-9.4 demonstrate that the mass transfer process, in droplets containing solids occurs in three periods. During the first period there is a sharp

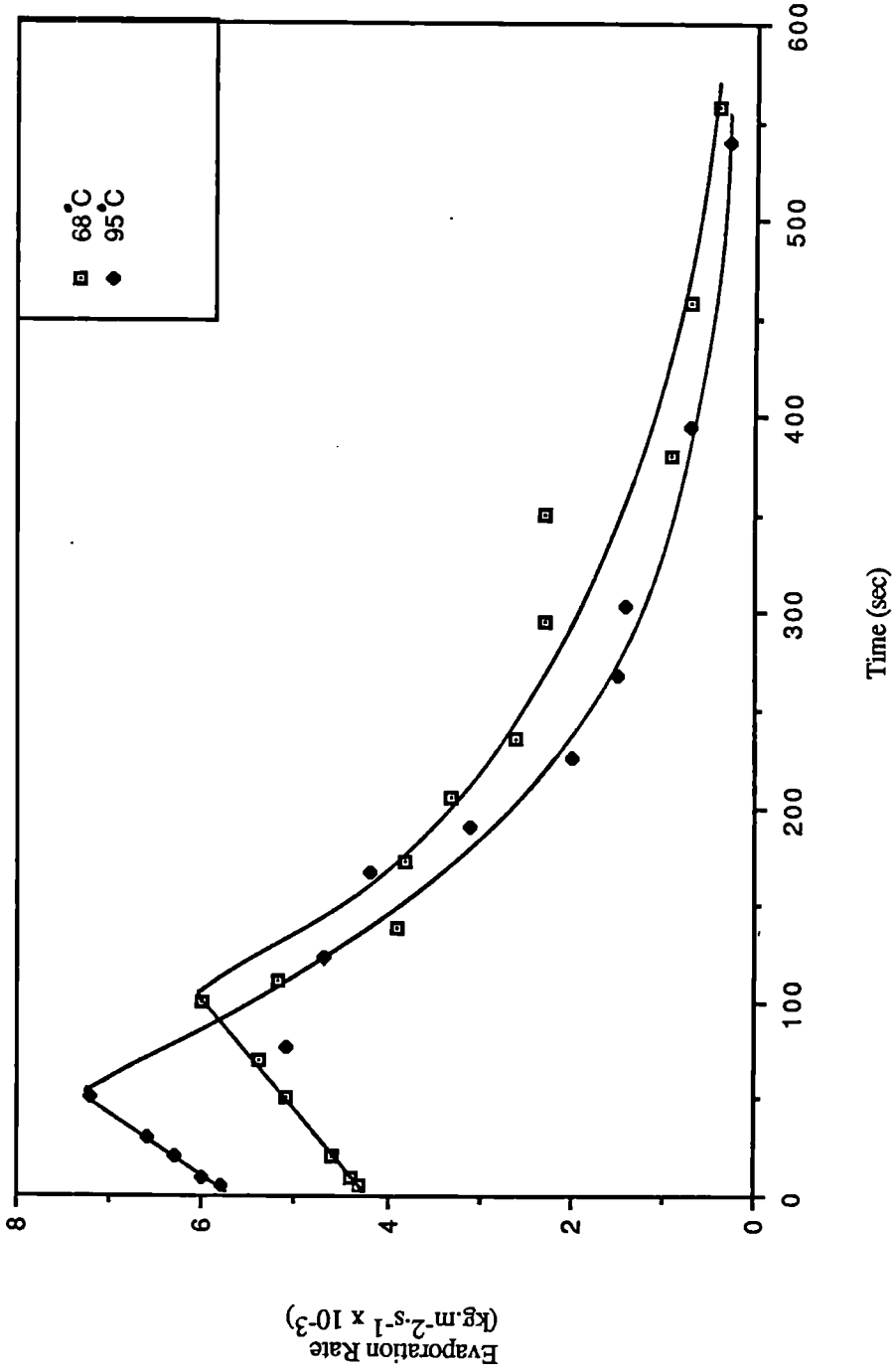


Figure 9.1 Drying Rate Curves For Drops of Sucrose Solution  
at 20 w/w% Solids and a 2mm Diameter Nozzle

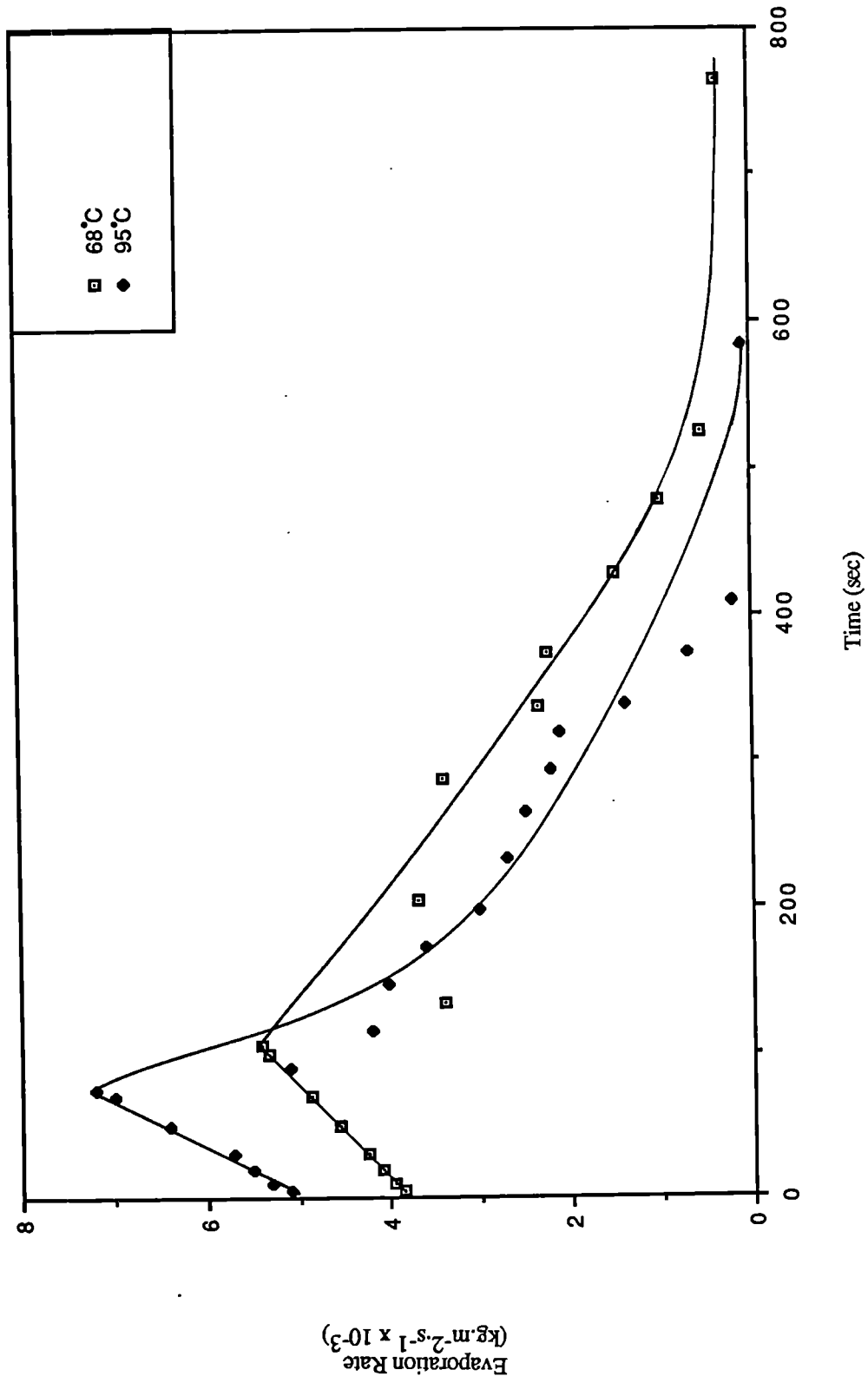


Figure 9.2 Drying Rate Curves For Drops of Sucrose Solution  
at 20 w/w% solids and a 4mm Diameter Nozzle

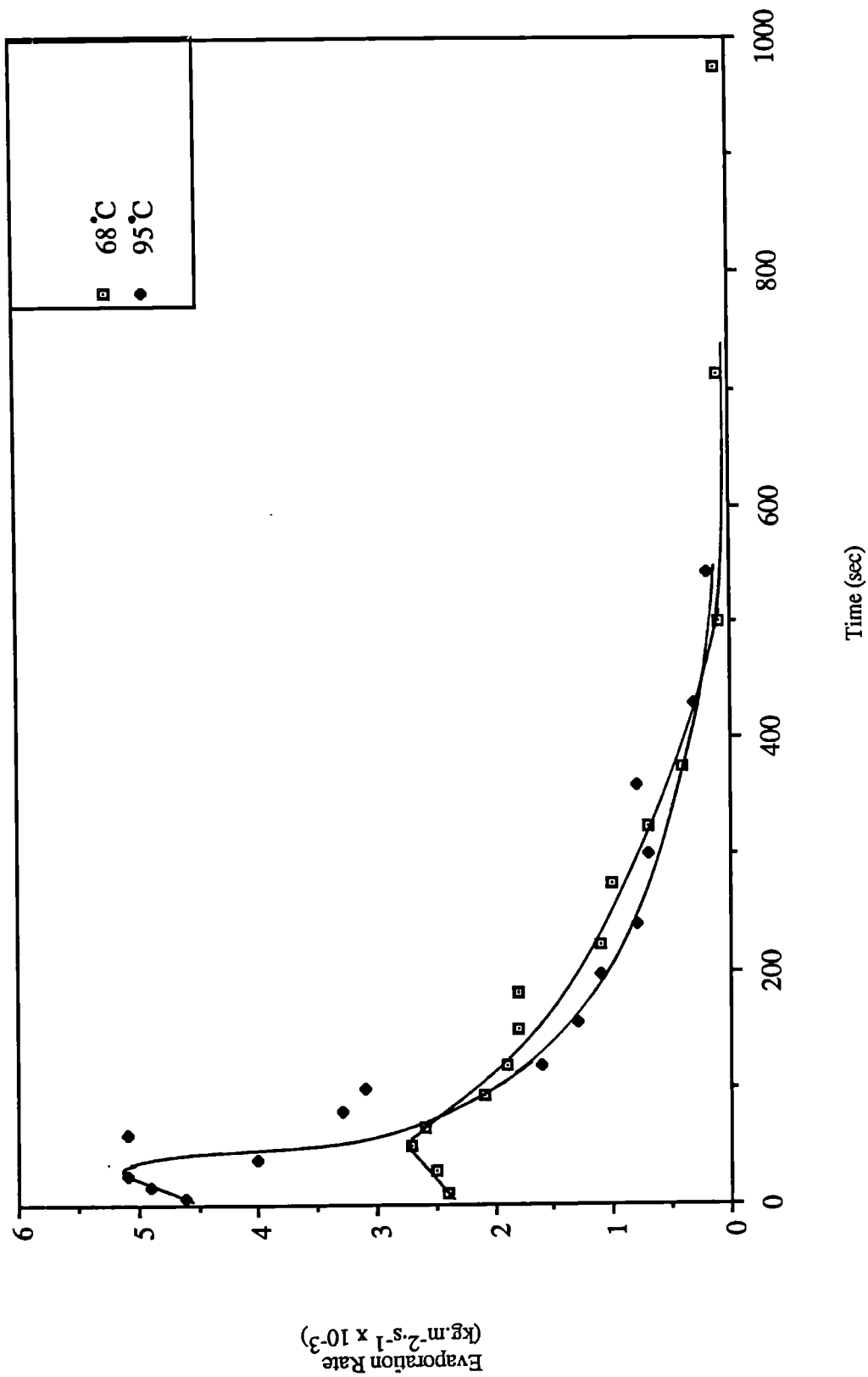


Figure 9.3 Drying Rate Curves For Drops of Sucrose Solution  
at 40 w/w% Solids and a 2mm Diameter Nozzle

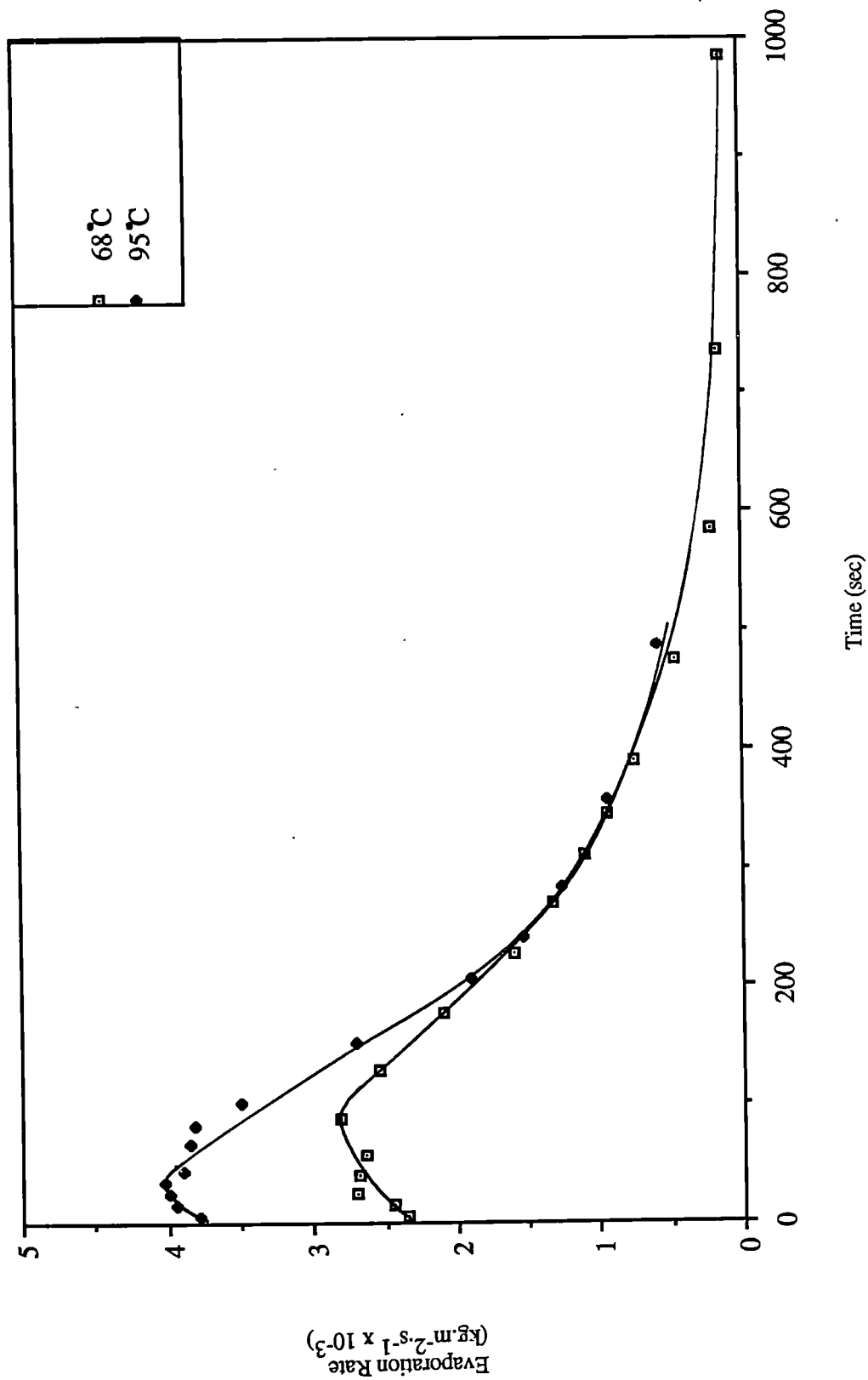


Figure 9.4 Drying Rate Curves For Drops of Sucrose Solution at 40 w/w% Solids and a 4mm Diameter Nozzle

increase in the evaporation rate as mass transfer occurs from a free-liquid surface, and the drop temperature decreases to the wet-bulb temperature. This initial stage is not accompanied by skin or crust formation. Once the drop attains the wet-bulb temperature a dynamic equilibrium exists between the rates of heat and mass transfer so that a period of constant-rate is observed. During this period material structure has no influence and the drying rate is, therefore, constant as long as the heat transfer rate is held constant by external conditions, i.e., that the temperature, humidity and velocity of the surrounding air remain constant. In the case of sucrose solution as well as potassium sulphate solution (section 9.2) a very short constant rate period was observed which was found to decrease with increasing temperature as the critical moisture content was attained more rapidly at higher temperatures.

Once the critical moisture content or the saturation point is attained the third period, or the falling-rate period, begins. This is characterised by the formation of a crust, or in the case of sucrose solution, a 'skin', a sharp decrease in the evaporation rate and a rise in drop temperature. At lower temperatures however, as seen in Figures 9.1-9.4, the decrease is more gradual as the time taken from partial to complete crust formation is longer.

During the falling rate period, a crust/skin providing the major resistance to mass transfer, originates on the underside facing the air stream and grows upwards around the drop. When the crust is complete there is a sharp fall in the evaporation rate and then a steady, gradual fall to 'complete' dryness, down to the bound moisture content. As expected, the latter is attained more quickly at a higher temperature.

A characteristic feature of the drying of drops of sucrose solution is that prior to crust formation a pliable and a relatively impervious skin forms over the

drop surface. For example a drop at an air temperature of 68°C (N.S=2mm, Conc=20w/w%) up to ~1200s did not exhibit crust formation, yet the rate of mass transfer after ~500s became very small (see Fig.9.5). This 'flattening' of the mass versus time curve, before crust formation, occurred for all the runs (see Figures 9.6-9.8). This suggested that a film or skin had encased the drop making moisture transfer very difficult, although not absent altogether. The formation of a skin over the drop surface resulted in extended drying times and a smooth crust of low porosity as shown in Figure 9.9. A similar phenomena was observed by Ali when drying from a nozzle an organic pigment which exhibited film formation (137). There is indeed a remarkable similarity between the crust appearance after ~2000s. A smooth outer surface would clearly be expected since the crust initially grows inwards from a smooth film.

At temperatures below 100°C, once the crust had formed around the drop, the latter assumed an almost spherical symmetry and thereafter the drop size remained constant. However, at higher temperatures, >100°C, after the skin had formed, occurrence of sudden inflation and bursting was observed. After a certain time, e.g on average 330s at 116°C, 190s at 127°C and 130s at 143°C, a bubble formed inside the drop and grew until the vapour-pressure build-up caused it to collapse. The bubble then reformed and grew until it collapsed once again due to the release of vapour from within the drop. This sequence of inflation, rupture and reformation occurred several times until the drop was carried away in the air stream. Figure 9.10 shows an initial part of one such cycle of events up to rupture for a drop of sucrose solution at an air temperature of 127°C.

Therefore, in a case such as for drops of sucrose solution where a relatively impervious skin or membrane forms, providing the initial resistance to

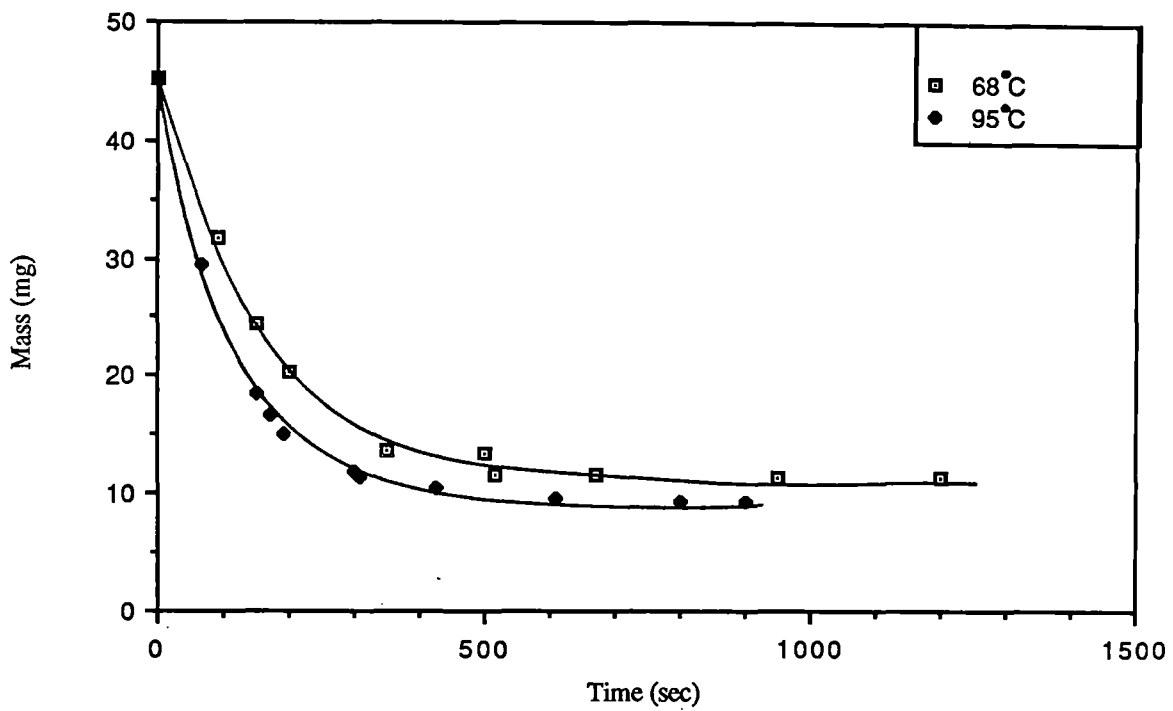


Figure 9.5 Drop Mass-vs-Time For Sucrose Solution (20w/w%) using a 2mm Diameter Nozzle

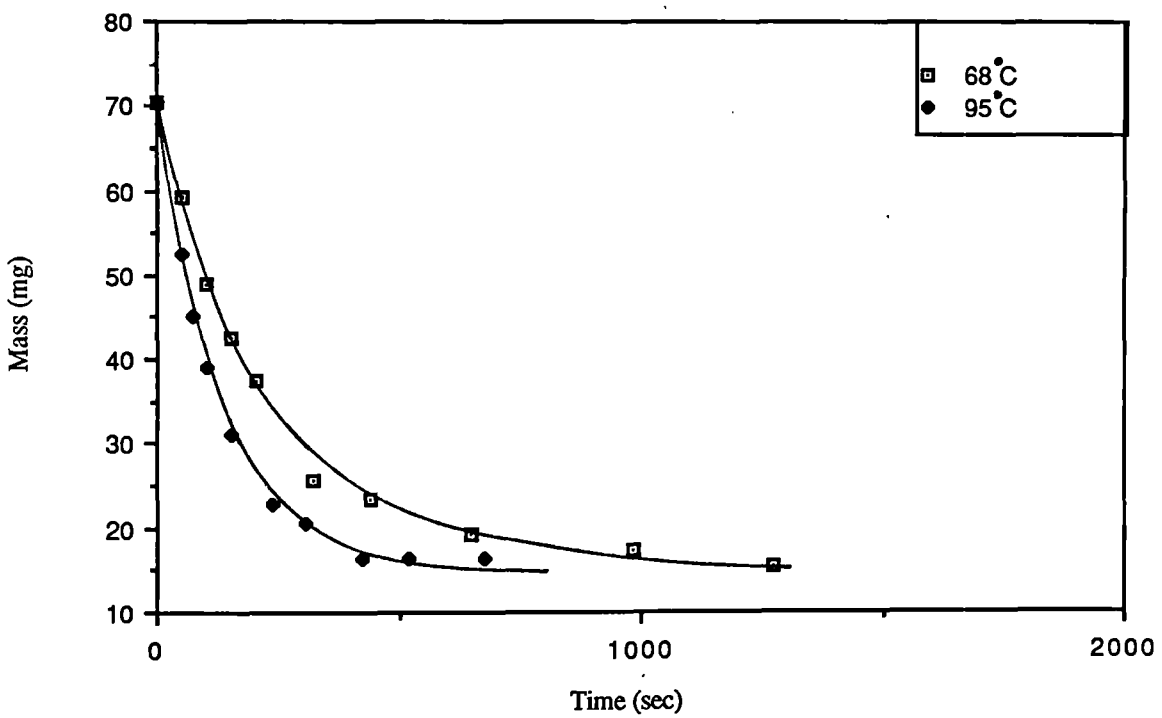


Figure 9.6 Drop Mass-vs- Time For Sucrose Solution (20w/w%) using a 4mm Diameter Nozzle

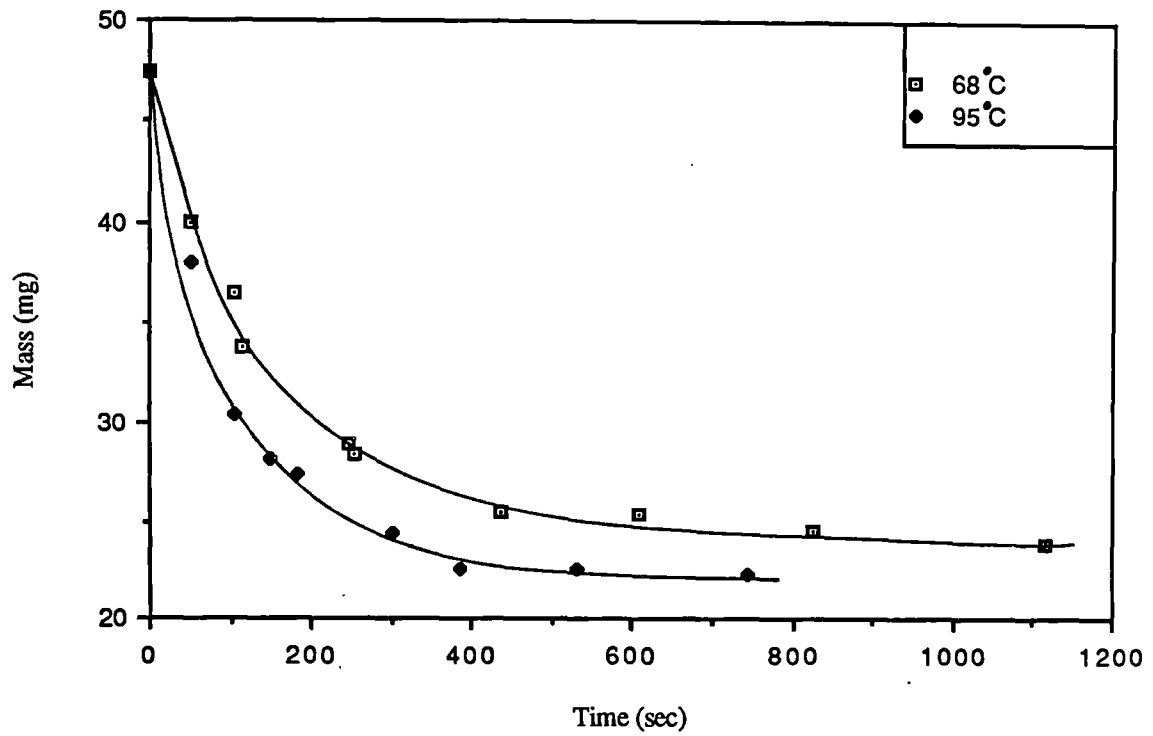


Figure 9.7 Drop Mass-vs-Time For Sucrose Solution (40w/w%) using a 2mm Diameter Nozzle

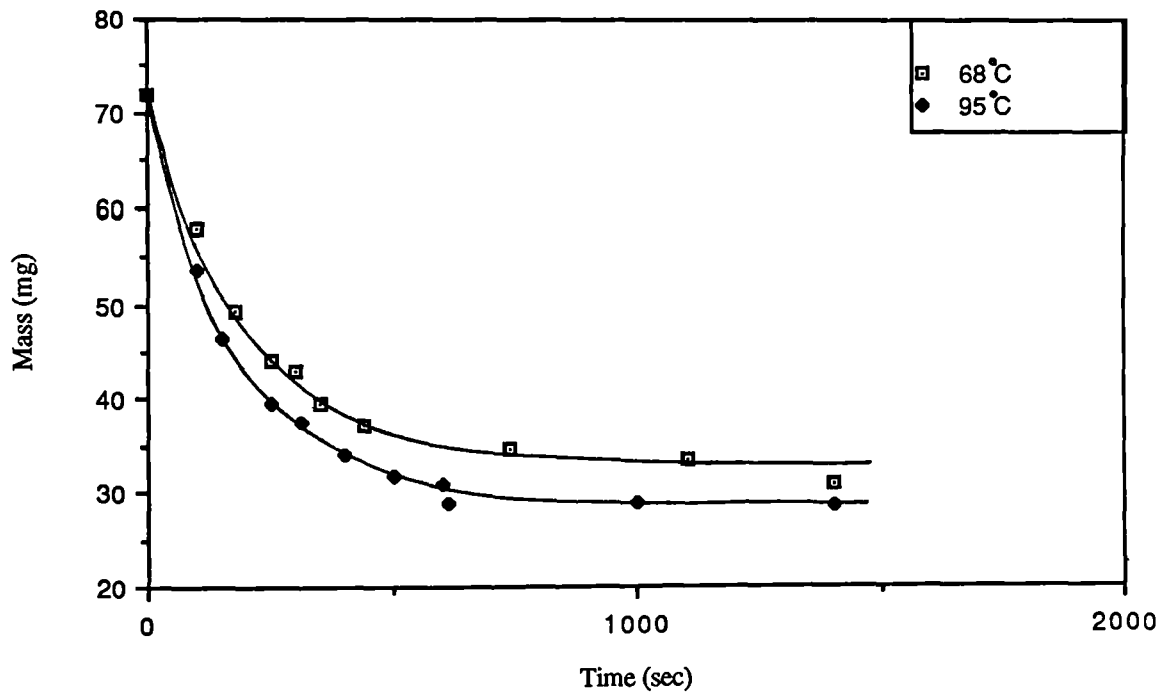


Figure 9.8 Drop Mass-vs-Time For Sucrose Solution (40w/w%) using a 4mm Diameter Nozzle



outer surface  
 $\theta = 2160$  s



Inner Surface  
 $\theta = 2160$  s

Figure 9.9 Electron micrographs of dried crusts of sucrose solution (40w/w%) at 68°C

mass transfer, the overall mass transfer coefficient, equation 5.30, must contain a term to include for the resistance to mass transfer due to this primary film . Normally when only a crust is formed, prior to crust formation the controlling resistance to mass transfer lies in the gas film around the drop. Once the crust starts to form the controlling resistance moves from the gas-film into the crust . In a previous study (137) with sodium sulphate decahydrate drops it was observed that a 32% thicker crust was obtained with an increase in air temperature from 100°C to 120°C. However, the crust only increased by 8% when the air velocity was increased by two fold from 0.6ms<sup>-1</sup> to 1.2 ms<sup>-1</sup>, confirming the relatively small resistance offered by the gas film once a crust is formed. However, when a skin forms prior to a crust, the overall mass transfer coefficient should include another term for skin mass transfer coefficient ( $k_s$ ), thus,

$$\frac{1}{K_o} = \frac{1}{k_g} + \frac{1}{k_s} \quad \text{--- 9.1}$$

Once the crust forms, the overall mass transfer coefficient reverts to,

$$\frac{1}{K_o} = \frac{1}{Hk_g} + \frac{1}{k_c} \quad \text{--- 9.2}$$

since the outer surface is, by definition, solid and not a film.

The driving force for mass transfer across a skin results from the difference in vapour pressure between the plane just beneath the skin and outside. No quantitative data are available on the skin resistance which would obviously depend upon the material and the drying temperature. However, in one case, from a comparison of evaporation rates of different pigment solutions of similar initial solids concentrations under identical conditions, one skin-forming and one normal, Ali (137) estimated that it accounted for 30% of

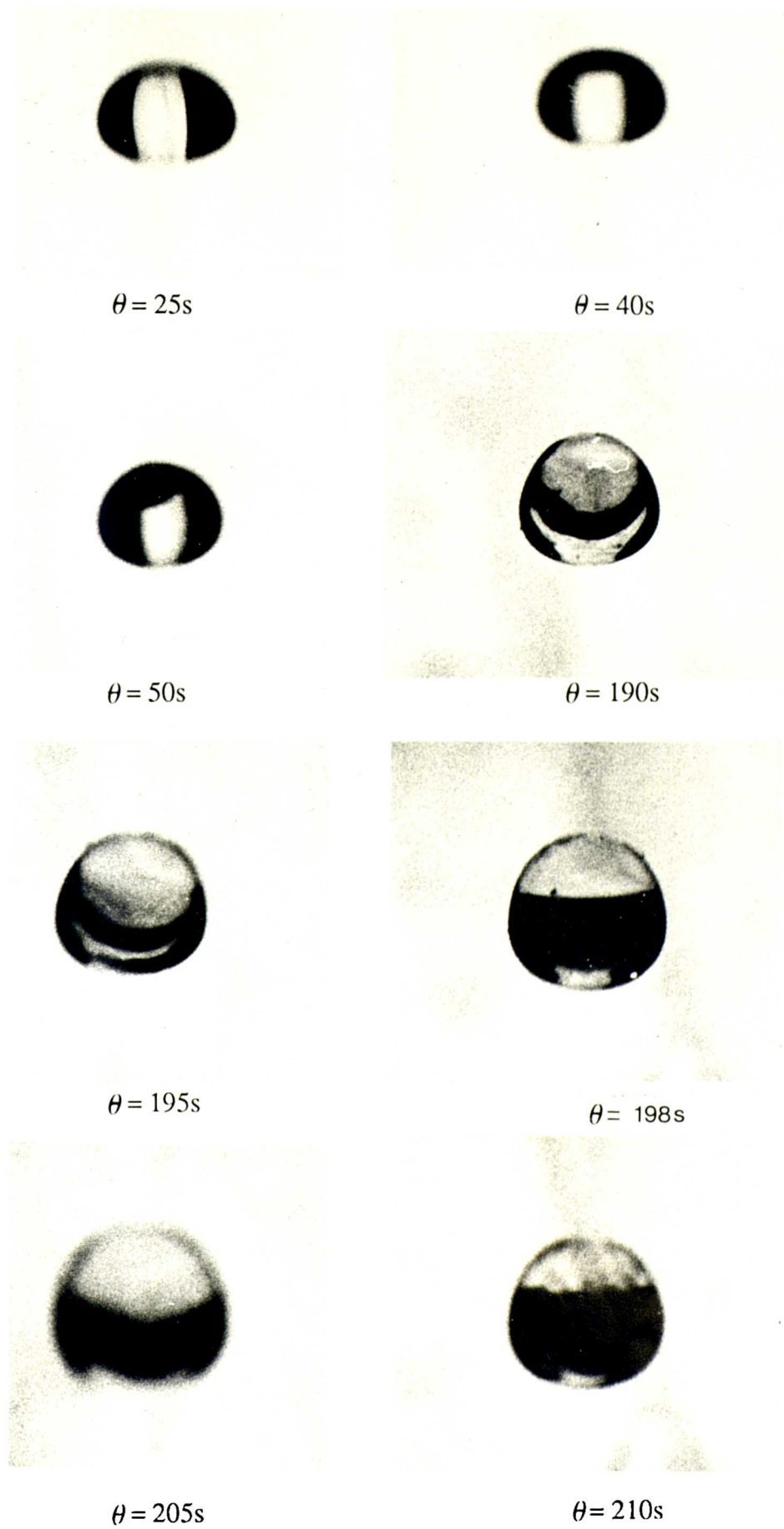


Figure 9.10 Photographs of a sucrose solution (40w/w%) drop exhibiting a 'ballooning' effect at 127°C.

the resistance to mass transfer prior to crust formation. Once a crust is formed the driving force is the concentration gradient. To increase mass transfer prior to crust formation the following considerations might be applicable:

(a) Increase the vapour pressure driving force across the skin. This could be achieved by ;

(i) Use of air of reduced humidity

(ii) Application of vacuum in conjunction with heat transfer by radiation, or with the feed initially heated then sprayed.

(b) Additives may be used to affect the skin structure and give a more porous membrane. For example in a previous study (137) Dispersol and sodium chloride were used as additives to an organic slurry and were found to increase evaporation rates. Furthermore the nature of the additive also affected the evaporation rate. For instance the formulation containing sodium chloride dried more rapidly.

(c) Application of microwave drying which might also induce turbulence within the drops. However, the critical rate of internal vapour generation would have to be carefully controlled depending upon the skin permeability. e.g attempts to microwave dry grapes have not been successful (147).

#### 9.1.2 Effect of Air temperature on the Rate of Mass Transfer

As expected increasing the air temperature increased the rate of mass transfer (see Figures 9.1-9.4) with the maximum rate being achieved more quickly. In fact , Table 9.1 shows that increasing the temperature from 68°C to 95°C almost halved the time to attain maximum evaporation rate.

#### 9.1.3 Effect of Concentration on the Rate of Mass Transfer

Figures 9.11 and 9.12 demonstrate that, as expected, increasing the initial concentration firstly reduced the time at which maximum evaporation was

Concentration ( wt/wt % )	Nozzle Size (mm)	Operating Temperature ( °C )	Critical Moisture Content $\epsilon_{crit}$	Corresponding Time $\theta_{crit}$ ( sec )
20	2	68	22.0	100
20	2	95	23.6	50
20	4	68	30.0	105
20	4	95	30.0	75
40	2	68	20.8	50
40	2	95	23.0	25
40	4	68	24.1	60
40	4	95	26.0	30

**Table 9.1 Effect of Operating Variables on the Critical Moisture Content**

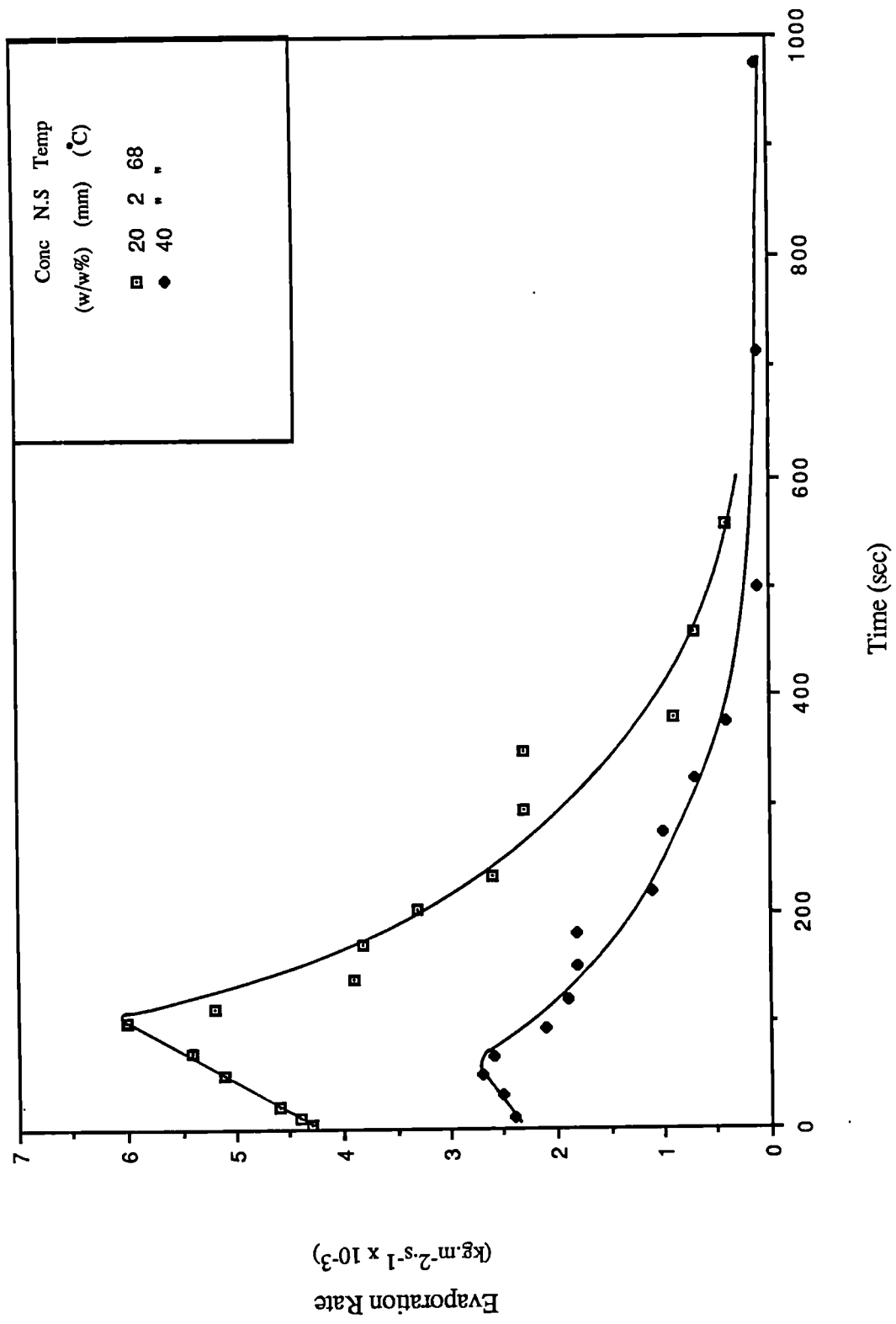


Figure 9.11 Effect of Concentration on the Evaporation Rate

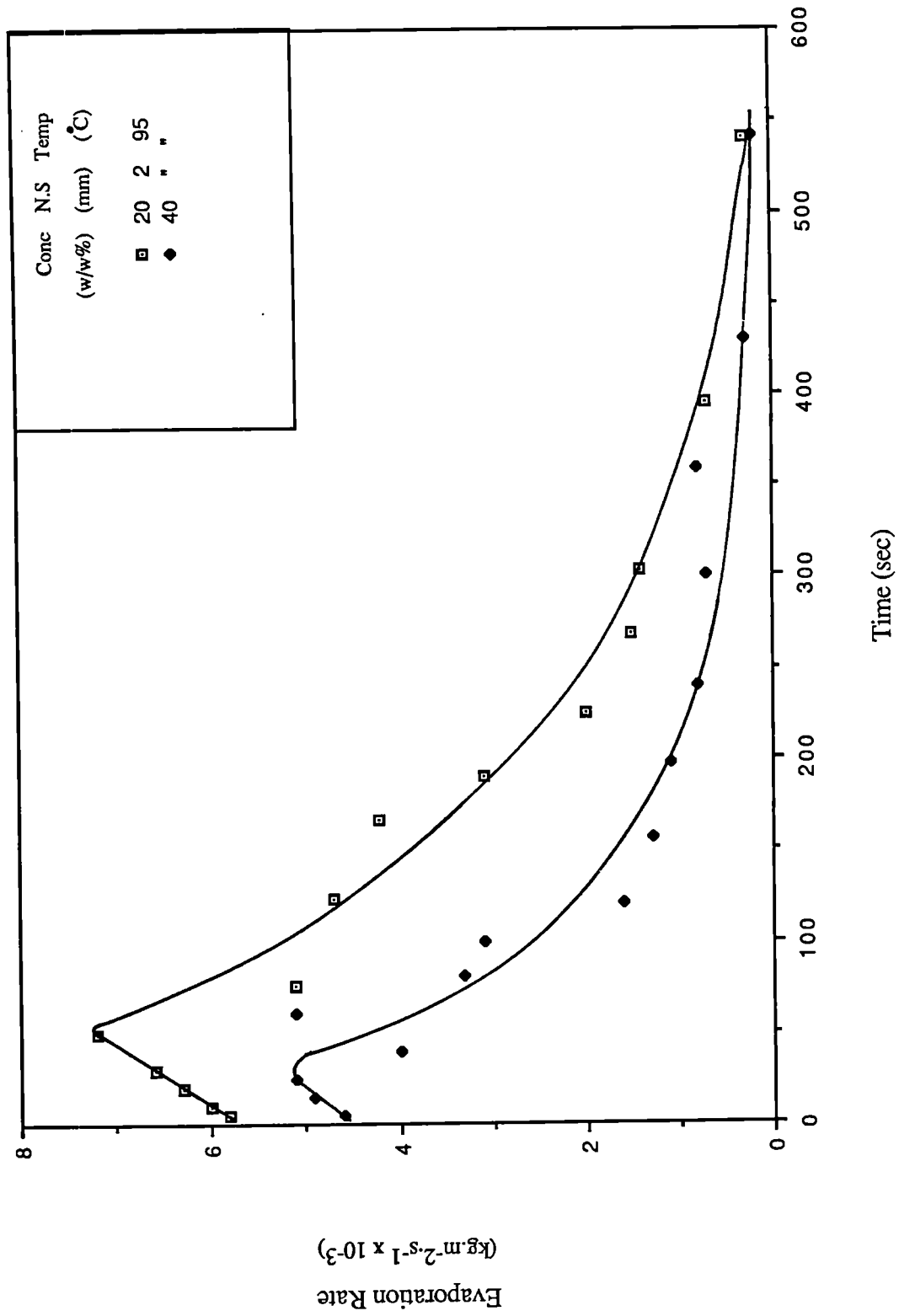


Figure 9.12 Effect of Concentration on the Evaporation Rate

achieved, i.e increasing solids content promotes more rapid solid phase formation, and secondly decreased the evaporation rate after corresponding times. Two effects may account for this ;

(i) The lowering of the vapour pressure of water as solution concentration is increased; and

(ii) The attainment of the critical moisture content, or the saturation point with concentrated solutions, before the maximum temperature driving force ( $T_a - T_{wb}$ ) is reached.

#### 9.1.4 Effect of Operating Temperature, Drop Diameter and Concentration on the Critical Moisture Content

The drying rate curve is used as fundamental data in process design and optimization of a drying plant. It is commonly accepted that the drying rate curve can be roughly divided into two sections: the first, wherein the rate remains relatively constant independent of moisture content, and the second, where the rate falls rapidly with diminishing moisture content. This drying rate curve may thus be characterised by the 'constant' drying rate, the critical moisture content of transition between the two drying periods, and the geometrical shape of the falling-rate curve.

In order to estimate the drying time in the falling-rate period, as well as the total drying time, it is necessary to know the values of the critical moisture content. This is defined as an averaged value, rather than a local one, so is not strictly a specific property for a given material (144). Kamei (142) and Krischer (143) reported that this value depended upon the initial drying rate, thickness of material or size of the element such as a droplet, and apparent diffusivity of moisture within the wet material. Table 9.1 confirms this to be the case for the solids studied here.

As the temperature is increased from 68°C to 95°C there is a slight increase in the critical moisture content possibly because of the greater rate of evaporation at the higher temperature, and because of differences in viscosities of the liquid at the two temperatures leading to differences in droplet perturbations and hence moisture migration. Drop size also appears to have an effect on the critical moisture content possibly because at different drop sizes the degree of drop distortion or oscillation is different which affects internal circulation, moisture migration and consequently rates of evaporation. Initial concentration also appears to have some bearing on the critical moisture content again possibly due to differences in viscosities, shape distortion and evaporation rates.

#### 9.1.5 Film Resistance Prior to Crust Formation

At temperatures below 100°C, for drops of sucrose solution, moisture transfer was by diffusion through the film, since intermittent drop inflation/collapse and reformation was not evident. Furthermore, the material also formed a smooth crust growing inwards from a smooth film.

This phenomena of film or skin formation may be described by analogy to transport coefficients in membranes. For the case of a solvent A diffusing across a membrane, diffusional flux is given by,

$$N_A = \frac{D_A}{x} (C_{A0} - C_{Ax}) \quad \text{---9.3}$$

where  $D_A$  = diffusion coefficient

$x$  = membrane thickness

If the values of  $N_A$ ,  $C_{A0}$ ,  $C_{Ax}$  and  $x$  are known, then the value of the

diffusion coefficient can be readily determined. However, the concentration of A on the surface of the membrane will be unknown. The driving force can be expressed in terms of the partial pressure of A on either side of the membrane. Therefore equation 9.3 becomes,

$$N_A = \frac{P_m}{x} (P_i - P_o) \quad \text{---9.4}$$

where  $P_m$  = permeability

$P_i$  = partial pressure beneath the membrane

$P_o$  = partial pressure outside the membrane

For the case of film forming materials  $P_i$ , prior to crust formation, will approximate to the vapour pressure at the wet-bulb temperature, although depressed as described in Chapter 4;  $P_o$  is the vapour pressure in the surrounding air at the known operating temperature  $T_a$ , and  $N_A$  can be determined experimentally. Therefore,  $P_m/x$  may be calculated and would represent the skin mass transfer coefficient.

In practical spray drying processes, the formation of a skin would strongly influence drying. The material will tend to produce products that might stick together which is undesirable. On the other hand particles which impinge on the chamber wall prior to 'dryness' may not adhere due to them bouncing. Conversely, materials which do not form a skin during drying form non-sticking products but may adhere to the chamber wall on impingement.

Furthermore, rupture of the drop skin should strongly influence drying. Rupture and collapse affect the developing morphology and may lead to an increase in the density of the particle. The inflate/deflate process can cause

mixing in the drop and in addition will expose the wet material inside the expanded drop to the outside environment. This mechanism of mass transfer by-passes the diffusional limitation of a non-rupturing or non-expanding drop and may therefore have significant effects on volatile retention and drying rates.

## **9.2 Drops of Potassium Sulphate Solution**

Section 9.1 dealt with the case of a film forming material. However, materials which educe crystals on drying and form a more open crust structure dry faster and exhibit totally different drying characteristics. The following section presents results for drops of potassium sulphate solution which forms a rigid, porous crust.

Investigations were carried out at varying air temperatures, initial drop diameters, air velocities and initial solids contents.

### **9.2.1 Drying Rates**

The drying rate curves and the changes in water content as a function of time are shown in Figures 9.13 - 9.18 and the data tabulated in Appendix A4.2. As for the case of drops of sucrose solution, the rate curves show an initial linear increase consistent with evaporation from liquid drops until the drop wet-bulb temperature and a maximum evaporation rate were reached. The moisture content during this initial stage of surface evaporation, correspondingly, decreases sharply especially at the higher temperatures of 65 and 95°C. This is followed by a short constant rate period, becoming shorter with increasing temperature, since the crust forms quickly once the drop has reached the critical moisture content or saturation point. As the crust grows over the drop surface there is a sharp fall in the rate, then a gradual fall to the bound

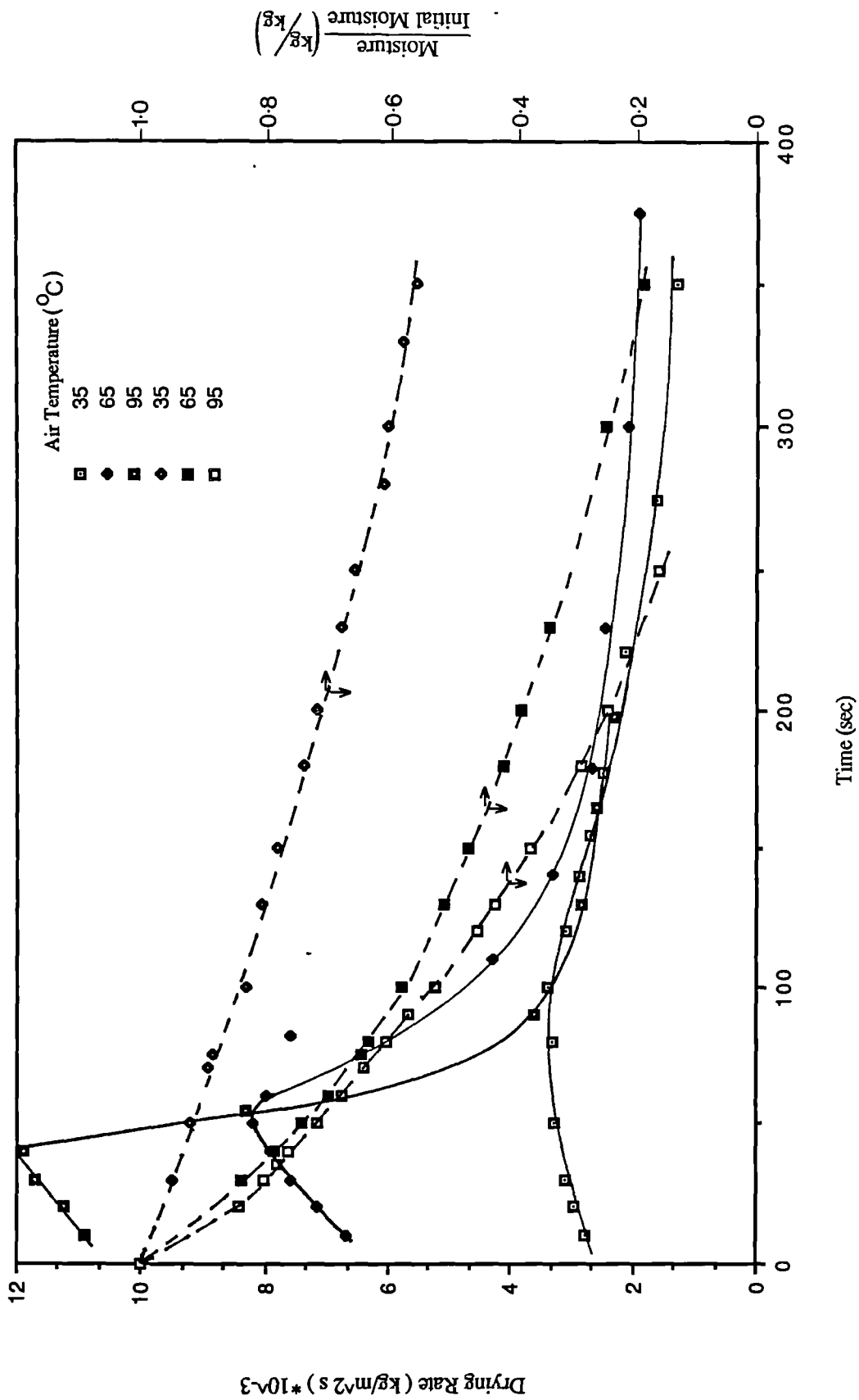


Figure 9.13 Drying Rate Curves and Water Content of 5w/w% Solution Drops of Potassium Sulphate using a 2mm Diameter Nozzle

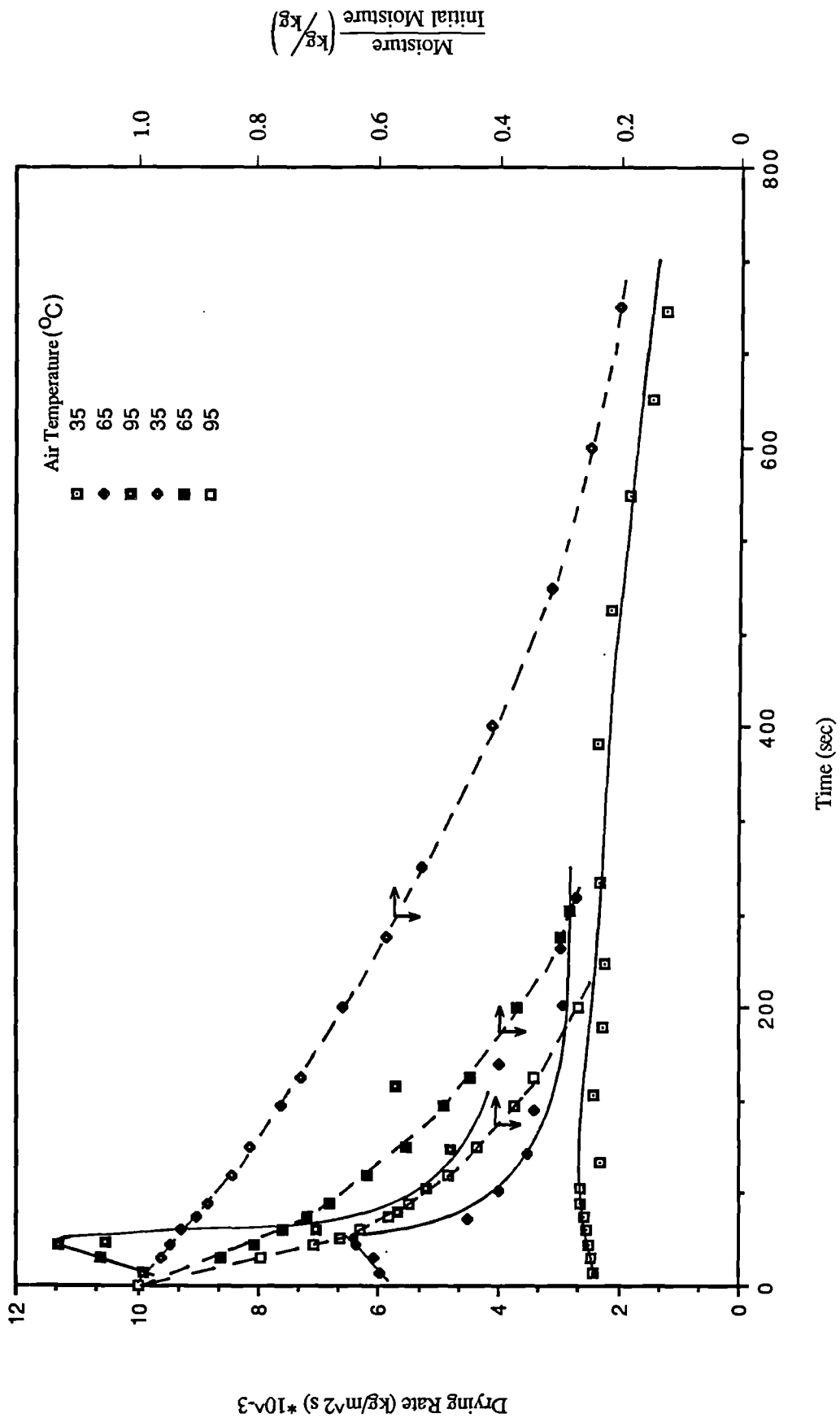


Figure 9.14 Drying Rate Curves and Water Content of 10w/w% Solution Drops of Potassium Sulphate using a 2mm Diameter Nozzle

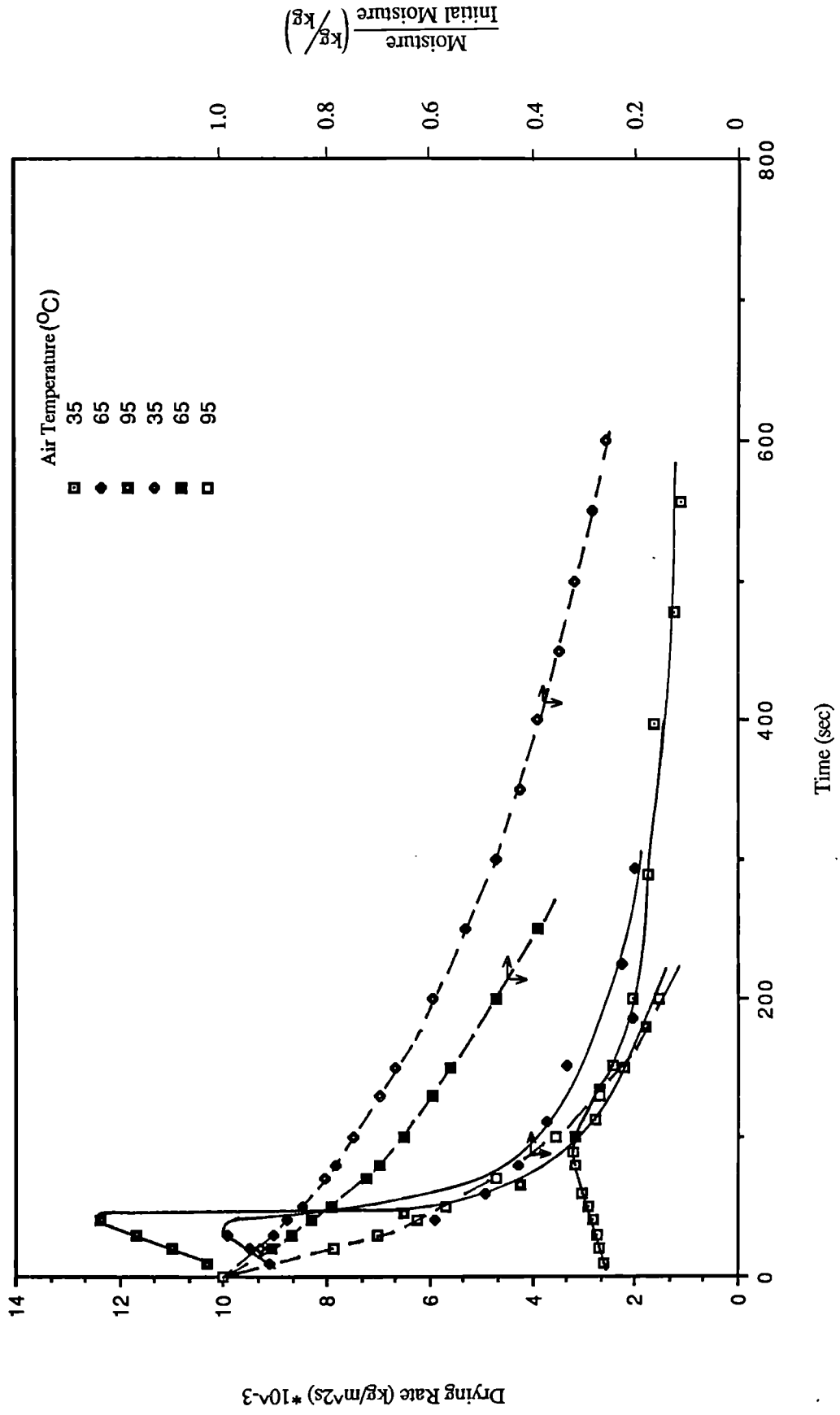


Figure 9.15 Drying rate Curves and Water Content of 5w/w% Solution Drops of Potassium Sulphate using a 3mm Diameter Nozzle

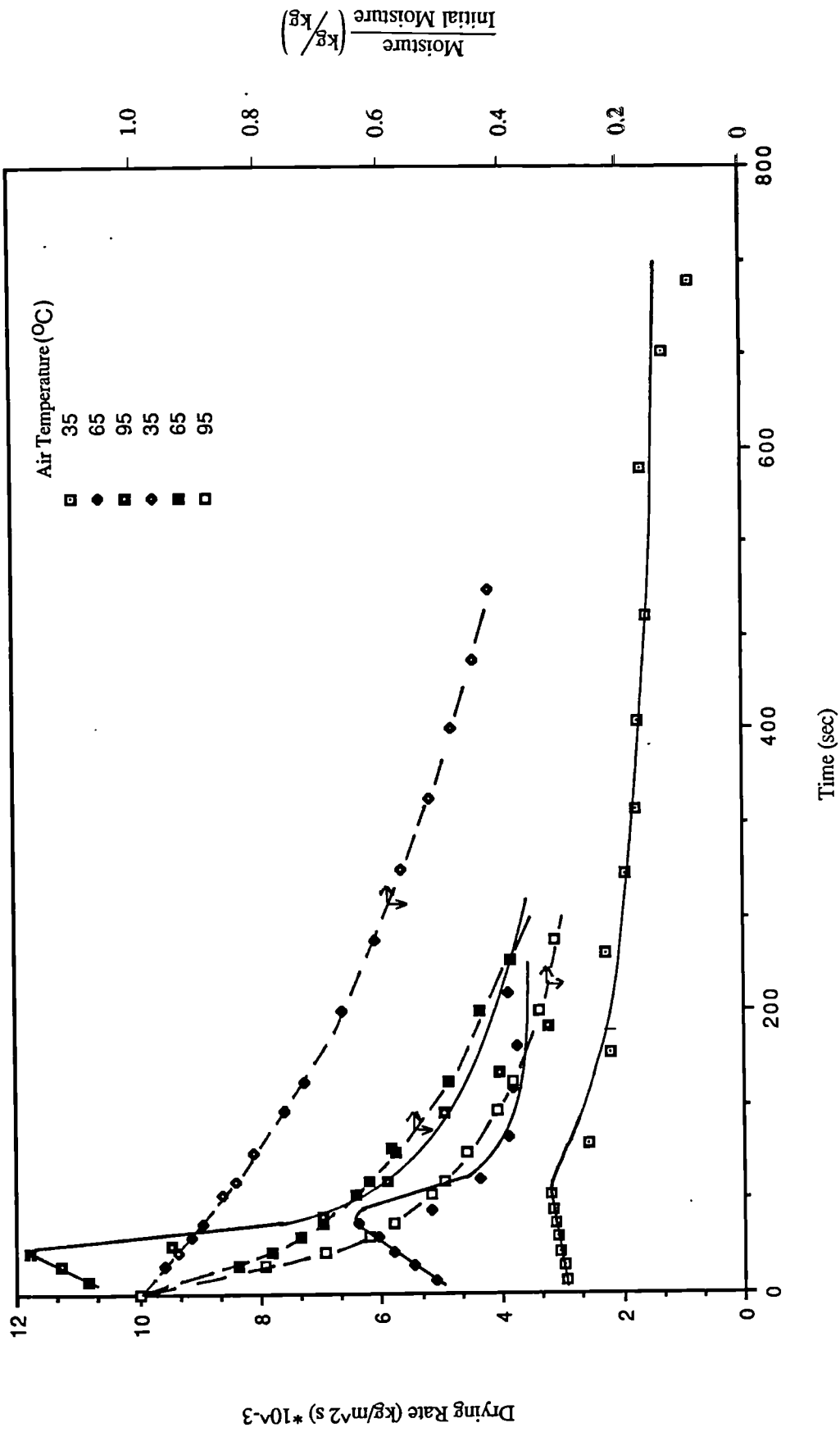


Figure 9.16 Drying Rate Curves and Water Content of 10w/w% Solution Drops of Potassium Sulphate using a 3mm Diameter Nozzle

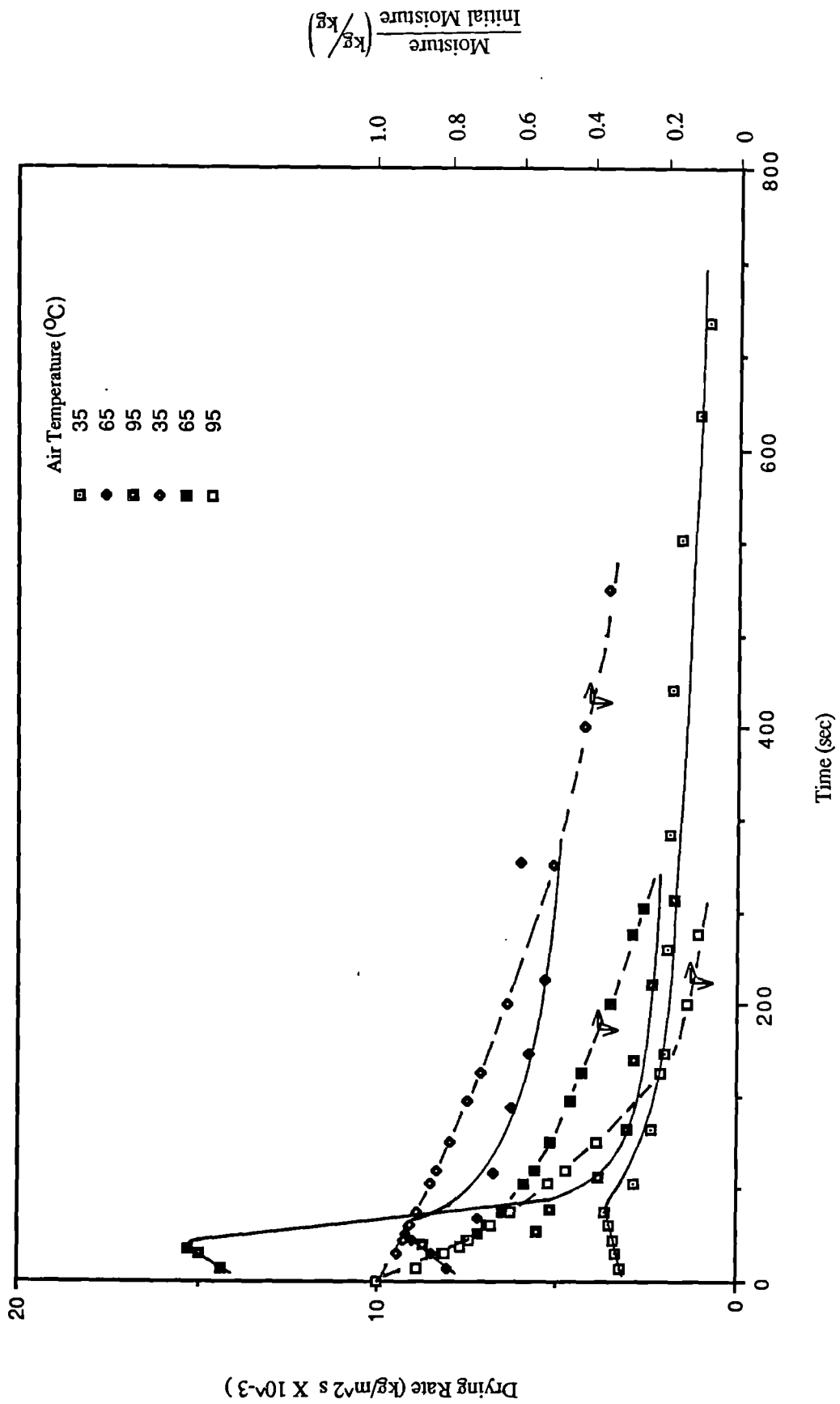


Figure 9.17 Drying Rate Curves and Water Content of 5w/w% Solution Drops of Potassium Sulphate using a 4mm Diameter Nozzle

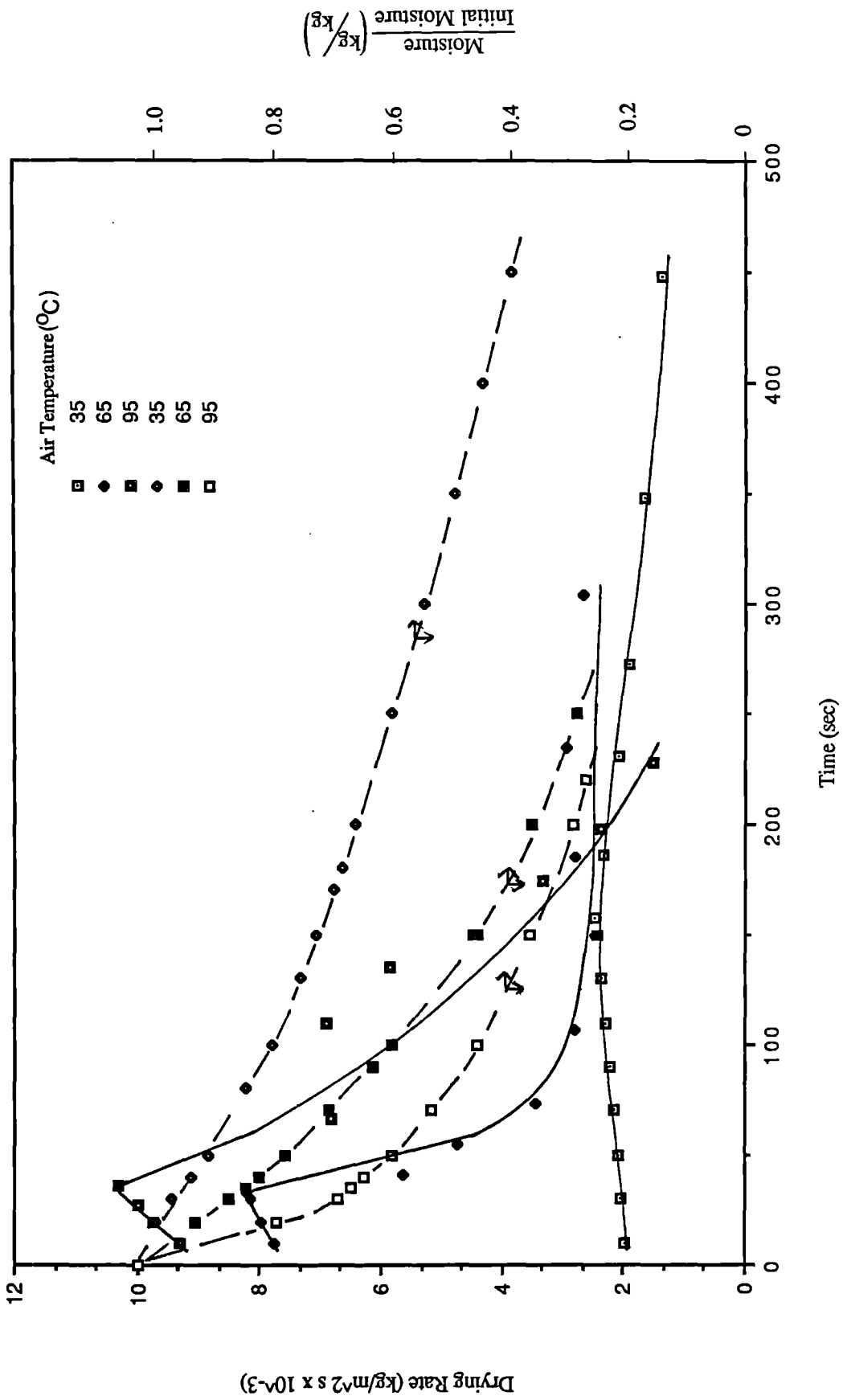


Figure 9.18 Drying Rate Curves and Water Content of 10w/w% Solution Drops of Potassium Sulphate using a 4mm Diameter Nozzle

or equilibrium moisture content. Figures 9.13-9.18 show, as expected, that increasing the temperature increased the rate of mass transfer while increasing the concentration decreased the evaporation rate and the time at which the maximum was achieved ( see section 9.13).

### 9.2.2 Appearance Changes and Drop Behaviour During Drying

Prior to crust formation drop behaviour was akin to pure liquid drops with the accompanying oscillations, deformations and rotations (see Chapter 8) and with a drop becoming more stable with decreasing size. However, once the crust had completely formed, drop behaviour became erratic making it difficult to retain the drop in the working section. Consequently, dried crusts could not be recovered for inspection under the Scanning Electron Microscope.

Sometimes, before deposition of the solid phase, the drop split up into two smaller droplets. This occasional break-up into two occurred through the air blowing a hole through the middle of the drop when the aerodynamic pressure exceeded the liquid head over the front stagnation point. Once the crust had formed around the drop its strength prevented the middle of the drop from being blown out.

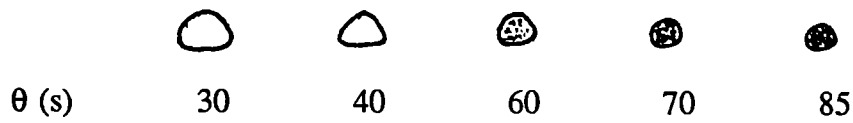
In a majority of the experimental runs, because of rotation about both the vertical and the horizontal axis, the crust grew randomly over the entire drop surface. This is shown diagrammatically in Figure 9.19 (a). Sometimes however, because of reduced rotation about the horizontal axis, the solid phase did not form randomly but started from the point of maximum evaporation, the front stagnation point on the leading face, and spread upwards. This behaviour resulted in a hollow saucer-shaped configuration as shown diagrammatically in Figure 9.19 (b) ; a particle shape not uncommon in spray dried powders (140). On occasions, an intermediate configuration was obtained with

the trailing surface showing a slight indentation. This is shown in Figure 9.19 (c). It was found that when the crust grew up to the equator and consequently formed a saucer-shape, Figure 9.19 (b), the drop became very stable in comparison with a drop whose surface was completely encrusted, Figure 9.19 (a). This of course resulted from the higher concentration of solute at the front of the droplet and hence greater density, a situation which would add to the droplet stability. Some of the saucer-shaped drops spun about the vertical axis and others floated without spinning. Figure 9.20 shows a drop in the process of forming a saucer-shape, whilst Figure 9.21 shows other configurations mentioned above. Saucer-like particles do sometimes occur in spray dried products but Charlesworth and Marshall (93), whilst postulating a partial localised crust -> complete crust mechanism for droplets drying in air below or above the boiling point of the solution, attributed non-spherical shapes to a pliable crust structure. In the drying of coffee extract below its boiling point for instance, the solid which encased the drop formed a pliable and relatively impervious skin, and the decrease in the particle volume which resulted from drying after completion of the skin caused it to dimple or wrinkle.

### **9.2.3 Comparison Between Predicted and Measured Drying Rates**

The drying rates of single drops were predicted using a modified version of Cheong's model (145) and the results are presented in Figures 9.22 - 9.30. An outline of the mathematical model is presented in Appendix A8. The plots demonstrate that the calculated rates are much lower than those determined experimentally, although the deviations generally decrease with time.

The explanation probably lies in the assumptions made when deriving the model. In the derivation drops were assumed to be perfect spheres. However,



(a) Conc = 10w/w%, N.S = 2mm, Ta = 95°C



(b) Conc = 10w/w%, N.S = 4mm, Ta = 65°C



(c) conc = 10w/w%, N.S = 3mm, Ta = 95°C

Figure 9.19 Changes in Appearance of Potassium Sulphate Drops

under the present experimental conditions, as discussed in Chapter 8, a drop exhibited oscillations, rotations and random deformations prior to crust formation which would tend to increase rates of heat and mass transfer. Because of the interaction of circulation, oscillation and deformation, quantitative determinations of individual contributions to mass transfer are difficult to obtain. However, Kronig and Brink (29) have shown theoretically that rates of mass transfer from drops in liquid-liquid systems should be increased by 2.5 times when circulation is present. Garner and Lane (75) obtained this figure experimentally by determining the effect of circulation on the absorption of

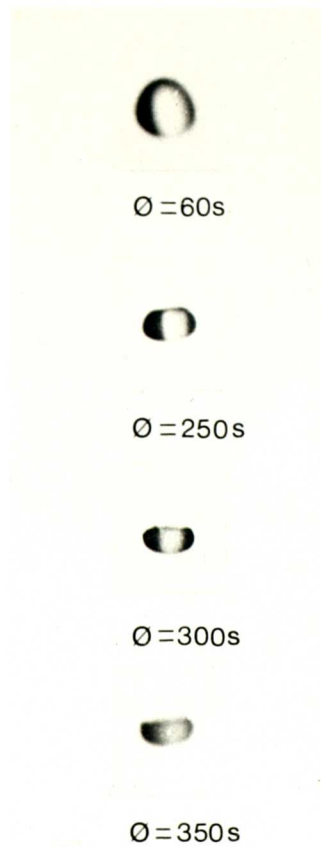


Figure 9.20 A drop of potassium sulphate solution forming a truncated spheroid  
 ( conc =5w/w%, N.S =4mm, T =65oC)

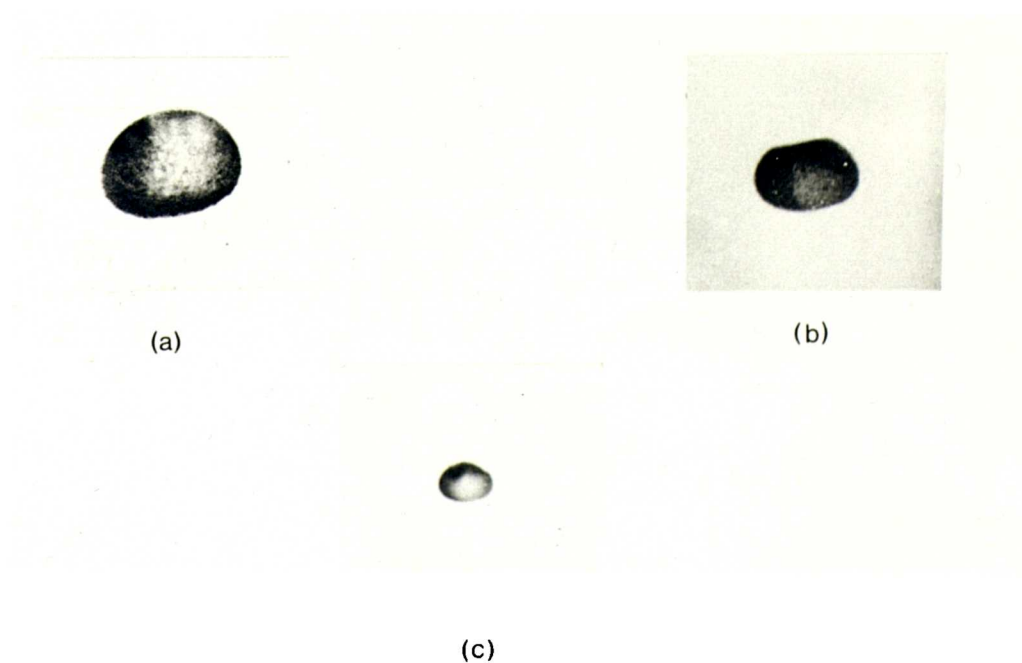


Figure 9.21 Photographs showing various configurations of dried crusts of potassium sulphate solution :  
 (a) Complete crust formation (conc =10w/w%, N.S=3mm, T=95°C)  
 (b) & (c) Slight indentation of trailing surface (conc =10w/w% , N.S =4mm, T =95°C)

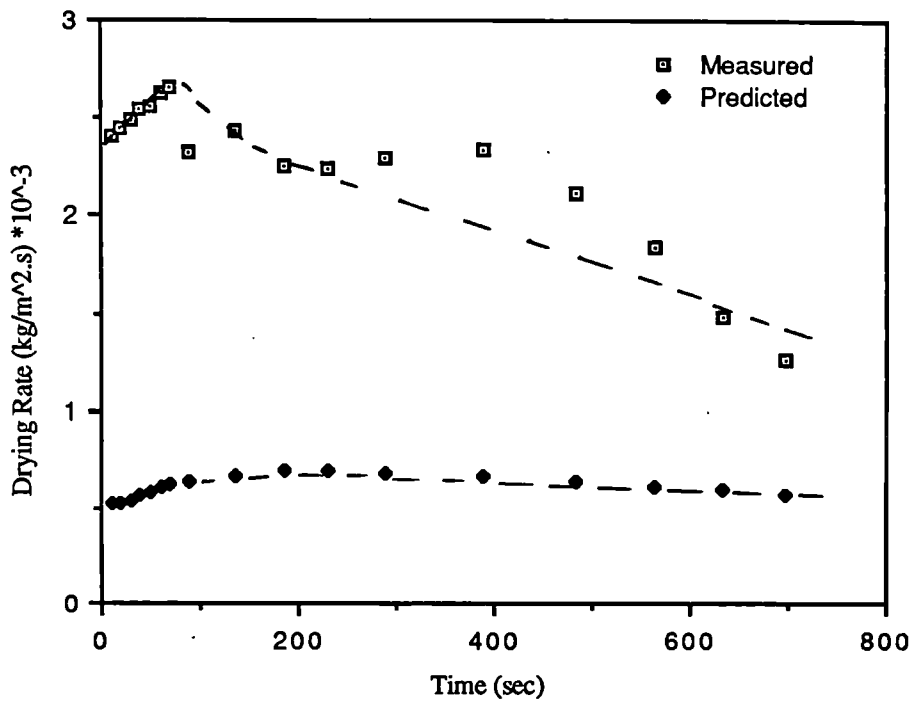


Figure 9.22 Comparison Between Measured and Predicted Drying rates of Potassium Sulphate Solution Drops at 36 C Using 10w/w% Solids and a 2mm Diameter Nozzle

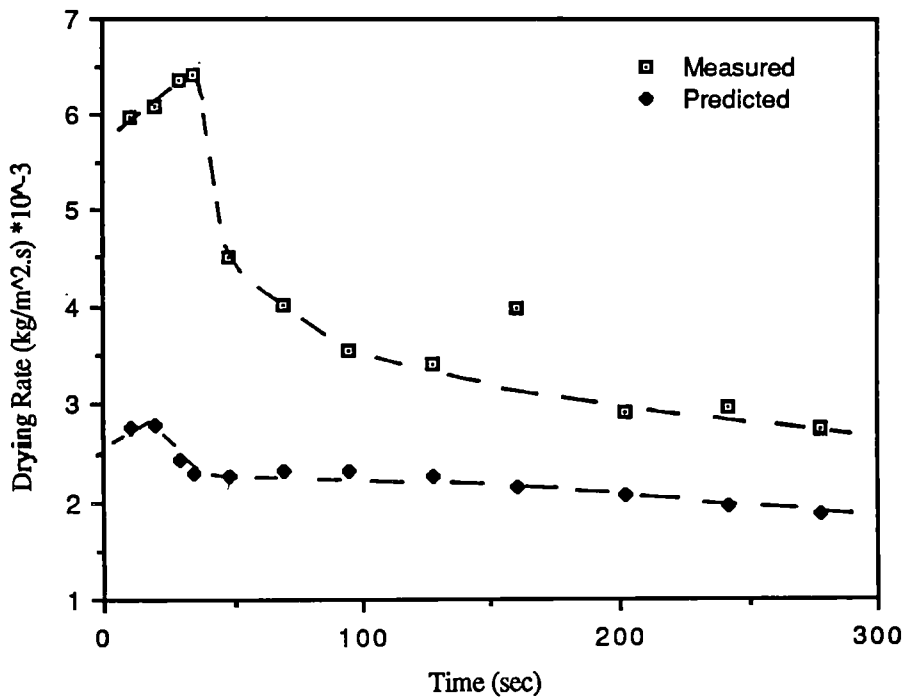


Figure 9.23 Comparison Between Measured and Predicted Drying Rates of Potassium Sulphate Solution Drops at 65 C Using 10w/w% Solids and a 2mm Diameter Nozzle

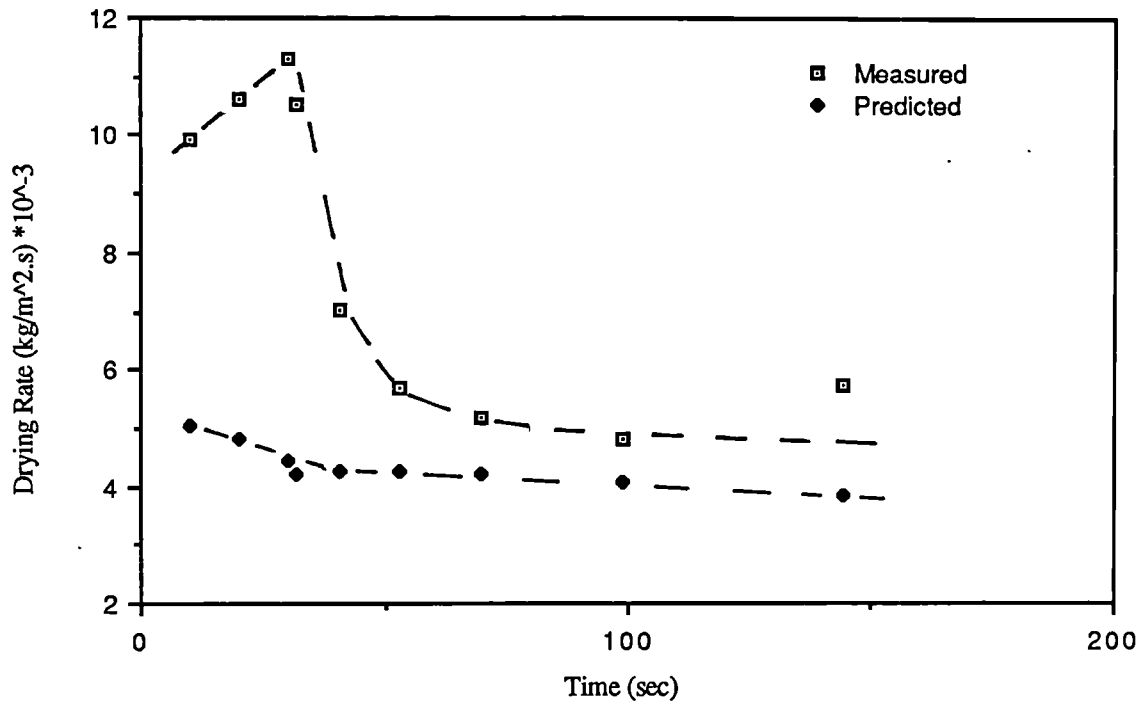


Figure 9.24 Comparison Between Measured and Predicted Drying Rates of Potassium Sulphate Solution Drops at 95 C Using 10w/w% Solids and a 2mm Diameter Nozzle

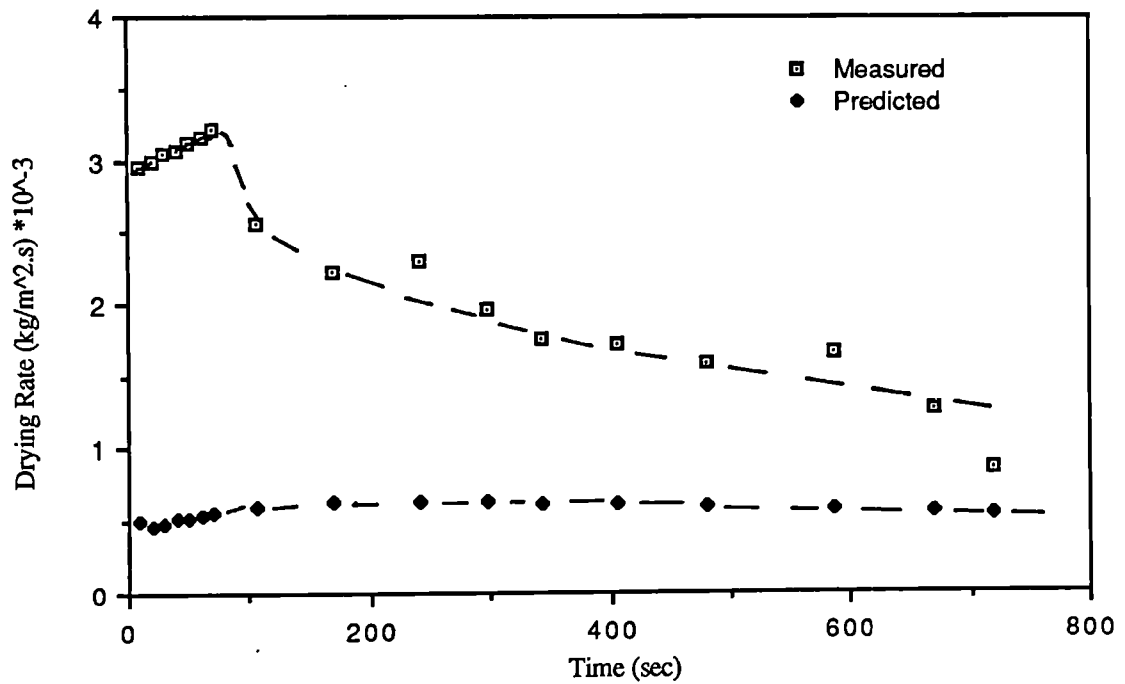


Figure 9.25 Comparison Between Measured and Predicted Drying Rates of Potassium Sulphate Solution Drops at 36 C Using 10w/w% Solids and a 3mm Diameter Nozzle

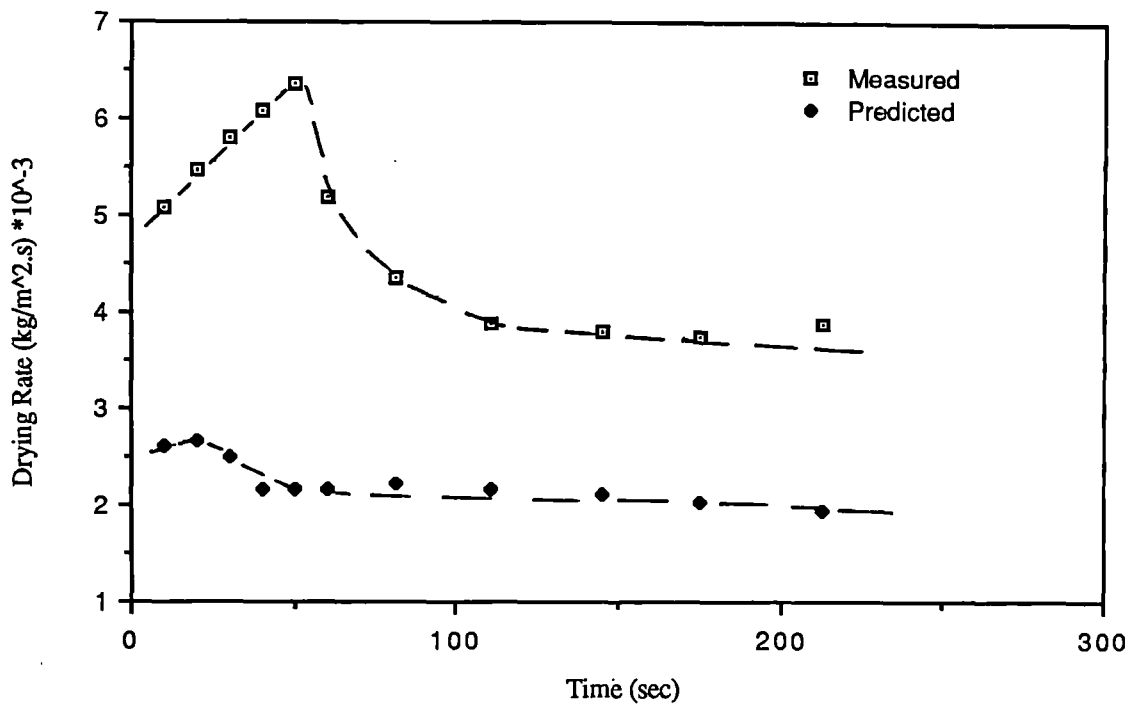


Figure 9.26 Comparison Between Measured and Predicted drying Rates of Potassium Sulphate Solution Drops at 65 C Using 10w/w% Solids and a 3mm Diameter Nozzle

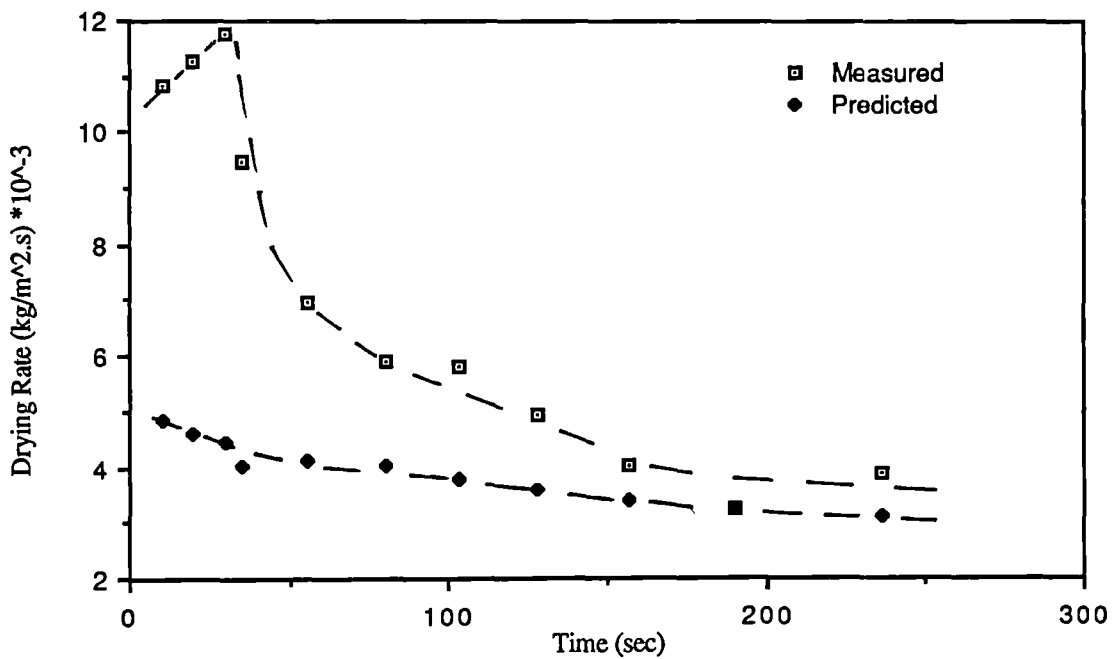


Figure 9.27 Comparison Between Measured and Predicted Drying Rates of Potassium Sulphate Solution Drops at 95 C Using 10w/w% Solids and a 3mm Diameter Nozzle

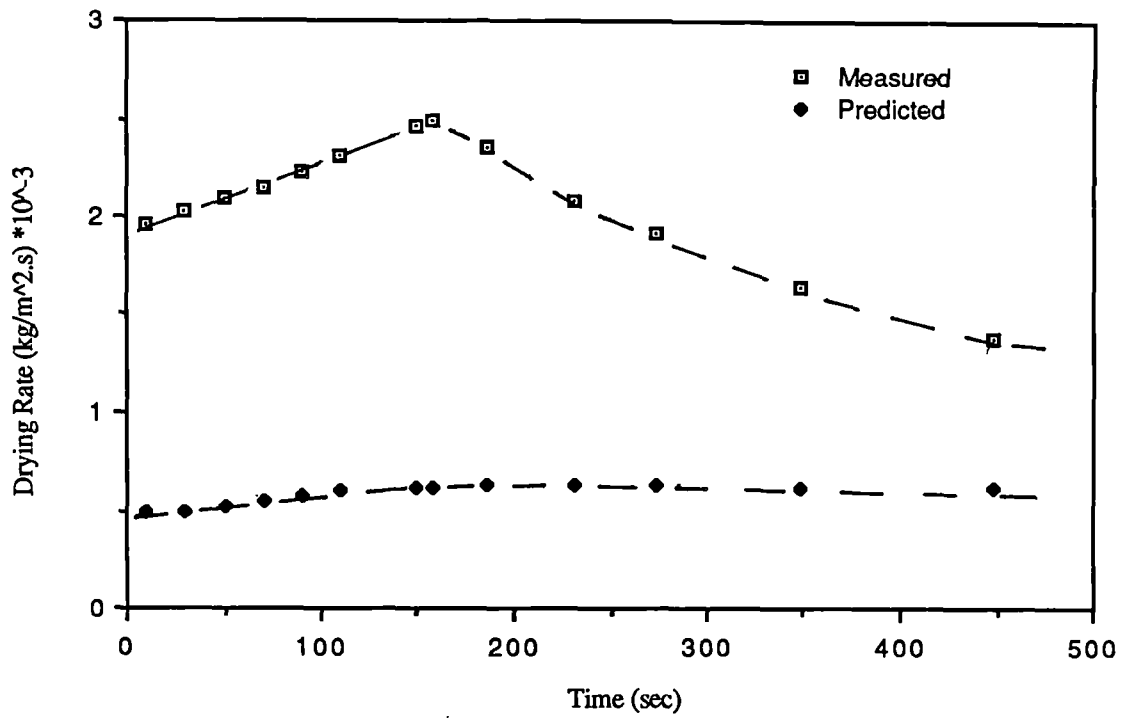


Figure 9.28 Comparison Between Predicted and Measured Drying Rates of Potassium Sulphate Solution Drops at 36 C Using 10w/w% Solids and a 4mm Diameter Nozzle

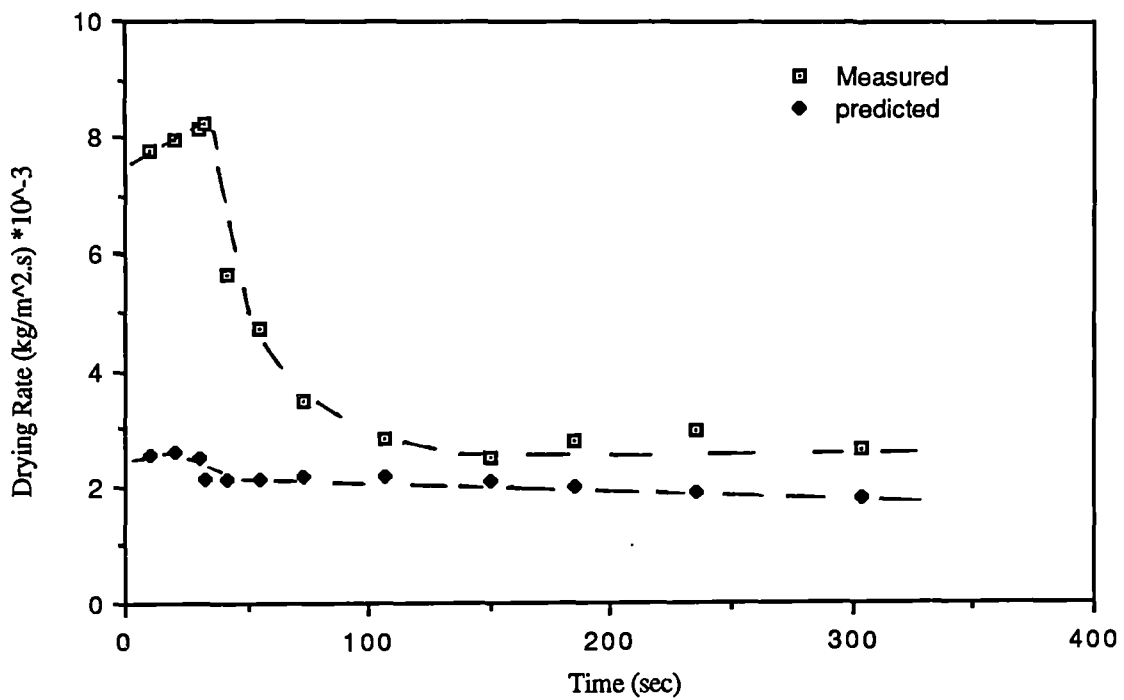
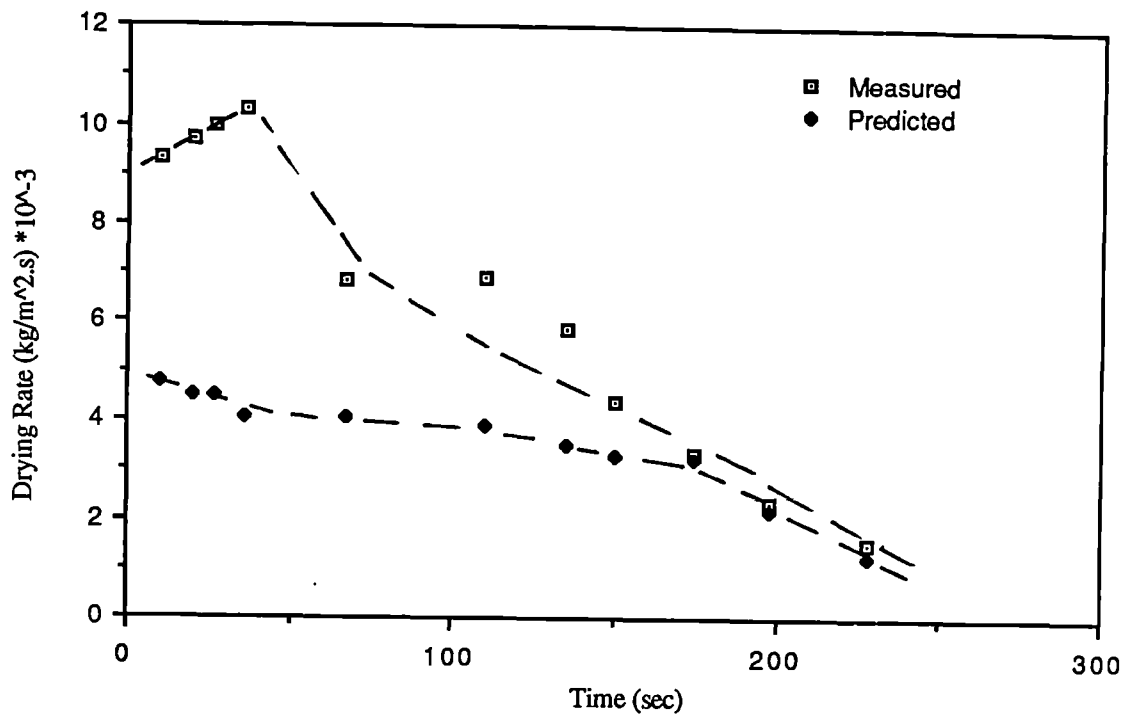


Figure 9.29 Comparison Between Measured and Predicted Drying Rates of Potassium Sulphate Solution Drops at 65 C Using 10w/w% Solids and a 4mm Diameter Nozzle



**Figure 9.30 Comparison Between Measured and Predicted Drying Rates of Potassium Sulphate Solution Drops at 95 C Using 10w/w% Solids and a 4mm Diameter Nozzle**

carbon dioxide into water drops. Studies on liquid-liquid systems (71) have shown mass transfer rates to increase by over 100% when vigorous prolate-oblate oscillations are present. The present study demonstrates an increase in mass transfer, in the earlier stages of drying, of up to 5 times the predicted value. This would take into account drop oscillation and deformation as well as circulation.

The model also (145) assumes uniform crust formation over the drop surface, yet under the present experimental conditions crusts were also observed to form at the leading surface, where maximum evaporation takes place, and grew up and around the drop. Furthermore, the model assumes that moisture transfer from the evaporation interface is by vapour diffusion alone. In reality however, a combination of mechanisms of flow may be effective at any one time. For example, vapour diffusion coupled with liquid moisture movement due to capillary forces or flow caused by a vaporization-condensation sequence (see section 4.3).

That the greatest deviations between calculated and measured values occur

for the earlier stages of surface evaporation is consistent with the observation that as the drop becomes smaller and a crust forms over its surface the deformations of the drop diminish and gradually cease altogether. Predicted and experimental drying rates then become closer, albeit still with a deviation of upto 40-50%. Therefore, for the case of small spherical particles or droplets < 2mm in diameter an ideal drying model such as presented by Cheong (115) or Bains (145) may be adequate to describe heat and mass transfer, provided of course the material concerned forms a porous, rigid crust. However, when a droplet undergoes changes in size and shape during part of its residence time, the situation becomes much more complicated to describe. Clearly, any description of the drying process of such a single droplet should take these effects into account.

### **2.3 Applicability of Single Drop Studies to Spray Drying**

In order to model drying behaviour, individual drops should ideally be of similar size to those encountered in a spray dryer i.e < 1000  $\mu\text{m}$  . However, the minimum drop size achieved by use of techniques such as nozzle or filament suspension or by suspending a drop in free-flight, is  $\sim 0.6\text{mm}$  . Therefore, the results have to be extrapolated to cover drop sizes in the range 10-1000 $\mu\text{m}$ . This can be justified since the rate controlling factors, in all cases, are vapour diffusion through the boundary layer during the constant rate period and crust formation and the process of moisture movement during the falling-rate period. The mechanisms are therefore comparable. The inherent assumption is however, that following crust formation the particle morphology is independent of particle size. Whilst this appears to be approximately correct (58,137) a separate study

(58,137) a separate study has been initiated to investigate this, the differing mechanisms when mixed solids are dried, and the effect of additives (140).

In section 9.1, at temperatures  $> 100^{\circ}\text{C}$ , single drops of sucrose solution were seen to inflate. In practical spray drying with co-current flow the inlet air temperature should be lower than this temperature to avoid this 'ballooning' phenomena. Therefore, this temperature represents a maximum for cocurrent spray dryer operation with flavour and volatiles retention. If there is no threat of product degradation a higher temperature is permissible with counter-current air flow.

The prediction and control of spray-air movement within the spray-drying chamber are important requirements for dryer design and performance. The manner in which the spray, on leaving the atomizer, combines with the drying air determines the rate and extent of drying and is dependent upon the nature of both the spray and product involved. For example, in the counter-current arrangement, the hottest drying air contacts the dried particles as they are about to leave the chamber. This layout is suitable for products that can withstand a very hot environment, and if a coarse product is required. If however, the product cannot withstand such high temperatures, alternative contacting methods must be employed and the co-current arrangement may be suitable. In this the hottest drying air contacts droplets at their maximum moisture content and the evaporation process prevents high droplet temperatures.

Retention of volatile flavour and aroma substances may also be an important consideration when deciding how best to contact the spray with the drying air. Important flavour and aroma substances tend to have very high activity coefficients in the aqueous phase (130) and are therefore highly volatile. If they are to be retained in the product, it is necessary that a substantial mass

transfer barrier to their loss be imposed within the particles. This is accomplished by the selective-diffusion mechanism, described by Thijssen and co-workers (131, 132), whereby the surface water content is reduced sufficiently so that the diffusion coefficients of volatile substances become substantially less than that of water. Through the selective-diffusion model one can reason that one method of improving volatile retention is to obtain a very rapid initial evaporation rate by using a high inlet air temperature. The addition of appropriate surfactants to the feed can also improve volatile retention by virtue of suppression of droplet circulation and oscillation (133).

The temperature to which droplets and particles are subjected in co-current, counter-current and mixed flow drying chambers can be easily appreciated from the air temperature profile characteristics (134). Ade-John (134) in his work on a 9ft high x 4ft diameter counter-current, perspex drying tower, confirmed his model of the air-flow pattern by smoke experiments on the tower.

White smoke was injected at the air inlet port of the dryer and the residence times measured. He proposed that the flow model consists of two, well-stirred tanks at the top and the conical bottom end of the dryer. In between there is a plug flow zone and in parallel with these three there is an inert by-pass stream.

It was shown in sections 9.1 and 9.2 that the initial solids content has a significant effect upon the rate of evaporation from droplets. Therefore, for any industrial drying process, a study of the evaporation rates from individual droplets gives some indication of the drying mechanisms and the drying characteristics. A substantial amount of evaporation takes place when the droplet surfaces are saturated and cool. Drying chamber design and air flow rate provide

a droplet residence time, such that the desired droplet moisture removal is completed, and product is removed from the dryer, before product temperatures can rise to the outlet drying air temperature of the chamber (for counter-current), or the inlet air temperature (for co-current). Hence, there is little chance of heat damage to the product. To meet product specification sufficient residence time is essential to allow completion of drying; means of prediction is important to avoid over sizing of the drying chamber.

In any spray-drying installation the drying chamber can represent a large cost item, therefore correct sizing is essential for minimising installation costs while maximising performance by producing high-quality dried powders at minimum operating costs. Drying chambers are designed therefore, to handle an air volume containing sufficient heat for drying the spray droplets, and to provide a residence time sufficient to yield particles of the desired moisture content. Hence, measurements of drying rates of single drops, as in section 9.1 and 9.2, give an estimate of the drop moisture content at any specific time. Application of the same parameters to a practical spray drying tower assists in avoiding either particles overheating or solids build-up, following particle impaction on the chamber walls, due to insufficient drying. In the latter case impingement of particles still containing high moisture contents causes them to adhere and to form a layer on the walls. Deposits which fall off may have been overheated, and hence changed in specification, or may still be wet and contaminate the products. Wall build-up of combustible material may also result in fires, or if dispersed, dust-explosions (1).

## CHAPTER 10

### Conclusions And Recommendations

The following major conclusions arise from this study :

#### 10.1 Pure liquid drops

(1) Drops in free-flight, unlike drops suspended on a nozzle or a filament, experienced oscillations, rotation and deformation. These effects led to a greater surface area, and a thinning of the boundary layer, and consequently to greater rates of heat and mass transfer. During this stage of evaporation, the experimental data lay well above the predictions using Ranz and Marshall's equations 3.15 and 3.16. However, as the drop size decreased below ~3mm the drop became more spherical, and more stable, and the experimental data were correlated reasonably well by previous equations.

(2) None of the previous correlations for pure liquid drops could adequately describe mass transfer from drops in free-flight. Hence, the following modified correlations were proposed;

(i) For droplets experiencing oscillations, rotation and deformation ;

$$Sh = - 105 + 3.9 \left( \frac{T_a - T_d}{T_{amb}} \right)^{0.18} Re^{0.5} Sc^{0.33} \quad \text{-----10.1}$$

for Re approx. > 1380

(ii) When the various drop movements have ceased or diminished ;

$$Sh = 2.0 + 0.71 \left( \frac{T_a - T_d}{T_{amb}} \right)^{0.18} Re^{0.5} Sc^{0.33} \quad \text{----10.2}$$

for Re approx. < 1060

Equations 10.1 and 10.2 are the first to be presented to correlate mass transfer film coefficients for free-flight drops of 0.7 to 4.6mm.

## 10.2 Drops Containing Dissolved Solids

### 10.2.1 Skin-Forming Materials

As an example of a skin-forming material this study investigated the drying behaviour of drops of sucrose solution. The following conclusions were drawn ;

(iii) When a drop of sucrose solution was dried, prior to crust formation, a relatively impervious skin formed around the drop which reduced the rate of evaporation substantially, leading to extended drying times and a smooth crust of negligible porosity.

(iv) The drying rate curves ( section 9.1) showed three distinct stages; an initial increase in the drying rate as drop temperature reduced to the wet-bulb temperature, a short constant rate period and a falling rate period as soon as the skin and then crust was formed. The drying rate after crust formation was, and in practical drying will always be, product specific.

(v) Initial conditions of drop temperature and concentration had the following effects upon the the drying rates :

The maximum evaporation rates were found to be higher for drops of low initial solids content , i.e the higher the solids content the lower the evaporation rates. Two effects may contribute to this :

(a) a lowering of the vapour pressure of water with increasing solution concentration; and

(b) the attainment of the critical saturation point with concentrated solutions before the maximum temperature driving force ( $T_a - T_{wb}$ ) is reached.

Increasing the air temperature, as, expected increased evaporation rates.

(vi) At higher temperatures ( $> 100^{\circ}\text{C}$ ), drops of sucrose solution exhibited a 'puffing' or 'ballooning' phenomena due to vapour pressure build-up inside the droplet because of resistance to vapour diffusion provided by the skin. The drop eventually collapsed to release the internal pressure before inflating again. A drop

inflated, collapsed and reformed many times before it was carried away in the air stream or hit a side wall. In practical spray drying such behaviour would have pronounced effects upon product quality factors such as bulk density, particle size, aroma and flavour retention.

(vii) The effect of various parameters such as air temperature, drop size and concentration upon the critical moisture content showed that its value depended upon the initial drying rate, thickness of material or size of the element such as a droplet, and apparent diffusivity of moisture within the material.

#### 10.2.2 Rigid Crust Forming Materials

Drops of potassium sulphate solution were studied as an example of a rigid, porous crust forming material and the following conclusions were drawn :

(viii) Comparison between measured and predicted drying rates, using Bains (145) receding interface model , showed the measured values to be much larger than predicted with the greatest deviations, up to 5 times the predicted value, occurring in the early stages of drying. The predicted values were smaller consistent with a number of assumptions made when deriving the model (Appendix A8), in particular the assumption that the drops were rigid spheres. In the present study, drops in the early stages of drying oscillated, rotated and deformed which increased mass transfer well above the predicted values. However, as the drop became smaller, and a crust formed on the surface these drop movements were damped out and the assumption of a rigid sphere became more realistic. Measured and predicted values now converged, although still with a deviation of up to 40-50%.

(ix) The rate curves showed a similar pattern to those for drops of sucrose solution (section 9.1) in that three distinct stages were observed; an initial period of increasing drying rate, a short constant-rate period, which decreased with an increase in the air temperature and concentration, and a falling-rate period following crust formation.

### 10.3 Experimental Technique

The novel apparatus and technique employed in this study represent a unique alternative method for investigating the evaporation of single drops of pure liquid, or drying of single drops of solutions or slurries, under unrestrained conditions. Previous investigators (8,22,58,93,115 ) studied evaporation from single stationary droplets suspended from a thermocouple or a glass filament, or from celite spheres of known porosities. These techniques are limited in application since the relative velocity present in the spray drying chamber is non-existent. Furthermore, in the later stages of drying the droplet climbs up the filament or thermocouple so that the entire drying history is not observed. Heat conduction along the suspension device, which can account for up to 21.7% of the total heat transferred to a suspended drop at an air temperature of 79°C, is yet another problem. The above disadvantages were overcome by suspending a droplet in free-flight. The main disadvantage of the present method was the difficulty of measuring directly the drop temperature. Nevertheless, free-flight drops bear a closer resemblance to the situation in a spray dryer, and the residence time can be increased beyond that in simple free-fall experiments which yield undried droplets.

### 10.4 Recommendations For Future Work

- (1) The effect of additives to improve drying characteristics of skin forming materials such as sucrose solution should be investigated. The study could be extended to cover natural products such as milk or coffee extract and detergent drops.
- (2) A further study could be carried out on the shape and oscillations of drops covering a wider range of materials , and hence physical properties. This would be useful in testing the proposed correlations (equations 10.1 and 10.2). Materials such as toluene, aniline, butanol or pentanol could be used for this study.
- (3) Internal circulation of drops and circulation velocities, which may have an effect

upon drop shape and hence mass transfer, could be studied by introducing aluminium or carbon particles into drops and tracing the circulation patterns.

- (4) The technique could be modified, to enable dried crusts to be collected with more ease, for example by introducing an inverted cup through the same hole (Figure 6.4 (K) ) used for the drop forming unit.
- (5) Very little work has been done on the effects of surfactants, which occur in many or all liquid foods naturally, on mass transfer. Addition of surfactants may be a convenient means to affect and control mass transfer rates and volatiles loss during spray drying and therefore single drop studies in this area are recommended. Surfactants such as sodium lauryl sulphate and sodium lauryl benzene sulphate in aqueous sucrose solutions are recommended. In subsequent development work it would of course be necessary to consider final product compatibility with food specifications.
- (6) The free-flight apparatus could be used to investigate mass transfer from aerated or foamed droplets. Theoretical predictions (110) from such drops, demonstrate a faster drying rate and a more uniform crust.
- (7) The apparatus could also be used to obtain basic particle drying data relevant to other types of dispersion dryers e.g. the recirculation type dryer used for grain, fluidised bed dryers, pneumatic-conveyer dryers or even the cascading rotary dryer.

## NOMENCLATURE

The symbols have the meaning listed below, unless stated otherwise in the text.

$$a_0 = \frac{[R(R - z) h_g]}{k_c z}$$

$$a_1 = \frac{(R^2 h_g k_c)}{[\rho_\infty (\lambda - C_d)]}$$

$$a_2 = k_{tc} - R h_g$$

$$a_3 = R^2 h_g$$

$$a_4 = \frac{(C_{pc})}{[3x(\lambda - C_d)]}$$

$$b_0 = \frac{[R(R - z) k_g]}{D_{eff} z}$$

$$b_1 = \frac{(R^2 D_{eff} M_w k_g)}{[\rho_\infty R_d]}$$

$$b_2 = D_{eff} - R k_g$$

$$b_3 = R^2 k_g$$

A Surface area of hemispherical droplet, m<sup>2</sup>

A<sub>e</sub> Equivalent surface area of a spheroid droplet, m<sup>2</sup>

A<sub>m</sub> Mass transfer area, m<sup>2</sup>

A<sub>h</sub> Heat transfer area, m<sup>2</sup>

a<sub>n</sub>, b<sub>n</sub> Constants

b Distance between water droplet surface and glass bead surface

c Concentration of solute

c<sub>0</sub> Initial concentration

C Concentration

C<sub>A</sub> Molar concentration of component A

$C_0$	Initial concentration
$C_1$	Solids content
$C_s$	Concentration on droplet surface
$C_\infty$	Concentration at infinite distance
$C_p$	Heat capacity of air, $J.kg^{-1}.k^{-1}$
$C_{pv}$	Heat capacity of diffusing vapour, $J.kg^{-1}.k^{-1}$
$C_c$	Heat of crystallisation per unit mass of water evaporated, $J.kg^{-1}$
$C_s'$	Humid heat, $J.kg^{-1}.k^{-1}$
$c$	Concentration of solute in equation 4.4.2, g-solute $mm^{-3}$ -solution
$c_0$	Initial concentration of solute in equation 4.4.2, g-solute $mm^{-3}$ -solution
$D$	Diffusivity, $m^2.s^{-1}$
$D_m$	Molecular diffusivity, $m^2.s^{-1}$
$D_{AB}$	Diffusion coefficient of A in a mixture of A and B
$D_v$	Effective diffusivity, $m^2.s^{-1}$
$d$	Diameter, m
$d'$	Maximum horizontal diameter of drop, m
$d_f$	Diameter of filament, m
$d_p$	Drop diameter, m
$\bar{d}_p$	Mean droplet diameter, m
$d(N)$	Number of droplets in size increment
$d_c$	Crust external diameter, m
$d_g$	Glass bead diameter, m
$d_{gm}$	Geometric mean droplet diameter, m
$d_{max}$	Maximum droplet diameter, m
$dm/d\theta$	Incremental change in drop mass with residence time, $kg s^{-1}$

$d_n$	Diameter of nozzle, m
$d_R$	Rosin - Rammler mean droplet diameter, m
$d_e$	Equivalent drop diameter, m
$d_h$	Horizontal drop diameter, m
$d_v$	Vertical drop diameter, m
$E$	Sphericity
$e$	Emissivity
$e_n$	Emissivity of nozzle
$f$	Dispersion coefficient in Table 4.5.1
$f'$	Wind factor
$F_a$	Geometry factor
$g$	Acceleration due to gravity, $m.s^{-2}$
$G$	Dry air mass flow rate, $kg.s^{-1}$
$\bar{G}$	Mass flow rate of air, $kg.s^{-1}$
$G'$	$=\phi/r_o$ in Eq.4.4.2
$H$	Humidity, kg/kg
$H_1$	Henry's Law constant
$H_i$	Inlet air humidity, kg/kg
$H_o$	Outlet air humidity, kg/kg
$H_d$	Downstream humidity, kg/kg
$H_u$	Upstream Humidity, kg/kg
$H_s$	Saturation humidity at drop temperature, kg/kg
$h$	Height of droplet in equation 3.9, m
$h'$	Height of droplet in equation 3.17, m
$h_f$	Heat transfer coefficient for glass filament, $Wm^{-2}K^{-1}$

$h_g$	Gas film heat transfer coefficient, $W.m^{-2}.K^{-1}$
$I$	Current, amp
$J_r$	Rate of mass transfer, $kg.m^{-2}.s^{-1}$
$k_c$	Crust mass transfer coefficient, $m.s^{-1}$
$k_g$	Gas film mass transfer coefficient, $m.s^{-1}$
$k_H$	Mass transfer coefficient in equation 5.6, $m.s^{-1}$
$k_s$	Skin mass transfer coefficient, $m.s^{-1}$
$k_p$	Mass transfer coefficient, $kg.m^{-2}.s^{-1}.atm^{-1}$
$k_{tc}$	Thermal conductivity of crust, $W.m^{-1}.K^{-1}$
$K$	Evaporation constant, $m^2/s$
$K_d$	Thermal Conductivity of air, $W.m^{-1}.K^{-1}$
$K_o$	Overall mass transfer coefficient, $m.s^{-1}$
$K_t$	Thermal conductivity of stainless steel, $W.m^{-1}.K^{-1}$
$K_v$	Thermal conductivity of diffusing vapour, $W.m^{-1}.K^{-1}$
$K'$	$= (M_a/M_w)k_g$
$M$	$= 1 - 0.4 ( 1 - T_s/T_g )$ in equation 3.51
$M_a$	Molecular weight of air
$M_w$	Molecular weight, $kg/kgmole$
$m$	Evaporation rate, $kg.m^{-2}.s^{-1}$
$m_o$	Evaporation rate in stagnant medium, $kg.m^{-2}.s^{-1}$
$m_o'$	Evaporation rate in stagnant medium neglecting radiation, $kg.m^{-2}.s^{-1}$
$N$	$1 - 0.4 ( 1 - \ln (1 + B) )/B$ in equation 3.51.
$N_A$	Rate of mass transfer per unit area, $kg.m^{-2}.s^{-1}$
$N.S$	Nozzle Size, m
$P$	Total pressure, atm

$p$	Partial pressure of water vapour, atm
$P_C$	Vapour Pressure on surface of core, atm.
$\Delta P$	Pressure drop through crust, atm.
$p_S$	Saturation vapour pressure, atm.
$p_g$	Partial pressure of air, atm.
$P_V$	Vapour pressure, atm.
$Q$	Total heat transferred
$Q_C$	Total heat transferred by convection
$Q_r$	Heat transfer rate within crust at radius $r$
$Q_R$	Total heat transferred by radiation
$Q'_R$	Heat transfer rate of surface of particle
$Q_Z$	Heat transfer rate at wet core surface
$q$	Rate of heat transfer
$q_e$	Rate of heat transfer by radiation
$q_n$	Rate of heat transfer to a drop through the nozzle
$r$	Radius of evaporating drop, mm
$r_1$	Radius of evaporating droplet in equation 3.47
$r_2$	Outer radius of evaporating droplet in equation 3.47
$r_0$	Initial radius of evaporating drop, mm
$R$	External drop radius, mm
$R_C$	Universal gas constant, $\text{Atm.m}^3.\text{kgmol}^{-1}.\text{K}^{-1}$
$S$	Fractional rate of replacement of elements
$S'$	Surface area of drop, $\text{m}^2$
$S_b$	Specific surface area, $\text{m}^{-2}$
$S_N$	Number standard deviation

$S_G$	Geometric standard deviation
$T$	Temperature, °C
$T_a$	Air temperature, °C
$T_c$	Core temperature, °C
$T_s$	Surface temperature, °C
$T_f$	Average film temperature, °C
$T_g, T'_g$	Gas temperature in °C and K respectively
$T_s, T'_s$	Drop temperature in °C and K respectively
$T_{amb}$	Ambient temperature
$v$	Velocity, $m.s^{-1}$
$V$	Volume of drop
$V_o$	Voltage, Volt
$W$	$= r/r_o$
$x$	Distance of fall, m
$x'$	Mass fraction of water
$x_o$	Initial diameter of droplet, m
$X$	Interface between crust and core
$X_w$	Mass fraction of water
$Y$	$= c/c_o$
$Z$	Distance in the direction of diffusion

### DIMENSIONLESS GROUPS

$B$	Transfer No. $= C_p \Delta T / \lambda$
$B'$	Spaldingtransfer No. $= C_p \Delta T / (\lambda - q/m)$

$B_f$	Transfer No. evaluated at film conditions
$Bo$	Bond No. $(\rho_d - \rho_c) d_p^2 g / \sigma_1$
$Gr$	Grashof No. $= d_p^3 \rho^2 g \beta_1 \Delta T / \mu^2$
$Nu$	Nusselt No. $= h_g d_p / K_d$
$Nu_f$	Nusselt No. evaluated at film conditions
$Nu_o$	Nusselt No. under stagnant conditions
$Nu_R$	Nusselt No. without neighbouring particles
$Pr$	Prandtl No. $= C_p \mu / K_d$
$Pr_f$	Prandtl No. evaluated at film conditions
$Pe$	Peclet No. $= Re.Pr = C_p v d_p \rho / K$
$Re$	Reynolds No. $= \rho d_e v / \mu$
$Re_f$	Reynolds No. evaluated using film conditions
$Re_g$	Reynolds No. of gas
$Re_m$	Reynolds No. defined as $\rho_g v_g d / \mu_f$
$Re_s$	Reynolds No. of sphere in equation 3.5.1
$Sc$	Schmidt No. $= \mu / \rho D_v$
$Sh$	Sherwood No. $= k_g d_e / D_v$
$Sh_o$	Sherwood No. under stagnant conditions
$Sh_R$	Sherwood No. without neighbouring particles
$St$	Stanton Number $= h_g / C_p \rho v$

## GREEK SYMBOLS

$\beta$	Dimensionless transfer coefficient defined by equation 3.7
$\beta_1$	Coefficient of expansion in equation 3.7
$\psi$	Crust thickness, m
$\varepsilon$	Crust porosity
$\theta$	Drying time, sec
$\Delta\theta$	Time interval , sec
$\theta_c$	Time for completion of solid crust formation , sec
$\gamma$	Dimensionless ratio in equation 4.4.1 = $K/D$
$\phi_y$	Positive root of $\tanh y = y/\gamma+1$
$\lambda$	Latent heat of vaporisation, $J.kg^{-1}$
$\sigma$	Stefan-Boltzman constant
$\sigma'$	Surface tension dyne / cm
$\phi$	Constant
$\rho$	Density, $kg.m^{-3}$
$\rho_c$	Density of continuous phase, $kgm^{-3}$
$\rho_{co}$	Density of wet core, $kgm^{-3}$
$\rho_d$	Drop density, $kgm^{-3}$
$\rho_g$	Density of gas, $kgm^{-3}$

$\mu$	Viscosity, $\text{kg.m}^{-1}.\text{s}^{-1}$
$\mu'$	Sphericity = $6V/S'd'$
$\mu_c$	Viscosity of continuous phase, $\text{kg.m}^{-1}.\text{s}^{-1}$
$\mu_d$	Viscosity of dispersed phase, $\text{kg.m}^{-1}.\text{s}^{-1}$
$\mu_f$	Film viscosity, $\text{kgm}^{-1}\text{s}^{-1}$
$\nu$	Kinematic viscosity, $\text{m}^2.\text{s}^{-1}$
$\eta$	Index constant
$\pi$	Constant = 3.1416

## REFERENCES

1. Keey, R.B. .,  
Drying Principles and Practice,  
1st ed., Pergamon Press, Oxford (1972).
2. Masters, K.,  
Spray Drying Handbook,  
3rd ed., John Wiley and Sons, New York (1979).
3. Fick, A.,  
Ann.Phys., 94, 59 (1855).
4. Whitman, W.G.,  
Chem. Met. Eng., 29, 147 (1923).
5. Higbie, R.,  
Trans.Amer.Inst.Chem.Eng., 31, 365 (1935).
6. Danckwerts, P.V.,  
Ind.Eng.Chem., 43, 1460 (1951).
7. Toor, H.L., Marchello, J.M.,  
A.I.Ch.E.J., 4, 97 (1958).
8. Frossling, N.,  
Gerlands Zeitr.Zurgeophysik, 52, 170 (1938).
9. Maxwell, J.C.,  
Collected Scientific Papers, Cambridge, 11,625 (1890).
10. Hsu, N.T., Sato, J., and Sage, B.H.  
Ind.Engng.Chem., 46, 870 (1954).
11. Garner, F.H., and Suckling, R.D.  
A.I.Ch.E.J, 4, 114 (1958).
12. Manning, W.P, and Gauvin, W.H.  
A.I.Ch.E.J, 6, 184 (1960).
13. Garner, F.H., and Tayeban, M.  
An.R.Soc.esp.Fis.Quim., 1960, 56B, 497.
14. Garner, F.H., and Grafton, R.W.  
Proc.R.Soc., 1954, A224, 64.
15. Maisel, D.S., and Sherwood, T.K.  
Chem.eng.Prog., 46,131 (1950) Idem. ibid., p 172.
16. Linton, W.H., and Sherwood, T.K.  
Chem.Eng.Prog., 46, 258 (1950).

17. Yen, Y.C., and Thodos, E.  
A.I.Ch.E.J., 8, 34, (1962).
18. Evnochides, S., and Thodos, E.  
A.I.Ch.E.J., 1961, 7, 78.
19. Powel, R.W.,  
Trans.Inst.Chem.Eng., 1940, 18, T36.
20. Aksel'rud, G.A.,  
Zh.Prikl.Khim., Leningr., 1953, 27, 1446.
21. Pasternak, I.S., and Gauvin, W.H.  
A.I.Ch.E.J., 7, 254, 1961.
22. Ranz, W.E., and Marshall, W.R.  
Ch.Eng.Prog., 48, 141, 1952. Idem.ibid., p. 173.
23. Dlouhy, J., and Gauvin, W.H.,  
Am.Inst.Chem.Eng.J., 6, 29 (1960).
24. Soo, S.L.,  
Chem.Eng.Sci., 5, 57 (1966).
25. Hoffman, T.W., and Gauvin, W.H.,  
Can.J.Chem.Eng., 40, 170 (1962).
26. Gwyn, J.E., Crosby, E.J., and Marshall, W.R.,  
Ind.Eng.Chem.Fund., 2, 204 (1965).
27. Brehaut, W.J., and Keey, R.B.,  
Zdravotni Techn. Vozduchotechn., 13, 23 (1970).
28. Frazer, R.P., Eisenklam, P., and Dombrowski, N.,  
Brit. Chem. Eng., 2, 414, 536, 610 (1957).
29. Frossling, N.,  
Lunds. Univ. Arskr., 36, No 4 (1940).
30. Sreznevskii, V.,  
Zh.R.Ph.Kh.O., 14, 420, 483 (1882).
31. Morse, H.W.,  
Proc. Amer. Acad. Sci., 45, 363 (1910).
32. Langmuir, I., Phy. Rev. Ser. II, 12, 368 (1918).
33. Whytlaw-Gray, R., Patterson, H.,  
Smoke (Dyme), Goskhimizdat, M., p.149 (1934).
34. Topley, B., Whytlaw-Gray, R.,  
Phyl.Mag., 4, 873 (1927).
35. Houghton, H.G.,  
Physics., 4, 419 (1933).

36. Kiriukhin, B.V.,  
Trudy NIU Gidrometsl., ser.1, 7, p.35 (1945).
37. Langstroth, G.O., Diel, C.H., Winhold, E.J.,  
Can.J.Research., 28A, 574 (1950).
38. Steinberger, R.L., Treybal, R.E.,  
A.I.Ch.E.J., 6, 227 (1960).
39. Yuge, T.,  
Trans. A.S.M.E., 82, Series C, 214 (1960).
40. Gudris, N., Kulikova, L.,  
Z.Physik , 25, 121 (1924).
41. Nestle, R.Z.,  
Physics., 77, 174 (1932).
42. Woodland, D.J., Mack, E.,  
J.Amer.Chem.Soc., 55,3149 (1933).
43. Majamo, Togino.,  
Bull,Inst.Phys.Chem.Res.(Tokyo), 9, 339 (1930).
44. Johnstone, H.F., Eades, D.K.,  
Ind.Eng.Chem., 42, 2293 (1950).
45. Tverskaia, N.P.,  
Uchen.Zap.Leningrad Univ., Series Phys. 7, 241 (1949).
46. Tverskaia, N.P.,  
IZV. Akad.Nauk sssR., series geogr. geoph. 14, 164 (1950).
47. Tverskaia, N.P.,  
IZV. Akad.Nauk sssR, series geoph. 259 (1953).
48. Sokol'skii, A.P; Timofeyeva, F.A;  
' Studies on the combustion process of natural fuels',  
Energoizdat, M.-L., p.182 (1948)
49. Van Krevelen, D.W., Hofstijzer, P.J.,  
J.Soc.Chem.Ind.,68, 59 (1949).
50. Ingebo, R.D.,  
Chem.eng.prog., 48, 403 (1952).
51. Garner, F.H., Keey, R.B.,  
Chem.Eng.Sci., 9, 119-129, 1958.
52. Garner, F.H., Hoffman, J.M.,  
A.I.Ch.E.J., 6, 579 (1960).

53. Pasternak, I.S., Gauvin, W.H.,  
Can.J.Chem.Eng., 38, 35 (1960).
54. Fuchs, N.A.,  
Evaporation and Droplet Growth in Gaseous Media, Pergamon  
Press, London (1959).
55. Bowman, C.W., Ward, D.M., Johnson, A.I., Trass, o.,  
Can.J.Chem.Eng., 39, 9 (1961).
56. Ward, D.M., Trass, O., Johnson, A.I.,  
Can.J.Chem.Eng., 40, 164 (1962).
57. Kinard, G.E., Manning, F.S., Manning, W.P.,  
Brit.Chem.Eng., 8, 326 (1963).
58. Audu, T.O.K.,  
Ph.D Thesis, University of Aston in Birmingham,  
England (1973)
59. Sandovles-Robles, J.G., Riba, J.P., Conderc, J.P.,  
Trans.Inst.Chem.Eng., 58, 132 (1980).
60. Sandovles-Robles, J.G., Delmas, H., Conderc, J.P.,  
A.I.Ch.E.J., 27, 819 (1981).
61. Davies, E.J., Ray, A.K., Chang, R.,  
A.I.Ch.E.Symp.Series., 74, 190 (1978).
62. Kramers, H.,  
Physica's Grav., 12, 61 (1946).
63. Tsubouchi,T., Sato, S.,  
Chem.Eng.Prog.Symp. Ser., 56, 269, 285 (1960).
64. Rowe, P.N., Claxton, K.T., Lewis, J.B.,  
Trans.Inst.Chem.Eng., 43, T14 (1965).
65. Adams, A.E.S., Pinder, K.L.,  
Canad.J.Chem.Eng., 50, 707, (1972).
66. Schafer, K.,  
Z.Physik., 77,198 (1932).
67. Monchik, L., Reiss, H.,  
J.Chem.Phys., 22, 831 (1954).
68. Vyrubov, D.N.,  
J.Tech.Phys.Moscow, 9, 1923 (1939), (Canadian Defence  
Research Board Translation, September 1949).
69. Kinzer, G.D., Gunn, R.,  
J.Meteor., 81, 71 (1951)

70. Jones, S.J.R., Smith, W.,  
Proc.Symp.Interaction Between Fluid and Particles.,  
Inst.Chem.Eng., London, 190 (1962).
71. Garner, F.H., Skelland, A.H.P.,  
Ind.Eng.Chem., 46, 1255 (1954).
72. Finlay, B.A.,  
Ph.D Thesis, University Of Birmingham, England (1957).
73. Jarvis, J., Ph.D Thesis.,  
University of Birmingham, England (1960).
74. Ahmadzadeh, J., Harker, J.H.,  
Trans.Inst.Chem.Eng., 52, 1974.
75. Garner, F.H., Lane, J.J.,  
Trans.Inst.Chem.Eng., 37, 155 (1959).
76. Miura, K., Miura, T., Ohtani., S.,  
A.I.Ch.E.Symp.Series, 73, 95 (1977).
77. Yao, S., Schrock, V.E.,  
Trans. of the ASME Journ.of Heat Tran., 120-126,  
February 1976.
78. Garner, F.H., Kendrick, P.,  
Trans.Inst.Chem.Eng., 37, 155 (1959).
79. Yuen, M.C., Chen, L.W.,  
Int.J.Heat Mass Trasfer, 21, 537-542 (9178).
80. Eisenklam, P., Armachalam, S.A., Weston, J.A.,  
'Evaporation rates and drag resistance of burning drops',  
in Eleventh Symposium (International) on Combustion., pp 715-725 (1967).
81. Marshall, W.R.,  
Trans. A.S.M.E., 77, 1377 (1955).
82. Ranz, W.E.,  
Trans. A.S.M.E., 78, 909 (1956).
83. Hoffman, T.W., Gauvin, W.H.,  
Canad.J.Chem.Eng., 35, 129 (1960).
84. Pei, D.C.T., Gauvin, W.H.,  
A.I.Ch.E.J., 9, 375 (1963).
85. Pei, D.C.T., Narasimhan, C., Gauvin, W.H.,  
Proc.Symp.Interaction between fluid and particles.,  
Inst.Chem.Eng. London, 243 (1962).
86. Downing, C.G.,  
A.I.Ch.E.J, 12, 760, (1966).

87. Narashimhan, C., Gauvin, W.H.,  
Can.J.Chem.Eng., Vol 45, pp 181-188, 1967.
88. Lee, K., Ryley, D.J.,  
J.Heat Transfer, Trans. A.S.M.E., 90, 445 (1968).
89. Frazier, G.C., Hellier, W.W.,  
Ind.Eng.Chem.Fundam., 8, 807 (1969).
90. Crosby, E.J. Stewart, W.E.,  
Ind.Eng.Chem.Fundam., 9, 515 (1970).
91. Trommelen, A.M., Crosby, E.J.,  
A.I.Ch.E.J., 16, 857 (1970).
92. Sano, U., Nishikawa,S.,  
Chem.Eng. (Japan), 28, 275 (1964).
93. Charlesworth, D.H., Marshall, W.R., Jr.,  
A.I.Ch.E.J., 6, 9, (1960).
94. Kadota, T., Hiroyasu, H.,  
Bull. J.S.M.E., 19, 1515 (1976).
95. Hiroyasu, H., etal.,  
Trans.J.S.M.E., 40, 3147 (1974).
96. Renksizbulut, M., Yuen, M.C.,  
Journal of Heat Transfer, 105, 384 (1983).
97. Van Arsdel, W.B.,  
'Food Dehydration -Principles',Vol 1, Avi, Westport, 1963.
98. Hougen, O.A., McCauley, H. J., Marshall, W.R.,  
Trans.Am.Inst.Ch,Eng., 36, 183 (1940).
99. Buckingham, E.,  
U.S. Dept. Agr. Bur. Solids, Bull., 38, (1907).
100. Lewis, W.K.,  
Ind.Eng.Chem., 13, 427 (1921).
101. Newman, A.B.,  
Trans.Am.Inst.Ch.Eng., 27, 203, 310 (1931).
102. Sherwood,T.K.,  
Ind.Eng.Chem., 21, 12, 976 (1929).
103. Gurr, C.J., Marshall. T.K., Hutton, J.T.,  
Soil Sci., 74, 335 (1952).
104. Kuzmak, J.M., Serada, P.J.,  
Soil Sci., 84, 419 (1957).

105. Harmathy, T.Z.,  
Ind.Eng.Chem.Fund., 8, 92 (1968).
106. Duffie, J.A., Marshall, W.R.Jr.,  
Chem.Eng.Prog., 49, 417 (1953).
107. Miura, K., Atarashiya, K., Ouchi, I., Ohtani, S.,  
Kagaku Kogaku, 35, 643 (1971) -Translation :  
Heat Trasfer, Jap.Res., 1, 11 (1972).
108. Audu, T.O.K., Jeffreys, G.V.,  
Trans.Inst.Chem.Eng., 53, 165 (1975).
109. Van der Lijn,  
J., Ph.D Thesis, Agricultural University Wageningen, Netherlands (1976).
110. Wijlhuizen, A.E., Kerkhof, R.J.A.M., Bruin, S.,  
Chem.Eng.Sci., 34, 651 (1979).
111. Haertling, M.,  
Drying '80, Vol 1, Hemisphere Publ. Corp., N.Y. (1980).
112. Esubiyi, A.O., Ph.D Thesis, University of Aston in Birmingham, England(1980).
113. Coulson, J.M., Richardson, J.F.,  
Chemical Engineering, Vol.2., 2nd ed., Pergamon Press, Oxford (1968).
114. Sano, Y., Keey, R.B.,  
Chem. Eng. Sci., 37, 881 (1982).
115. Cheong, H.W.,  
Ph.D Thesis, University of Aston in Birmingham, England (1983).
116. Rosin, P., Rammler, E.,  
J.Inst.Fuel, 7, 29 (1933).
117. Fledderman, R.G., Hanson, A.R.,  
Univ.Michigan Res.Dept. CM 667 (1951).
118. Nukiyama, S., Tanasawa, Y.,  
Trans. Soc. Mech. Eng., (Japan), 4, 86 (1937).
119. Bose, A.K., Pei, D.C.T.,  
Can.J.Chem.Eng., 42, 259 (1964).
120. Dickinson, D.R., Marshall, W.R.,  
A.I.Ch.E.J, 14, 541 (1968).
121. Miura, T., Ohtani, S.,  
Kagaku Kogaku Ronbunshu, 5, 130 (1979).
122. Baltas, L., Gauvin, W.H.,  
A.I.Ch.E.J, 15, 764, 764, 772 (1969).

123. Katta, S., Gauvin, W.H.,  
A.I.Ch.E.J, 21, 143 (1975).
124. Miura, T., Ohtani, S., Maeda, S.,  
Drying '80, Vol.1, Hemisphere Publ. Corp., N.Y. (1980).
125. Williams, G.C., Schmidt, R.O.,  
Ind.Eng.Chem., 38, 967 (1946).
126. Perry, J.H.,  
Chemical Engineering Handbook, 4th ed., McGraw Hill (1936).
127. Hinchley, J.W., Himus, G.W.,  
Trans.I.Ch.Eng., 2, 57 (1924).
128. Coulson, J.M., and Richardson, J.F.,  
Chem.Eng., Vol.2, 2nd ed., Pergamon Press, Oxford (1976).
129. Kronig, R., and Brink, J.C.,  
Appl.Sci.Res., 1950, A2, 142, 439.
130. Bomben, J.L., Bruin, S., Thijssen, H.A.C., and Merson, R.L.,  
'Aroma Recovery and Retention in Concentration and Drying of Food',  
in Advances in Food Research, eds. G.F. Stewart, et al.,  
Vol.20, Academic press, New York (1973).
131. Thijssen, H.A.C.,  
Lebensm. Wiss. u. Technol ., vol.12, 308 (1979).
132. Thijssen, H.A.C., and Rulkens, W.H.,  
De Ingenieur, (The Hague), vol.80, Ch.45 (1968)
133. Frey, D.D, and King, C.J.,  
A.I.Ch.E. Natl.Mtg., Denver,co. August (1983).
134. Ade-John, A.O.,  
PhD Thesis, University of Aston in Birmingham, England.
135. Flick, D., Lenoir, Ph., Gilbert, H.,  
Sixth IDS'88, vol.1, (1988).
136. King, C.J.,  
Drying'85, p.59-66, Hemisphere Publ.Co.
137. Ali, H.H., Mumford, C.J., Jeffreys, G.V., Bains, G.S.,  
Sixth IDS'88, vol.1, pp 463-470 (1988).
138. Probert, R.P.,  
Phil.Mag., 37, 94 (1946).
139. Bedingfield and Drew;  
Ind. Eng. Chem., 42 , 1164 (1950).

140. Walton, D.E,  
Unpublished work, Aston University (1988).
141. Khiabani, G.,  
Unpublished work, Aston University (1984).
142. Kamei, S., Mizuno, S., and Shiomi, S;  
Kogyo Kwagaku Zasshi, J.Soc.Chem.Ind.Japan, 1077(1935).
143. Krischer, O.,  
Die Wissenschaftlichen Grundlagen Der Trocknungstechnik,  
Springer-verlag, 2/e, Berlin/Gottingen/Heidelberg (1963).
144. Marshall, W.R.Jr.,  
'Drying', 85, Vol 7, pp 326-378.
145. Bains, G.S.,  
Unpublished work, Department of Chemical Engineering,  
Aston University (1988).
146. International Critical Tables.,  
Vol.3, pp 292-
147. Sixth International Drying Symposium.,  
IDS'88, Versailles, (1988).
148. Foord, A.,  
PhD Thesis, Birmingham University (1956).
149. Lihou, D.A.,  
PhD Thesis, Birmingham University (1963).

## APPENDIX A1

### A1 Least Squares Method For Data Correlation

#### A1.1 Constant Air Temperature

From equation 8.1

$$Sh=2+\beta Re^{0.5} Sc^{0.33}$$

By rearrangement and taking logarithms to the base e,

$$\log_e(Sh-2)=\log_e\beta + \log_e(Re^{0.5} Sc^{0.33}) \quad \text{----A.1}$$

Let  $x1=\log_e (Sh-2)$

$$x2=\log_e (Re^{0.5} Sc^{0.33})$$

$$x3=\log_e\beta$$

The error between the given data and the approximating function at  $x2_i$  can be expressed by,

$$E(x1_i)=x1_i-x2_i-x3 \quad \text{----A.2}$$

The objective function is to minimise the sum of the errors squared, expressed as,

$$E(x1_i)^2 = S = \sum_{i=1}^n (x1_i - x2_i - x3)^2 \quad \text{----A.3}$$

Differentiating S with respect to  $x3$ , and setting the resultant differential equation to zero,

$$\frac{ds}{dx3} = -2 \sum_{i=1}^n (x1_i - x2_i - x3) = 0 \quad \text{----A.4}$$

Thus,

$$\Sigma x1_i - \Sigma x2_i - \Sigma nx3 = 0 \quad \text{----A.5}$$

Hence,

$$x3 = 1/n (\Sigma x1_i - \Sigma x2_i) \quad \text{----A.6}$$

The value of  $\beta$  can then be evaluated by taking the exponential of  $x3$ ,

$$\beta = \exp(x3) \quad \text{----A.7}$$

The correlation coefficient C, can be evaluated by,

$$C = [1 - \frac{\sum (x_{1i} - x_{2i} - x_3)^2}{\sum (x_{1i} - x'_1)^2}]^{1/2} \quad \text{----A.8}$$

where  $x'_1 = 1/n \sum x_{1i}$

The same analytical procedure was followed to find the value of  $\phi$  in equation 8.2, and hence equation A.7 becomes,

$$\phi = \exp(x_3) \quad \text{----A.9}$$

In this case let,

$$x_1 = \log_e (\text{Nu} - 2)$$

$$x_2 = \log_e (\text{Re}^{0.5} \text{Pr}^{0.33})$$

$$x_3 = \log_e \phi$$

Computer programs "Constant1" and "Constant 2" listed in APPENDIX A2 were used for data analysis at constant temperature.

### A1.2 Variable Air Temperature

From the proposed equation 8.3,

$$\text{Sh} = A + \beta \left[ \frac{\text{Ta} - \text{Ts}}{\text{Tamb}} \right]^n \text{Re}^{0.5} \text{Sc}^{0.33}$$

rearranging and taking logarithms to the base e,

$$\log_e (\text{Sh} - A) = \log_e \beta + n \log_e [(\text{Ta} - \text{Ts}) / \text{Tamb}] + \log_e (\text{Re}^{0.5} \text{Sc}^{0.33}) \quad \text{---A.10}$$

Let,

$$x_1 = \log_e (\text{Sh} - A)$$

$$x_2 = \log_e (\text{Re}^{0.5} \text{Sc}^{0.33})$$

$$x_3 = \log \beta$$

$$x_4 = \log_e [(\text{Ta} - \text{Ts}) / \text{Tamb}]$$

The errors squared  $E(x_{1i})^2$ , is thus expressed as,

$$E(x_{1i})^2 = S = \sum_{i=1}^n (x_{1i} - x_{2i} - x_3 - nx_{4i})^2 \quad \text{----A.11}$$

Differentiating S with respect to  $x_3$  and  $n$  respectively, and equating both equations to zero,

$$\frac{ds}{dx_3} = -2 \sum_{i=1}^n (x_{1i} - x_{2i} - x_3 - nx_{4i}) = 0 \quad \text{----A.12}$$

and

$$\frac{ds}{dn} = -2 \sum_{i=1}^n x_{4i} (x_{1i} - x_{2i} - x_3 - nx_{4i}) = 0 \quad \text{----A.13}$$

Rewriting equation A.12,

$$\sum x_{1i} - \sum x_{2i} - nx_3 - n \sum x_{4i} = 0 \quad \text{----A.14}$$

and therefore,

$$x_3 = 1/n (\sum x_{1i} - \sum x_{2i} - n \sum x_{4i}) \quad \text{----A.15}$$

Equation A.12 can similarly be expressed as,

$$\sum (x_{4i} \cdot x_{1i}) - \sum (x_{4i} \cdot x_{2i}) - x_3 \sum x_{4i} - n \sum (x_{4i})^2 = 0 \quad \text{----A.16}$$

Substituting equation A.15 into A.16 and rearranging,

$$n = \frac{n \sum (x_{4i} \cdot x_{1i}) - n \sum (x_{4i} \cdot x_{2i}) - (\sum x_{4i}) (\sum x_{1i}) + (\sum x_{4i}) (\sum x_{2i})}{n \sum (x_{4i})^2 - (\sum x_{4i})^2} \quad \text{----A.17}$$

The value of  $n$  can then be used in equation A.15 to evaluate  $x_3$ , and hence

$$\beta = \exp(x_3) \quad \text{----A.18}$$

The correlation coefficient  $C$ , is expressed as,

$$C = \left[ 1 - \frac{\sum (x_{1i} - x_{2i} - x_3 - nx_{4i})^2}{\sum (x_{1i} - \bar{x}_1)^2} \right]^{1/2} \quad \text{----A.19}$$

$$\text{where } \bar{x}_1 = \frac{1}{n} \sum x_i .$$

A computer program "VarTemp", listed in APPENDIX A2 was used to analyse the results according to the above equations.

## APPENDIX A2

**program** Constant 1;

{Program to obtain the value of B in the equation :  $Sh = 2.0 + B * Re^{0.5} Sc^{0.33}$  using a least squares technique }

**var**

A1,A2,A3,Sh,Re,Sc,x1,x2,x3,Barx1,Sumx1,Sumx2,B,C: real ;

N: integer ;

InputEnd : boolean ;

**begin**

N:=0;

Sumx1 :=0;

Sumx2 :=0;

writeln;

write ( 'Write the value of Sh,Re,Sc : ');

read ( Sh,Re,Sc);

writeln;

**while not** InputEnd **do**

**begin**

N:= N + 1;

x1:= Ln ( Sh - 2 );

x2:= ( 0.5 \* Ln ( Re ) ) + 0.33 \* Ln ( Sc );

Sumx1:= Sumx1 + x1;

Sumx2:= Sumx2 + x2;

writeln;

write ( ' Write the value of Sh, Re, Sc: ');

read (Sh, Re, Sc);

writeln;

**if** ((Sh = 0) **and** ( Re = 0) **and** ( Sc = 0)) **then**

**begin**

InputEnd := True;

writeln

**end**

**end;**

x3 := 1/N \* ( Sumx1 - Sumx2 );

Barx1 := 1/N \* Sumx1;

B :=Exp ( x3 );

A1 := Sqr ( Sumx1 - Sumx2 -x3 );

A2 := Sqr ( Sumx1 - Barx1 );

A3 := ( A1/A2 );

```

C := Sqr ( 1 - A3 );
Writeln ( ' The value of beta = ', B : 5 : 3 );
Write ( ' The value of the correlation coefficient = ', C : 5 : 3 );
end.

```

---

```

program Constant 2;

```

```

{ Program to obtain the values of Z in the equation :  $Nu = 2.0 + Z * Re^{0.5}Pr^{0.33}$  using a
least squares method}

```

```

var

```

```

A1, A2, A3, Nu, Re, Pr, x1, x2, x3, Barx1, Sumx1, Sumx2, Z, C : real;

```

```

N : integer;

```

```

InputEnd : boolean;

```

```

begin

```

```

N := 0;

```

```

Sumx1 := 0;

```

```

Sumx2 := 0;

```

```

writeln;

```

```

write ( 'Write the values of Nu,Re,Pr : ' );

```

```

read (Nu,Re,Pr );

```

```

writeln;

```

```

while not InputEnd do

```

```

begin

```

```

N := N + 1;

```

```

x1 := Ln ( Nu-2);

```

```

x2 := (0.5 * Ln(Re) ) +0.33 * Ln(Pr);

```

```

Sumx1 := Sumx1 + x1;

```

```

Sumx2 := Sumx2 + x2;

```

```

writeln;

```

```

write ( 'Write the values of Nu,Re,Pr : ' );

```

```

read (Nu,Re,Pr );

```

```

writeln;

```

```

if (( Nu = 0 ) and ( Re = 0 ) and ( Pr = 0 )) then

```

```

begin

```

```

InputEnd := True;

```

```

writeln

```

```

end

```

```

end;

```

```

x3 := 1/N * ( Sumx1 - Sumx2 );

```

```

Barx1 := 1/N * Sumx1;

```

```

Z := Exp (x3);

```

```

A1 := Sqr ( Sumx1 -Sumx2 -x3 );
A2 := Sqr (Sumx1 -Barx1 );
A3 := ( A1/A2);
C := Sqr (1 -A3 );
Writeln ( ' The value of Phye =', Z : 5 : 3);
Write ( ' The value of the correlation coefficient =', C : 5 : 3);
end.

```

---

**program** VarTemp

{ Program to obtain the values of A, B and N in the equation :

$Sh = A + B (( Ta -Ts)/Tamb)^N Re^{0.5} Sc^{0.33}$ , using a least squares technique to give the best fit to the data}

**var**

A1,A2,A3,A4,Sh,Re,Sc,Ta,Ts,Tamb,X1,X2,X3,X4,BarX1,SumX1,SumX2,SumX4,  
SX4ASX1,SX4ASX2,SX4ASX4,B,N,C : real;

I : integer;

InputEnd : boolean;

(\* Note: SX4ASX1 = Sum (X4 \* X1), SX4ASX2 = Sum (X4 \* X2), SX4ASX4 =  
Sum (X4 \*X4) \* )

**begin**

I := 0;

SumX1 := 0;

SumX2 := 0;

SumX4 := 0;

SX4ASX1 := 0;

SX4ASX2 := 0;

SX4ASX4 := 0;

writeln;

write ( ' Write the values of Sh, Re, Sc, Ta, Ts, Tamb, A4: ');

read (Sh, Re, Sc, Ta, Ts, Tamb, A4 );

writeln;

**while not** InputEnd **do**

**begin**

I := I + 1;

X1 := Ln (Sh -A4 );

X2 := (0.5 \* Ln( Re )) + 0.33 \* Ln (Sc);

X4 := Ln (( Ta -Ts)/ Tamb );

SumX1 := SumX1 + X1;

```

SumX2 := SumX2 + X2;
SumX4 := SumX4 + X4;
SX4ASX1 := SX4ASX1 + (X4 * X1 );
SX4ASX2 := SX4ASX2 + (X4 * X2 );
SX4ASX4 := SX4ASX4 + (X4 *X4 );
writeln;
write ( ' Write the values of Sh, Re, Sc, Ta, Ts, Tamb, A4 : ');
read ( Sh, Re, Sc, Ta, Ts, Tamb, A4 );
writeln;
if ( Sh = 0 ) and ( Re = 0 ) and ( Sc = 0 ) then
  begin
    InputEnd := True;
    writeln
  end
end;
N := ( I * SX4ASX1 - I * SX4ASX2 -SumX4 * SumX1 +SumX4 * SumX2 ) /
      (SX4ASX4 - Sqr ( SumX4 ));
X3 := 1/I * ( SumX1 -SumX2 -N *SumX4 );
BarX1 := 1/I *SumX1;
B := Exp (X3);
A1 := Sqr ( SumX1 -SumX2 -X3 -N *SumX4 );
A2 := Sqr (SumX1 -BarX1);
C := Sqr (1 -A3);
writeln ('The value of A4 =' A4 : 5 :3);
writeln ( ' The value of Beta = ', B : 5: 3);
writeln ('The value of N = ', N : 5 : 3 );
write ( ' The value of the correlation coefficient = ', C : 5 : 3);
end.

```

## APPENDIX A3

### A3.1 Tabulation of Results of Pure Liquid Drops

#### A3.1.1 Pure Water Drops

Table A1

Operating Temperature = 37°C

Drop Temperature = 14°C

Nozzle Size = 2.0 mm

Time (sec)	Drop Mass (mg)	Time (sec)	Equivalent Drop Diameter (m $\times 10^{-3}$ )	Air Velocity (m/s)	Re
0	48.1	60	3.5	8.1	1730
64	36.8	80	3.4	8.0	1677
128	32.8	100	3.3	8.0	1634
192	27.6	120	3.3	8.0	1595
244	25.4	140	3.2	7.9	1556
330	21.4	160	3.2	7.9	1524
354	18.7	200	3.1	7.8	1455
447	14.4	250	2.9	7.6	1367
		300	2.8	7.5	1290

Table A2

Operating Temperature = 67°C

Drop Temperature = 25°C

Nozzle Size = 2.0 mm

Time (sec)	Drop Mass (mg)	Time (sec)	Equivalent Drop Diameter (m $\times 10^{-3}$ )	Air Velocity (m/s)	Re
0	47.7	40	3.4	8.1	1417
32	37.7	80	3.1	7.9	1260
65	30.3	100	3.0	7.8	1190
77	28.3	120	2.8	7.8	1125
126	21.2	140	2.7	7.7	1061
155	18.6	160	2.6	7.6	1003
164	19.2	180	2.4	7.5	941
256	9.0	200	2.4	7.4	891
308	5.5				
330	3.9				

Table A3

Operating Temperature = 97°C  
Drop Temperature = 32°C  
Nozzle Size = 2.0 mm

Time (sec)	Drop Mass (mg)	Time (sec)	Equivalent Drop Diameter(m*10 <sup>-3</sup> )	Air Velocity (m/s)	Re
0	48.0	40	3.1	8.0	1400
25	32.6	60	2.9	7.9	977
37	29.7	80	2.7	7.8	896
69	22.9	100	2.5	7.6	813
81	21.4	120	2.3	7.5	724
123	12.3	140	2.1	7.3	643
173	7.5	160	1.9	7.0	562
177	7.4				
206	4.3				
224	3.3				

Table A4

Operating Temperature =37°C  
Drop Temperature = 14°C  
Nozzle Size = 4.0 mm

Time (sec)	Drop Mass (mg)	Time (sec)	Equivalent Drop Diameter(m*10 <sup>-3</sup> )	Air Velocity (m/s)	Re
0	70.1	50	4.3	8.5	2211
31	53.4	100	4.0	8.4	2092
51	49.3	150	3.9	8.4	1990
147	45.9	200	3.7	8.3	1903
279	35.8	300	3.5	8.1	1716
430	25.0	400	3.2	7.9	1541
573	17.7	500	2.9	7.7	1371
583	15.0	600	2.6	7.5	1183
802	10.0				

Table A5

Operating Temperature = 67°C  
Drop Temperature = 25°C  
Nozzle Size = 4.0 mm

Time (sec)	Drop Mass (mg)	Time (sec)	Equivalent Drop Diameter(m*10 <sup>-3</sup> )	Air Velocity (m/s)	Re
0	70.9	50	4.1	8.4	1759
28	56.5	100	3.8	8.2	1593
38	47.3	150	3.5	8.0	1428
80	45.6	200	3.2	7.9	1289
150	33.0	250	2.9	7.7	1139
246	21.9	300	2.6	7.4	988
386	8.5	400	1.9	6.6	643
482	3.2				

Table A6

Operating Temperature = 97°C  
Drop Temperature = 32°C  
Nozzle Size = 4.0 mm

Time (sec)	Drop Mass (mg)	Time (sec)	Equivalent Drop Diameter(m*10 <sup>-3</sup> )	Air Velocity (m/s)	Re
0	70.3	40	4.1	8.2	1445
35	52.0	50	4.0	8.1	1347
77	39.9	80	3.6	7.9	1211
131	26.0	100	3.4	7.7	1124
164	20.4	120	3.3	7.6	1047
185	18.1	140	3.1	7.5	971
		160	2.9	7.3	894
		180	2.7	7.1	824

### A3.1.2 Pure Isopropanol Drops

Table A7

Operating Temperature = 37°C  
 Drop Temperature = 13°C  
 Nozzle Size = 4.0 mm

Time (sec)	Drop Mass (mg)	Time (sec)	Equivalent Drop Diameter(m*10 <sup>-3</sup> )	Air Velocity (m/s)	Re
0	20.1	17	2.5	6.8	1012
10	13.5	27	2.4	6.8	949
31	10.5	40	2.2	6.6	877
42	8.8	52	2.0	6.4	809
84	4.7	65	1.9	6.3	736
121	3.0	83	1.7	6.1	627
156	1.6	101	1.4	5.9	528
173	1.2	121	1.2	5.7	
		148	0.8	5.3	

Table A8

Operating Temperature = 67°C  
 Drop Temperature = 20°C  
 Nozzle Size = 4.0 mm

Time (sec)	Drop Mass (mg)	Time (sec)	Equivalent Drop Diameter(m*10 <sup>-3</sup> )	Air Velocity (m/s)	Re
0	20.2	16	2.3	6.5	806
8	12.5	20	2.2	6.5	767
16	8.8	25	2.1	6.4	728
22	7.5	30	2.0	6.4	687
35	5.1	43	1.7	6.4	572
43	4.3	51	1.6	6.1	520
72	1.7	59	1.5	5.8	455
		67	1.4	5.4	395

## APPENDIX A4

### A4.1 Tabulation of Data for Evaluation of Drying Characteristics of Drops of Sucros Solution

Table A9

Operating Temperature = 68°C  
Drop Temperature = 25.5°C  
Nozzle Size = 2.0 mm  
Initial Concentration = 20 w/w%

Time (sec)	Drop Mass (mg)	Time (sec)	Equivalent Drop Diameter(m*10 <sup>-3</sup> )	Air Velocity (m/s)
0	45.1	20	3.5	9.4
90	31.7	50	3.3	9.3
150	24.5	70	3.1	9.2
200	20.4	100	2.9	9.0
350	13.8	111	2.9	8.9
500	13.5	138	2.8	8.9
515	11.7	172	2.7	8.8
670	11.6	205	2.6	8.7
950	11.5	235	2.5	8.7
1200	11.4	295	2.3	8.6
		350	2.2	8.5
		380	2.2	8.5
		458	2.1	8.5
		558	2.0	8.4

Table A10

Operating Temperature = 95°C  
Drop Temperature = 31.5°C  
Nozzle Size = 2.0 mm  
Initial Concentration = 20 w/w%

Time (sec)	Drop Mass (mg)	Time (sec)	Equivalent Drop Diameter(m*10 <sup>-3</sup> )	Air Velocity (m/s)
0	46.0	20	3.3	9.2
65	29.5	50	3.2	9.1
150	18.5	76	3.1	9.0
170	16.7	123	2.8	9.0
192	15.0	167	2.6	8.9
300	11.8	190	2.5	8.8
310	11.5	225	2.4	8.7
423	10.5	268	2.2	8.5
610	9.5	303	2.1	8.4
800	9.4	395	2.0	8.2
900	9.3	540	2.0	7.9

Table A11

Operating Temperature = 68°C  
Drop Temperature = 25.5°C  
Nozzle Size = 4.0 mm  
Initial Concentration = 20 w/w%

Time (sec)	Drop Mass (mg)	Time (sec)	Equivalent Drop Diameter(m*10 <sup>-3</sup> )	Air Velocity (m/s)
0	70.5	20	4.2	10.2
50	59.3	30	4.1	10.2
100	49.0	50	3.9	10.2
150	42.6	70	3.7	10.1
200	37.4	100	3.5	10.1
320	25.7	105	3.4	10.0
435	23.5	135	3.3	10.0
643	19.2	205	3.0	9.9
980	17.5	288	2.7	9.8
1270	15.5	338	2.6	9.7
		375	2.6	9.7
		429	2.5	9.6
		479	2.5	9.6
		525	2.4	9.5
		765	2.3	9.4

Table A12

Operating Temperature = 95°C  
Drop Temperature = 31.3°C  
Nozzle Size = 4.0 mm  
Initial Concentration = 20 w/w%

Time (sec)	Drop Mass (mg)	Time (sec)	Equivalent Drop Diameter(m*10 <sup>-3</sup> )	Air Velocity (m/s)
0	70.8	20	3.9	9.6
50	52.5	30	3.9	9.6
75	45.0	50	3.7	9.6
100	39.0	70	3.6	9.5
154	31.0	75	3.6	9.5
235	22.8	90	3.5	9.5
300	20.7	115	3.4	9.4
420	16.5	147	3.2	9.3
515	16.4	173	3.1	9.3
675	16.3	199	3.0	9.3
		233	2.9	9.2
		265	2.8	9.2
		295	2.8	8.9
		320	2.7	8.7
		340	2.7	8.7
		375	2.6	8.6
		410	2.6	8.5

Table A13

Operating Temperature = 68°C  
Drop Temperature = 26.1°C  
Nozzle Size = 2.0 mm  
Initial Concentration = 40 w/w%

Time (sec)	Drop Mass (mg)	Time (sec)	Equivalent Drop Diameter(m*10 <sup>-3</sup> )	Air Velocity (m/s)
0	47.5	30	3.6	10.4
50	40.0	50	3.5	10.3
105	36.5	67	3.4	10.3
115	33.8	93	3.3	10.3
246	29.0	120	3.2	10.2
255	28.4	182	3.2	10.2
435	25.5	182	3.1	10.1
610	25.3	222	3.1	10.1
825	24.5	275	3.0	10.0
1115	23.9	325	3.0	10.0
		375	2.9	9.9
		500	2.8	9.9
		500	2.8	9.9
		712	2.7	9.8
		975	2.7	9.7

Table A14

Operating Temperature = 95°C  
Drop Temperature = 32°C  
Nozzle Size = 2.0 mm  
Initial Concentration = 40 w/w%

Time (sec)	Drop Mass (mg)	Time (sec)	Equivalent Drop Diameter(m*10 <sup>-3</sup> )	Air Velocity (m/s)
0	47.9	25	3.6	9.9
50	37.9	40	3.5	9.7
104	30.4	61	3.4	9.5
150	28.2	81	3.3	9.4
182	27.4	100	3.2	9.2
300	24.4	120	3.1	9.1
385	22.5	156	3.0	9.0
530	22.5	197	2.9	8.9
745	22.3	240	2.8	8.8
		300	2.7	8.8
		359	2.6	8.7
		430	2.6	8.6
		542	2.5	8.4

Table A15

Operating Temperature = 68°C  
Drop Temperature = 26°C  
Nozzle Size = 4.0 mm  
Initial Concentration = 40 w/w%

Time (sec)	Drop Mass (mg)	Time (sec)	Equivalent Drop Diameter(m*10 <sup>-3</sup> )	Air Velocity (m/s)
0	72.1	26	4.1	10.2
100	58.0	40	4.0	10.2
180	49.3	57	4.0	10.1
250	44.0	88	3.9	10.1
300	43.0	130	3.7	10.1
350	39.6	177	3.7	10.0
435	37.3	227	3.6	10.0
735	34.5	270	3.5	10.0
1100	33.5	311	3.5	9.9
1400	31.0	345	3.4	9.9
		389	3.4	9.8
		474	3.3	9.7
		585	3.3	9.7
		735	3.2	9.5
		985	3.2	9.5

Table A16

Operating Temperature = 95°C  
Drop Temperature = 32°C  
Nozzle Size = 4.0 mm  
Initial Concentration = 40 w/w%

Time (sec)	Drop Mass (mg)	Time (sec)	Equivalent Drop Diameter(m*10 <sup>-3</sup> )	Air Velocity (m/s)
0	72.3	25	4.1	9.7
100	53.5	35	4.0	9.7
150	46.5	45	4.0	9.6
250	39.5	68	3.9	9.6
313	37.5	83	3.8	9.6
400	34.0	102	3.8	9.5
500	31.7	152	3.6	9.5
600	31.0	207	3.5	9.4
610	29.0	241	3.4	9.4
1000	28.8	283	3.3	9.4
1400	28.5	358	3.2	9.3

**A4.2 Tabulation of Data for Evaluation of Drying Characteristics of Drops of Potassium Sulphate Solution**

**Table A17**

Operating Temperature = 35°C  
 Drop Temperature = °C  
 Nozzle Size = 2.0 mm  
 Initial Concentration = 5 w/w%

Time (sec)	Drop Mass (mg)	Time (sec)	Equivalent Drop Diameter(m*10 <sup>-3</sup> )	Air Velocity (m/s)
0	47.7	20	3.7	8.4
60	43.6	30	3.6	8.4
165	37.0	40	3.6	8.3
300	30.1	50	3.5	8.2
450	23.7	60	3.5	8.2
603	17.7	82	3.3	8.1
611	16.7	110	3.1	8.0
808	12.7	141	2.9	7.9
893	8.3	179	2.7	7.8
		230	2.4	7.7
		300	2.0	7.7

**Table A18**

Operating Temperature = 65°C  
 Drop Temperature = °C  
 Nozzle Size = 2.0 mm  
 Initial Concentration = 5 w/w%

Time (sec)	Drop Mass (mg)	Time (sec)	Equivalent Drop Diameter(m*10 <sup>-3</sup> )	Air Velocity (m/s)
0	47.6	20	3.6	8.3
56	35.1	30	3.5	8.2
148	24.7	40	3.4	8.1
149	24.2	55	3.3	8.0
236	16.8	90	3.0	7.8
241	16.2	130	2.6	7.7
324	11.8	165	2.3	7.6
		198	2.0	7.5
		226	1.9	7.5

Table A19

Operating Temperature = 95°C  
Drop Temperature = °C  
Nozzle Size = 2.0 mm  
Initial Concentration = 5 w/w%

Time (sec)	Drop Mass (mg)	Time (sec)	Equivalent Drop Diameter(m*10 <sup>-3</sup> )	Air Velocity (m/s)
0	47.3	20	3.5	8.2
71	32.5	30	3.4	8.1
74	31.4	50	3.2	7.9
119	23.2	80	3.1	7.7
186	13.4	100	3.1	7.6
319	8.0	120	3.0	7.5
582	4.5	140	2.4	7.5
		177	2.2	7.3
		221	1.8	7.2

Table A20

Operating Temperature = 35°C  
Drop Temperature = °C  
Nozzle Size = 2.0 mm  
Initial Concentration = 10 w/w%

Time (sec)	Drop Mass (mg)	Time (sec)	Equivalent Drop Diameter(m*10 <sup>-3</sup> )	Air Velocity (m/s)
0	50.1	20	3.8	8.8
58	40.4	30	3.7	8.7
118	39.6	35	3.7	8.7
145	39.1	48	3.6	8.7
200	33.0	69	3.5	8.6
252	31.4	95	3.3	8.6
256	33.0	137	3.1	8.5
405	23.7	187	3.0	8.3
518	20.6	231	2.9	8.2
642	15.2	290	2.8	8.2
717	14.0	388	2.6	8.1
		483	2.4	8.0
		565	2.3	8.0
		634	2.1	7.9
		696	1.9	7.8

Table A21

Operating Temperature = 65°C  
Drop Temperature = °C  
Nozzle Size = 2.0 mm  
Initial Concentration = 10 w/w%

Time (sec)	Drop Mass (mg)	Time (sec)	Equivalent Drop Diameter(m*10 <sup>-3</sup> )	Air Velocity (m/s)
0	50.0	20	3.6	8.7
52	37.1	30	3.5	8.7
124	29.1	32	3.5	8.6
127	27.6	41	3.4	8.6
157	26.0	50	3.3	8.6
196	21.2	60	3.3	8.5
		70	3.3	8.5
		90	3.2	8.4
		127	3.1	8.2
		160	2.8	8.1
		202	2.7	7.8
		242	2.5	7.7
		278	2.4	7.5

Table A22

Operating Temperature = 95°C  
Drop Temperature = °C  
Nozzle Size = 2.0 mm  
Initial Concentration = 10 w/w%

Time (sec)	Drop Mass (mg)	Time (sec)	Equivalent Drop Diameter(m*10 <sup>-3</sup> )	Air Velocity (m/s)
0	504	20	3.4	8.5
29	37.1	30	3.4	8.4
31	35.6	40	3.4	8.4
69	31.3	53	3.2	8.3
91	26.2	70	3.0	8.1
125	22.1	99	2.6	8.0
320	12.3	144	2.1	7.7

Table A23

Operating Temperature = 35°C  
Drop Temperature = °C  
Nozzle Size = 3.0 mm  
Initial Concentration = 5 w/w%

Time (sec)	Drop Mass (mg)	Time (sec)	Equivalent Drop Diameter(m*10 <sup>-3</sup> )	Air Velocity (m/s)
0	66.5	20	4.1	8.8
69	56.2	30	4.0	8.8
129	48.1	40	3.9	8.7
136	47.0	60	3.8	8.6
199	45.0	80	3.7	8.5
203	40.0	90	3.7	8.5
310	33.6	112	3.6	8.4
509	25.0	152	3.5	8.2
695	16.6	200	3.4	8.1
		290	3.3	7.8
		397	3.1	7.6

Table A24

Operating Temperature = 65°C  
Drop Temperature = °C  
Nozzle Size = 3.0 mm  
Initial Concentration = 5 w/w%

Time (sec)	Drop Mass (mg)	Time (sec)	Equivalent Drop Diameter(m*10 <sup>-3</sup> )	Air Velocity (m/s)
0	67.1	20	4.0	8.6
62	54.5	30	4.0	8.6
152	39.9	40	3.9	8.5
256	28.0	65	3.7	8.4
405	16.0	100	3.4	8.2
514	14.6	135	3.3	8.0
		180	3.1	7.9
		283	3.0	7.6

Table A25

Operating Temperature = 95°C  
Drop Temperature = °C  
Nozzle Size = 3.0 mm  
Initial Concentration = 5 w/w%

Time (sec)	Drop Mass (mg)	Time (sec)	Equivalent Drop Diameter(m*10 <sup>-3</sup> )	Air Velocity (m/s)
0	68.0	20	3.8	8.4
40	46.1	30	3.7	8.3
50	41.6	41	3.6	8.2
112	27.6	60	3.5	8.1
165	16.7	80	3.3	8.0
184	14.7	111	3.2	7.8
287	9.6	152	3.0	7.6
		186	2.8	7.5
		225	2.6	7.4

Table A26

Operating Temperature = 35°C  
Drop Temperature = °C  
Nozzle Size = 3.0 mm  
Initial Concentration = 10 w/w%

Time (sec)	Drop Mass (mg)	Time (sec)	Equivalent Drop Diameter(m*10 <sup>-3</sup> )	Air Velocity (m/s)
0	71.5	20	4.2	8.8
51	65.0	30	4.1	8.8
148	54.8	35	4.1	8.7
151	51.1	50	3.9	8.7
298	42.3	60	3.9	8.6
510	33.8	70	3.9	8.6
702	29.7	107	3.8	8.5
843	27.5	170	3.6	8.3
		241	3.4	8.1
		298	3.3	8.0
		343	3.2	7.9
		405	3.1	7.7

Table A27

Operating Temperature = 65°C  
Drop Temperature = °C  
Nozzle Size = 3.0 mm  
Initial Concentration = 10 w/w%

Time (sec)	Drop Mass (mg)	Time (sec)	Equivalent Drop Diameter(m*10 <sup>-3</sup> )	Air Velocity (m/s)
0	69.5	20	4.1	8.7
50	51.7	30	4.0	8.7
103	43.1	40	4.0	8.6
203	37.0	50	3.8	8.6
204	32.8	60	3.8	8.5
303	30.5	81	3.7	8.4
		111	3.5	8.3
		145	3.3	8.2
		175	3.1	8.1
		213	3.0	8.0

Table A28

Operating Temperature = 95°C  
Drop Temperature = °C  
Nozzle Size = 3.0 mm  
Initial Concentration = 10 w/w%

Time (sec)	Drop Mass (mg)	Time (sec)	Equivalent Drop Diameter(m*10 <sup>-3</sup> )	Air Velocity (m/s)
0	70.5	20	4.0	8.5
42	46.9	30	4.0	8.5
68	42.8	40	3.9	8.4
113	31.3	80	3.7	8.2
197	30.9	103	3.5	8.1
227	26.8	128	3.3	8.0
		157	3.0	7.9
		190	2.7	7.7
		236	2.3	7.6

Table A29

Operating Temperature = 35°C  
Drop Temperature = °C  
Nozzle Size = 4.0 mm  
Initial Concentration = 5 w/w%

Time (sec)	Drop Mass (mg)	Time (sec)	Equivalent Drop Diameter(m*10 <sup>-3</sup> )	Air Velocity (m/s)
0	68.3	20	4.3	9.5
78	59.0	27	4.3	9.5
130	51.8	36	4.2	9.4
200	42.4	50	4.1	9.4
248	41.4	70	4.0	9.3
320	40.6	110	3.8	9.2
420	31.4	165	3.6	9.1
		239	3.5	8.9
		322	3.4	8.7
		428	3.2	8.4
		535	3.0	8.3

Table A30

Operating Temperature = 65°C  
Drop Temperature = °C  
Nozzle Size = 4.0 mm  
Initial Concentration = 5 w/w%

Time (sec)	Drop Mass (mg)	Time (sec)	Equivalent Drop Diameter(m*10 <sup>-3</sup> )	Air Velocity (m/s)
0	67.1	20	4.3	9.4
42	48.6	30	4.2	9.3
94	37.6	40	4.1	9.3
155	35.5	50	4.1	9.2
225	23.3	75	3.9	9.2
321	14.5	110	3.6	9.1
393	13.8	160	3.3	8.9
		215	3.2	8.6
		275	3.0	8.2

Table A31

Operating Temperature = 95°C  
Drop Temperature = °C  
Nozzle Size = 4.0 mm  
Initial Concentration = 5 w/w%

Time (sec)	Drop Mass (mg)	Time (sec)	Equivalent Drop Diameter(m*10 <sup>-3</sup> )	Air Velocity (m/s)
0	69.6	20	3.8	9.0
34	52.3	30	3.7	8.9
42	47.2	35	3.7	8.8
52	46.2	45	3.6	8.7
93	32.2	78	3.3	8.4
128	16.3	125	3.0	8.1
148	17.5	165	2.8	7.8
187	13.6	218	2.5	7.6
239	11.9	302	2.0	7.4

Table A32

Operating Temperature = 35°C  
Drop Temperature = °C  
Nozzle Size = 4.0 mm  
Initial Concentration = 10 w/w%

Time (sec)	Drop Mass (mg)	Time (sec)	Equivalent Drop Diameter(m*10 <sup>-3</sup> )	Air Velocity (m/s)
0	76.0	30	4.3	9.7
42	66.4	50	4.2	9.6
86	59.6	70	4.2	9.5
135	55.7	90	4.1	9.4
205	53.1	110	4.0	9.3
304	46.8	130	4.0	9.3
424	31.8	150	3.9	9.2
524	27.1	158	3.9	9.2
671	26.3	186	3.8	9.1
756	25.0	231	3.6	9.0
		273	3.5	8.9
		348	3.4	8.8
		448	3.2	8.5

Table A33

Operating Temperature = 65°C  
Drop Temperature = °C  
Nozzle Size = 4.0 mm  
Initial Concentration = 10 w/w%

Time (sec)	Drop Mass (mg)	Time (sec)	Equivalent Drop Diameter(m*10 <sup>-3</sup> )	Air Velocity (m/s)
0	75.4	30	4.3	9.5
74	52.2	33	4.2	9.5
159	25.8	41	4.2	9.4
216	30.6	55	4.1	9.3
284	24.6	73	4.0	9.2
319	19.9	107	3.8	9.1
320	25.1	150	3.58	8.9
		185	3.4	8.9
		235	3.1	8.7
		304	2.9	8.6

Table A34

Operating Temperature = 95°C  
Drop Temperature = °C  
Nozzle Size = 4.0 mm  
Initial Concentration = 10 w/w%

Time (sec)	Drop Mass (mg)	Time (sec)	Equivalent Drop Diameter(m*10 <sup>-3</sup> )	Air Velocity (m/s)
0	76.4	27	4.3	9.3
41	50.0	36	4.2	9.2
88	40.0	67	3.9	9.0
114	30.5	110	3.5	8.8
141	34.6	135	3.3	8.7
230	24.0	150	3.2	8.6
366	17.9	174	3.0	8.5
486	25.2	198	3.0	8.4
		228	2.8	8.4

## APPENDIX A5

### Derivation of the Crust Coefficient, $k_c$

By analogy to the Two Film Theory (3) the crust mass transfer coefficient can be defined as,

$$k_c = \frac{D_e}{\beta} \quad \text{---A5.1}$$

where,  $D_e$  = effective diffusivity of water vapour through the crust

$\beta$  = crust thickness

since the hold-up of solvent in the crust is negligible. The effective diffusivity (42) is proportional to the molecular diffusivity,  $D_m$ , porosity,  $\epsilon$ , the constriction factor,  $\sigma$ , and the tortuosity factor,  $\tau$ . These quantities are related to  $D_e$  according to the expression,

$$\frac{D_e}{D_m} = \frac{\epsilon \sigma}{\tau} \quad \text{---A5.2}$$

The porosity factor,  $\epsilon$ , is included to account for the effective reduction in the area for the diffusion of moisture at a particular point in the porous medium. The tortuosity factor is a measure of the ratio of the distance which a diffusing species must travel on the average, and the linear distance between the two points in the solid. The constriction factor takes into account the fact that channels are not uniform in cross-section but vary with position.

The tortuosity and constriction factors are functions of the porosity, and Bruggeman's equation predicts,

$$\frac{\sigma}{\tau} = \varepsilon^{1/2} \quad \text{---A5.3}$$

On substituting equation A5.3 into A5.2, the effective diffusivity becomes,

$$D_e = D_m \varepsilon^{1.5} \quad \text{---A5.4}$$

The mass transfer coefficient from equations A5.1 and A5.4, becomes,

$$k_c = \frac{D_m \varepsilon^{1.5}}{\beta} \quad \text{---A5.5}$$

## APPENDIX A6

List of videos deposited in the Departmental Library :

<u>Tape Number</u>	<u>Title</u>
1	A study of pure liquid droplets; water
2	A study of pure liquid droplets; isopropanol
3	A study of drops of potassium sulphate solution (N.S = 2&3mm)
4	A study of drops of potassium sulphate solution (N.S = 4mm)
5	A study of drops of sucrose solution (N.S =2mm, T <sub>a</sub> = 68°C)
6	A study of drops of sucrose solution (N.S =2mm, T <sub>a</sub> = 95°C)
7	A study of drops of sucrose solution (N.S =4mm)

## APPENDIX A7

Determination of the pressure driving force for mass transfer for systems other than air-water vapour:

At equilibrium, assuming negligible change in the dry-bulb temperature, a heat balance over a saturated surface gives the wet-bulb equation as,

$$k_g \lambda (p_s - p_g) = h_c (t_a - t_w) \quad (1)$$

Under ordinary conditions the partial pressure and vapour pressure are small relative to the total pressure, and the wet-bulb equation can be written as,

$$H_s - H_a = \frac{h_c}{\lambda K'} (t_a - t_w) \quad (2)$$

$$\text{where } K' = (M_a/M_w) k_g = 1.6k_g \quad (3)$$

Now, the equation for the adiabatic- saturation line is (126);

$$H_s - H_a = \frac{C'_s}{\lambda} (t_a - t_w) \quad (4)$$

Experimentally it has been shown that for air-water systems the value of  $h_c/K'C'_s$ , the psychrometric ratio, is approximately equal to 1. Under these conditions the wet-bulb temperatures and adiabatic saturation temperatures are substantially equal and can be used interchangeably.

For systems other than air-water vapour, such as air-isopropanol vapour, the value of  $h_c/K'C'_s$  may differ appreciably from unity, and the wet-bulb and adiabatic saturation temperatures are no longer equal. For these systems the psychrometric ratio may be obtained by determining  $h_c/K'$  from heat- and mass-transfer analogies. For example Bedingfield and Drew (139), for wet-bulb thermometers in air, give the following expression ;

$$\frac{h_c}{K'} = 0.294 \left[ \frac{\mu_a}{\rho_a D_v} \right]^{0.56} \quad (5)$$

## APPENDIX A8

### Mathematical Model for the Prediction of Drying Rates

The drying rate after crust formation is generally controlled by the resistance of the crust to vapour diffusion. Heat is transferred through the crust into the wet core where evaporation occurs at the interface between the core and the crust. The vapour then diffuses through the pores of the crust into the drying medium. Capillary effects are negligible. On this basis consider a slurry droplet after a crust has been formed as depicted in Figure A8.1. Let the outer radius of the crust be  $r=R$  and the

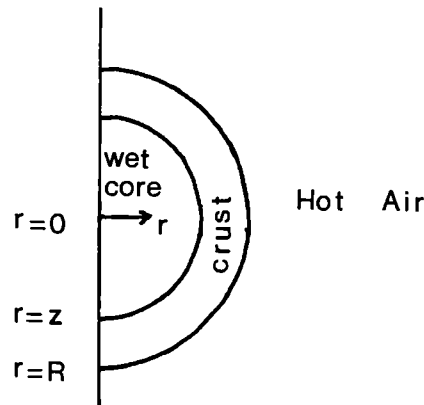


Figure A8.1 Spherical slurry droplet after crust formation

evaporation interface be  $r=z$ . Further assumptions are:

1. Evaporation only occurs at the evaporation interface, which is the interface between the wet core and the crust.
2. The evaporation interface,  $r=z$ , recedes into the wet core as evaporation proceeds.
3. Once formed, the crust does not shrink or inflate, i.e.,  $R$  remains constant. It is also assumed that no fractures or large blow-holes occur.
4. The core temperature,  $T_c$ , is uniform throughout the core.
5. Heat transfer from the drying air to the crust is solely by convection.
6. Heat transfer through the crust is solely by conduction.
7. Moisture is transferred from the evaporation interface by vapour diffusion through the pores and can be represented by an effective diffusivity  $D_{eff}$ .
8. The wet core density of the slurry remains constant during the evaporation process, i.e., as water evaporates at the interface it precipitates an equivalent amount

of solid as crust, between the surface of the particle and the wet core. The core continues to be a slurry.

9. The energy and water vapour storage within the crust are assumed to be negligible because the crusts produced are thin.

Then a heat balance over the evaporation interface at  $r=z$  can be expressed as :

Rate of heat supplied through crust = Rate of heat loss by evaporation + Rate of sensible heat supply into core

or,

$$4\pi z^2 k_{tc} \left. \frac{\delta T}{\delta r} \right|_{r=z} = -4\pi z^2 \rho_w \dot{x} (\lambda - C_c) \left( \frac{dz}{d\theta} \right) + \frac{4}{3} \pi z^3 C_p \rho_c \left( \frac{dT_c}{d\theta} \right) \quad --(1)$$

which reduces to

$$\frac{dz}{d\theta} = \left[ \frac{k_{tc}}{\rho_w \dot{x} (\lambda - C_c)} \right] \left. \frac{\delta T}{\delta r} \right|_{r=z} - \left[ \frac{C_p z}{3 \dot{x} (\lambda - C_c)} \right] \left( \frac{dT_c}{d\theta} \right) \quad --(2)$$

The final assumption (9) implies a linear temperature gradient within the crust. Then the rate of heat transfer can be expressed as,

$$4\pi r^2 k_{tc} \frac{\delta T}{\delta r} = \text{Constant} \quad --(3)$$

Integrating Eq.3 between the limits  $r=R$  and  $r=z$ , gives

$$Q_r = 4\pi k_{tc} (T_R - T_z) \left. \frac{R_z}{R - z} \right) \quad --(4)$$

At  $r = R$ ,

$$Q'_R = 4\pi k_{tc} R^2 \left. \frac{\delta T}{\delta r} \right|_R \quad --(5)$$

and at  $r=z$ ,

$$Q_z = 4\pi k_{tc} z^2 \left. \frac{\delta T}{\delta r} \right|_{r=z} \quad --(6)$$

but  $Q_r = Q'_R = Q_z$ , so that

$$\left. \frac{\delta T}{\delta r} \right|_R = \frac{z(T_R - T_z)}{R(R - z)} \quad \text{--(7)}$$

and

$$\left. \frac{\delta T}{\delta r} \right|_{r=z} = \frac{R^2}{z^2} \left. \frac{\delta T}{\delta r} \right|_R \quad \text{--(8)}$$

but  $T_z = T_c$  at the surface of the wet core so that Eq.7 becomes

$$\left. \frac{\delta T}{\delta r} \right|_R = \frac{z(T_R - T_c)}{R(R - z)} \quad \text{--(7)}$$

Also at  $r = R$ ,

$$4\pi R^2 k_c \left. \frac{\delta T}{\delta r} \right|_R = 4\pi R^2 h_g (T_g - T_R) \quad \text{--(10)}$$

where  $h_g$  = gas film heat transfer coefficient.

Substituting Eq.9 into Eq.10 gives,

$$(T_R - T_c) = R(R - z)(T_g - T_R)/k_{tc} z \quad \text{--(11)}$$

Let  $a_0 = R(R - z)h_g/k_{tc}z$

Rearranging gives,

$$(T_R - T_c) = (a_0/(1 + a_0))(T_g - T_c) \quad \text{--(12)}$$

Substituting Eq.12 into Eq.9 and the resulting equation into Eq.8 gives,

$$\left. \frac{\delta T}{\delta r} \right|_z = \left( \frac{a_0}{1 + a_0} \right) \left[ \frac{R}{z(R - z)} \right] (T_g - T_c) \quad \text{--(13)}$$

Substituting Eq.13 and the value of  $a_0$  into the heat balance, Eq.2 gives,

$$\frac{dz}{d\theta} = \left( \frac{R^2 h_g k_c}{\rho_w \lambda (\lambda - C_d)} \right) \left[ \frac{1}{[k_c - R h_g z^2 + R^2 h_g z]} \right] (T_g - T_c) - \left[ \frac{C_p z}{3\lambda (\lambda - C_c)} \right] \frac{dT_c}{d\theta} \quad \text{--(14)}$$

Let

$$a_1 = \frac{R^2 h_g k_c}{\rho_w \lambda (\lambda - C_d)}$$

$$a_2 = k_{tc} - R h_g$$

$$a_3 = R^2 h_g$$

$$a_4 = \frac{C_p}{3x(\lambda - C_d)}$$

Then Eq.14 becomes,

$$\frac{dz}{d\theta} = \left( \frac{a_1}{a_2z^2 + a_3z} \right) (\Gamma_g - T_c) - a_4z \frac{dT_c}{d\theta} \quad --(15)$$

### Mass Transfer at Evaporation Interface

A mass balance over the evaporation interface for low rates of mass transfer, the conditions pertaining to the drying of particulate slurries, can be expressed by

$$-4\pi z^2 \rho_{\omega} x' \frac{dz}{d\theta} = -4\pi z^2 D_{ef} \left( \frac{M_w}{R_c T_c} \right) \frac{\delta p}{\delta r} \Big|_{r=z} \quad --(16)$$

This reduces to

$$\frac{dz}{d\theta} = \left( \frac{D_{ef}}{\rho_{\omega} x'} \right) \left( \frac{M_w}{R_c T_c} \right) \frac{\delta p}{\delta r} \Big|_{r=z} \quad --(17)$$

As in the case of heat transfer, a linear concentration gradient can be assumed for the thin crusts. Hence, the rate of mass transfer can be expressed as ,

$$J_r = -4\pi r^2 D_{ef} \left( \frac{\delta p}{\delta r} \right) = \text{C onstant} \quad --(18)$$

where  $D_{eff}$  is evaluated at the mean crust temperature. A similar analysis to that for heat transfer yields,

$$\frac{dz}{d\theta} = \left( \frac{b_1}{b_2z^2 + b_3z} \right) \left( \frac{p_g}{T_g} - \frac{p_c}{T_c} \right) \quad --(19)$$

where  $b_0, b_1, b_2, etc.$  are functions as defined in the Nomenclature.

Equations 19 and 15 have to be solved simultaneously since they are coupled heat and mass transfer equations. Thus,

$$\frac{dT_c}{d\theta} = \left( \frac{a_1/a_4}{a_2 z^2 + a_3 z} \right) \left( \frac{T_g - T_d}{z} \right) + \left( \frac{b_1/a_4}{b_2 z^2 + b_3 z} \right) \left( \frac{p_g - p_d}{T_g - T_d} \right) \frac{1}{z} \quad --(20)$$

Also, from Eq.16, the rate of mass transfer can be expressed as,

$$-\frac{dW}{d\theta} = -4\pi z^2 \rho_c \delta' \frac{dz}{d\theta} \quad --(21)$$

Substituting for  $dz/d\theta$  from Eq.19 gives

$$-\frac{dW}{d\theta} = -4\pi z^2 \rho_c \delta' \left( \frac{b_1}{b_2 z^2 + b_3 z} \right) \left( \frac{p_g - p_c}{T_g - T_c} \right) \quad --(22)$$

Equations 19, 20, and 22 can be solved simultaneously by the Runge-Kutta fourth order method to give the crust thickness, core temperature, and weight of the drop as a function of time, using the boundary conditions pertaining to the different experiments, i.e., air and wet-bulb temperatures, initial concentration and drop weight, partial pressure of water-vapour in air and air velocities.